

DATA-INFUSED FRACTIONAL MODELING AND SPECTRAL NUMERICAL ANALYSIS
FOR ANOMALOUS TRANSPORT AND TURBULENCE

By

Mehdi Samiee

A DISSERTATION

Submitted to
Michigan State University
in partial fulfillment of the requirements
for the degree of

Mechanical Engineering – Doctor of Philosophy
Computational Mathematics, Science and Engineering – Dual Major

2021

ABSTRACT

DATA-INFUSED FRACTIONAL MODELING AND SPECTRAL NUMERICAL ANALYSIS FOR ANOMALOUS TRANSPORT AND TURBULENCE

By

Mehdi Samiee

Fractional calculus introduces tractable mathematical tools for accurate description of anomalous phenomena, regarded as a manifestation of self-similar structures and memory effects. Fractional approaches in modeling anomalous dynamics have been increasingly employed over the last decade in a disparate range of applications, where the standard methods have been found experimentally to be inadequate. The physical significance of employing fractional operators in such models is indicated by their potentials in describing the inherent abnormal-exponential or heavy-tailed processes due to their power-law or logarithmic kernels of convolution type. However, it is also inevitably challenging to provide efficient and yet accurate numerical methods for fractional differential equations. More concretely, history-dependent and nonlocal characteristics of fractional operators impose further numerical complexities, ranging from theoretical analysis to large memory requirement. Therefore, to establish a robust framework for developing fractional models, a great deal of attention is required in theoretical and numerical studies of fractional calculus. In particular, developing a fractional model depends on some key elements, given as: stochastic interpretation, theoretical analysis, numerical methods, and optimization of model parameters. In this dissertation, we provide a robust framework for fractional modeling of anomalous features in the applied areas of research such as solute transport in underground waters and homogeneous isotropic turbulent flows.

Inspired by the stochastic interpretation of fractional diffusion problems in terms of time-changed Markov processes, we develop a unified Petrov-Galerkin (PG) spectral method for a class of fractional partial differential equations (FPDEs) with two-sided derivatives and constant coefficients. We employ the eigenfunctions of the fractional Sturm-Liouville eigen-problems, called Jacobi poly-fractonomials, as temporal bases and test functions. Furthermore, we formulate

a novel unified fast linear solver for the resulting high-dimensional linear system based on the solution of generalized eigenproblem of spatial mass matrices with respect to the corresponding stiffness matrices. On the theoretical side, we prove existence and uniqueness of the solution to the corresponding bilinear form of the problem and subsequently, provide the corresponding stability and error analyses. Moreover, we compare the theoretical and computational rates of spectral convergence by performing several numerical simulations. Motivated by the multifractal characteristics of anomalous phenomena, we extend the unified PG method to the generalized form of FPDEs with distributed-order two-sided derivatives and carry out the corresponding stability and error analyses.

In the large-eddy simulation of homogeneous turbulence, presence of nonlocal triad interactions and intermittent structures urges developing new nonlocal closure models. Such anomalous effects become even more pronounced when the filter-width enlarges. Within the proposed framework, we start modeling of turbulent effects at the Boltzmann transport using fractional calculus. In practice, we approximate the filtered collision operator with a power-law function which contributes to the corresponding fractional subgrid-scale (SGS) model in the filtered NS equations through a meticulous derivation. Inspired by the self-similar cascading of energy from large to small scales and the exponential decay in the dissipation range, we adopt tempered Lévy-stable distribution as a statistically-consistent choice at the kinetic level and subsequently, we derive the corresponding operator in terms of the tempered fractional Laplacian, $(\Delta + \lambda)^\alpha(\cdot)$, $\alpha \in (0, 1]$, $\alpha \neq \frac{1}{2}$, and $\lambda > 0$ in the filtered NS equations, termed as tempered fractional SGS (TFSGS) model. The model parameters appear to be strictly depending on the filter-width and the flow Reynolds number. Such a tractable fractional operator offers a great flexibility in characterizing nonlocal structures in the turbulent inertial and dissipation ranges through fractional and tempering parameters. To infer optimum values of the model parameters, we develop a robust optimization algorithm, involving two-point structure functions and conventional correlation coefficients. In *a priori / a posteriori* statistical analyses, we evaluate capabilities of the TFSGS model in fulfilling the closed essential requirements and also study the numerical stability of LES solutions in time.

Copyright by
MEHDI SAMIEE
2021

To my parents

ACKNOWLEDGEMENTS

First and foremost I am extremely grateful to my supervisor, Professor Zayernouri for his invaluable advice, continuous support, and illuminating guidance throughout my doctoral program. My sincere gratitude extends to my committee members, Professor Brereton, Professor Jaber, and Professor Murillo, for their thoughtful and meticulous comments and suggestions. I also appreciate Professor Meerschaert for the informative and helpful conversations during his class and group meetings.

I would like to thank to my dear peers in the FMATH group for a cherished time spent together in the lab and in social settings especially Dr. Jorge Suzuki for sharing his invaluable thoughts and experiences. I would like to acknowledge my great collaborators Mr. Ali Akhavan-Safaei and Dr. Ehsan Kharazmi for the fruitful discussions and being open to exchanging ideas. Additionally, I would like to express my deepest gratitude to my friends who offered me their gracious supports and encouragements in good times and tough times during my PhD.

My most special appreciations and heartfelt thanks go to my parents, Muhammad Hussein and Zahra, and to my kind brother, Milad, for all the love and endless encouragements they have given me to shape my life. Their sacrifices and support have helped me complete this achievement. As a small token of my appreciation, this dissertation is dedicated to them.

This dissertation was supported by the department of mechanical engineering and department of computational mathematics, science and engineering in the college of engineering at Michigan State University. The high-performance computing resources and services were provided by the Institute for Cyber-Enabled Research (ICER) at Michigan State University.

TABLE OF CONTENTS

LIST OF TABLES	x
LIST OF FIGURES	xi
LIST OF ALGORITHMS	xiv
CHAPTER 1 INTRODUCTION	1
1.1 Anomalous Transport	1
1.2 Fractional Calculus	4
1.2.1 Preliminaries on Fractional Calculus	7
1.2.2 Fractional Modeling	8
1.3 Outline of the Present Work	9
CHAPTER 2 A UNIFIED SPECTRAL METHOD FOR FPDES WITH TWO-SIDED DERIVATIVES	17
2.1 Background	17
2.2 Preliminaries on Fractional Calculus	19
2.3 Problem Definition	21
2.3.1 Stochastic Interpretation of the FPDEs	21
2.4 Petrov-Galerkin Mathematical Formulation	22
2.4.1 Mathematical Framework	22
2.4.2 Solution and Test Function Spaces	29
2.4.3 Petrov-Galerkin Method	31
2.5 Well-posedness Analysis	32
2.6 Discrete Form Formulation	35
2.6.1 Space of Basis Functions (U_N)	36
2.6.2 Space of Test Functions (V_N)	37
2.7 Implementation of PG Spectral Method	37
2.8 Unified Fast FPDE Solver	43
2.8.1 Computational Considerations	45
2.9 Stability and Error Analysis	45
2.10 Error Analysis	46
2.11 Numerical Tests	50
CHAPTER 3 A UNIFIED PG METHOD FOR DISTRIBUTED-ORDER FPDES	54
3.1 Background	54
3.2 Preliminaries on Fractional Calculus	56
3.3 Mathematical Formulation	58
3.3.1 Mathematical Framework	58
3.3.2 Solution and Test Function Spaces	66
3.3.3 Well-posedness Analysis	68
3.4 Petrov Galerkin Method	71

3.4.1	Space of Basis (U_N) and Test (V_N) Functions	72
3.4.2	Implementation of the PG Spectral Method	72
3.4.3	Unified Fast FPDE Solver	73
3.5	Stability and Error Analysis	74
3.5.1	Stability Analysis	74
3.5.2	Error Analysis	75
3.6	Numerical Tests	80
CHAPTER 4	A FRACTIONAL SUBGRID-SCALE MODEL FOR TURBULENT FLOWS	84
4.1	Background	84
4.2	Preliminaries on Fractional Laplacian	87
4.3	Governing Equations	89
4.3.1	Boltzmann Transport Equation (BTE)	89
4.3.2	Filtered Boltzmann Transport Equation (FBTE)	91
4.3.3	Derivation of the FS _{SGS} model	94
4.3.4	Physical Properties	97
4.3.4.1	<i>Second-law of Thermodynamics</i>	97
4.3.4.2	<i>Frame Invariance</i>	98
4.4	<i>A Priori</i> Analysis of the Fractional SGS Model	98
4.4.1	Estimation of Fractional Exponent α	101
4.4.2	Analysis of the Model Performance	104
4.4.3	Towards Modeling Nonlocal Effects	107
CHAPTER 5	A TEMPERED FRACTIONAL APPROACH TO LES OF TURBULENT FLOWS	109
5.1	Background	109
5.2	Preliminaries on Tempered Fractional Calculus	113
5.2.1	Tempered fractional Laplacian	115
5.3	Boltzmannian Framework	115
5.3.1	A review on the subgrid-scale modeling	116
5.3.2	The BGK equation and the closure problem	117
5.3.3	Tempered fractional SGS modeling	120
5.3.4	TF _{SGS} formulations for the SGS stresses	123
5.4	Statistical Analysis	123
5.4.1	Optimization strategy	125
5.5	<i>A Priori</i> Study	126
5.5.1	DNS Database and LES Platform	127
5.5.2	Optimal estimation of fractional parameters	128
5.5.3	Interpretation of two-point structure functions	131
5.5.4	PDF of SGS stresses	134
5.6	<i>A Posteriori</i> Analysis	136
CHAPTER 6	SUMMARY AND FUTURE WORKS	138
6.1	Concluding Remarks	138
6.2	Future Works	141

APPENDICES	142	
APPENDIX A	DERIVATIONS IN CHAPTER 2	143
APPENDIX B	DERIVATIONS IN CHAPTER 3	149
APPENDIX C	DERIVATIONS IN CHAPTER 4	151
APPENDIX D	DERIVATIONS IN CHAPTER 5	155
BIBLIOGRAPHY	160	

LIST OF TABLES

Table 1.1: Variety of the underlying anomalous stochastic processes [1].	5
Table 2.1: Convergence study of the PG spectral method for (1+1)-D diffusion problem, where $\kappa_{l_1} = \kappa_{r_1} = \frac{2}{10}$ and $T = 2$. Besides, $p_1 = 5\frac{1}{20}$, $p_2 = 5\frac{3}{4}$ and $p_3 = 5\frac{1}{5}$ in (2.105). Here, we denote by \bar{r}_0 the practical rate of the convergence, numerically achieved.	51
Table 2.2: Here, we set $p_1 = 5\frac{1}{20}$ and $n = 1$ in (2.106) to study the convergence of the PG spectral method for (1+1)-D diffusion problem, where $\kappa_{l_1} = \kappa_{r_1} = \frac{2}{10}$ and $T = 2$. Besides, the limit orders are $\nu_1 = \frac{11}{20}$ and $\nu_1 = \frac{19}{20}$, where $\tau = \frac{5}{20}$ is fixed.	53
Table 3.1: CPU time, PG spectral method for fully distributed (1+d)-dimensional diffusion problems. $u^{ext} = t^{p_1+\alpha} \times \prod_{i=1}^3 (1+x_i)^{p_{2i}} (1-x_i)^{p_{2i+1}}$, where $\alpha = 10^{-4}$, $p_1 = 3$, and the expansion order is 4×11^d	83
Table 4.1: Computational parameters and statistical features of a forced HIT problem, provided by JHTDB [2]	99
Table 4.2: Micro-scale statistical characteristics of turbulence for the applied initial condition in DNS of decaying HIT.	100
Table 4.3: <i>A priori</i> results for the correlation coefficients, ϱ_{ij} , of SGS stresses obtained from the FSGS and SMG models at two different Reynolds numbers, \mathcal{L}_δ	105
Table 4.4: Study of FSGS model in terms of \mathcal{L} through <i>a priori</i> analysis at other time instants of Case (I)	106
Table 5.1: Flow parameters and statistical properties in the DNS of a forced HIT flow.	128
Table 5.2: The ensemble-averaged correlation coefficients (ϱ_{ii}) between SGS stresses obtained by the filtered DNS data ($T_{ii}^{R,D}$) and the TFSGS model ($T_{ii}^{R,TF}$) for $i = 1, 2, 3$. In the fractional models, α^{opt} is set as 0.76, 0.58, and 0.51 for $\mathcal{L}_\delta = 4, 8, 12$ respectively.	129
Table 5.3: Optimized parameters associated with the TFSGS model in terms of Algorithm 5.1 for differing filter widths.	132

LIST OF FIGURES

<p>Figure 1.1: [3] Overlay of a migrating MDCK-F NHE cell with its path covered within 480 minutes. The cell frequently changes its shape and direction during migration. Double-logarithmic plot of the mean squared displacement as a function of time. Experimental data points for both cell types are symbolized by triangles and circles.</p> <p>Figure 1.2: [4] Positions of 10 small particles (distinguished by different colors) (left) $\delta = 0.2$, (middle) $\delta = 0.35$, and (right) $\delta = 0.5$, for a fixed total time. Note that δ denotes the size ratio of small and large particles. The distribution, $n(s)$, of the size, s, of clusters follow a power-law dependence, $n(s) \sim s^{-2.19}$.</p> <p>Figure 1.3: [5] (left) Dispersal of bank notes on geographical scales originating from three different places. (middle) In the quantitative analysis of bank note dispersal, the measured probability density function, $p(r)$, of traversing a distance, r, in 4 days undergoes a power-law $p(r) \sim r^{-1.59}$. (right) $p(r)$ for three classes of initial entry locations (black triangles for metropolitan areas, diamonds for cities of intermediate size, and circles for small towns).</p> <p>Figure 1.4: [6] The trajectories of Lagrangian particles in a heterogeneous porous media; (left) probability distributions of normalized Lagrangian longitudinal velocity increments, $\frac{\Delta V}{\sigma_{\Delta V}(\tau)}$ for the different time lags, (right) colored normalized mean squared displacement of purely advected particles, $\sigma_x = <\Delta x^2>$, versus normalized time.</p> <p>Figure 1.5: [7] Ramp-cliff structures in a scalar field at $Re_\lambda = 650$ and $Sc = 1$. The vertical colored solid line show the spatial positions for the magnifications of the scalar fluctuation profiles, plotted in the right.</p> <p>Figure 1.6: Schematic framework of the thesis with main focus on developing fractional models for anomalous transport, e.g., solute particle transport in underground waters and SGS motions in turbulent flows. The proposed framework is established based on the key elements, listed as: mathematical formulation of the fractional model starting at the kinetic level, theoretical analysis, developing numerical schemes for the proposed FPDE approaches, and optimizing performance of the model.</p> <p>Figure 3.1: Temporal/Spatial p-refinement for case I with singularity of order $\alpha = 10^{-4}$. (Left): $p_1 = 3$, $p_2 = p_3 = 2$, and expansion order of $\mathcal{N} \times 9$. (Middle): $p_1 = 2$, $p_2 = p_3 = 2$, and expansion order of $3 \times \mathcal{M}$. (Right): $p_1 = 3$, $p_2 = p_3 = 2$, and expansion order of $4 \times \mathcal{M}$.</p>	<p>2</p> <p>2</p> <p>3</p> <p>3</p> <p>5</p> <p>10</p> <p>81</p>
---	--

Figure 3.2: Spatial p -refinement for case II, $p_1 = 3$, $\alpha = 0.1$, and $\alpha = 0.9$.	82
Figure 3.3: Spatial p -refinement for case III with singularity of order $\alpha = 10^{-4}$. (Left): $(1+2)$ -dimensional, $p_1 = 3$, $p_{2i} = p_{2i+1} = 1$, where the expansion order is $\mathcal{N} \times \mathcal{M}_1 \times \mathcal{M}_2$. (Left): $(1+3)$ -dimensional, $p_1 = 3$, $p_{2i} = p_{2i+1} = 1$, where the expansion order is $\mathcal{N} \times \mathcal{M}_1 \times \mathcal{M}_2 \times \mathcal{M}_3$.	82
Figure 4.1: Time evolution of $K(t')/K_0$, $\varepsilon(t')/\varepsilon_0$, and $Re_\lambda(t')$ during the DNS of decaying HIT	101
Figure 4.2: v_α versus α for $\nu = 1.85 \times 10^{-4}$ in Case (I) and $\nu = 10^{-3}$ in Case (II)	102
Figure 4.3: Variation of the correlation coefficient, ϱ_i , and the regression coefficient, β_i , in terms of the fractional exponent, $\alpha \in (0, 1)$ using the DNS database of Case (I) for (a) $i = 1, 2, 3$ at $\mathcal{L}_\delta = 4$, and (b) $i = 1$ at $\mathcal{L}_\delta = 2, 8, 32$	103
Figure 4.4: α^{opt} versus \mathcal{L}_δ for the Case (I) , of properties are given in Table 4.1	103
Figure 4.5: (a) The surface of α^{opt} , obtained by the Kriging method, versus \mathcal{L}_δ and Re_λ using the data points, denoted by \star , which are estimated by the <i>a priori</i> tests of FSGS model for Case (II) and (b) comparison between the curves of α^{opt} versus \mathcal{L}_δ , which are designated by $Re_\lambda \approx 26, 35, 45$	104
Figure 4.6: Comparing the correlation coefficients, ϱ_i , from the FSGS model using the optimum fractional exponent, with the corresponding ones implied by the Smagorinsky model	105
Figure 4.7: <i>A priori</i> results for the correlation between the true and model values for the components of $\nabla \cdot \mathcal{T}^R$, where $[\nabla \cdot \mathcal{T}^R]^{FSGS} = \mu_\alpha (-\Delta)^\alpha \bar{\mathbf{V}} _{\alpha=\alpha^{opt}}$, yielding the correlation coefficients, as shown	106
Figure 4.8: Comparison of Kriging-constructed surfaces of ϱ_i for $i = 1, 2, 3$, obtained from <i>a priori</i> study of the FSGS and the SMG models, versus \mathcal{L}_δ and Re_λ on Case (II)	106
Figure 4.9: <i>A priori</i> results for the PDF of the true and modeled $(\nabla \cdot \mathcal{T}^R)_1$ regarding α variations at each \mathcal{L}_δ	107
Figure 5.1: variation of the correlation coefficients (a) ϱ_{11} , (b) ϱ_{22} , and (c) ϱ_{33} versus $\alpha \in (0, 1)$ for $\mathcal{L}_\delta = 4, 8, 12$ by setting $\lambda \simeq 0$ in (5.41). The maximum values lie in the dashed boxes.	129

Figure 5.2: (a) Comparing results of the normalized two-point stress-strain rate correlation functions (S_Δ) and (b) error analysis of the longitudinal dissipation spectrum (\mathcal{E}_H) for fractional SGS and Smagorinsky models, where $\mathcal{L}_\delta = 8$ and ξ represents the radius of Fourier wave numbers. In both plots, the arrows point to the dissipation range.	130
Figure 5.3: Comparing results of the normalized two-point stress-strain rate correlation functions for (a) $\mathcal{L}_\delta = 4$ and (b) $\mathcal{L}_\delta = 12$. The inset plots illustrate the scaled error of longitudinal dissipation spectrum (\mathcal{E}_H) versus the radius of Fourier wave numbers (ξ). The arrows point to the dissipation range.	131
Figure 5.4: Two-point velocity-stress correlation function in a stationary HIT flow for $\mathcal{L}_\delta = 8$ using box filtering. The segment of balance region (BR) has been thickened up in (a) for all the graphs. The dissipation and the inertial ranges have been enlarged in plots (b) with semi-logarithmic scale on the x-axis and (c) with logarithmic scale on the both axes.	133
Figure 5.5: Two-point velocity-stress correlation function in a stationary HIT flow for (a) $\mathcal{L}_\delta = 4$ and (b) $\mathcal{L}_\delta = 12$ using box filtering. The inertial range has been enlarged in the inset plots with logarithmic scale on the both axes.	133
Figure 5.6: Scatter plots of the SGS stresses obtained by the filtered DNS data ($T_{33}^{R,D}$) versus the modeled stresses ($T_{33}^{R,TF}$) using optimized parameters in Table 5.3 for (a) $\mathcal{L}_\delta = 4$, (b) $\mathcal{L}_\delta = 8$, and (c) $\mathcal{L}_\delta = 12$	135
Figure 5.7: PDF of the ensemble-averaged $(\nabla \cdot \mathbf{T})_{i=3}$ for the optimized (tempered) fractional and the SMG models at (a) $\mathcal{L}_\delta = 4$, (b) $\mathcal{L}_\delta = 8$, and (c) $\mathcal{L}_\delta = 12$	135
Figure 5.8: PDF of the ensemble-averaged SGS dissipation for the optimized (tempered) fractional and the SMG models at (a) $\mathcal{L}_\delta = 4$, (b) $\mathcal{L}_\delta = 8$, and (c) $\mathcal{L}_\delta = 12$	136
Figure 5.9: Decaying of the resolved turbulent kinetic energy, \bar{K}_{tot} , for the optimized TFSGS and the SMG models with (a) 40^3 and (b) 20^3 grid points.	137
Figure 5.10: Time-evolution of the resolved enstrophy, $\bar{\mathcal{E}}$, for the optimized TFSGS and the SMG models with (a) 40^3 and (b) 20^3 grid points.	137

LIST OF ALGORITHMS

Algorithm 5.1: Estimation of the optimal parameters for a specific \mathcal{L} 126

CHAPTER 1

INTRODUCTION

1.1 Anomalous Transport

Anomalous transport represents a proper kinetic description of dynamical systems with much more complex behavior than the standard diffusion. In classical physics, standard diffusion equation governs the probability distribution function (PDF) of the underlying Brownian motion, in which $\overline{(\Delta r)^2} \sim t$, where Δr denotes the displacement of the scalar particle in a given time, t , and $\overline{(\cdot)}$ denotes ensemble averaging. In contrast, for describing anomalous diffusion a large variety of stochastic processes have been proposed over the last decade, in which the characteristics grow non-linearly in time, i.e., $\overline{(\Delta r)^2} \sim t^\gamma$. If $\gamma < 1$, the phenomenon undergoes sub-diffusion and if $\gamma > 1$, it is called super-diffusion. Modern non-intrusive experimental techniques disclosed significance of anomalous dynamics in a disparate range of dynamical systems such as turbulence [8, 1, 9, 10], porous media [11, 12, 13, 14, 15, 16], geoscience [17], bioscience [18, 19, 20], and viscoelastic material [21, 22, 23, 24]. Some of the important evidences are discussed as follows.

Biology: By analyzing the trajectories of wild-type and mutated epithelial (transformed Madin-Darby canine kidney) cells, Dieterich et al. [3] presented the anomalous characteristics of cell migration in an experimental study. In figure 1.1, they depicted the contours and the path of a migrating MDCK-F NHE cell monitored for 480 minutes. At first sight, the underlying stochastic process of particles by a mean squared displacement, which is proportional to t^2 at short times corresponding to ballistic motion and t for long time intervals designating normal diffusion. More recently, Sentjabrskaja et al. [4] investigated anomalous dynamics such as proteins moving through cells in a colloidal model system, in which dilute small spheres move in a glassy matrix of large spheres. As illustrated in figure 1.2, they monitored the evolution of the position of small particles and reported the anomalous behavior of small spheres, which is strongly connected to slow dynamics of the matrix of large particles.

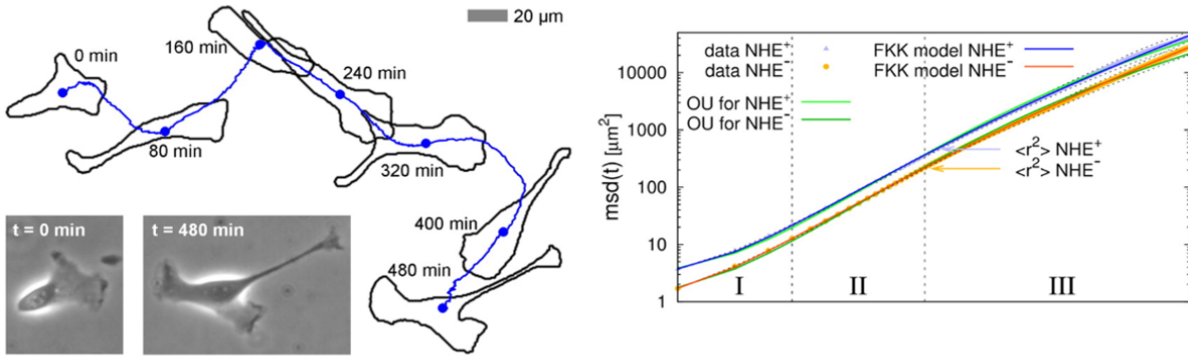


Figure 1.1: [3] Overlay of a migrating MDCK-F NHE cell with its path covered within 480 minutes. The cell frequently changes its shape and direction during migration. Double-logarithmic plot of the mean squared displacement as a function of time. Experimental data points for both cell types are symbolized by triangles and circles.

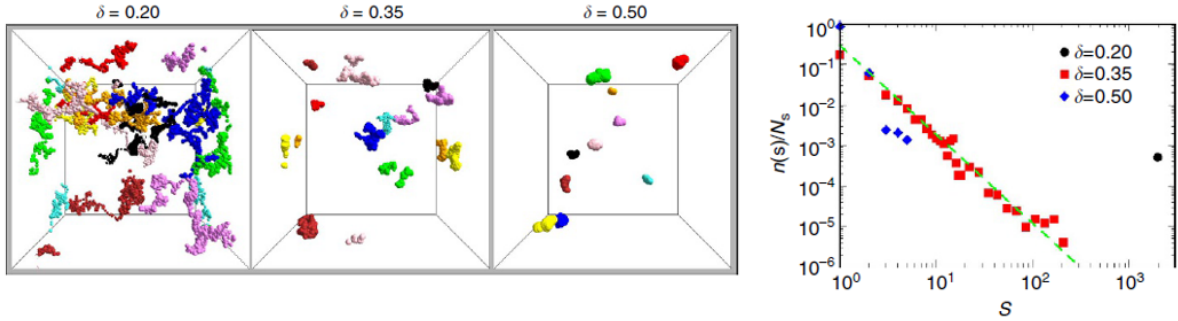


Figure 1.2: [4] Positions of 10 small particles (distinguished by different colors) (left) $\delta = 0.2$, (middle) $\delta = 0.35$, and (right) $\delta = 0.5$, for a fixed total time. Note that δ denotes the size ratio of small and large particles. The distribution, $n(s)$, of the size, s , of clusters follow a power-law dependence, $n(s) \sim s^{-2.19}$.

Human transportation: Brockmann [5] presented the super-diffusive statistics of human travel by analyzing the geographical circulation of individual bank notes. In figure 1.3, they illustrated qualitative features of bank notes which is described by a power-law distribution. For more information the reader is referred to [25].

Heterogeneous porous media: Many laboratory experiments confirmed the existence of non-Gaussian processes, which govern the PDF of particle dispersion in porous media. Recently, Anna et al. [6] conducted an experimental study on the intermittent structures of fluid velocities and its relation to the anomalous dispersion of solute particles. In figure 1.4, they plotted the super-

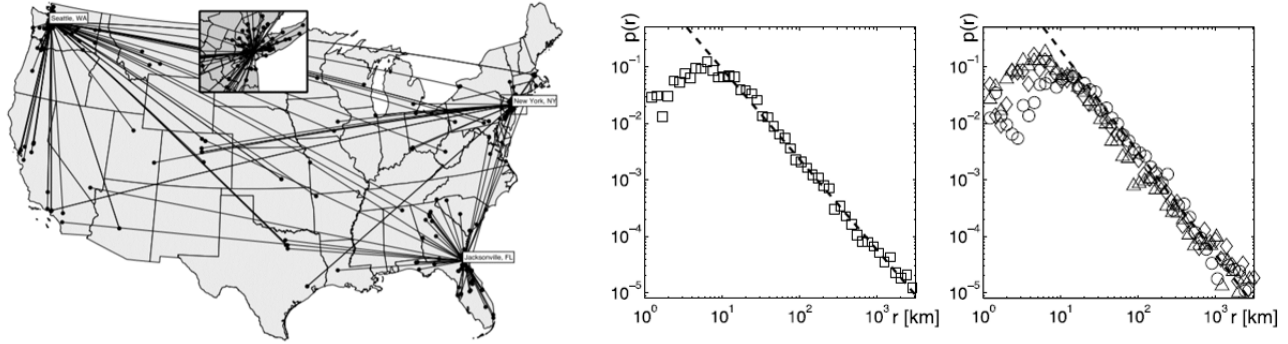


Figure 1.3: [5] (left) Dispersal of bank notes on geographical scales originating from three different places. (middle) In the quantitative analysis of bank note dispersal, the measured probability density function, $p(r)$, of traversing a distance, r , in 4 days undergoes a power-law $p(r) \sim r^{-1.59}$. (right) $p(r)$ for three classes of initial entry locations (black triangles for metropolitan areas, diamonds for cities of intermediate size, and circles for small towns).

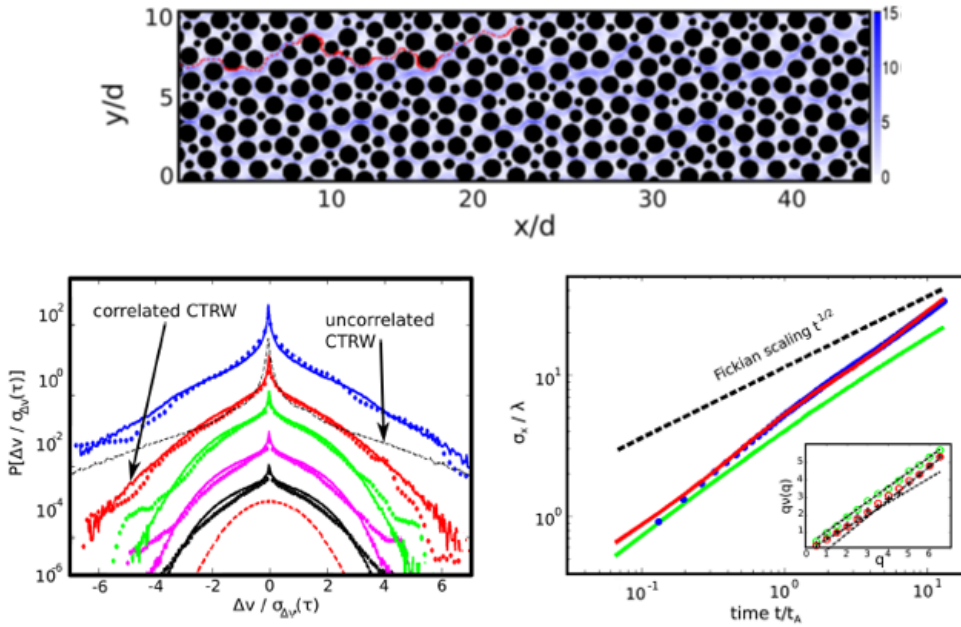


Figure 1.4: [6] The trajectories of Lagrangian particles in a heterogeneous porous media; (left) probability distributions of normalized Lagrangian longitudinal velocity increments, $\frac{\Delta V}{\sigma_{\Delta V}(\tau)}$ for the different time lags, (right) colored normalized mean squared displacement of purely advected particles, $\sigma_x = \langle \Delta x^2 \rangle$, versus normalized time.

diffusive transport of the particles. Moreover, Yang and Wang [26] conducted a numerical study on the anomalous transport of solute particles using lattice Boltzmann method at high Peclet numbers. Supported by their results and other experimental findings in [27, 28], anomalous transport is

indeed ubiquitous in porous media.

Turbulence: One hallmark of fully-developed turbulent flows is the emergence of non-Gaussian statistics in the velocity field using Gaussian initial conditions. Wilczek et al. [29] discussed some aspects of the relation between non-Gaussianity, coherent structures and phase correlations in turbulence. The connection between intermittent behavior and the presence of organized structures, embedded within turbulent background, have been discussed numerically and experimentally over the past decade (see e.g., [30, 31, 32]). Camussi and Verzicco [33] elaborated on the relation between anomalies and coherent structures. Rosales and Meneveau [34] proposed the multiscale minimal Lagrangian map (MMLM) approach to generate synthetic turbulent vector fields. They used the MMLM method in [35] to focus mainly on the intermittency and scaling properties of the synthetic velocity field in the inertial range. In this study, they presented an analysis of multifractal characteristics of energy dissipation for the description of strongly intermittent structures. Moreover, by measuring scalar intermittent moments of high orders, Iyer et al. [7] provided unequivocal evidence on the scalar intermittency and multifractal statistical process. In figure 1.5, they illustrated the generic existence of scalar cliffs. Such ramp-cliff structures suggested that the local spatial barriers to scalar mixing have a significant impact on scalar intermittency. Moreover, Shraiman and Siggia [8] reviewed recent progresses in the statistical description of passive scalar turbulence, centered on the anomalous scaling properties and the appearance of coherent structures in the scalar field. For more information on anomalous dynamics of turbulent flows, the reader is referred to [31, 36].

More concretely, anomalous phenomena undergo a large variety of stochastic processes than a simple power-law, which describe the continuous time random walk (CTRW) of particles at the kinetic level. We summarized some of the processes in Table 1.1.

1.2 Fractional Calculus

Fractional calculus seamlessly generalizes the notion of standard integer-order calculus to its fractional-order counterpart, leading to a broader class of mathematical models, namely fractional

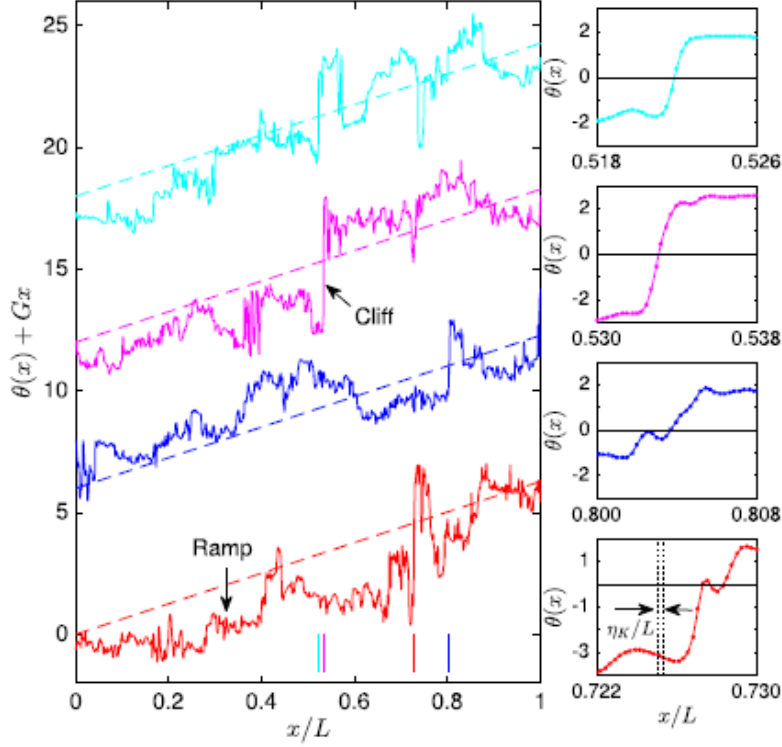


Figure 1.5: [7] Ramp-cliff structures in a scalar field at $Re_\lambda = 650$ and $Sc = 1$. The vertical colored solid line show the spatial positions for the magnifications of the scalar fluctuation profiles, plotted in the right.

Table 1.1: Variety of the underlying anomalous stochastic processes [1].

Stochastic Process	Correlation Function	Application
Normal Diffusion	$\langle \Delta X^2 \rangle \sim t^2$	Homogeneous media
Sub-Diffusion	$\langle \Delta X^2 \rangle \sim t^\beta, \quad 0 < \beta < 1$	Particle-laden flows, Biological media & Porous media
Super-Diffusion (ballistic motion)	$\langle \Delta X^2 \rangle \sim t^{2/\alpha}, \quad 0 < \alpha \leq 2 \ (\alpha=2)$	Plasma turbulence & Chaotic motion in a turbulent flow
Super slow Sub-Diffusion	$\langle \Delta X^2 \rangle \sim \ln^\nu t$	Sinai diffusion ($\nu = 4$)
Tempered Super-Diffusion (Truncated Lévy Process)	$\langle \Delta X^2 \rangle \sim t^{2/\alpha} e^{(-\lambda t)} \quad 0 < \lambda$	Scalar dispersion in shear flows, Plasma & Scalar dispersion in bounded flows

ordinary differential equations (FODEs) and fractional partial differential equations (FPDEs) [37, 38, 39, 40, 41]. Despite the considerable progresses in developing nonlocal models using standard methods for anomalous phenomena, fractional calculus appears to be a mathematical tractable

tool, which deals with integro-differential equations with mainly singular kernels of power law or logarithm type. As alternative approaches in the recent decades, the fractional derivatives have been found helpful and effective in modeling anomalous diffusion processes due to their inherent potentials in describing nonlocal interactions, self-similar structures, sharp peaks, and memory effects (see e.g., [42, 43]). In the following, we provide a brief review of fractional models in variety of applications.

Fractional Rheology: Regarding the mathematical modeling of irreversible mechanical processes, fractional calculus is used as a robust tool to provide more precise constitutive models. Suzuki et al. [22] proposed two fractional-order models for unaxial large strains, which interpolates between the standard elasto-plastic and visco-elasto-plastic models. In this respect, we refer to these papers: [44] where a 3D non-local in the stress state model was defined; [45] where a new constitutive equation was proposed based on a time–space fractional derivative to characterize the visco-elasto-plastic behavior of metals and alloys. For more details, we refer the reader to [46].

Biology: Complex dynamic processes of biological tissues can be represented by fractional-order formulations, which incorporates the memory effects. Goran et al. [47] presented a modified single-dispersion cole model for more accurate description of bioimpedance properties of human skin. Recently, Baleanue et al. [48] presented a new fractional model for a tumor-immune surveillance mechanism. This model formulates the interactions between various tumor cell populations and immune response by a system of FODEs. More information is provided in [49] and the references therein.

Porous Media: In the standard advection-dispersion equations, solute transport in ground water has been modeled traditionally based on the underlying Fickian process (equivalently a process of Brownian motion). Supported by the experimental evidence (see e.g., [50]), solute particles do not follow a Fickian process particularly in heterogeneous porous media. Accordingly, standard approaches are found to be inherently insufficient to reproduce long-range interactions and memory effects. Regarding that, FPDE approaches have been introduced widely to provide more adequate and accurate models, i.e., fractional advection-dispersion equations, for transport of solute particles

[51]. Suzuki et al. [52] developed a fractional heat transfer equation to describe anomalous diffusion in a fractured reservoir. Sapora et al. [53] investigated the diffusion processes on finite porous domains using fractional finite difference methods. More details on this topic can be found in [54].

1.2.1 Preliminaries on Fractional Calculus

Here, we obtain some basic definitions from fractional calculus [38, 55]. Denoted by ${}_a\mathcal{D}_x^\sigma g(x)$, the left-sided Reimann-Liouville fractional derivative of order ν in which $g(x) \in C^n[a, b]$ and $n = \lceil \sigma \rceil$, is defined as:

$${}_{RL}^L {}_a\mathcal{D}_x^\sigma g(x) = \frac{1}{\Gamma(n-\sigma)} \frac{d^n}{dx^n} \int_a^x \frac{g(s)}{(x-s)^{\sigma+1-n}} ds, \quad x \in [a, b], \quad (1.1)$$

where Γ represents the Euler gamma function. The corresponding right-sided Reimann-Liouville fractional derivative of order ν , ${}_x\mathcal{D}_b^\sigma g(x)$, is given by

$${}_{RL}^R {}_x\mathcal{D}_b^\sigma g(x) = \frac{1}{\Gamma(n-\sigma)} (-1)^n \frac{d^n}{dx^n} \int_x^b \frac{g(s)}{(s-x)^{\sigma+1-n}} ds, \quad x \in [a, b]. \quad (1.2)$$

In (1.1) and (1.2), as $\sigma \rightarrow n$, the fractional derivatives tend to the standard n -th order derivative with respect to x . We recall from [56, 57] that the following link between the Reimann-Liouville and Caputo fractional derivatives, where

$${}_{RL}^L {}_a\mathcal{D}_x^\sigma f(x) = \frac{f(a)}{\Gamma(1-\sigma)(x-a)^\sigma} + {}_a^C\mathcal{D}_x^\sigma f(x) \quad (1.3)$$

$${}_{RL}^R {}_x\mathcal{D}_b^\sigma f(x) = \frac{f(b)}{\Gamma(1-\sigma)(b-x)^\sigma} + {}_x^C\mathcal{D}_b^\sigma f(x), \quad (1.4)$$

when $\lceil \sigma \rceil = 1$. Generally

$${}_a^C\mathcal{D}_x^\sigma f(x) = \frac{1}{\Gamma(n-\sigma)} \int_a^x \frac{g^{(n)}(s)}{(x-s)^{\sigma+1-n}} ds, \quad x \in [a, b], \quad (1.5)$$

$${}_x^C\mathcal{D}_b^\sigma f(x) = \frac{(-1)^n}{\Gamma(n-\sigma)} \int_x^b \frac{g^{(n)}(s)}{(s-x)^{\sigma+1-n}} ds, \quad x \in [a, b], \quad (1.6)$$

where $\lceil \sigma \rceil = n$. In (1.3) and (1.4), ${}_{RL}^L {}_a\mathcal{D}_x^\sigma g(x) = {}_a^C\mathcal{D}_x^\sigma g(x) = {}_a\mathcal{D}_x^\sigma g(x)$ when homogeneous Dirichlet initial and boundary conditions are enforced.

1.2.2 Fractional Modeling

The advantage of fractional model lies in the straightforward way of modeling the underlying heavy-tailed, self-similar, and non-Markovian processes for anomalous phenomena. With increasing number of fractional models in diverse applications, the development of robust mathematical theories and efficient computational methods has become urgent for approximating the solutions of FPDEs. History-dependent and nonlocal characteristics of fractional operators impose further numerical complexities, ranging from theoretical analysis to large memory requirement.

On the theoretical side, the notion of well-posedness analysis is very significant to ensure the existence and uniqueness of the solution to FPDEs. In particular, well-posedness analysis plays even a more crucial role when the proper boundary conditions of fractional equations are under doubt. Additionally, several mathematical rules such as the integration by parts formula cannot be applied in the standard way for fractional operators. In the context of numerical analysis, the computational costs of the numerical solutions for FPDEs are heavier than the classical PDEs due to the complicated forms of fractional operators, involving power-law to logarithmic kernels of convolution type. Moreover, the huge memory requirement of FPDEs/FODEs is computationally demanding especially for the temporal fractional problems.

Over the past decade, fractional calculus has gained considerable attention from the engineering and computational science communities to address some key challenges and approximate solutions of fractional equations more precisely and faster. It also inspired the engineering communities to allow the real world scientific applications come true by using fractional approaches. However, according to the computational challenges and complex formulations of fractional models, further theoretical and numerical studies are required to establish a robust framework for developing accurate and efficient models for anomalous transport.

In order to build a framework for developing fractional models, there are some essential elements, which are listed as follows.

- **Stochastic formulation:** From the point of view of CTRW, motion of particles are modeled

by a proper random walk at the kinetic level for a precise and comprehensive understanding of the anomalous system. Such stochastic interpretations can give rise to fractional differential equations such as FPDEs, where the associated fractional exponents are connected with the anomalous features.

- **Theoretical analysis:** In dealing with FPDEs, the well-posedness analysis plays a crucial role in studying the existence and uniqueness of the underlying solutions and preventing any instability in the numerical method. The primary step in performing such analysis is to construct solution spaces, equipped with the proper equivalent norms.
- **Numerical methods:** Developing reliable numerical schemes for approximating the solution of FPDEs requires a great deal of attention especially in treating fractional operators. It is of great importance and necessity to propose efficient computational methods, which can resolve the singularity in a fractional equation accurately.
- **Optimization:** In order to introduce a mathematical representation of anomalous structures and improve the accuracy of fractional models in statistical features, it is markedly essential to construct a mapping function from the underlying physical properties of anomalous phenomena to the model parameters through using proper optimization algorithms. The key idea is to use higher-order nonlocal statistical properties to offer a better representation of anomalous dynamics.

1.3 Outline of the Present Work

The overall goal of this research is to develop fractional models in a robust framework, incorporating the aforementioned key elements. In this study, we employ some useful mathematical and computational tools to extend the framework to more applied areas of research such as solute transport in underground water and turbulent flows. The proposed framework for developing fractional models are illustrated in figure 1.6. The dissertation is divided to six chapters, which a short summary of each is presented in the following.

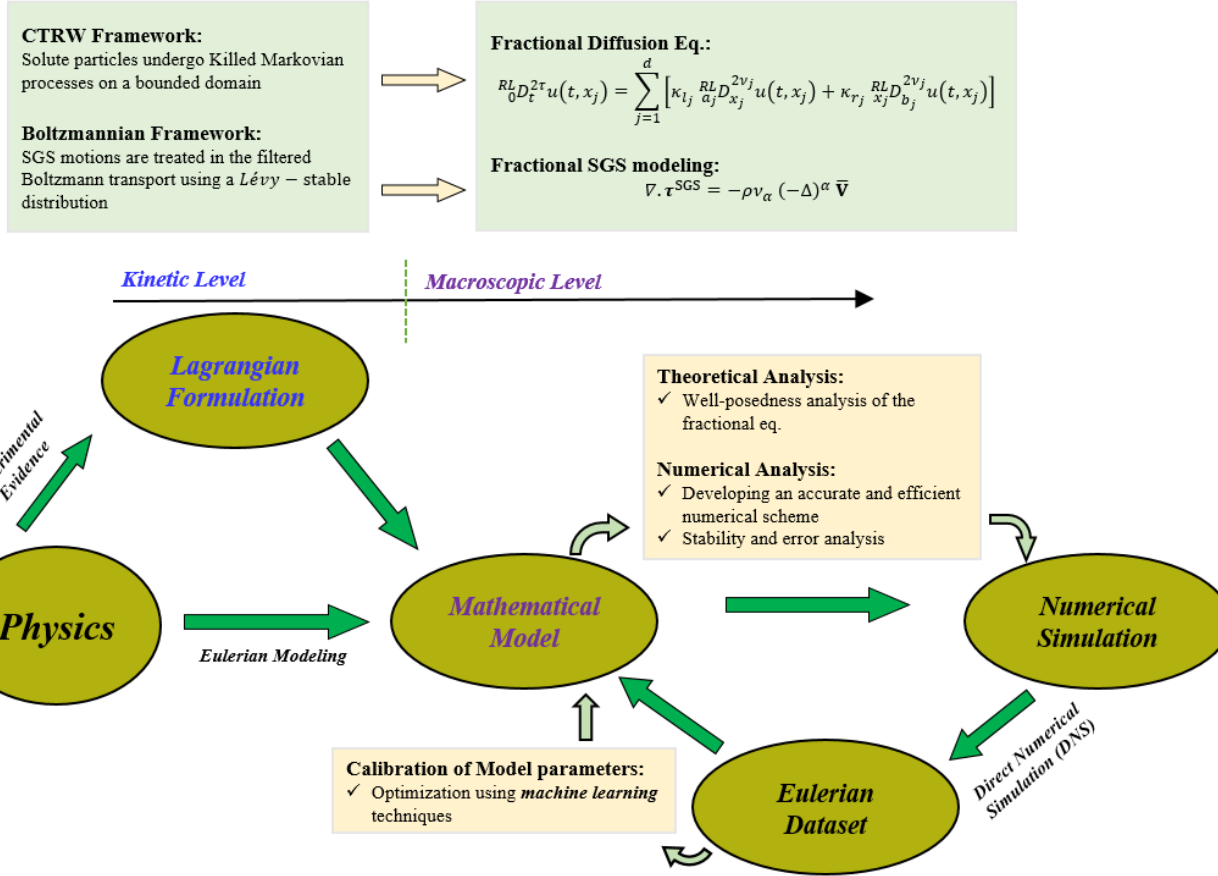


Figure 1.6: Schematic framework of the thesis with main focus on developing fractional models for anomalous transport, e.g., solute particle transport in underground waters and SGS motions in turbulent flows. The proposed framework is established based on the key elements, listed as: mathematical formulation of the fractional model starting at the kinetic level, theoretical analysis, developing numerical schemes for the proposed FPDE approaches, and optimizing performance of the model.

Chapter 2:

Supported by the macroscopic experiments at the Columbus Air Force Base in Mississippi in [58], dispersion of particles in a highly heterogeneous aquifer undergoes time-changed Le y processes rather than Brownian motion. Within the framework of CTRW, Baeumer et al. in [59] established the stochastic interpretation for the FPDEs on a bounded domain in terms of time-changed Markov processes by an inverse stable subordinator whose index equals the order of the fractional temporal derivative. Inspired by that, we consider a class of FPDEs with two-sided

derivatives and constant coefficients of the form

$${}_0\mathcal{D}_t^{2\tau} u + \sum_{i=1}^d [c_{l_i} a_i \mathcal{D}_{x_i}^{2\mu_i} u + c_{r_i} x_i \mathcal{D}_{b_i}^{2\mu_i} u] = \sum_{j=1}^d [\kappa_{l_j} a_j \mathcal{D}_{x_j}^{2\nu_j} u + \kappa_{r_j} x_j \mathcal{D}_{b_j}^{2\nu_j} u] - \gamma u + f$$

in a $(1+d)$ -dimensional *space-time* hypercube, where $2\mu_i, \in (0, 1)$, $2\nu_i, \in (1, 2)$, and $2\tau, \in (0, 2)$, $2\tau \neq 1$, subject to Dirichlet initial and boundary conditions, where $i = 1, 2, \dots, d$.

In this chapter, we make several key contributions to the field of fractional calculus by developing a unified PG spectral method for the FPDEs and performing the corresponding numerical analysis (see [60, 61]). These contributions are mainly listed as follows.

- We develop a unified PG spectral method for the FPDEs employing the Legendre polynomials as the spatial basis/test functions and the eigenfunctions of the fractional Sturm-Liouville eigen-problems of the first/second kinds in [56], called Jacobi *poly-fractonomials*, as temporal basis/test functions, respectively.
- We construct the underlying solution/test spaces, associated with the equivalent norms induced by the corresponding weak form of (1.7). Subsequently, we perform the well-posedness analysis using the Babuška-Lax-Milgram theorem [62] to guarantee the existence and uniqueness of solutions of the bilinear form.
- We formulate a novel unified fast linear solver for the resulting high-dimensional linear system based on the solution of generalized eigen-problem of spatial mass matrices with respect to the corresponding stiffness matrices, hence, making the complexity of the problem optimal, i.e., $O(N^{d+2})$.
- We provide the stability analysis of the PG method for the finite-dimensional subspaces of solution/test spaces. Moreover, we perform the corresponding error analysis to find the spectral accuracy of the PG method.
- We carry out several numerical test cases using non-smooth exact solutions to examine the CPU time and compare the practical and theoretical convergence rate of the PG method.

Chapter 3: In many complex multi-fractal anomalous phenomena described by accelerating super-diffusion and decelerating sub-diffusion processes [63, 64, 65, 38, 66, 67, 68, 69], a single power-law scaling is not observed over the whole domain. A faithful description of such anomalous transport requires exploiting distributed-order derivatives, in which the underlying derivative orders are distributed over a range of values.

Let define the distributed-order derivative as

$${}^D \mathcal{D}_t^\phi f(t, x) := \int_{\tau_{\min}}^{\tau_{\max}} \phi(\tau) {}_0 \mathcal{D}_t^\tau f(t, x) d\tau, \quad (1.7)$$

where $\alpha \rightarrow \phi(\alpha)$ be a continuous mapping in $[\alpha^{\min}, \alpha^{\max}]$ [70] and $t > 0$. We note that by choosing the distribution function in the distributed-order derivatives to be the Dirac delta function $\delta(\tau - \tau_0)$, we recover a single (fixed) term fractional derivative, i.e.,

$$\int_{\tau_{\min}}^{\tau_{\max}} \delta(\tau - \tau_0) {}_0 \mathcal{D}_t^\tau f(t, x) d\tau = {}_0 \mathcal{D}_t^{\tau_0} f(t, x), \quad (1.8)$$

where $\tau_0 \in (\tau^{\min}, \tau^{\max})$. The main purpose of this chapter [71, 72] is to develop and analyze a Petrov-Galerkin (PG) spectral method to solve a $(1+d)$ -dimensional fully distributed-order FPDE with two-sided derivatives of the form

$$\begin{aligned} & \int_{\tau_{\min}}^{\tau_{\max}} \varphi(\tau) {}_0^C \mathcal{D}_t^{2\tau} u d\tau + \sum_{i=1}^d \int_{\mu_i^{\min}}^{\mu_i^{\max}} \varrho_i(\mu_i) [c_{l_i} {}_{a_i}^{RL} \mathcal{D}_{x_i}^{2\mu_i} u + c_{r_i} {}_{x_i}^{RL} \mathcal{D}_{b_i}^{2\mu_i} u] d\mu_i \\ &= \sum_{j=1}^d \int_{\nu_j^{\min}}^{\nu_j^{\max}} \rho_j(\nu_j) [\kappa_{l_j} {}_{a_j}^{RL} \mathcal{D}_{x_j}^{2\nu_j} u + \kappa_{r_j} {}_{x_j}^{RL} \mathcal{D}_{b_j}^{2\nu_j} u] d\nu_j - \gamma u + f, \end{aligned} \quad (1.9)$$

subject to homogeneous Dirichlet boundary conditions and initial condition, where $t \in [0, T]$, $x_j \in [a_j, b_j]$, $2\tau^{\min} < 2\tau^{\max} \in (0, 2]$, $2\tau^{\min} \neq 1$, $2\tau^{\max} \neq 1$, $2\mu_i^{\min} < 2\mu_i^{\max} \in (0, 1]$, and $2\nu_j^{\min} < 2\nu_j^{\max} \in (1, 2]$ for $i, j = 1, 2, \dots, d$. The coefficients c_{l_i} , c_{r_i} , κ_{l_i} , κ_{r_i} , and γ are considered to be constant. Besides, the distribution function $0 < \varphi(\tau) \in L^1([\tau^{\min}, \tau^{\max}])$, $0 < \varrho_i(\mu_i) \in L^1([\mu_i^{\min}, \mu_i^{\max}])$, and $0 < \rho_j(\nu_j) \in L^1([\nu_j^{\min}, \nu_j^{\max}])$. We carry out the following main contributions as listed here.

- We construct the underlying function spaces by extending the *distributed Sobolev* space in [70] to higher dimensions in time and space. These solution/test spaces are endowed with the equivalent norms, which are induced by the corresponding bilinear form of (1.9).

- We develop a unified PG spectral method, employing Legendre polynomials and Jacobi *poly-fractonomials* [56] as spatial and temporal basis/test functions, respectively. We also formulate a fast solver for the corresponding weak form of (1.9), which significantly reduces the computational expenses in high-dimensional problems.
- We prove the existence and uniqueness of the solutions to the weak form of (1.9) in the underlying solution/test spaces. Additionally, we performed the stability analysis of the PG method for the finite-dimensional subspaces of solution/test spaces.
- We perform the corresponding error analysis, where the *distributed Sobolev* spaces enable us to obtain accurate error estimate of the scheme.
- We carry out several numerical test cases using non-smooth exact solutions to examine the CPU time and compare the practical and theoretical convergence rate of the PG method.
- To examine the performance and convergence of the developed PG method, we also perform several numerical simulations using smooth and non-smooth test cases.

Chapter 4:

Supported by several numerical and empirical studies (see e.g., [31, 73, 74, 75, 76]), SGS motions are characterized by the intermittent structures and anomalous scaling properties in turbulent flows. Such anomalous features become even more pronounced when the filter-width enlarges. That inspires the development of new nonlocal closure models, which captures the anomalous scaling of the structure function exponents. In this chapter, we outline a new framework to the functional modeling of SGS stresses in large eddy simulation (LES) of turbulent flows, starting from the kinetic theory.

The Boltzmann transport equation [77, 78] is given by

$$\frac{\partial f}{\partial t} + \mathbf{u} \cdot \nabla f = \left(\frac{\partial f}{\partial t} \right)_{coll} \equiv -\frac{f - f^{eq}}{\tau}, \quad (1.10)$$

where $f^{eq} = f^{eq}(t, \mathbf{x}, \mathbf{u})$ represents the equilibrium distribution function and τ is the relaxation time. Assuming that the system of gaseous particles is in thermodynamic equilibrium, the equi-

librium distribution is given by a Maxwell (Gaussian) distribution function [79]. To proceed for the LES of a turbulent flow, we can decompose f to the filtered, \bar{f} , and the residual values, f' . The overbar represents the spatial isotropic filtering, i.e. $\bar{f} = G * f$, where G is the kernel of any generic spatial filtering. Then, we formulate the filtered Boltzmann transport according to

$$\frac{\partial \bar{f}}{\partial t} + \mathbf{u} \cdot \nabla \bar{f} = -\frac{\bar{f} - \overline{f^{eq}(\Delta)}}{\tau}, \quad (1.11)$$

where $\bar{\Delta} := \frac{|\mathbf{u} - \bar{\mathbf{V}}|^2}{U^2}$ and U and $\bar{\mathbf{V}}$ represent the agitation speed and the filtered velocity field, respectively.

Within the proposed framework, we treat the resource of turbulent small scale motions by modeling $\overline{f^{eq}(\Delta)} - f^{eq}(\bar{\Delta})$ with a Lévy-stable distribution. Subsequently, by ensemble-averaging (1.11), we derive the corresponding filtered Navier-Stokes equations, where the divergence of SGS stresses emerges as a single-parameter fractional Laplacian, $(-\Delta)^\alpha(\cdot)$, $\alpha \in (0, 1]$, of the filtered velocity field. The only model parameter, i.e., the fractional exponent, appears to be strictly depending on the filter-width and the flow Reynolds number.

Here, we briefly highlight the main contributions of this work as follows:

- We develop a new functional approach to model the SGS stresses by employing the fractional Laplacian of the filtered velocity within the Boltzmann transport framework. The fractional exponent in the model arises from the heavy-tailed behavior of the SGS stresses.
- We show that the model is frame invariant and constrain it to a set of conditions to preserve the second-law of thermodynamics.
- We perform the *a priori* studies to assess performance of the model primarily by the correlation and regression coefficients utilizing the results of direct numerical simulation (DNS) for three-dimensional forced and decaying homogeneous isotropic turbulence (HIT) problems. We also investigate statistical characteristics of the proposed model, as a hallmark of fractional operators, in a range of filter widths.

On the basis of the theoretical background and the *a priori* analyses provided in this study, the proposed framework show a remarkable potential for developing more sophisticated SGS models in LES of turbulent flows by leveraging proper mathematical tools in fractional calculus.

Chapter 5: Presence of nonlocal triad interactions and intermittent structures in homogeneous turbulence give a key role to multi-point statistical functions in formulating an ideal LES model [80, 81, 76]. Such nonlocality, caused by filtering pressure terms in the NS equations, leave urges for developing nonlocal and fractional LES models [82]. Within the fractional framework, introduced in chapter 4, we take a step forward in modeling the real physics of turbulent energy cascade by employing a tempered *Lévy*-stable distribution at the kinetic level. Subsequently, we derive the corresponding operator in terms of the tempered fractional Laplacian, $(\Delta + \lambda)^\alpha(\cdot)$, for $\alpha \in (0, 1)$ and $\lambda > 0$ at the filtered NS equations, where the model parameters depend on the filter width. The significance of this approach lies in:

- We treat the source of turbulent small-scale motions at the kinetic level, by employing a tempered heavy-tailed distribution in approximating $\overline{f^{eq}}$. This leads us to the tempered fractional operator in the filtered NS equations as a proper choice for modeling a power-law like behavior in the mid-range and a Gaussian tail in real-physics anomalous phenomena.
- The proposed TFSGS model sets the ground for fulfilling essential statistical conditions as a relatively best approximation of an ideal LES model through fractional and tempering parameters. To achieve an optimized edition of the TFSGS model, we devise an optimization strategy, which involves conventional one-point correlation coefficients, two-point structures, and the SGS dissipation.
- The optimized TFSGS model presents reasonably accurate predictions of two-point structure functions for a range of filter widths while maintaining the expected correlations between the modeled and true SGS stresses.

- The corresponding fractional LES solutions present a stable prediction of energy and enstrophy decays in the *a posteriori* analysis.

Chapter 6: The dissertation is concluded with the discussed findings and possible future works extended from the current investigation.

CHAPTER 2

A UNIFIED SPECTRAL METHOD FOR FPDES WITH TWO-SIDED DERIVATIVES

2.1 Background

Due to the history dependence and non-local character of fractional differential equations (FDEs), their discretization becomes computationally challenging. Numerical methods, developed to discretize FPDEs, can be categorized in two major classes: i) local methods, e.g., finite difference method (FDM), finite volume method (FVM), and finite element method (FEM), and ii) global methods, e.g., single and multi-domain spectral methods (SM).

Local schemes have been studied extensively in the literature. Lubich introduced the discretized fractional calculus within the spirit of FDM [83]. Sugimoto employed a FDM scheme for approximating fractional Burger's equation [84, 85]. Meerschaert and Tadjeran [86] developed finite difference approximations to solve one-dimensional advection-dispersion equations with variable coefficients on a finite domain. Tadjeran and Meerschaert [87] employed a practical alternating directions implicit (ADI) method to solve a class of fractional partial differential equations with variable coefficients in bounded domain. Hejazi et al. [88] developed a finite-volume method utilizing fractionally shifted grunwald formula for the fractional derivatives for space-fractional advection-dispersion equation on a finite domain. To solve the two-dimensional two-sided space-fractional convection diffusion equation, Chen and Deng [89] proposed a practical alternating directions implicit method. Zeng et al. [90] constructed a finite element method and a multistep method for unconditionally stable time-integration of sub-diffusion problem. In addition, Zhao et al. developed second-order FDM for the variable-order FPDEs in [91]. Li et al. [92] proposed an implicit finite difference scheme for solving the generalized time-fractional Burger's equation. Recently, Feng et al. [93] proposed a second-order Crank-Nicolson scheme to approximate the Riesz space-fractional advection-dispersion equations (FADE). Recently, Zayernouri and Matzavinos [94] have developed an explicit fractional adams/Bashforth/Moulton and implicit fractional

Adams-Moulton finite difference methods, applicable to high-order time-integration of nonlinear FPDEs and amenable for formulating implicit/explicit (IMEX) splitting methods.

Regarding global methods, Sugimoto [84, 85] used Fourier SM in a fractional Burger's equation. Shen and Wang [95] constructed a set of Fourier-like basis functions for Legendre-Galerkin method for non-periodic boundary value problems and proposed a new space-time spectral method. Sweilam et al. [96] considered Chebyshev Pseudo-spectral method for solving one-dimensional FADE, where the fractional derivative is described in Caputo sense. Chen et al. [97] developed an approach for high-order time integration within multi-domain setting for time-fractional diffusion equations. Mokhtary developed a fully discrete Galerkin method to numerically approximate initial value fractional integro-differential equations [98]. More recent works in this area can be found in [99, 100].

Moreover, Zayernouri and Karniadakis [56, 101] introduced a new family of basis/test functions, called (tempered)Jacobi *poly-fractonomials*, known as the explicit eigenfunctions of (tempered) fractional Strum-Liouville problems in bounded domains of the first and second kind. Following this new spectral theory, they have developed a number of single- and multi-domain spectral methods [102, 103, 55]. Recently, Zaho et al. [104] developed a spectral method for the tempered fractional diffusion equations (TFDEs) using the generalized Jacobian functio [105]. Mao and Shen [106] developed Galerkin spectral methods for solving multi-dimensional fractional elliptic equations with variable coefficients.

The main contribution of the present work is to construct a unified Petrov-Galerkin spectral method and a unified fast solver for the weak form of linear FPDEs with constant coefficients in (1+d) dimensional *space-time* hypercube of the form

$${}_0\mathcal{D}_t^{2\tau} u + \sum_{i=1}^d [c_{l_i} {}_a\mathcal{D}_{x_i}^{2\mu_i} u + c_{r_i} {}_x\mathcal{D}_{b_i}^{2\mu_i} u] = \sum_{j=1}^d [\kappa_{l_j} {}_a\mathcal{D}_{x_j}^{2\nu_j} u + \kappa_{r_j} {}_x\mathcal{D}_{b_j}^{2\nu_j} u] - \gamma u + f, \quad (2.1)$$

where $2\mu_i, \in (0, 1)$, $2\nu_i, \in (1, 2)$, and $2\tau, \in (0, 2)$, $2\tau \neq 1$, subject to Dirichlet initial and boundary conditions, where $i = 1, 2, \dots, d$. Compared to the problem considered in [45], we

extend the one-sided spatial derivatives to two-sided ones, also, we include an advection term in order to consider the drift effects. Employing different (Legendre polynomial) spatial basis/test functions and the additional advection term then would not allow employing the fast linear solver developed in [45]. Accordingly, we formulate a new fast linear solver for advection-dispersion problems. We additionally aim to perform the well-posedness and stability analysis in any (1+d) dimensions in [2], while in [45], only the stability of 1-D problem has been carried out. Furthermore, we briefly presented the stochastic interpretation of FADE on bounded domain which sheds light on the well-posedness of the problem from the perspective of the probability theory.

The outline of this chapter is as follows: in section 2.2, we introduce some definitions from fractional calculus. In section 2.3, we present the strong form definition of the problem. In section 2.4, we construct the solution/test spaces and develop the PG method. Next, We prove the well-posedness of the weak form and perform the stability analysis in section 2.5. In section 2.6 to 2.8, we develop a unified fast linear solver and obtain the closed-form solution in terms of the generalized eigenvalues and eigenvectors of the corresponding mass and stiffness matrices. In section 2.11, the performance of the PG method is examined via several numerical simulations for low-to-high dimensional problems with smooth and non-smooth solutions.

2.2 Preliminaries on Fractional Calculus

Here, we obtain some basic definitions from fractional calculus [38, 55]. Denoted by ${}_a\mathcal{D}_x^\sigma g(x)$, the left-sided Reimann-Liouville fractional derivative of order ν in which $g(x) \in C^n[a, b]$ and $n = \lceil \sigma \rceil$, is defined as:

$${}_{RL}^L \mathcal{D}_x^\sigma g(x) = \frac{1}{\Gamma(n - \sigma)} \frac{d^n}{dx^n} \int_a^x \frac{g(s)}{(x - s)^{\sigma+1-n}} ds, \quad x \in [a, b], \quad (2.2)$$

where Γ represents the Euler gamma function. The corresponding right-sided Reimann-Liouville fractional derivative of order ν , ${}_x\mathcal{D}_b^\sigma g(x)$, is given by

$${}_{RL}^R \mathcal{D}_b^\sigma g(x) = \frac{1}{\Gamma(n - \sigma)} (-1)^n \frac{d^n}{dx^n} \int_x^b \frac{g(s)}{(s - x)^{\sigma+1-n}} ds, \quad x \in [a, b]. \quad (2.3)$$

In (2.2) and (2.3), as $\sigma \rightarrow n$, the fractional derivatives tend to the standard n -th order derivative with respect to x . We recall from [56, 57] that the following link between the Reimann-Liouville and Caputo fractional derivatives, where

$${}_{a}^{Rl}\mathcal{D}_x^{\sigma}f(x) = \frac{f(a)}{\Gamma(1-\sigma)(x-a)^{\sigma}} + {}_a^C\mathcal{D}_x^{\sigma}f(x) \quad (2.4)$$

$${}_{x}^{Rl}\mathcal{D}_b^{\sigma}f(x) = \frac{f(b)}{\Gamma(1-\sigma)(b-x)^{\sigma}} + {}_x^C\mathcal{D}_b^{\sigma}f(x), \quad (2.5)$$

when $\lceil \sigma \rceil = 1$. Generally

$${}_a^C\mathcal{D}_x^{\sigma}f(x) = \frac{1}{\Gamma(n-\sigma)} \int_a^x \frac{g^{(n)}(s)}{(x-s)^{\sigma+1-n}} ds, \quad x \in [a, b], \quad (2.6)$$

$${}_x^C\mathcal{D}_b^{\sigma}f(x) = \frac{(-1)^n}{\Gamma(n-\sigma)} \int_x^b \frac{g^{(n)}(s)}{(s-x)^{\sigma+1-n}} ds, \quad x \in [a, b], \quad (2.7)$$

where $\lceil \sigma \rceil = n$. In (2.4) and (2.5), ${}_{-1}^{RL}\mathcal{I}_x^{\sigma}g(x) = {}_a^C\mathcal{D}_x^{\sigma}g(x) = {}_a\mathcal{D}_x^{\sigma}g(x)$ when homogeneous Dirichlet initial and boundary conditions are enforced.

To analytically obtain the fractional differentiation of our basis function, we employ the following relations [56] as:

$${}_{-1}^{RL}\mathcal{I}_x^{\sigma}\{(1+x)^{\beta}P_n^{\alpha,\beta}(x)\} = \frac{\Gamma(n+\beta+1)}{\Gamma(n+\beta+\sigma+1)} (1+x)^{\beta+\sigma} P_n^{\alpha-\sigma,\beta+\sigma}(x), \quad (2.8)$$

and

$${}_{x}^{RL}\mathcal{I}_1^{\sigma}\{(1-x)^{\alpha}P_n^{\alpha,\beta}(x)\} = \frac{\Gamma(n+\alpha+1)}{\Gamma(n+\alpha+\sigma+1)} (1-x)^{\alpha+\sigma} P_n^{\alpha+\sigma,\beta-\sigma}(x), \quad (2.9)$$

where $0 < \sigma < 1$, $\alpha > -1$, $\beta > -1$ and $P_n^{\alpha,\beta}(x)$ denotes the standard Jacobi Polynomials of order n and parameters α and β . It is worth mentioning that

$${}_{a}^{RL}\mathcal{I}_x^{\sigma}\{f(x)\} = \frac{1}{\Gamma(\sigma)} \int_a^x \frac{f(s)}{(x-s)^{1-\sigma}} ds, \quad x \in [a, b],$$

and

$${}_{x}^{RL}\mathcal{I}_b^{\sigma}\{f(x)\} = \frac{1}{\Gamma(\sigma)} \int_x^b \frac{f(s)}{(s-x)^{1-\sigma}} ds, \quad x \in [a, b].$$

By substituting $\alpha = \sigma$ and $\beta = -\sigma$, we can simplify equations (2.8) and (2.9), thereby we have:

$${}_{-1}^{RL}\mathcal{I}_x^{\sigma}\{(1+x)^{-\sigma}P_n^{\sigma,-\sigma}(x)\} = \frac{\Gamma(n-\sigma+1)}{\Gamma(n+1)} P_n(x), \quad x \in [-1, 1] \quad (2.10)$$

and

$${}^{RL}_x \mathcal{I}_1^\sigma \{(1-x)^{-\sigma} P_n^{-\sigma, \sigma}(x)\} = \frac{\Gamma(n-\sigma+1)}{\Gamma(n+1)} P_n(x), \quad x \in [-1, 1]. \quad (2.11)$$

Accordingly, we have the fractional derivative of Legendre polynomial by differentiating (2.10) and (2.11) as

$${}_1 \mathcal{D}_x^\sigma P_n(x) = \frac{\Gamma(n+1)}{\Gamma(n-\sigma+1)} P_n^{\sigma, -\sigma}(x) (1+x)^{-\sigma} \quad (2.12)$$

and

$${}_x \mathcal{D}_1^\sigma P_n(x) = \frac{\Gamma(n+1)}{\Gamma(n-\sigma+1)} P_n^{-\sigma, \sigma}(x) (1-x)^{-\sigma}, \quad (2.13)$$

where $P_n(x) = P_n^{0,0}(x)$ represents Legendre polynomial of degree n.

2.3 Problem Definition

Let $u : \mathbb{R}^{d+1} \rightarrow \mathbb{R}$ for some positive integer d and $\Omega = [0, T] \times [a_1, b_1] \times [a_2, b_2] \times \cdots \times [a_d, b_d]$,

where

$$\begin{aligned} {}_0 \mathcal{D}_t^{2\tau} u &+ \sum_{i=1}^d [c_{l_i} a_i \mathcal{D}_{x_i}^{2\mu_i} u + c_{r_i} x_i \mathcal{D}_{b_i}^{2\mu_i} u] \\ &- \sum_{j=1}^d [\kappa_{l_j} a_j \mathcal{D}_{x_j}^{2\nu_j} u + \kappa_{r_j} x_j \mathcal{D}_{b_j}^{2\nu_j} u] + \gamma u = f, \end{aligned} \quad (2.14)$$

and $\gamma, c_{l_i}, c_{r_i}, \kappa_{l_j}$, and κ_{r_j} are all constant. Besides, $2\mu_i \in (0, 1)$, $2\nu_j \in (1, 2)$, and $2\tau \in (0, 2)$, $2\tau \neq 1$, for $j = 1, 2, \dots, d$. This equation is subject to the following Dirichlet initial and boundary conditions as:

$$\begin{aligned} u|_{t=0} &= 0, \quad \tau \in (0, 1/2), \\ u|_{t=0} &= \frac{\partial u}{\partial t}|_{t=0} = 0, \quad \tau \in (1/2, 1), \\ u|_{x_j=a_j} = u|_{x_j=b_j} &= 0, \quad \nu_j \in (1/2, 1), \quad j = 1, 2, \dots, d. \end{aligned}$$

2.3.1 Stochastic Interpretation of the FPDEs

Following [59], we provide a brief stochastic interpretation of the FPDEs in (2.14) that further sheds light on the well-posedness of the problem from the perspective of probability theory. Let

suppose that in (2.14), $f \equiv 0$ and $\gamma = 0$ and $0 < 2\tau < 1$ and that $a_i = -\infty$ and $b_i = +\infty$ for $i = 1, 2, \dots$. Then (2.14) governs [59] a time-changed Lévy process $X(E_t)$ on \mathbb{R}^d whose Fourier transform is $\mathbb{E}[e^{-ik \cdot X(t)}] = e^{t\psi(k)}$ with the Fourier symbol

$$\psi(k) = - \sum_{n=1}^d [c_{l_n}(ik_n)^{2\mu_n} + c_{r_n}(-ik_n)^{2\mu_n}] + \sum_{m=1}^d [\kappa_{l_m}(-ik_m)^{2\nu_m} + \kappa_{r_m}(ik_m)^{2\nu_m}]. \quad (2.15)$$

Recalling that in one dimension the Lévy process $Y(t)$ with Fourier Transform $\mathbb{E}[e^{-ikY(t)}] = e^{t\psi_0(k)}$ where $\psi_0(k) = pD(ik)^\alpha + qD(-ik)^\alpha$ for $D > 0$ and $1 < \alpha \leq 2$, $p \geq 0$, $q \geq 0$, and $p + q = 1$ is a stable Lévy process with index α and skewness $p - q$ [38, 59].

Then $X(t)$ has d independent components, each of which is the sum of two independent stable Lévy processes with index $2\mu_m$ and $2\nu_m$, respectively. Furthermore, for a bounded domain Λ_d , letting $X'(t)$ denote the modification of the process $X(t)$ that vanishes the first time it leaves the domain, (2.14) governs the time-changed Markov process $X'(E_t)$. You can find complete details in [38].

2.4 Petrov-Galerkin Mathematical Formulation

We introduce the underlying solution and test spaces with their proper norms. Moreover, we provide some lemmas in order to prove the well-posedness of the problem in addition to constructing the spatial basis/test functions and performing the discrete stability and convergence analysis of the PG spectral method.

2.4.1 Mathematical Framework

We first recall the definition of the Sobolev space for real $s \geq 0$ from [70, 107]. Let

$$H^s(\mathbb{R}) = \{u \in L^2(\mathbb{R}) \mid (1 + |\omega|^2)^{\frac{s}{2}} \mathcal{F}(u)(\omega) \in L^2(\mathbb{R})\}, \quad (2.16)$$

endowed with the norm $\|u\|_{H^s(\mathbb{R})} = \|(1 + |\omega|^2)^{\frac{s}{2}} F(u)(\omega)\|_{L^2(\mathbb{R})}$, where $\mathcal{F}(u)$ is the Fourier transform of u . For bounded domain $I = (0, T)$, we define

$$H^s(I) = \{u \in L^2(I) \mid \exists \tilde{u} \in H^s(\mathbb{R}) \text{ s.t. } \tilde{u}|_I = u\}, \quad (2.17)$$

associated with $\|u\|_{H^s(I)} = \inf_{\tilde{u} \in H^s(\mathbb{R}), \tilde{u}|_I = u} \|\tilde{u}\|_{H^s(\mathbb{R})}$. Let ${}_0C^\infty(I)$ and $C_0^\infty(I)$ be the spaces of smooth functions with compact support in $(0, T]$ and $[0, T)$, respectively. Then, denoted by ${}^lH^s(I)$ and ${}^rH^s(I)$ are the closure of ${}_0C^\infty(I)$ and $C_0^\infty(I)$ with respect to the norm $\|\cdot\|_{H^s(I)}$ in $(0, T]$ and $[0, T)$, respectively. Here, we recall from [107, 108] that

$$|\cdot|_{H^s(I)} \equiv |\cdot|_{lH^s(I)} \equiv |\cdot|_{rH^s(I)}, \quad (2.18)$$

where " \equiv " denotes equivalence relation and $|\cdot|_{lH^s(I)} = \|{}_0\mathcal{D}_t^s(\cdot)\|_{L^2(I)}$, $|\cdot|_{rH^s(I)} = \|{}_t\mathcal{D}_T^s(\cdot)\|_{L^2(I)}$.

Take $\Lambda = (a, b)$. $H^\sigma(\Lambda)$ denotes the usual Sobolev space associated with the real index $\sigma \geq 0$ and $\sigma \neq n - \frac{1}{2}$ on the bounded interval Λ , and equipped with the norm $\|\cdot\|_{H^\sigma(\Lambda)}$. In [109], it has been shown that the following norms are equivalent:

$$\|\cdot\|_{H^\sigma(\Lambda)} \equiv \|\cdot\|_{lH^\sigma(\Lambda)} \equiv \|\cdot\|_{rH^\sigma(\Lambda)} \equiv |\cdot|_{H^\sigma(\Lambda)}^*, \quad (2.19)$$

where $\|\cdot\|_{lH^\sigma(\Lambda)} = \left(\|{}_a\mathcal{D}_x^\sigma(\cdot)\|_{L^2(\Lambda)}^2 + \|\cdot\|_{L^2(\Lambda)}^2 \right)^{\frac{1}{2}}$, $\|\cdot\|_{rH^\sigma(\Lambda)} = \left(\|{}_x\mathcal{D}_b^\sigma(\cdot)\|_{L^2(\Lambda)}^2 + \|\cdot\|_{L^2(\Lambda)}^2 \right)^{\frac{1}{2}}$, and $|\cdot|_{H^\sigma(\Lambda)}^* = |({}_a\mathcal{D}_x^\sigma(\cdot), {}_x\mathcal{D}_b^\sigma(\cdot))_\Lambda|^{\frac{1}{2}}$. It follows from Lemma 5.2 in [108] that

$$|\cdot|_{H^\sigma(\Lambda)}^* \equiv |\cdot|_{lH^\sigma(\Lambda)}^{\frac{1}{2}} |\cdot|_{rH^\sigma(\Lambda)}^{\frac{1}{2}} = \|{}_a\mathcal{D}_x^\sigma(\cdot)\|_{L^2(\Lambda)}^{\frac{1}{2}} \|{}_x\mathcal{D}_b^\sigma(\cdot)\|_{L^2(\Lambda)}^{\frac{1}{2}}. \quad (2.20)$$

Lemma 2.4.1. *Let $\sigma \geq 0$ and $\sigma \neq n - \frac{1}{2}$. Then, the norms $\|\cdot\|_{lH^\sigma(\Lambda)}$ and $\|\cdot\|_{rH^\sigma(\Lambda)}$ are equivalent to $\|\cdot\|_{cH^\sigma(\Lambda)}$ in space $C_0^\infty(\Lambda)$, where*

$$\|\cdot\|_{cH^\sigma(\Lambda)} = \left(\|{}_x\mathcal{D}_b^\sigma(\cdot)\|_{L^2(\Lambda)}^2 + \|{}_a\mathcal{D}_x^\sigma(\cdot)\|_{L^2(\Lambda)}^2 + \|\cdot\|_{L^2(\Lambda)}^2 \right)^{\frac{1}{2}}. \quad (2.21)$$

Proof. See Appendix A. □

In the usual Sobolev space, for $u \in H^\sigma(\Lambda)$ we define $|u|_{H^\sigma(\Lambda)}^* = |({}_a\mathcal{D}_x^\sigma u, {}_x\mathcal{D}_b^\sigma v)_\Lambda|^{\frac{1}{2}}$ $\forall v \in H^\sigma(\Lambda)$, assuming $\sup_{u \in H^\sigma(\Lambda)} |({}_a\mathcal{D}_x^\sigma u, {}_x\mathcal{D}_b^\sigma v)_\Lambda|^{\frac{1}{2}} > 0$ $\forall v \in H^\sigma(\Lambda)$.

Denoted by ${}^lH_0^\sigma(\Lambda)$ and ${}^rH_0^\sigma(\Lambda)$ are the closure of $C_0^\infty(\Lambda)$ with respect to the norms $\|\cdot\|_{lH^s(\Lambda)}$ and $\|\cdot\|_{rH^s(\Lambda)}$ in Λ , respectively, where $C_0^\infty(\Lambda)$ is the space of smooth functions with compact support in Λ .

Lemma 2.4.2. For $\sigma \geq 0$ and $\sigma \neq n - \frac{1}{2}$, ${}^l H_0^\sigma(\Lambda)$, ${}^r H_0^\sigma(\Lambda)$, and ${}^c H_0^\sigma(\Lambda)$ are equal and their seminorms are equivalent to $|\cdot|_{H^\sigma(\Lambda)}^*$, where ${}^l H_0^\sigma(\Lambda)$, ${}^r H_0^\sigma(\Lambda)$, and ${}^c H_0^\sigma(\Lambda)$ denotes the closure of $C_0^\infty(\Lambda)$ with compact support on Λ with respect to the norms $\|\cdot\|_{l H^\sigma(\Lambda)}$ and $\|\cdot\|_{r H^\sigma(\Lambda)}$.

Proof. In [108, 109], it has been shown that the spaces ${}^l H_0^\sigma(\Lambda)$ and ${}^r H_0^\sigma(\Lambda)$ are equal. Following similar steps, we can show that ${}^c H_0^\sigma(\Lambda)$ is equal with ${}^l H_0^\sigma(\Lambda)$ and ${}^r H_0^\sigma(\Lambda)$ and the corresponding seminorms are equivalent. \square

Assuming $|({}_a \mathcal{D}_x^\sigma u, {}_x \mathcal{D}_b^\sigma v)_\Lambda|$ and $|({}_x \mathcal{D}_b^\sigma u, {}_a \mathcal{D}_x^\sigma v)_\Lambda| > 0$, Lemma 2.4.2 directly respectively results in $|({}_a \mathcal{D}_x^\sigma u, {}_x \mathcal{D}_b^\sigma v)_\Lambda| \geq \beta_1 |u|_{l H^\sigma(\Lambda)} |v|_{r H^\sigma(\Lambda)}$ and $|({}_x \mathcal{D}_b^\sigma u, {}_a \mathcal{D}_x^\sigma v)_\Lambda| \geq \beta_2 |u|_{r H^\sigma(\Lambda)} |v|_{l H^\sigma(\Lambda)}$, where β_1 and β_2 are positive constants and independent of σ .

Let $\Lambda_1 = (a_1, b_1)$, $\Lambda_i = (a_i, b_i) \times \Lambda_{i-1}$ for $i = 2, \dots, d$, and $\mathcal{X}_1 = H_0^{\nu_1}(\Lambda_1)$ with the associated norm $\|\cdot\|_{c H^{\nu_1}(\Lambda_1)}$. Accordingly, we construct \mathcal{X}_d such that

$$\begin{aligned} \mathcal{X}_2 &= H_0^{\nu_2}\left((a_2, b_2); L^2(\Lambda_1)\right) \cap L^2((a_2, b_2); \mathcal{X}_1), \\ &\vdots \\ \mathcal{X}_d &= H_0^{\nu_d}\left((a_d, b_d); L^2(\Lambda_{d-1})\right) \cap L^2((a_d, b_d); \mathcal{X}_{d-1}), \end{aligned} \quad (2.22)$$

associated with the norm

$$\|\cdot\|_{\mathcal{X}_d} = \left\{ \|\cdot\|_{c H^{\nu_d}\left((a_d, b_d); L^2(\Lambda_{d-1})\right)}^2 + \|\cdot\|_{L^2\left((a_d, b_d); \mathcal{X}_{d-1}\right)}^2 \right\}^{\frac{1}{2}}. \quad (2.23)$$

Lemma 2.4.3. Let $\nu_i > 0$ and $\nu_i \neq n - \frac{1}{2}$ for $i = 1, \dots, d$. Then

$$\|\cdot\|_{\mathcal{X}_d} \equiv \left\{ \sum_{i=1}^d \left(\|{}_x \mathcal{D}_{b_i}^{\nu_i}(\cdot)\|_{L^2(\Lambda_d)}^2 + \|{}_a \mathcal{D}_{x_i}^{\nu_i}(\cdot)\|_{L^2(\Lambda_d)}^2 \right) + \|\cdot\|_{L^2(\Lambda_d)}^2 \right\}^{\frac{1}{2}}. \quad (2.24)$$

Proof. \mathcal{X}_1 is endowed with the norm $\|\cdot\|_{\mathcal{X}_1}$, where $\|\cdot\|_{\mathcal{X}_1} \equiv \|\cdot\|_{H^{\nu_1}(\Lambda_1)}$ (see Lemma 2.4.1).

Moreover, \mathcal{X}_2 is associated with the norm

$$\|\cdot\|_{\mathcal{X}_2} \equiv \left\{ \|\cdot\|_{c H^{\nu_2}\left((a_2, b_2); L^2(\Lambda_1)\right)}^2 + \|\cdot\|_{L^2\left((a_2, b_2); \mathcal{X}_1\right)}^2 \right\}^{\frac{1}{2}}, \quad (2.25)$$

where

$$\begin{aligned}\|u\|_{cH^{\nu_2}((a_2,b_2);L^2(\Lambda_1))}^2 &= \int_{a_1}^{b_1} \left(\int_{a_2}^{b_2} |{}_{a_2}\mathcal{D}_{x_2}^{\nu_2} u|^2 dx_2 + \int_{a_2}^{b_2} |{}_{x_2}\mathcal{D}_{b_2}^{\nu_2} u|^2 dx_2 \right. \\ &\quad \left. + \int_{a_2}^{b_2} |u|^2 dx_2 \right) dx_1 \\ &= \|{}_{x_2}\mathcal{D}_{b_2}^{\nu_2}(u)\|_{L^2(\Lambda_2)}^2 + \|{}_{a_2}\mathcal{D}_{x_2}^{\nu_2}(u)\|_{L^2(\Lambda_2)}^2 + \|u\|_{L^2(\Lambda_2)}^2,\end{aligned}$$

and

$$\begin{aligned}\|u\|_{L^2((a_2,b_2);\chi_1)}^2 &= \int_{a_2}^{b_2} \left(\int_{a_1}^{b_1} |{}_{a_1}\mathcal{D}_{x_1}^{\nu_1} u|^2 dx_1 + \int_{a_1}^{b_1} |{}_{x_1}\mathcal{D}_{b_1}^{\nu_1} u|^2 dx_1 + \int_{a_1}^{b_1} |u|^2 dx_1 \right) dx_2 \\ &= \|{}_{x_1}\mathcal{D}_{b_1}^{\nu_1} u\|_{L^2(\Lambda_2)}^2 + \|{}_{a_1}\mathcal{D}_{x_1}^{\nu_1} u\|_{L^2(\Lambda_2)}^2 + \|u\|_{L^2(\Lambda_2)}^2.\end{aligned}$$

Now, we assume that

$$\|\cdot\|_{\chi_{d-1}} \equiv \left\{ \sum_{i=1}^{d-1} \left(\|{}_{x_i}\mathcal{D}_{b_i}^{\nu_i}(\cdot)\|_{L^2(\Lambda_{d-1})}^2 + \|{}_{a_i}\mathcal{D}_{x_i}^{\nu_i}(\cdot)\|_{L^2(\Lambda_{d-1})}^2 \right) + \|\cdot\|_{L^2(\Lambda_{d-1})}^2 \right\}^{\frac{1}{2}}. \quad (2.26)$$

Then,

$$\begin{aligned}\|u\|_{cH^{\nu_d}((a_d,b_d);L^2(\Lambda_{d-1}))}^2 &= \int_{\Lambda_{d-1}}^{b_d} \left(\int_{a_d}^{b_d} |{}_{a_d}\mathcal{D}_{x_d}^{\nu_d} u|^2 dx_d + \int_{a_d}^{b_d} |{}_{x_d}\mathcal{D}_{b_d}^{\nu_d} u|^2 dx_d + \int_{a_d}^{b_d} |u|^2 dx_d \right) d\Lambda_{d-1} \\ &= \|{}_{x_d}\mathcal{D}_{b_d}^{\nu_d}(u)\|_{L^2(\Lambda_d)}^2 + \|{}_{a_d}\mathcal{D}_{x_d}^{\nu_d}(u)\|_{L^2(\Lambda_d)}^2 + \|u\|_{L^2(\Lambda_d)}^2,\end{aligned}$$

and

$$\begin{aligned}\|u\|_{L^2((a_d,b_d);\chi_{d-1})}^2 &= \sum_{i=1}^{d-1} \left(\int_{\Lambda_d} |{}_{a_i}\mathcal{D}_{x_i}^{\nu_i} u|^2 d\Lambda_d + \int_{\Lambda_d} |{}_{x_i}\mathcal{D}_{b_i}^{\nu_i} u|^2 d\Lambda_d \right) + \int_{\Lambda_d} |u|^2 d\Lambda_d \\ &= \sum_{i=1}^{d-1} \left(\|{}_{x_i}\mathcal{D}_{b_i}^{\nu_i} u\|_{L^2(\Lambda_d)}^2 + \|{}_{a_i}\mathcal{D}_{x_i}^{\nu_i} u\|_{L^2(\Lambda_d)}^2 \right) + \|u\|_{L^2(\Lambda_d)}^2.\end{aligned}$$

Therefore, (2.24) arises from (2.26). \square

In Lemma 2.8 in [109], it is shown that if $u, v \in H_0^\alpha(\Lambda_1)$ for $0 < 2\alpha < 2$ and $2\alpha \neq 1$, then $({}_{x_1}\mathcal{D}_{b_1}^{2\alpha} u, v)_{\Lambda_1} = ({}_{x_1}\mathcal{D}_{b_1}^\alpha u, {}_{a_1}\mathcal{D}_{x_1}^\alpha v)_{\Lambda_1}$, and $({}_{a_1}\mathcal{D}_{x_1}^{2\alpha} u, v)_{\Lambda_1} = ({}_{a_1}\mathcal{D}_{x_1}^\alpha u, {}_{x_1}\mathcal{D}_{b_1}^\alpha v)_{\Lambda_1}$. Here, we generalize this lemma for the corresponding (1+d)-D case.

Lemma 2.4.4. If $0 < 2\nu_i < 2$ and $2\nu_i \neq 1$ for $i = 1, \dots, d$, and $u, v \in \mathcal{X}_d$, then $({}_{x_i} \mathcal{D}_{b_i}^{2\nu_i} u, v)_{\Lambda_d} = ({}_{x_i} \mathcal{D}_{b_i}^{\nu_i} u, {}_{a_i} \mathcal{D}_{x_i}^{\nu_i} v)_{\Lambda_d}$, and $({}_{a_i} \mathcal{D}_{x_i}^{2\nu_i} u, v)_{\Lambda_d} = ({}_{a_i} \mathcal{D}_{x_i}^{\nu_i} u, {}_{x_i} \mathcal{D}_{b_i}^{\nu_i} v)_{\Lambda_d}$.

Proof. See Appendix A. \square

Additionally, in the light of Lemma 2.4.2, we can prove that

$$\begin{aligned} |({}_{a_d} \mathcal{D}_{x_d}^{\nu_d} u, {}_{x_d} \mathcal{D}_{b_d}^{\nu_d} v)_{\Lambda_d}| + |({}_{x_d} \mathcal{D}_{b_d}^{\nu_d} u, {}_{a_d} \mathcal{D}_{x_d}^{\nu_d} v)_{\Lambda_d}| \\ \equiv \|u\|_{{}^c H_0^{\nu_d}((a_d, b_d); L^2(\Lambda_{d-1}))}^{|v|} \|v\|_{{}^c H^{\nu_d}((a_d, b_d); L^2(\Lambda_{d-1}))}, \end{aligned} \quad (2.27)$$

where we assume $\sup_{u \in {}^c H_0^{\nu_d}((a_d, b_d); L^2(\Lambda_{d-1}))} (|({}_{a_d} \mathcal{D}_{x_d}^{\nu_d} u, {}_{x_d} \mathcal{D}_{b_d}^{\nu_d} v)_{\Lambda_d}| + |({}_{x_d} \mathcal{D}_{b_d}^{\nu_d} u, {}_{a_d} \mathcal{D}_{x_d}^{\nu_d} v)_{\Lambda_d}|) > 0$ for any $v \in {}^c H_0^{\nu_d}((a_d, b_d); L^2(\Lambda_{d-1}))$. Next, we study the property of the fractional time derivative in the following lemmas.

Lemma 2.4.5. If $0 < 2\tau < 1$ ($1 < 2\tau < 2$) and $u, v \in H^\tau(I)$, when $u|_{t=0} (= \frac{du}{dt}|_{t=0}) = 0$, then $({}_0 \mathcal{D}_t^{2\tau} u, v)_I = ({}_0 \mathcal{D}_t^\tau u, {}_t \mathcal{D}_T^\tau v)_I$, where $I = (0, T)$.

Proof. See [70]. \square

Lemma 2.4.4 and 2.4.5 will help us obtain the corresponding weak form of (2.14). Let $2\tau \in (0, 1)$ and $\Omega = I \times \Lambda_d$. We define

$${}_0^l H^\tau(I; L^2(\Lambda_d)) := \left\{ u \mid \|u(t, \cdot)\|_{L^2(\Lambda_d)} \in H^\tau(I), u|_{t=0} = u|_{x_i=a_i} = u|_{x_i=b_i} = 0, i = 1, \dots, d \right\}, \quad (2.28)$$

which is equipped with the norm $\|u\|_{{}^l H^\tau(I; L^2(\Lambda_d))}$. For real $0 < 2\tau < 1$, ${}_0^l H^\tau(I; L^2(\Lambda_d))$ is associated with the norm $\|\cdot\|_{{}^l H^\tau(I; L^2(\Lambda_d))}$, which is defined as

$$\|u\|_{{}^l H^\tau(I; L^2(\Lambda_d))} = \left\| \|u(t, \cdot)\|_{L^2(\Lambda_d)} \right\|_{H^\tau(I)}.$$

Therefore, we have

$$\begin{aligned}
\|u\|_{lH^\tau(I;L^2(\Lambda_d))} &= \left\| \|u(t,\cdot)\|_{L^2(\Lambda_d)} \right\|_{lH^\tau(I)} \\
&= \left\{ \int_0^T \left(\left(\int_{\Lambda_d} |{}_0\mathcal{D}_t^\tau u|^2 d\Lambda_d \right)^{\frac{1}{2}} \right)^2 dt + \int_0^T \int_{\Lambda_d} |u|^2 d\Lambda_d dt \right\}^{\frac{1}{2}} \\
&= \left(\|{}_0\mathcal{D}_t^\tau(u)\|_{L^2(\Omega)}^2 + \|u\|_{L^2(\Omega)}^2 \right)^{\frac{1}{2}}.
\end{aligned} \tag{2.29}$$

Similarly, we define

$${}^r_0H^\tau\left(I; L^2(\Lambda_d)\right) := \left\{ v \mid \|v(t,\cdot)\|_{L^2(\Lambda_d)} \in H^\tau(I), v|_{t=T} = v|_{x_i=a_i} = v|_{x_i=b_i} = 0, i = 1, \dots, d \right\}, \tag{2.30}$$

which is equipped with the norm $\|v\|_{{}^r_0H^\tau(I;L^2(\Lambda_d))}$. Following (2.29),

$$\begin{aligned}
\|v\|_{{}^r_0H^\tau(I;L^2(\Lambda_d))} &= \left\| \|v(t,\cdot)\|_{L^2(\Lambda_d)} \right\|_{{}^r_0H^\tau(I)} \\
&= \left(\|{}_t\mathcal{D}_T^\tau(v)\|_{L^2(\Omega)}^2 + \|v\|_{L^2(\Omega)}^2 \right)^{\frac{1}{2}}.
\end{aligned} \tag{2.31}$$

Lemma 2.4.6. If $0 < 2\tau < 2$, $2\tau \neq 1$ and $u \in {}^l_0H^\tau(I;L^2(\Lambda_d))$, then

$$({}_0\mathcal{D}_t^{2\tau}u, v)_\Omega = ({}_0\mathcal{D}_t^\tau u, {}_t\mathcal{D}_T^\tau v)_\Omega \quad \forall v \in {}^r_0H^\tau(I;L^2(\Lambda_d))$$

Proof. Following Lemma 2.4.5,

$$\begin{aligned}
({}_0\mathcal{D}_t^{2\tau}u, v)_\Omega &= \int_0^T \int_{\Lambda_d} {}_0\mathcal{D}_t^{2\tau}u v d\Lambda_d dt = \int_{\Lambda_d} \int_0^T {}_0\mathcal{D}_t^\tau u {}_t\mathcal{D}_T^\tau v d\Lambda_d dt \\
&= ({}_0\mathcal{D}_t^\tau u, {}_t\mathcal{D}_T^\tau v)_\Omega.
\end{aligned} \tag{2.32}$$

□

Lemma 2.4.7. For $u \in {}^l_0H^\tau(I;L^2(\Lambda_d))$ and $2\tau \in (0, 1)$, $|({}_0\mathcal{D}_t^\tau u, {}_t\mathcal{D}_T^\tau v)_\Omega| \leq \|u\|_{{}^l_0H^\tau(I;L^2(\Lambda_d))} \|v\|_{{}^r_0H^\tau(I;L^2(\Lambda_d))} \forall v \in {}^r_0H^\tau(I;L^2(\Lambda_d))$.

Proof.

$$|({}_0\mathcal{D}_t^\tau u, {}_t\mathcal{D}_T^\tau v)_\Omega| = \left(\int_{\Lambda_d} \int_0^T |{}_0\mathcal{D}_t^\tau u {}_t\mathcal{D}_T^\tau v| dt d\Lambda_d \right) \tag{2.33}$$

By Hölder inequality,

$$\begin{aligned}
& |({}_0\mathcal{D}_t^\tau u, {}_t\mathcal{D}_T^\tau v)_\Omega| \tag{2.34} \\
& \leq \left(\int_{\Lambda_d} \int_0^T |{}_0\mathcal{D}_t^\tau u|^2 dt d\Lambda_d \right)^{\frac{1}{2}} \left(\int_{\Lambda_d} \int_0^T |{}_t\mathcal{D}_T^\tau v|^2 dt d\Lambda_d \right)^{\frac{1}{2}} \\
& \leq \left(\int_{\Lambda_d} \int_0^T |{}_0\mathcal{D}_t^\tau u|^2 dt d\Lambda_d + \int_{\Lambda_d} \int_0^T |u|^2 dt d\Lambda_d \right)^{\frac{1}{2}} \\
& \quad \times \left(\int_{\Lambda_d} \int_0^T |{}_t\mathcal{D}_T^\tau v|^2 dt d\Lambda_d + \int_{\Lambda_d} \int_0^T |v|^2 dt d\Lambda_d \right)^{\frac{1}{2}} \\
& = \left(\|{}_0\mathcal{D}_t^\tau u\|_{L^2(\Omega)}^2 + \|u\|_{L^2(\Omega)}^2 \right)^{\frac{1}{2}} \left(\|{}_t\mathcal{D}_T^\tau v\|_{L^2(\Omega)}^2 + \|v\|_{L^2(\Omega)}^2 \right)^{\frac{1}{2}} \\
& = \|u\|_{lH^\tau(I; L^2(\Lambda_d))} \|v\|_{rH^\tau(I; L^2(\Lambda_d))}.
\end{aligned}$$

□

Lemma 2.4.8. For any $u \in {}_0^lH^\tau(I; L^2(\Lambda_d))$ and $2\tau \in (0, 1)$, there exists a constant $c > 0$ and independent of τ and u such that

$$\sup_{0 \neq v \in {}_0^rH^\tau(I; L^2(\Lambda_d))} \frac{|({}_0\mathcal{D}_t^\tau u, {}_t\mathcal{D}_T^\tau v)_\Omega|}{|v|_{rH^\tau(I; L^2(\Lambda_d))}} \geq c|u|_{lH^\tau(I; L^2(\Lambda_d))}, \tag{2.35}$$

assuming $\sup_{u \in {}_0^lH^\tau(I; L^2(\Lambda_d))} |({}_0\mathcal{D}_t^\tau u, {}_t\mathcal{D}_T^\tau v)_\Omega| > 0 \quad \forall v \in {}_0^rH^\tau(I; L^2(\Lambda_d))$.

Proof. Following Lemma 2.4 in [110] and Lemma 3.1 in [111], for any given $u \in {}_0^lH^\tau(I; L^2(\Lambda_d))$ let $\mathcal{V}_u = {}_t\mathcal{I}_T^\tau(f(t) {}_0\mathcal{D}_t^\tau u)$ under the assumption of $\sup_{u \in {}_0^lH^\tau(I; L^2(\Lambda_d))} |({}_0\mathcal{D}_t^\tau u, {}_t\mathcal{D}_T^\tau v)_\Omega| > 0$, where $f(t) = (1 - H(t-T))$ and $H(t)$ is the Heaviside function. Clearly $\mathcal{V}_u \in {}_0^rH^\tau(I; L^2(\Lambda_d))$. Therefore, by Hölder inequality we obtain

$$\begin{aligned}
|\mathcal{V}_u|_{rH^\tau(I; L^2(\Lambda_d))}^2 &= \|{}_t\mathcal{D}_T^\tau({}_t\mathcal{I}_T^\tau(f(t) {}_0\mathcal{D}_t^\tau u))\|_{L^2(\Omega)}^2 = \|f(t) {}_0\mathcal{D}_t^\tau u\|_{L^2(\Omega)}^2 \\
&\leq \|f(t)\|_{L^2(\Omega)}^2 \|{}_0\mathcal{D}_t^\tau u\|_{L^2(\Omega)}^2 = \tilde{\beta}_1 \|{}_0\mathcal{D}_t^\tau u\|_{L^2(\Omega)}^2,
\end{aligned} \tag{2.36}$$

where $\tilde{\beta}_1 = \|f(t)\|_{L^2(\Omega)}^2$ and independent of τ and u . Using \mathcal{V}_u , we have

$$\begin{aligned} |(0\mathcal{D}_t^\tau u, {}_t\mathcal{D}_T^\tau \mathcal{V}_u)_\Omega| &= \int_{\Lambda_d} \int_0^T |{}_0\mathcal{D}_t^\tau u \cdot {}_t\mathcal{D}_T^\tau ({}_t\mathcal{I}_T^\tau(f(t) {}_0\mathcal{D}_t^\tau u))| dt d\Lambda_d \\ &= \int_{\Lambda_d} \int_0^T |{}_0\mathcal{D}_t^\tau u|^2 |f(t)| dt d\Lambda_d. \end{aligned}$$

According to the second mean value theorem for integrals [112],

$$\int_{\Lambda_d} \int_0^T |{}_0\mathcal{D}_t^\tau u|^2 |f(t)| dt d\Lambda_d \geq \bar{\beta}_1 \int_{\Lambda_d} \int_0^T |{}_0\mathcal{D}_t^\tau u|^2 dt d\Lambda_d = \bar{\beta}_1 \|u\|_{l^H(I; L^2(\Lambda_d))}^2, \quad (2.37)$$

where $\bar{\beta}_1 = \lim_{t \rightarrow T^-} |f(t)| = 1$. Considering (2.36) and (2.37), we obtain

$$\sup_{0 \neq v \in r_{H^\tau}(I; L^2(\Lambda_d))} \frac{|(0\mathcal{D}_t^\tau u, {}_t\mathcal{D}_T^\tau v)_\Omega|}{\|v\|_{r_{H^\tau}(I; L^2(\Lambda_d))}} \geq \frac{|(0\mathcal{D}_t^\tau u, {}_t\mathcal{D}_T^\tau \mathcal{V}_u)_\Omega|}{\|\mathcal{V}_u\|_{r_{H^\tau}(I; L^2(\Lambda_d))}} \geq \frac{\bar{\beta}_1}{\tilde{\beta}_1} \|u\|_{l^H(I; L^2(\Lambda_d))}, \quad (2.38)$$

where $c = \frac{\bar{\beta}_1}{\tilde{\beta}_1} > 0$ and independent of τ and u . \square

2.4.2 Solution and Test Function Spaces

Let $2\tau \in (0, 1)$ and $2\nu_i \in (1, 2)$ for $i = 1, \dots, d$. We define the solution space

$$\mathcal{B}^{\tau, \nu_1, \dots, \nu_d}(\Omega) := l^H(I; L^2(\Lambda_d)) \cap L^2(I; X_d), \quad (2.39)$$

endowed with the norm

$$\|u\|_{\mathcal{B}^{\tau, \nu_1, \dots, \nu_d}(\Omega)} = \left\{ \|u\|_{l^H(I; L^2(\Lambda_d))}^2 + \|u\|_{L^2(I; X_d)}^2 \right\}^{\frac{1}{2}}, \quad (2.40)$$

where due to (2.23) and Lemma 2.4.3,

$$\begin{aligned} \|u\|_{L^2(I; X_d)} &= \left\| \|u(t, .)\|_{X_d} \right\|_{L^2(I)} \\ &= \left\{ \|u\|_{L^2(\Omega)}^2 + \sum_{i=1}^d (\|{}_{x_i}\mathcal{D}_{b_i}^{\nu_i}(u)\|_{L^2(\Omega)}^2 + \|{}_{a_i}\mathcal{D}_{x_i}^{\nu_i}(u)\|_{L^2(\Omega)}^2) \right\}^{\frac{1}{2}}. \end{aligned} \quad (2.41)$$

Therefore, by (2.29) and (2.41),

$$\|u\|_{\mathcal{B}^{\tau, \nu_1, \dots, \nu_d}(\Omega)} = \left\{ \|u\|_{L^2(\Omega)}^2 + \|{}_0\mathcal{D}_t^\tau(u)\|_{L^2(\Omega)}^2 + \sum_{i=1}^d (\|{}_{x_i}\mathcal{D}_{b_i}^{\nu_i}(u)\|_{L^2(\Omega)}^2 + \|{}_{a_i}\mathcal{D}_{x_i}^{\nu_i}(u)\|_{L^2(\Omega)}^2) \right\}^{\frac{1}{2}}. \quad (2.42)$$

Likewise, we define the test space

$$\mathfrak{B}^{\tau, \nu_1, \dots, \nu_d}(\Omega) := {}_0^r H^\tau \left(I; L^2(\Lambda_d) \right) \cap L^2(I; \mathcal{X}_d), \quad (2.43)$$

endowed with the norm

$$\begin{aligned} \|v\|_{\mathfrak{B}^{\tau, \nu_1, \dots, \nu_d}(\Omega)} &= \left\{ \|v\|_{r H^\tau(I; L^2(\Lambda_d))}^2 + \|v\|_{L^2(I; \mathcal{X}_d)}^2 \right\}^{\frac{1}{2}}. \\ &= \left\{ \|v\|_{L^2(\Omega)}^2 + \|{}_t \mathcal{D}_T^\tau(v)\|_{L^2(\Omega)}^2 \right. \\ &\quad \left. + \sum_{i=1}^d (\|{}_{x_i} \mathcal{D}_{b_i}^{\nu_i}(v)\|_{L^2(\Omega)}^2 + \|{}_{a_i} \mathcal{D}_{x_i}^{\nu_i}(v)\|_{L^2(\Omega)}^2) \right\}^{\frac{1}{2}}. \end{aligned} \quad (2.44)$$

Remark 2.4.9. If $2\tau \in (0, 1)$, our method is essentially Galerkin in the ∞ -dimensional space. Yet in the discretization, we choose two different subspaces as basis and test spaces, leading to the PG spectral method; that is, $U_N \subset \mathcal{B}^{\tau, \nu_1, \dots, \nu_d}(\Omega)$ and $V_N \subset \mathfrak{B}^{\tau, \nu_1, \dots, \nu_d}(\Omega)$ such that $U_N \neq V_N$.

In case $2\tau \in (1, 2)$, we define the solution space as

$$\mathcal{B}^{\tau, \nu_1, \dots, \nu_d}(\Omega) := {}_{0,0}^l H^\tau \left(I; L^2(\Lambda_d) \right) \cap L^2(I; \mathcal{X}_d), \quad (2.45)$$

where

$$\begin{aligned} {}_{0,0}^l H^\tau \left(I; L^2(\Lambda_d) \right) &:= \left\{ u \mid \|u(t, \cdot)\|_{L^2(\Lambda_d)} \in H^\tau(I), \right. \\ &\quad \left. \frac{\partial u}{\partial t}|_{t=0} = u|_{t=0} = u|_{x_i=a_i} = u|_{x_i=b_i} = 0, i = 1, \dots, d \right\}, \end{aligned}$$

which is associated with $\|\cdot\|_{\mathcal{B}^{\tau, \nu_1, \dots, \nu_d}(\Omega)}$. The corresponding test space is also defined as

$$\mathfrak{B}^{\tau, \nu_1, \dots, \nu_d}(\Omega) := {}_{0,0}^r H^\tau \left(I; L^2(\Lambda_d) \right) \cap L^2(I; \mathcal{X}_d), \quad (2.46)$$

where

$$\begin{aligned} {}_{0,0}^r H^\tau \left(I; L^2(\Lambda_d) \right) &:= \left\{ v \mid \|v(t, \cdot)\|_{L^2(\Lambda_d)} \in H^\tau(I), \right. \\ &\quad \left. \frac{\partial v}{\partial t}|_{t=T} = v|_{t=T} = v|_{x_i=a_i} = v|_{x_i=b_i} = 0, i = 1, \dots, d \right\}, \end{aligned}$$

which is endowed with $\|\cdot\|_{\mathfrak{B}^{\tau, \nu_1, \dots, \nu_d}(\Omega)}$. It should be noted that similar to Lemma 2.4.7, for any $u \in {}_{0,0}^l H^\tau(I; L^2(\Lambda_d))$ and $2\tau \in (1, 2)$, we obtain

$$\sup_{0 \neq v \in {}_{0,0}^r H^\tau(I; L^2(\Lambda_d))} \frac{|({}_0 \mathcal{D}_t^\tau u, {}_t \mathcal{D}_T^\tau v)_\Omega|}{|v|_{{}_{0,0}^r H^\tau(I; L^2(\Lambda_d))}} \geq |u|_{{}_{0,0}^l H^\tau(I; L^2(\Lambda_d))}, \quad (2.47)$$

assuming $\sup_{u \in {}_{0,0}^l H^\tau(I; L^2(\Lambda_d))} |({}_0 \mathcal{D}_t^\tau u, {}_t \mathcal{D}_T^\tau v)_\Omega| > 0 \quad \forall v \in {}_{0,0}^r H^\tau(I; L^2(\Lambda_d))$.

2.4.3 Petrov-Galerkin Method

Let $u \in \mathcal{B}^{\tau, \nu_1, \dots, \nu_d}(\Omega)$ and $\Omega = (0, T) \times (a_1, b_1) \times (a_2, b_2) \times \dots \times (a_d, b_d)$, where d is a positive integer. We define the corresponding bilinear form as

$$\begin{aligned} a(u, v) = & ({}_0 \mathcal{D}_t^\tau u, {}_t \mathcal{D}_T^\tau v)_\Omega \\ & + \sum_{i=1}^d [c_{l_i} ({}_i \mathcal{D}_{x_i}^{\mu_i} u, {}_i \mathcal{D}_{b_i}^{\mu_i} v)_\Omega + c_{r_i} ({}_i \mathcal{D}_{a_i}^{\mu_i} u, {}_i \mathcal{D}_{x_i}^{\mu_i} v)_\Omega] \\ & - \sum_{j=1}^d [\kappa_{l_j} ({}_j \mathcal{D}_{x_j}^{\nu_j} u, {}_j \mathcal{D}_{b_j}^{\nu_j} v)_\Omega + \kappa_{r_j} ({}_j \mathcal{D}_{b_j}^{\nu_j} u, {}_j \mathcal{D}_{x_j}^{\nu_j} v)_\Omega] \\ & + \gamma(u, v)_\Omega, \end{aligned} \quad (2.48)$$

where $\gamma, c_{l_i}, c_{r_i}, \kappa_{l_i}$, and κ_{r_i} are all constant. $2\mu_j \in (0, 1)$, $2\nu_j \in (1, 2)$, and $2\tau \in (0, 2)$ for $j = 1, 2, \dots, d$. Now, the problem reads as: find $u \in \mathcal{B}^{\tau, \nu_1, \dots, \nu_d}(\Omega)$ such that

$$a(u, v) = (f, v)_\Omega, \quad \forall v \in \mathfrak{B}^{\tau, \nu_1, \dots, \nu_d}(\Omega), \quad (2.49)$$

where $a(u, v)$ is a continuous bilinear form and $f \in (\mathcal{B}^{\tau, \nu_1, \dots, \nu_d})^*(\Omega)$, which is the dual space of $\mathcal{B}^{\tau, \nu_1, \dots, \nu_d}(\Omega)$. It should be noted that $({}_0 \mathcal{D}_t^{2\tau} u, v)_\Omega = ({}_0 \mathcal{D}_t^\tau u, {}_t \mathcal{D}_T^\tau v)_\Omega$ is proven in Proposition 1 in [113] and later in [70] requiring less regularity and constraint.

Remark 2.4.10. In case $\tau < \frac{1}{2}$, the solution to the bilinear form in (2.48) does not lead to the homogeneous initial condition in the strong form. To guarantee the equivalence between the problem under the strong formulation and the bilinear form, we assume that f in (2.14) possesses enough regularity [114].

2.5 Well-posedness Analysis

Based upon the Lemmas provided in Section 2.4, we are able to prove the well-posed and further the stability of the problem (2.49) in the following theorems.

Assumption 1. For any $v \in \mathfrak{B}^{\tau, v_1, \dots, v_d}(\Omega)$ with $v \neq 0$, we assume that

$$\begin{aligned} & \sup_{u \in \mathcal{B}^{\tau, v_1, \dots, v_d}(\Omega)} \left(|(_0\mathcal{D}_t^\tau u, {}_t\mathcal{D}_T^\tau v)_\Omega| \right) > 0 \text{ and} \\ & \sup_{u \in \mathcal{B}^{\tau, v_1, \dots, v_d}(\Omega)} \left(|(a_j \mathcal{D}_{x_j}^{v_j} u, {}_{x_j} \mathcal{D}_{b_j}^{v_j} v)_\Omega| + |(x_j \mathcal{D}_{b_j}^{v_j} u, {}_{a_j} \mathcal{D}_{x_j}^{v_j} v)_\Omega| \right) > 0 \text{ for } j = 1, \dots, d. \end{aligned}$$

Lemma 2.5.1. (Continuity) The bilinear form in (2.48) is continuous, i.e., for $u \in \mathcal{B}^{\tau, v_1, \dots, v_d}(\Omega)$,

$$\exists \beta > 0, \quad |a(u, v)| \leq \beta \|u\|_{\mathcal{B}^{\tau, v_1, \dots, v_d}(\Omega)} \|v\|_{\mathfrak{B}^{\tau, v_1, \dots, v_d}(\Omega)} \quad \forall v \in \mathfrak{B}^{\tau, v_1, \dots, v_d}(\Omega). \quad (2.50)$$

Proof. The proof follows easily using (2.27) and Lemma 2.4.7. \square

Theorem 2.5.2. The inf-sup condition for the bilinear form, defined in (2.48) when $d = 1$, i.e.,

$$\inf_{0 \neq u \in \mathcal{B}^{\tau, v_1}(\Omega)} \sup_{0 \neq v \in \mathfrak{B}^{\tau, v_1}(\Omega)} \frac{|a(u, v)|}{\|v\|_{\mathfrak{B}^{\tau, v_1}(\Omega)} \|u\|_{\mathcal{B}^{\tau, v_1}(\Omega)}} \geq \beta > 0, \quad (2.51)$$

holds with $\beta > 0$, where $\Omega = I \times \Lambda_1$ and Assumption 1 holds.

Proof. It is evident that u and v are in Hilbert spaces (see [108, 109]). By Assumption 1, we can prove that

$$\begin{aligned} |a(u, v)| & \equiv |(_0\mathcal{D}_t^\tau u, {}_t\mathcal{D}_T^\tau v)_\Omega| + \left(|(a_1 \mathcal{D}_{x_1}^{\mu_1} u, {}_{x_1} \mathcal{D}_{b_1}^{\mu_1} v)_\Omega| + |(x_1 \mathcal{D}_{a_1}^{\mu_1} u, {}_{a_1} \mathcal{D}_{x_1}^{\mu_1} v)_\Omega| \right) \\ & \quad + \left(|(a_1 \mathcal{D}_{x_1}^{v_1} u, {}_{x_1} \mathcal{D}_{b_1}^{v_1} v)_\Omega| + |(x_1 \mathcal{D}_{b_1}^{v_1} u, {}_{a_1} \mathcal{D}_{x_1}^{v_1} v)_\Omega| \right) + |(u, v)_\Omega|. \end{aligned} \quad (2.52)$$

Next, by (2.27) and Lemma 2.4.8 we obtain

$$\begin{aligned} \sup_{0 \neq v \in \mathfrak{B}^{\tau, v_1}(\Omega)} \frac{|(_0\mathcal{D}_t^\tau u, {}_t\mathcal{D}_T^\tau v)_\Omega|}{\|v\|_{\mathfrak{B}^{\tau, v_1}(\Omega)}} & \equiv \sup_{0 \neq v \in \mathfrak{B}^{\tau, v_1}(\Omega)} \frac{|(_0\mathcal{D}_t^\tau u, {}_t\mathcal{D}_T^\tau v)_\Omega|}{\|v\|_{r_{H^\tau}((0,T);L^2(\Lambda_1))}} \\ & \geq C_1 |u|_{l_{H^\tau}((0,T);L^2(\Lambda_1))}, \end{aligned} \quad (2.53)$$

$$\begin{aligned} & \frac{\sup_{0 \neq v \in \mathcal{B}^{\tau, \nu_1}(\Omega)} |(a_1 \mathcal{D}_{x_1}^{\nu_1}(u), {}_{x_1} \mathcal{D}_{b_1}^{\nu_1}(v))_{\Omega}| + |({}_{x_1} \mathcal{D}_{b_1}^{\nu_1}(u), a_1 \mathcal{D}_{x_1}^{\nu_1}(v))_{\Omega}|}{\|v\|_{\mathcal{B}^{\tau, \nu_1}(\Omega)}} \equiv \\ & \sup_{0 \neq v \in \mathcal{B}^{\tau, \nu_1}(\Omega)} \frac{|(a_1 \mathcal{D}_{x_1}^{\nu_1}(u), {}_{x_1} \mathcal{D}_{b_1}^{\nu_1}(v))_{\Omega}| + |({}_{x_1} \mathcal{D}_{b_1}^{\nu_1}(u), a_1 \mathcal{D}_{x_1}^{\nu_1}(v))_{\Omega}|}{\|v\|_{cH^{\nu_1}(\Lambda_1; L^2(I))}} \geq C_2 \|u\|_{cH^{\nu_1}(\Lambda_1; L^2(I))}, \end{aligned}$$

and $\sup_{0 \neq v \in \mathcal{B}^{\tau, \nu_1}(\Omega)} \frac{|(u, v)_{\Omega}|}{\|v\|_{L^2(\Omega)}} \geq \|u\|_{L^2(\Omega)}$, where C_1, C_2 , and C_3 are positive constants and independent and Assumption 1 holds. Therefore, for $u \in \mathcal{B}^{\tau, \nu_1, \dots, \nu_d}(\Omega)$

$$\begin{aligned} & \sup_{0 \neq v \in \mathcal{B}^{\tau, \nu_1}(\Omega)} \frac{|a(u, v)|}{\|v\|_{\mathcal{B}^{\tau, \nu_1}(\Omega)}} \\ & \geq \bar{\beta} \sup_{0 \neq v \in \mathcal{B}^{\tau, \nu_1}(\Omega)} \frac{|({}_0 \mathcal{D}_t^{\tau}(u), {}_t \mathcal{D}_T^{\tau}(v))_{\Omega}| + |(a_1 \mathcal{D}_{x_1}^{\nu_1}(u), {}_{x_1} \mathcal{D}_{b_1}^{\nu_1}(v))_{\Omega}|}{\|v\|_{\mathcal{B}^{\tau, \nu_1}(\Omega)}} \\ & \quad + \bar{\beta} \sup_{0 \neq v \in \mathcal{B}^{\tau, \nu_1}(\Omega)} \frac{|({}_{x_1} \mathcal{D}_{b_1}^{\nu_1}(u), a_1 \mathcal{D}_{x_1}^{\nu_1}(v))_{\Omega}| + |(u, v)_{\Omega}|}{\|v\|_{\mathcal{B}^{\tau, \nu_1}(\Omega)}} \\ & \geq \bar{\beta} \tilde{C} \left\{ |u|_{lH^{\tau}((0, T); L^2(\Lambda_1))} + |u|_{cH^{\nu_1}(\Lambda_1; L^2(I))} + \|u\|_{L^2(\Omega)} \right\}, \end{aligned} \quad (2.54)$$

where \tilde{C} is $\min\{C_1, C_2, C_3, C_4\}$ and $\bar{\beta}$ is a positive constant from (2.52). Accordingly,

$$\sup_{0 \neq v \in \mathcal{B}^{\tau, \nu_1}(\Omega)} \frac{|a(u, v)|}{\|v\|_{\mathcal{B}^{\tau, \nu_1}(\Omega)}} \geq \beta \|u\|_{\mathcal{B}^{\tau, \nu_1}(\Omega)}, \quad (2.55)$$

where $\beta = \bar{\beta} \tilde{C}$ is a positive constant and independent of τ, ν_1 , and u . \square

In Theorem 2.5.3, we extend the proof of Theorem 2.5.2 to the corresponding (1+d)-dimensional problem in (2.48).

Theorem 2.5.3. *The inf-sup condition of the bilinear form, defined in (2.48) for any $d \geq 1$, i.e.,*

$$\inf_{0 \neq u \in \mathcal{B}^{\tau, \nu_1, \dots, \nu_d}(\Omega)} \sup_{0 \neq v \in \mathcal{B}^{\tau, \nu_1, \dots, \nu_d}(\Omega)} \frac{|a(u, v)|}{\|v\|_{\mathcal{B}^{\tau, \nu_1, \dots, \nu_d}(\Omega)} \|u\|_{\mathcal{B}^{\tau, \nu_1, \dots, \nu_d}(\Omega)}} \geq \beta > 0, \quad (2.56)$$

holds with $\beta > 0$, where $\Omega = I \times \Lambda_d$ and Assumption 1 holds.

Proof. By Assumption 1,

$$\begin{aligned} |a(u, v)| &\equiv |(0\mathcal{D}_t^\tau u, {}_t\mathcal{D}_T^\tau v)_\Omega| + \sum_{i=1}^d \left(|({}_{a_i}\mathcal{D}_{x_i}^{\mu_i} u, {}_{x_i}\mathcal{D}_{b_i}^{\mu_i} v)_\Omega| + |({}_{x_i}\mathcal{D}_{a_i}^{\mu_i} u, {}_{a_i}\mathcal{D}_{x_i}^{\mu_i} v)_\Omega| \right) \\ &\quad + \sum_{j=1}^d \left(|({}_{a_j}\mathcal{D}_{x_j}^{\nu_j} u, {}_{x_j}\mathcal{D}_{b_j}^{\nu_j} v)_\Omega| + |({}_{x_j}\mathcal{D}_{b_j}^{\nu_j} u, {}_{a_j}\mathcal{D}_{x_j}^{\nu_j} v)_\Omega| \right) + |(u, v)_\Omega|. \end{aligned} \quad (2.57)$$

It follows from (2.27) that for $u \in \mathcal{B}^{\tau, \nu_1, \dots, \nu_d}(\Omega)$ and $v \in \mathfrak{B}^{\tau, \nu_1, \dots, \nu_d}(\Omega)$ we have

$$\begin{aligned} &\sum_{i=1}^d \left(|({}_{a_i}\mathcal{D}_{x_i}^{\nu_i} (u), {}_{x_i}\mathcal{D}_{b_i}^{\nu_i} (v))_\Omega| + |({}_{x_i}\mathcal{D}_{b_i}^{\nu_i} (u), {}_{a_i}\mathcal{D}_{x_i}^{\nu_i} (v))_\Omega| \right) \\ &\geq \tilde{C}_1 \sum_{i=1}^d \left(\|{}_{a_i}\mathcal{D}_{x_i}^{\nu_i} (u)\|_{L^2(\Omega)} \|{}_{x_i}\mathcal{D}_{b_i}^{\nu_i} (v)\|_{L^2(\Omega)} + \|{}_{x_i}\mathcal{D}_{b_i}^{\nu_i} (u)\|_{L^2(\Omega)} \|{}_{a_i}\mathcal{D}_{x_i}^{\nu_i} (v)\|_{L^2(\Omega)} \right). \end{aligned}$$

Thus

$$\begin{aligned} &\sum_{i=1}^d \left(|({}_{a_i}\mathcal{D}_{x_i}^{\nu_i} (u), {}_{x_i}\mathcal{D}_{b_i}^{\nu_i} (v))_\Omega| + |({}_{x_i}\mathcal{D}_{b_i}^{\nu_i} (u), {}_{a_i}\mathcal{D}_{x_i}^{\nu_i} (v))_\Omega| \right) \\ &\geq \tilde{C}_1 \sum_{i=1}^d \left(\|{}_{a_i}\mathcal{D}_{x_i}^{\nu_i} (u)\|_{L^2(\Omega)} + \|{}_{x_i}\mathcal{D}_{b_i}^{\nu_i} (u)\|_{L^2(\Omega)} \right) \\ &\quad \times \sum_{j=1}^d \left(\|{}_{x_j}\mathcal{D}_{b_j}^{\nu_j} (v)\|_{L^2(\Omega)} + \|{}_{a_j}\mathcal{D}_{x_j}^{\nu_j} (v)\|_{L^2(\Omega)} \right) \\ &= \tilde{C}_1 |u|_{L^2(I; \mathcal{X}_d)} |v|_{L^2(I; \mathcal{X}_d)}. \end{aligned} \quad (2.58)$$

where \tilde{C}_1 is a positive constant and independent of u and v_i . Considering Lemma 2.4.8, there exists a positive constant $\tilde{C}_2 > 0$ independent of u and τ such that

$$\begin{aligned} \sup_{0 \neq v \in \mathfrak{B}^{\tau, \nu_1}(\Omega)} \frac{|(0\mathcal{D}_t^\tau u, {}_t\mathcal{D}_T^\tau v)_\Omega|}{|v|_{\mathfrak{B}^{\tau, \nu_1, \dots, \nu_d}(\Omega)}} &\equiv \sup_{0 \neq v \in \mathfrak{B}^{\tau, \nu_1, \dots, \nu_d}(\Omega)} \frac{|(0\mathcal{D}_t^\tau u, {}_t\mathcal{D}_T^\tau v)_\Omega|}{|v|_{rH^\tau((0,T); L^2(\Lambda_d))}} \\ &\geq \tilde{C}_2 |u|_{lH^\tau((0,T); L^2(\Lambda_d))}. \end{aligned} \quad (2.59)$$

It follows from (2.58) and (2.59) that

$$\begin{aligned}
& \sup_{0 \neq v \in \mathfrak{B}^{\tau, \nu_1, \dots, \nu_d}(\Omega)} \frac{|a(u, v)|}{\|v\|_{\mathfrak{B}^{\tau, \nu_1, \dots, \nu_d}(\Omega)}} \\
& \geq \bar{\beta} \sup_{0 \neq v \in \mathfrak{B}^{\tau, \nu_1, \dots, \nu_d}(\Omega)} \frac{|(0 \mathcal{D}_t^\tau u, {}_t \mathcal{D}_T^\tau v)_\Omega|}{\|v\|_{\mathfrak{B}^{\tau, \nu_1, \dots, \nu_d}(\Omega)}} \\
& + \bar{\beta} \sup_{0 \neq v \in \mathfrak{B}^{\tau, \nu_1, \dots, \nu_d}(\Omega)} \frac{\sum_{j=1}^d \left(|(a_j \mathcal{D}_{x_j}^{\nu_j} u, {}_{x_j} \mathcal{D}_{b_j}^{\nu_j} v)_\Omega| + |({}_{x_j} \mathcal{D}_{b_j}^{\nu_j} u, {}_{a_j} \mathcal{D}_{x_j}^{\nu_j} v)_\Omega| \right)}{\|v\|_{\mathfrak{B}^{\tau, \nu_1, \dots, \nu_d}(\Omega)}} \\
& \geq \bar{\beta} \left(\tilde{C}_2 \|u\|_{l_{H^\tau}(I; L^2(\Lambda_d))} + \tilde{C}_1 \|u\|_{L^2(I; \mathcal{X}_d)} + \|u\|_{L^2(\Omega)} \right) \\
& \geq \bar{\beta} \bar{C} \|u\|_{\mathcal{B}^{\tau, \nu_1, \dots, \nu_d}(\Omega)},
\end{aligned} \tag{2.60}$$

where $\bar{C} = \min\{\tilde{C}_2, \tilde{C}_1\}$ and also $\bar{\beta} > 0$ form (2.57). Therefore,

$$\inf_{0 \neq u \in \mathcal{B}^{\tau, \nu_1, \dots, \nu_d}(\Omega)} \sup_{0 \neq v \in \mathfrak{B}^{\tau, \nu_1, \dots, \nu_d}(\Omega)} \frac{|a(u, v)|}{\|u\|_{\mathcal{B}^{\tau, \nu_1, \dots, \nu_d}(\Omega)} \|v\|_{\mathfrak{B}^{\tau, \nu_1, \dots, \nu_d}(\Omega)}} \geq \beta, \tag{2.61}$$

where $\beta = \bar{\beta} \bar{C}$ is a positive constant and independent of u and τ . \square

Theorem 2.5.4. (well-posedness) For all $0 < \tau < 2$, $2\tau \neq 1$, and $1 < 2\nu_i < 2$, and $i = 1, \dots, d$, there exists a unique solution to (2.49), which is continuously dependent on $f \in (\mathcal{B}^{\tau, \nu_1, \dots, \nu_d})^*(\Omega)$, where $(\mathcal{B}^{\tau, \nu_1, \dots, \nu_d})^*(\Omega)$ is the dual space of $\mathcal{B}^{\tau, \nu_1, \dots, \nu_d}(\Omega)$ and Assumption 1 holds.

Proof. The continuity and the inf-sup condition, which are proven in Lemmas 2.5.1 and Theorem 2.5.3 respectively, yield the well-posedness of the weak form in (2.49) in $(1+d)$ -dimension due to the generalized Babuška-Lax-Milgram theorem [62]. \square

2.6 Discrete Form Formulation

We choose proper subspaces of $\mathcal{B}^{\tau, \nu_1, \dots, \nu_d}(\Omega)$ and $\mathfrak{B}^{\tau, \nu_1, \dots, \nu_d}(\Omega)$ as finite dimensional U_N and V_N with $\dim(U_N) = \dim(V_N) = N$. Now, the discrete problem reads: find $u_N \in U_N$ such that

$$a(u_N, v_N) = (f, v_N), \quad \forall v_N \in V_N. \tag{2.62}$$

By representing u_N as a linear combination of points/elements in U_N , i.e., the corresponding $(1+d)$ -dimensional space-time basis functions, the finite-dimensional problem (2.62) leads to a

linear system known as *Lyapunov* system. For instance, when $d = 1$, we obtain the corresponding Lyapunov equation in the space-time domain $(0, T) \times (a_1, b_1)$ as

$$\begin{aligned} S_\tau \mathcal{U} M_1^T + c_{l1} M_\tau \mathcal{U} S_{\mu_1, l}^T + c_{r1} M_\tau \mathcal{U} S_{\mu_1, r}^T \\ - \kappa_{l1} M_\tau \mathcal{U} S_{\nu_1, l}^T - \kappa_{r1} M_\tau \mathcal{U} S_{\nu_1, r}^T + \gamma M_\tau \mathcal{U} M_1^T = F, \end{aligned} \quad (2.63)$$

where all are defined in 2.7. To find the general form of Lyapunov equation, we can define S^{Tot} as

$$-\kappa_{l1} S_{\nu_1, l} - \kappa_{r1} S_{\nu_1, r} + c_{l1} S_{\mu_1, l} + c_{r1} S_{\mu_1, r} = S_1^{Tot}. \quad (2.64)$$

Considering equation (2.64), we obtain the (1+1)-D space-time Lyapunov system as

$$S_\tau \mathcal{U} M_1^T + M_\tau \mathcal{U} S_1^{TotT} + \gamma M_\tau \mathcal{U} M_1^T = F.$$

We present a new class of basis and test functions yielding *symmetric* stiffness matrices. Moreover, we compute exactly the corresponding mass matrices, which are either *symmetric* and *pentadiagonal*. In the following, we extensively study the properties of the aforementioned matrices, allowing us to formulate a general fast linear solver.

2.6.1 Space of Basis Functions (U_N)

We construct the basis for the spatial discretization employing the Legendre polynomials defined as

$$\phi_m(\xi) = \sigma_m (P_{m+1}(\xi) - P_{m-1}(\xi)), \quad m = 1, 2, \dots \quad \text{and } \xi \in [-1, 1], \quad (2.65)$$

where $\sigma_m = 2 + (-1)^m$. The definition reflects the fact that for $\mu_j \leq 1/2$ and $1/2 \leq \nu_j \leq 1$, then both boundary conditions needs to be presented. Naturally, for the temporal basis functions only initial conditions are prescribed and the basis function for the temporal discretization is constructed based on the univariate poly-fractonomials [56] as

$$\psi_n^\tau(\eta) = \sigma_n (1 + \eta)^\tau P_{n-1}^{-\tau, \tau}(\eta), \quad n = 1, 2, \dots \quad \text{and } \eta \in [-1, 1], \quad (2.66)$$

for $n \geq 1$. With the notation established, we define the space-time trial space to be

$$U_N = \text{span} \left\{ \left(\psi_n^\tau \circ \eta \right)(t) \prod_{j=1}^d \left(\phi_{m_j} \circ \xi_j \right)(x_j) : n = 1, \dots, N, m_j = 1, \dots, M_j \right\}, \quad (2.67)$$

where $\eta(t) = 2t/T - 1$ and $\xi_j(s) = 2\frac{s-a_j}{b_j-a_j} - 1$.

2.6.2 Space of Test Functions (V_N)

We construct the *spatial* test functions using Legendre polynomial as well as the basis function in the Petrov-Galerkin method as

$$\Phi_k(\xi) = \tilde{\sigma}_k (P_{k+1}(\xi) - P_{k-1}(\xi)), \quad k = 1, 2, \dots \quad \text{and} \quad \xi \in [-1, 1], \quad (2.68)$$

where $\tilde{\sigma}_k = 2(-1)^k + 1$. Next, we define the *temporal* test functions using the univariate polyfractonomials

$$\Psi_r^\tau(\eta) = \tilde{\sigma}_r (1-\eta)^\tau P_{r-1}^{\tau, -\tau}(\eta), \quad r = 1, 2, \dots \quad \text{and} \quad \eta \in [-1, 1], \quad (2.69)$$

and we construct the corresponding space-time test space as

$$V_N = \text{span} \left\{ \left(\Psi_r^\tau \circ \eta \right)(t) \prod_{j=1}^d \left(\Phi_{k_j} \circ \xi_j \right)(x_j) : r = 1, \dots, N, k_j = 1, \dots, M_j \right\}. \quad (2.70)$$

Remark 2.6.1. *The choices of σ_m in (2.65) and (2.66), also $\tilde{\sigma}_k$ in (2.68) and (2.69), result in the spatial/temporal mass and stiffness matrices being symmetric, which are discussed in Theorems 2.7.1, 2.7.2, and 2.7.3 in more details.*

2.7 Implementation of PG Spectral Method

We now seek the solution to (2.14) in terms of a linear combination of elements in the space U_N of the form

$$u_N(x, t) = \sum_{n=1}^N \sum_{m_1=1}^{M_1} \cdots \sum_{m_d=1}^{M_d} \hat{u}_{n,m_1, \dots, m_d} \left[\psi_n^\tau(t) \prod_{j=1}^d \phi_{m_j}(x_j) \right] \quad (2.71)$$

in Ω . We enforce the corresponding residual

$$\begin{aligned}
R_N(t, x_1, \dots, x_d) &= {}_0\mathcal{D}_t^{2\tau} u_N + \sum_{i=1}^d [c_{l_i} {}_{a_i} \mathcal{D}_{x_i}^{2\mu_i} u_N + c_{r_i} {}_{x_i} \mathcal{D}_{b_i}^{2\mu_i} u_N] \\
&\quad - \sum_{j=1}^d [\kappa_{l_j} {}_{a_j} \mathcal{D}_{x_j}^{2\nu_j} u_N + \kappa_{r_j} {}_{x_j} \mathcal{D}_{b_j}^{2\nu_j} u_N] \\
&\quad + \gamma u_N - f
\end{aligned} \tag{2.72}$$

to be L^2 -orthogonal to $v_N \in V_N$, which leads to the finite-dimensional variational weak form in (2.62). Specifically, by choosing $v_N = \Psi_r^\tau(t) \prod_{j=1}^d \Phi_{k_j}(x_j)$, when $r = 1, \dots, N$ and $k_j = 1, \dots, \mathcal{M}_j$, $j = 1, 2, \dots, d$, we have

$$\begin{aligned}
&\sum_{n=1}^N \sum_{m_1=1}^{\mathcal{M}_1} \dots \sum_{m_d=1}^{\mathcal{M}_d} \hat{u}_{n,m_1, \dots, m_d} \left(\{S_\tau\}_{r,n} \{M_1\}_{k_1,m_1} \dots \{M_d\}_{k_d,m_d} \right. \\
&\quad + \sum_{i=1}^d [c_{l_i} \{M_\tau\}_{r,n} \{M_1\}_{k_1,m_1} \dots \{S_{v_i,l}\}_{k_i,m_i} \dots \{M_d\}_{k_d,m_d}] \\
&\quad + c_{r_i} \{M_\tau\}_{r,n} \{M_1\}_{k_1,m_1} \dots \{S_{v_i,r}\}_{k_i,m_i} \dots \{M_d\}_{k_d,m_d}] \\
&\quad - \sum_{j=1}^d [\kappa_{l_j} \{M_\tau\}_{r,n} \{M_1\}_{k_1,m_1} \dots \{S_{v_j,l}\}_{k_j,m_j} \dots \{M_d\}_{k_d,m_d}] \\
&\quad + \kappa_{r_j} \{M_\tau\}_{r,n} \{M_1\}_{k_1,m_1} \dots \{S_{v_j,r}\}_{k_j,m_j} \dots \{M_d\}_{k_d,m_d}] \\
&\quad \left. + \gamma \{M_\tau\}_{r,n} \{M_1\}_{k_1,m_1} \dots \{M_d\}_{k_d,m_d} \right) \\
&= F_{r,k_1, \dots, k_d},
\end{aligned}$$

where S_τ and M_τ denote, respectively, the temporal stiffness and mass matrices whose entries are defined as

$$\{S_\tau\}_{r,n} = \int_0^T {}_0\mathcal{D}_t^\tau (\psi_n^\tau \circ \eta)(t) {}_T\mathcal{D}_T^\tau (\Psi_r^\tau \circ \eta)(t) dt,$$

and

$$\{M_\tau\}_{r,n} = \int_0^T (\Psi_r^\tau \circ \eta)(t) (\psi_n^\tau \circ \eta)(t) dt.$$

Moreover, S_{μ_j} and M_{μ_j} , $j = 1, 2, \dots, d$, are the corresponding spatial stiffness and mass matrices where the left-sided and right-sided entries of the spatial stiffness matrices are obtained as

$$\begin{aligned}\{S_{\mu_j,l}\}_{k_j,m_j} &= \int_{a_j}^{b_j} a_j \mathcal{D}_{x_j}^{\mu_j} (\phi_{m_j} \circ \xi_j)(x_j) x_j \mathcal{D}_{b_j}^{\mu_j} (\Phi_{k_j} \circ \xi_j)(x_j) dx_j = \{S_{\mu_j}\}_{k_j,m_j}, \\ \{S_{\mu_j,r}\}_{k_j,m_j} &= \int_{a_j}^{b_j} x_j \mathcal{D}_{b_j}^{\mu_j} (\phi_{m_j} \circ \xi_j)(x_j) a_j \mathcal{D}_{x_j}^{\mu_j} (\Phi_{k_j} \circ \xi_j)(x_j) dx_j = \{S_{\mu_j}\}_{k_j,m_j}^T,\end{aligned}$$

and the corresponding entries of the spatial mass matrix are given by

$$\{M_j\}_{k_j,m_j} = \int_{a_j}^{b_j} (\Phi_{k_j} \circ \xi_j)(x_j) (\phi_{m_j} \circ \xi_j)(x_j) dx_j.$$

Moreover, the components of the load vector are computed as

$$F_{r,k_1, \dots, k_d} = \int_{\Omega} f(t, x_1, \dots, x_d) (\Psi_r^\tau \circ \eta)(t) \prod_{j=1}^d (\Phi_{k_j} \circ \xi_j)(x_j) d\Omega. \quad (2.73)$$

The linear system (2.73) can be exhibited as the following general Lyapunov equation

$$\begin{aligned} & \left(S_\tau \otimes M_1 \otimes M_2 \cdots \otimes M_d \right. \\ & + \sum_{i=1}^d c_{l_i} M_\tau \otimes M_1 \otimes \cdots \otimes S_{\mu_i,l} \otimes M_{i+1} \cdots \otimes M_d \\ & + \sum_{i=1}^d c_{r_i} M_\tau \otimes M_1 \otimes \cdots \otimes S_{\mu_i,r} \otimes M_{i+1} \cdots \otimes M_d \\ & - \sum_{i=1}^d \kappa_{l_i} M_\tau \otimes M_1 \otimes \cdots \otimes S_{\nu_i,l} \otimes M_{i+1} \cdots \otimes M_d \\ & - \sum_{i=1}^d \kappa_{r_i} M_\tau \otimes M_1 \otimes \cdots \otimes S_{\nu_i,r} \otimes M_{i+1} \cdots \otimes M_d \\ & \left. + \gamma M_\tau \otimes M_1 \otimes M_2 \cdots \otimes M_d \right) \mathcal{U} = F.\end{aligned} \quad (2.74)$$

Let

$$c_{l_i} \times S_{\mu_i,l} + c_{r_i} \times S_{\mu_i,r} - \kappa_{l_i} \times S_{\nu_i,l} - \kappa_{r_i} \times S_{\nu_i,r} = S_i^{Tot}. \quad (2.75)$$

Considering the fact that all the aforementioned stiffness and mass matrices are *symmetric*, $S_{\mu_i,l}$, $S_{\mu_i,r}$, $S_{\nu_i,l}$, and $S_{\nu_i,r}$ can be replaced by S_i^{Tot} which remains symmetric. Therefore,

$$\begin{aligned} & \left(S_\tau \otimes M_1 \otimes M_2 \cdots \otimes M_d \right. \\ & + \sum_{i=1}^d [M_\tau \otimes M_1 \otimes \cdots \otimes M_{i-1} \otimes S_i^{Tot} \otimes M_{i+1} \cdots \otimes M_d] \\ & \left. + \gamma M_\tau \otimes M_1 \otimes M_2 \cdots \otimes M_d \right) \mathcal{U} = F, \end{aligned} \quad (2.76)$$

in which \otimes represents the Kronecker product, F denotes the multi-dimensional load matrix whose entries are given in (2.73), and \mathcal{U} denotes the corresponding multi-dimensional matrix of unknown coefficients with entries $\hat{u}_{n,m_1,\dots,m_d}$.

In the Theorems 2.7.1, 2.7.2, and 2.7.3, we study the properties of the aforementioned matrices. Besides, we present efficient ways of deriving the spatial mass and the temporal stiffness matrices analytically and exact computation of the temporal mass and the spatial stiffness matrices through proper quadrature rules.

Theorem 2.7.1. *The temporal stiffness matrix S_τ corresponding to the time-fractional order $\tau \in (0, 1)$ is a diagonal $N \times N$ matrix, whose entries are obtained as*

$$\{S_\tau\}_{r,n} = \tilde{\sigma}_r \sigma_n \frac{\Gamma(n+\tau)}{\Gamma(n)} \frac{\Gamma(r+\tau)}{\Gamma(r)} \left(\frac{2}{T}\right)^{2\tau-1} \frac{2}{2n-1} \delta_{r,n}, \quad r, n = 1, 2, \dots, N.$$

Moreover, the entries of temporal mass matrices M_τ can be computed exactly by employing a Gauss-Lobatto-Jacobi (GLJ) rule with respect to the weight function $(1-\eta)^\tau (1+\eta)^\tau$, $\eta \in [-1, 1]$, where $\alpha = \tau/2$. Moreover, M_τ is symmetric.

Proof. See [55]. □

Theorem 2.7.2. *The spatial mass matrix M is a pentadiagonal $M \times M$ matrix, whose entries are explicitly given as*

$$M_{k,r} = \tilde{\sigma}_k \sigma_r \left[\frac{2}{2k+3} \delta_{k,r} - \frac{2}{2k+3} \delta_{k+1,r-1} - \frac{2}{2k-3} \delta_{k-1,r+1} + \frac{2}{2k-3} \delta_{k-1,r-1} \right]. \quad (2.77)$$

Proof. The (k, r) th-entry of the spatial mass matrix is given by

$$M_{k,r} = \int_a^b \phi_r \circ \xi(x) \Phi_k \circ \xi(x) dx = \left(\frac{b-a}{2}\right) \int_{-1}^1 \phi_r(\xi) \Phi_k(\xi) d\xi, \quad (2.78)$$

where $\xi = 2\frac{x-a}{b-a} - 1$ and $\xi \in (-1, 1)$. Substituting the spatial basis/test functions, we have

$$M_{k,r} = \left(\frac{b-a}{2}\right) \tilde{\sigma}_k \sigma_r [\tilde{M}_{k,r} - \tilde{M}_{k+1,r-1} - \tilde{M}_{k-1,r+1} + \tilde{M}_{k,r}], \quad (2.79)$$

in which

$$\tilde{M}_{i,j} = \int_{-1}^1 P_i(\xi) P_j(\xi) d\xi = \frac{2}{2i+1} \delta_{ij}. \quad (2.80)$$

Therefore, we have

$$M_{k,r} = \left(\frac{b-a}{2}\right) \tilde{\sigma}_k \sigma_r \left[\frac{2}{2k+3} \delta_{k,r} - \frac{2}{2k+3} \delta_{k+1,r-1} - \frac{2}{2k-3} \delta_{k-1,r+1} + \frac{2}{2k-3} \delta_{k,r} \right]$$

as a pentadiagonal matrix. Moreover,

$$\begin{aligned} M_{r,k} &= \left(\frac{b-a}{2}\right) \tilde{\sigma}_r \sigma_k \left[\frac{2}{2r+3} \delta_{r,k} - \frac{2}{2r+3} \delta_{r+1,k-1} - \frac{2}{2r-3} \delta_{r-1,k+1} + \frac{2}{2r-3} \delta_{r,k} \right] \\ &= M_{k,r}. \end{aligned}$$

□

Theorem 2.7.3. *The total spatial stiffness matrix S_i^{Tot} is symmetric and its entries can be exactly computed as:*

$$c_{l_i} \times S_{\mu_i,l} + c_{r_i} \times S_{\mu_i,r} - \kappa_{l_i} \times S_{\nu_i,l} - \kappa_{r_i} \times S_{\nu_i,r} = S_i^{Tot}, \quad (2.81)$$

where $i = 1, 2, \dots, d$.

Proof. Regarding the definition of stiffness matrix, we have

$$\begin{aligned} \{S_{\mu_i,l}\}_{r,n} &= \int_{a_i}^{b_i} a_i \mathcal{D}_{x_i}^{\mu_i} (\phi_n \circ \xi_i(x_i))_{x_i} \mathcal{D}_{b_i}^{\mu_i} (\Phi_r \circ \xi_i(x_i)) dx_i, \\ &= \left(\frac{b_i - a_i}{2}\right)^{-2\mu_i+1} \tilde{\sigma}_r \sigma_n \int_{-1}^1 \mathcal{D}_{\xi_i}^{\mu_i} (P_{n+1}(\xi_i) - P_{n-1}(\xi_i)) \times \\ &\quad \xi_i \mathcal{D}_1^{\mu_i} (P_{k+1}(\xi_i) - P_{k-1}(\xi_i)) d\xi_i \\ &= \left(\frac{b_i - a_i}{2}\right)^{-2\mu_i+1} \tilde{\sigma}_r \sigma_n \left[\tilde{S}_{r+1,n+1}^{\mu_i} - \tilde{S}_{r+1,n-1}^{\mu_i} - \tilde{S}_{r-1,n+1}^{\mu_i} + \tilde{S}_{r-1,n-1}^{\mu_i} \right], \end{aligned}$$

where

$$\begin{aligned}\tilde{S}_{r,n}^{\mu_i} &= \int_{-1}^1 -1 \mathcal{D}_{\xi_i}^{\mu_i} \left(P_n(\xi_i) \right) \xi_i \mathcal{D}_1^{\mu_i} \left(P_r(\xi_i) \right) d\xi_i \\ &= \int_{-1}^1 \frac{\Gamma(r+1)}{\Gamma(r-\mu_i+1)} \frac{\Gamma(n+1)}{\Gamma(n-\mu_i+1)} (1+\xi_i)^{-\mu_i} (1-\xi_i)^{-\mu_i} P_r^{-\mu_i, \mu_i}(\xi_i) P_n^{\mu_i, -\mu_i}(\xi_i) d\xi_i.\end{aligned}$$

$\tilde{S}_{r,n}^{\mu_i}$ can be computed accurately using Guass-Jacobi quadrature rule as

$$\tilde{S}_{r,n}^{\mu_i} = \frac{\Gamma(r+1)}{\Gamma(r-\mu_i+1)} \frac{\Gamma(n+1)}{\Gamma(n-\mu_i+1)} \sum_{q=1}^Q w_q P_r^{-\mu_i, \mu_i}(\xi_q) P_n^{\mu_i, -\mu_i}(\xi_q), \quad (2.82)$$

in which $Q \geq N + 2$ represents the minimum number of GJ quadrature points $\{\xi_q\}_{q=1}^Q$, associated with the weigh function $(1-\xi_q)^{-\mu_i}(1+\xi_q)^{-\mu_i}$, for *exact* quadrature, and $\{w_q\}_{q=1}^Q$ are the corresponding quadrature weights. Employing the property of the Jacobi polynomials where $P_n^{\alpha, \beta}(-x_i) = (-1)^n P_n^{\beta, \alpha}(x_i)$, we can re-express $\tilde{S}_{r,n}^{\mu_i}$ as $(-1)^{(r+n)} \tilde{S}_{n,r}^{\mu_i}$. Accordingly,

$$\begin{aligned}\{S_{\mu_i}\}_{r,n} &= \left(\frac{b_i - a_i}{2} \right)^{-2\mu_i+1} \tilde{\sigma}_r \sigma_n \left[(-1)^{(n+r+2)} \tilde{S}_{n+1,r+1}^{\mu_i} - (-1)^{(n+r)} \tilde{S}_{n+1,r-1}^{\mu_i} \right. \\ &\quad \left. - (-1)^{(n+r)} \tilde{S}_{n-1,r+1}^{\mu_i} + (-1)^{(n+r-2)} \tilde{S}_{n-1,r-1}^{\mu_i} \right] \\ &= \tilde{\sigma}_r \sigma_n (-1)^{(n+r)} \left[\tilde{S}_{n+1,r+1}^{\mu_i} - \tilde{S}_{n+1,r-1}^{\mu_i} - \tilde{S}_{n-1,r+1}^{\mu_i} + \tilde{S}_{n-1,r-1}^{\mu_i} \right].\end{aligned} \quad (2.83)$$

According to (2.83),

$$\{S_{\mu_i}\}_{r,n} = \{S_{\mu_i}\}_{n,r} \times \frac{\tilde{\sigma}_r \sigma_n}{\tilde{\sigma}_n \sigma_r} (-1)^{(n+r)}. \quad (2.84)$$

In fact, $\tilde{\sigma}_r$ and σ_n are chosen such that $(-1)^{(n+r)}$ is canceled. Furthermore,

$$\begin{aligned}\{S_{\mu_i,r}\}_{r,n} &= \int_{a_i}^{b_i} a_i \mathcal{D}_{x_i}^{\mu_i} \left(\Phi_r(x_i) \right) x_i \mathcal{D}_{b_i}^{\mu_i} \left(\phi_n(x_i) \right) dx_i, \\ &= \int_{a_i}^{b_i} a_i \mathcal{D}_{x_i}^{\mu_i} \left(\phi_n(x_i) \right) x_i \mathcal{D}_{b_i}^{\mu_i} \left(\Phi_r(x_i) \right) dx_i, \\ &= \{S_{\mu_i,l}\}_{n,r},\end{aligned} \quad (2.85)$$

where $\{S_{\mu_i,l}\}_{n,r} = \{S_{\mu_i,l}\}_{r,n} = \{S_{\mu_i,r}\}_{r,n} = \{S_{\mu_i}\}_{r,n}$ due to symmetry of $S_{\mu_i,l}$ and $S_{\mu_i,r}$. Similar to (2.85), we get $\{S_{\nu_i,l}\}_{r,n} = \{S_{\nu_i,r}\}_{r,n} = \{S_{\nu_i}\}_{r,n}$; therefore,

$$-(\kappa_{l_i} + \kappa_{r_i}) S_{\nu_i} + (c_{l_i} + c_{r_i}) S_{\mu_i} = S_i^{Tot}. \quad (2.86)$$

Hence it can be easily concluded that the stiffness matrix $S_{n,r}^{\mu_i}$, $S_{n,r}^{\nu_i}$ and thereby $\{S_i^{Tot}\}_{n,r}$ as the sum of two symmetric matrices are symmetric. \square

2.8 Unified Fast FPDE Solver

We formulate a closed-form solution for the Lyapunov system (2.76) in terms of the generalised eigensolutions that can be computed very efficiently, leading to the following unified fast solver for the development of Petrov-Galerkin spectral method.

Theorem 2.8.1. *Let $\{\vec{e}^j, \lambda^j\}_{m_j=1}^{\mathcal{M}_j}$ be the set of general eigen-solutions of the spatial stiffness matrix S_j^{Tot} with respect to the mass matrix M_j . Moreover, let $\{\vec{e}^\tau, \lambda^\tau\}_{n=1}^N$ be the set of general eigen-solutions of the temporal mass matrix M_τ with respect to the stiffness matrix S_τ . (I) if $d > 1$, then the multi-dimensional matrix of unknown coefficients \mathcal{U} is explicitly obtained as*

$$\mathcal{U} = \sum_{n=1}^N \sum_{m_1=1}^{\mathcal{M}_1} \cdots \sum_{m_d=1}^{\mathcal{M}_d} \kappa_{n,m_1, \dots, m_d} \vec{e}_n^\tau \otimes \vec{e}_{m_1}^1 \otimes \cdots \otimes \vec{e}_{m_d}^d, \quad (2.87)$$

where $\kappa_{n,m_1, \dots, m_d}$ are given by

$$\kappa_{n,m_1, \dots, m_d} = \frac{(\vec{e}_n^\tau \vec{e}_{m_1}^1 \cdots \vec{e}_{m_d}^d)F}{\left[(\vec{e}_n^\tau S_\tau \vec{e}_n^\tau) \prod_{j=1}^d ((\vec{e}_{m_j}^j)^T M_j \vec{e}_{m_j}^j) \right] \Lambda_{n,m_1, \dots, m_d}}, \quad (2.88)$$

in which the numerator represents the standard multi-dimensional inner product, and $\Lambda_{n,m_1, \dots, m_d}$ are obtained in terms of the eigenvalues of all mass matrices as

$$\Lambda_{n,m_1, \dots, m_d} = \left[(1 + \gamma \lambda_n^\tau) + \lambda_n^\tau \sum_{j=1}^d (\lambda_{m_j}^j) \right].$$

(II) If $d = 1$, then the two-dimensional matrix of the unknown solution \mathcal{U} is obtained as

$$\mathcal{U} = \sum_{n=1}^N \sum_{m_1=1}^{\mathcal{M}_1} \kappa_{n,m_1} \vec{e}_n^\tau (\vec{e}_{m_1}^1)^T,$$

where κ_{n,m_1} is explicitly obtained as

$$\kappa_{n,m_1} = \frac{\vec{e}_n^\tau F \vec{e}_{m_1}^1}{(\vec{e}_n^\tau S_\tau \vec{e}_n^\tau)((\vec{e}_{m_1}^1)^T M_1 \vec{e}_{m_1}^1) \left[(1 + \gamma \lambda_n^\tau) + \lambda_n^\tau \lambda_{m_1}^1 \right]}.$$

Proof. Let us consider the following generalised eigenvalue problems as

$$S_j^{Tot} \vec{e}_{m_j}^j = \lambda_{m_j}^j M_j \vec{e}_{m_j}^j, \quad m_j = 1, \dots, \mathcal{M}_j, \quad j = 1, 2, \dots, d, \quad (2.89)$$

and

$$M_\tau \vec{e}_n^\tau = \lambda_n^\tau S_\tau \vec{e}_n^\tau, \quad n = 1, 2, \dots, N. \quad (2.90)$$

Having the spatial and temporal eigenvectors determined in equations (2.90) and (2.89), we can represent the unknown coefficient matrix \mathcal{U} in (2.71) in terms of the aforementioned eigenvectors as

$$\mathcal{U} = \sum_{n=1}^N \sum_{m_1=1}^{M_1} \cdots \sum_{m_d=1}^{M_d} \kappa_{n,m_1, \dots, m_d} \vec{e}_n^\tau \otimes \vec{e}_{m_1}^1 \otimes \cdots \otimes \vec{e}_{m_d}^d, \quad (2.91)$$

where $\kappa_{n,m_1, \dots, m_d}$ are obtained as follows. First, we take the multi-dimensional inner product of $\vec{e}_q^\tau \vec{e}_{p_1}^1 \cdots \vec{e}_{p_d}^d$ on both sides of the Lyapunov equation (2.76) as

$$\begin{aligned} & (\vec{e}_q^\tau \vec{e}_{p_1}^1 \vec{e}_{p_2}^2 \cdots \vec{e}_{p_d}^d) \left[S_\tau \otimes M_1 \otimes \cdots \otimes M_d \right. \\ & + \sum_{j=1}^d [M_\tau \otimes M_1 \otimes \cdots \otimes M_{j-1} \otimes S_j^{Tot} \otimes M_{j+1} \cdots \otimes M_d] \\ & \left. + \gamma M_\tau \otimes M_1 \otimes \cdots \otimes M_d \right] \mathcal{U} = (\vec{e}_q^\tau \vec{e}_{p_1}^1 \cdots \vec{e}_{p_d}^d) F. \end{aligned}$$

Then, by replacing (2.89) and (2.90) into (2.88) and re-arranging the terms, we get

$$\begin{aligned} & \sum_{n=1}^N \sum_{m_1=1}^{M_1} \cdots \sum_{m_d=d}^{M_d} \kappa_{n,m_1, \dots, m_d} \times \left(\vec{e}_q^\tau S_\tau \vec{e}_n^\tau (\vec{e}_{p_1}^1)^T M_1 \vec{e}_{m_1}^1 \cdots (\vec{e}_{p_d}^d)^T M_d \vec{e}_{m_d}^d \right. \\ & + \sum_{j=1}^d \vec{e}_q^\tau T M_\tau \vec{e}_n^\tau (\vec{e}_{p_1}^1)^T M_1 \vec{e}_{m_1}^1 \cdots (\vec{e}_{p_j}^j)^T S_j^{Tot} \vec{e}_{m_j}^j (\vec{e}_{p_{j+1}}^{j+1})^T M_{j+1} \vec{e}_{m_{j+1}}^{j+1} \cdots (\vec{e}_{p_d}^d)^T M_d \vec{e}_{m_d}^d \\ & \left. + \gamma \vec{e}_q^\tau T M_\tau \vec{e}_n^\tau (\vec{e}_{p_1}^1)^T M_1 \vec{e}_{m_1}^1 (\vec{e}_{p_2}^2)^T M_2 \vec{e}_{m_2}^2 \cdots (\vec{e}_{p_d}^d)^T M_d \vec{e}_{m_d}^d \right) \\ & = (\vec{e}_q^\tau \vec{e}_{p_1}^1 \vec{e}_{p_2}^2 \cdots \vec{e}_{p_d}^d) F. \end{aligned}$$

Recalling that $S_j^{Tot} \vec{e}_{m_j}^j = (\lambda_{m_j}^j M_j \vec{e}_{m_j}^j)$ and $M_\tau \vec{e}_n^\tau = (\lambda_n^\tau S_\tau \vec{e}_n^\tau)$, we have

$$\begin{aligned} & \sum_{n=1}^N \sum_{m_1=1}^{M_1} \cdots \sum_{m_d=1}^{M_d} \kappa_{n,m_1, \dots, m_d} \left(\vec{e}_q^\tau S_\tau \vec{e}_n^\tau (\vec{e}_{p_1}^1)^T M_1 \vec{e}_{m_1}^1 (\vec{e}_{p_2}^2)^T M_2 \vec{e}_{m_2}^2 \cdots (\vec{e}_{p_d}^d)^T M_d \vec{e}_{m_d}^d \right. \\ & + \sum_{j=1}^d \vec{e}_q^\tau (\lambda_n^\tau S_\tau \vec{e}_n^\tau) (\vec{e}_{p_1}^1)^T M_1 \vec{e}_{m_1}^1 \cdots (\vec{e}_{p_j}^j)^T (\lambda_{m_j}^j M_j \vec{e}_{m_j}^j) \cdots (\vec{e}_{p_d}^d)^T M_d \vec{e}_{m_d}^d \\ & + \left. \gamma \vec{e}_q^\tau (\lambda_n^\tau S_\tau \vec{e}_n^\tau) (\vec{e}_{p_1}^1)^T M_1 \vec{e}_{m_1}^1 (\vec{e}_{p_2}^2)^T M_2 \vec{e}_{m_2}^2 \cdots (\vec{e}_{p_d}^d)^T M_d \vec{e}_{m_d}^d \right) \\ & = (\vec{e}_q^\tau \vec{e}_{p_1}^1 \vec{e}_{p_2}^2 \cdots \vec{e}_{p_d}^d) F. \end{aligned}$$

Therefore,

$$\kappa_{n,m_1,\dots,m_d} = \frac{(\vec{e}_n^\tau \vec{e}_{m_1}^1 \cdots \vec{e}_{m_d}^d)F}{\left[(\vec{e}_n^\tau)^T S_\tau \vec{e}_n^\tau \right] \prod_{j=1}^d ((\vec{e}_{m_j}^j)^T M_j \vec{e}_{m_j}^j)} \times \left[(1 + \gamma \lambda_n^\tau) + \lambda_n^\tau \sum_{j=1}^d (\lambda_{m_j}^j) \right].$$

Then, we have

$$\begin{aligned} \sum_{n=1}^N \sum_{m_1=1}^{M_1} \cdots \sum_{m_d=1}^{M_d} \kappa_{n,m_1,\dots,m_d} (\vec{e}_q^\tau)^T S_\tau \vec{e}_n^\tau ((\vec{e}_{p_1}^1)^T M_1 \vec{e}_{m_1}^1) \cdots ((\vec{e}_{p_d}^d)^T M_d \vec{e}_{m_d}^d) \\ \times \left[(1 + \gamma \lambda_n^\tau) + \lambda_n^\tau \sum_{j=1}^d (\lambda_{m_j}^j) \right] = (\vec{e}_q^\tau \vec{e}_{p_1}^1 \vec{e}_{p_2}^2 \cdots \vec{e}_{p_d}^d) F. \end{aligned}$$

Due to the fact that the spatial Mass M_j and temporal stiffness matrices S_τ are diagonal (see Theorems 2.7.2 and 2.7.1), we have $(\vec{e}_q^\tau)^T S_\tau \vec{e}_n^\tau = 0$ if $q \neq n$, and also $((\vec{e}_{p_j}^j)^T M_j \vec{e}_{m_j}^j) = 0$ if $p_j \neq m_j$, which completes the proof for the case $d > 1$.

Following similar steps for the two-dimensional problem, it is easy to see that if $d = 1$, the relationship for κ can be derived as

$$\kappa_{q,p_1} = \frac{\vec{e}_q^\tau F \vec{e}_{p_1}^1}{(\vec{e}_q^\tau)^T S_\tau \vec{e}_q^\tau ((\vec{e}_{p_1}^1)^T M_1 \vec{e}_{p_1}^1) \left[(1 + \gamma \lambda_n^\tau) + \lambda_n^\tau \lambda_{m_1}^1 \right]}. \quad (2.92)$$

In 2.8.1, we present a computational method for the fast solver which reduces the computational cost significantly. \square

2.8.1 Computational Considerations

Employing the fast solver in $(1+d)$ dimensional problem $d \geq 1$ reduces the dominant computational cost of the eigensolver from $O(N^{2(1+d)})$ to $O(N^{2+d})$, which becomes even more efficient in higher dimensional problems. This approach is extensively discussed in [55].

2.9 Stability and Error Analysis

Theorem 2.9.1. *The Petrov-Galerkin spectral method for (2.62) is stable, i.e.,*

$$\inf_{0 \neq u_N \in U_N} \sup_{0 \neq v \in V_N} \frac{|a(u_N, v_N)|}{\|v_N\|_{\mathcal{B}^{\tau, v_1, \dots, v_d}(\Omega)} \|u_N\|_{\mathcal{B}^{\tau, v_1, \dots, v_d}(\Omega)}} \geq \beta > 0, \quad (2.93)$$

holds with $\beta > 0$ and independent of N , where $\sup_{0 \neq v_N \in V_N} |a(u_N, v_N)| > 0$.

Proof. It is clear that the basis /test spaces are Hilbert spaces. Since $U_N \subset \mathcal{B}^{\tau, \nu_1, \dots, \nu_d}(\Omega)$ and $V_N \subset \mathfrak{B}^{\tau, \nu_1, \dots, \nu_d}(\Omega)$, (2.93) follows directly from Theorem 2.5.4. \square

2.10 Error Analysis

Let $P_{\mathcal{M}}(\Lambda)$ denote the space of all polynomials of degree $\leq \mathcal{M}$ on Λ , where $\Lambda \subset \mathbb{R}$. $P_{\mathcal{M}}^s(\Lambda)$ denotes $P_{\mathcal{M}}(\Lambda) \cap H_0^s(\Lambda)$ for any real positive s , where $H_0^s(\Lambda)$ is the closure of $C_0^\infty(\Lambda)$ in Λ with respect to $\|\cdot\|_{cH^s(\Lambda)}$. In this section, $I_i = (a_i, b_i)$ for $i = 1, \dots, d$, $\Lambda_i = I_i \times \Lambda_{i-1}$, and $\Lambda_i^j = \prod_{\substack{k=1 \\ k \neq j}}^i I_k$.

Theorem 2.10.1. [115] Let r_1 be a real number, where $r_1 \neq \mathcal{M}_1 + \frac{1}{2}$, and $1 \leq r_1$. There exists a projection operator $\Pi_{r_1, \mathcal{M}_1}^{\nu_1}$ from $H^{r_1}(\Lambda_1) \cap H_0^{\nu_1}(\Lambda_1)$ to $P_{\mathcal{M}_1}^{\nu_1}(\Lambda_1)$ such that for any $u \in H^{r_1}(\Lambda_1) \cap H_0^{\nu_1}(\Lambda_1)$, we have $\|u - \Pi_{r_1, \mathcal{M}_1}^{\nu_1} u\|_{cH^{\nu_1}(\Lambda_1)} \leq c_1 \mathcal{M}_1^{\nu_1 - r_1} \|u\|_{H^{r_1}(\Lambda_1)}$, where c_1 is a positive constant.

Maday in [115] proved Theorem 2.10.1 using the error estimate provided in [116] for Legendre and Chebyshev polynomials. Next, this theorem is extended to Jacobi *polyfractonomials* of first kind.

Theorem 2.10.2. [55] Let $r_0 \geq \lceil 2\tau \rceil$, $r_0 \neq \mathcal{N} + \frac{1}{2}$ and $2\tau \in (0, 2)$, $2\tau \neq 1$. There exists an operator $\Pi_{r_0, \mathcal{N}}^\tau$ from $H^{r_0}(I) \cap {}^l H^\tau(I)$ to $P_{\mathcal{N}}^\tau(\Lambda_1)$ such that for any $u \in H^{r_0}(I) \cap {}^l H^\tau(I)$, we have

$$\|u - \Pi_{r_0, \mathcal{N}}^\tau u\|_{{}^l H^\tau(I)} \leq c_0 \mathcal{N}^{\tau - r_0} \|u\|_{H^{r_0}(I)},$$

where c_0 is a positive constant.

Li and Xu in [109] performed the error analysis for the space-time fractional diffusion equation, employing Lagrangian polynomials. Here, employing Theorems 2.10.1 and 2.10.2 and Theorem A.3 from [117], we study the properties of higher-dimensional approximation operators in the following lemmas.

Lemma 2.10.3. Let the real-valued $1 \leq r_1, r_2, I_i = (a_i, b_i)$ $i = 1, 2$, $\Omega = I_1 \times I_2$, and $\frac{1}{2} < \nu_1, \nu_2 < 1$. If $u \in H_0^{\nu_2}(I_2, H^{r_1}(I_1)) \cap H^{r_2}(I_2, H_0^{\nu_1}(I_1))$, then

$$\begin{aligned} & \|u - \Pi_{r_1, \mathcal{M}_1}^{\nu_1} \Pi_{r_2, \mathcal{M}_2}^{\nu_2} u\|_{\mathcal{B}^{\nu_1, \nu_2}(\Omega)} \leq \\ & \mathcal{M}_2^{\nu_2-r_2} \|u\|_{H^{r_2}(I_2, L^2(I_1))} + \mathcal{M}_2^{\nu_2-r_2} \mathcal{M}_1^{-r_1} \|u\|_{H^{r_2}(I_2, H^{r_1}(I_1))} + \mathcal{M}_1^{-r_1} \|u\|_{cH^{\nu_2}(I_2, H^{r_1}(I_1))} \\ & + \mathcal{M}_1^{\nu_1-r_1} \|u\|_{H^{r_1}(I_1, L^2(I_2))} + \mathcal{M}_1^{\nu_1-r_1} \mathcal{M}_2^{-r_2} \|u\|_{H^{r_1}(I_1, H^{r_2}(I_2))} \\ & + \mathcal{M}_2^{-r_2} \|u\|_{cH^{\nu_1}(I_1, H^{r_2}(I_2))}, \end{aligned} \quad (2.94)$$

where $\|\cdot\|_{\mathcal{B}^{\nu_1, \nu_2}(\Omega)} = \{\|\cdot\|_{cH^{\nu_1}(I_1, L^2(I_2))}^2 + \|\cdot\|_{cH^{\nu_2}(I_1, L^2(I_1))}^2\}^{\frac{1}{2}}$, and $\beta > 0$.

Proof. If $u \in H_0^{\nu_2}(I_2, H^{r_1}(I_1)) \cap H^{r_2}(I_2, H_0^{\nu_1}(I_1))$, then evidently $u \in H^{r_2}(I_2, H^{r_1}(I_1))$, $u \in H^{r_2}(I_2, L^2(I_1))$, and $u \in H^{r_1}(I_1, L^2(I_2))$. By the real-valued positive constant β , we have

$$\begin{aligned} & \|u - \Pi_{r_1, \mathcal{M}_1}^{\nu_1} \Pi_{r_2, \mathcal{M}_2}^{\nu_2} u\|_{\mathcal{B}^{\nu_1, \nu_2}(\Omega)} \\ &= \left(\|u - \Pi_{r_1, \mathcal{M}_1}^{\nu_1} \Pi_{r_2, \mathcal{M}_2}^{\nu_2} u\|_{cH^{\nu_2}(I_2, L^2(I_1))}^2 + \|u - \Pi_{r_1, \mathcal{M}_1}^{\nu_1} \Pi_{r_2, \mathcal{M}_2}^{\nu_2} u\|_{L^2(I_2, cH^{\nu_1}(I_1))}^2 \right)^{\frac{1}{2}} \\ &\leq \|u - \Pi_{r_1, \mathcal{M}_1}^{\nu_1} \Pi_{r_2, \mathcal{M}_2}^{\nu_2} u\|_{cH^{\nu_2}(I_2, L^2(I_1))} + \|u - \Pi_{r_1, \mathcal{M}_1}^{\nu_1} \Pi_{r_2, \mathcal{M}_2}^{\nu_2} u\|_{L^2(I_2, cH^{\nu_1}(I_1))}. \end{aligned} \quad (2.95)$$

By Theorem 2.10.1, (2.95) can be simplified to

$$\begin{aligned} & \|u - \Pi_{r_1, \mathcal{M}_1}^{\nu_1} \Pi_{r_2, \mathcal{M}_2}^{\nu_2} u\|_{cH^{\nu_2}(I_2, L^2(I_1))} \\ &= \|u - \Pi_{r_2, \mathcal{M}_2}^{\nu_2} u + \Pi_{r_2, \mathcal{M}_2}^{\nu_2} u - \Pi_{r_1, \mathcal{M}_1}^{\nu_1} \Pi_{r_2, \mathcal{M}_2}^{\nu_2} u\|_{cH^{\nu_2}(I_2, L^2(I_1))} \\ &\leq \|u - \Pi_{r_2, \mathcal{M}_2}^{\nu_2} u\|_{cH^{\nu_2}(I_2, L^2(I_1))} + \|\Pi_{r_2, \mathcal{M}_2}^{\nu_2} u - \Pi_{r_1, \mathcal{M}_1}^{\nu_1} \Pi_{r_2, \mathcal{M}_2}^{\nu_2} u\|_{cH^{\nu_2}(I_2, L^2(I_1))} \\ &\leq \mathcal{M}_2^{\nu_2-r_2} \|u\|_{H^{r_2}(I_2, L^2(I_1))} + \|(\Pi_{r_2, \mathcal{M}_2}^{\nu_2} - \mathcal{I})(u - \Pi_{r_1, \mathcal{M}_1}^{\nu_1} u)\|_{cH^{\nu_2}(I_2, L^2(I_1))} \\ &\quad + \|u - \Pi_{r_1, \mathcal{M}_1}^{\nu_1} u\|_{cH^{\nu_2}(I_2, L^2(I_1))} \\ &\leq \mathcal{M}_2^{\nu_2-r_2} \|u\|_{H^{r_2}(I_2, L^2(I_1))} + \mathcal{M}_2^{\nu_2-r_2} \mathcal{M}_1^{-r_1} \|u\|_{H^{r_2}(I_2, H^{r_1}(I_1))} \\ &\quad + \mathcal{M}_1^{-r_1} \|u\|_{cH^{\nu_2}(I_2, H^{r_1}(I_1))}, \end{aligned} \quad (2.96)$$

where \mathcal{I} is the identity operator.

Since $\|u - \Pi_{r_1, \mathcal{M}_1}^{\nu_1} \Pi_{r_2, \mathcal{M}_2}^{\nu_2} u\|_{L^2(I_2, {}^c H^{\nu_1}(I_1))} = \|u - \Pi_{r_1, \mathcal{M}_1}^{\nu_1} \Pi_{r_2, \mathcal{M}_2}^{\nu_2} u\|_{{}^c H^{\nu_1}(I_1, L^2(I_2))}$, we obtain

$$\begin{aligned}
& \|u - \Pi_{r_1, \mathcal{M}_1}^{\nu_1} \Pi_{r_2, \mathcal{M}_2}^{\nu_2} u\|_{L^2(I_2, {}^c H^{\nu_1}(I_1))} \\
&= \|u - \Pi_{r_1, \mathcal{M}_1}^{\nu_1} u + \Pi_{r_1, \mathcal{M}_1}^{\nu_1} u - \Pi_{r_1, \mathcal{M}_1}^{\nu_1} \Pi_{r_2, \mathcal{M}_2}^{\nu_2} u\|_{{}^c H^{\nu_1}(I_1, L^2(I_2))} \\
&\leq \|u - \Pi_{r_1, \mathcal{M}_1}^{\nu_1} u\|_{{}^c H^{\nu_1}(I_1, L^2(I_2))} + \|\Pi_{r_1, \mathcal{M}_1}^{\nu_1} u - \Pi_{r_1, \mathcal{M}_1}^{\nu_1} \Pi_{r_2, \mathcal{M}_2}^{\nu_2} u\|_{{}^c H^{\nu_1}(I_1, L^2(I_2))} \\
&\leq \mathcal{M}_1^{\nu_1 - r_1} \|u\|_{H^{r_1}(I_1, L^2(I_2))} + \|(\Pi_{r_1, \mathcal{M}_1}^{\nu_1} - \mathcal{I})(u - \Pi_{r_2, \mathcal{M}_2}^{\nu_2} u)\|_{{}^c H^{\nu_1}(I_1, L^2(I_2))} \\
&\quad + \|u - \Pi_{r_2, \mathcal{M}_2}^{\nu_2} u\|_{{}^c H^{\nu_1}(I_1, L^2(I_2))} \\
&\leq \mathcal{M}_1^{\nu_1 - r_1} \|u\|_{H^{r_1}(I_1, L^2(I_2))} + \mathcal{M}_1^{\nu_1 - r_1} \mathcal{M}_2^{-r_2} \|u\|_{H^{r_1}(I_1, H^{r_2}(I_2))} \\
&\quad + \mathcal{M}_2^{-r_2} \|u\|_{{}^c H^{\nu_1}(I_1, H^{r_2}(I_2))}. \tag{2.97}
\end{aligned}$$

Accordingly, (2.94) can be derived immediately from (2.97) and (2.96). \square

In order to perform the error analysis of (1+d)-dimensional PG method, we first study the approximation properties in three dimensions and then extend it to (1+d)-dimensions. It should be noted that in the following lemmas, $H^{r_{i+1}, r_{i+2}, \dots, r_{i+k}}(I_{i+1} \times \dots \times I_{i+k}, L^2(\Lambda_d^{i+1, \dots, i+k})) = H^{r_{i+1}}(I_{i+1}, H^{r_{i+2}}(I_{i+2}, \dots, H^{r_{i+k}}(I_{i+k}, L^2(\Lambda_d^{i+1, \dots, i+k})))$, where $\Lambda_d^{i+1, \dots, i+k} = \prod_{\substack{j=1 \\ k \neq i+1, \dots, i+k}}^d I_j$.

Following Lemma 2.10.3, we introduce

Lemma 2.10.4. *Let the real-valued $1 \leq r_i$, $I_i = (a_i, b_i)$, $\Omega = \prod_{i=1}^d I_i$, $\Lambda_k = \prod_{i=1}^k I_i$, $\Lambda_k^j = \prod_{\substack{i=1 \\ i \neq j}}^k I_i$ and $\frac{1}{2} < \nu_i < 1$ for $i = 1, \dots, d$. If $u \in {}^c H_0^{\nu_1}(I_1, H^{r_2, r_3}(\Lambda_3^1)) \cap H^{r_1, r_3}(\Lambda_3^2, {}^c H_0^{\nu_2}(I_2)) \cap H^{r_1, r_2}(\Lambda_2, {}^c H_0^{\nu_3}(I_3))$, then*

$$\begin{aligned}
& \|u - \Pi_{r_1, \mathcal{M}_1}^{\nu_1} \Pi_{r_2, \mathcal{M}_2}^{\nu_2} \Pi_{r_3, \mathcal{M}_3}^{\nu_3} u\|_{{}^c H^{\nu_i}(I_i, L^2(\Lambda_3^i))} \tag{2.98} \\
&\leq \mathcal{M}_i^{\nu_i - r_i} \|u\|_{H^{r_i}(I_i, L^2(\Lambda_3^i))} + \mathcal{M}_i^{\nu_i - r_i} \mathcal{M}_j^{-r_j} \mathcal{M}_k^{-r_k} \|u\|_{H^{r_i, r_j, r_k}(\Lambda_3)} \\
&\quad + \mathcal{M}_j^{-r_j} \mathcal{M}_k^{-r_k} \|u\|_{{}^c H^{\nu_i}(I_i, H^{r_j}(I_j, L^2(I_k)))} \\
&\quad + \sum_{\substack{j=1 \\ j \neq i}}^3 (\mathcal{M}_i^{\nu_i - r_i} \mathcal{M}_2^{-r_j} \|u\|_{H^{r_i, r_j}(I_i \times I_j, L^2(\Lambda_3^{i,j}))} + \mathcal{M}_j^{-r_j} \|u\|_{{}^c H^{\nu_i}(I_i, H^{r_j}(I_j, L^2(\Lambda_3^{i,j})))})
\end{aligned}$$

for $i = 1, 2, 3$, $j = 1, 2, 3$ and $j \neq i$, and $k = 1, 2, 3$ and $k \neq i, j$, where $\beta > 0$.

Proof. see Appendix A. \square

Lemma 2.10.4 can be easily extended to the d-dimensional approximation operator as

$$\begin{aligned}
\|u - \Pi_d^h u\|_{c H^{\nu_i}(I_i, L^2(\Lambda_d^i))} &\leq \\
&\quad \mathcal{M}_i^{\nu_i - r_i} \|u\|_{H^{r_i}(I_i, L^2(\Lambda_d^i))} + \sum_{\substack{j=1 \\ j \neq i}}^d \mathcal{M}_j^{-r_j} \|u\|_{c H^{\nu_i}(I_i, H^{r_j}(I_j, L^2(\Lambda_d^{i,j})))} \\
&\quad + \mathcal{M}_i^{\nu_i - r_i} \sum_{\substack{j=1 \\ j \neq i}}^d \mathcal{M}_j^{-r_j} \|u\|_{H^{r_i}(I_i, H^{r_j}(I_j, L^2(\Lambda_d^{i,j})))} \\
&\quad + \sum_{\substack{k=1 \\ k \neq i}}^d \sum_{\substack{j=1 \\ j \neq i, k}}^d \mathcal{M}_j^{-r_j} \mathcal{M}_k^{-r_k} \|u\|_{c H^{\nu_i}(I_i, H^{r_k, r_j}(I_k \times I_j, L^2(\Lambda_d^{i,j,k})))} \\
&\quad + \cdots + \mathcal{M}_i^{\nu_i - r_i} \left(\prod_{\substack{j=1 \\ j \neq i}}^d \mathcal{M}_j^{-r_j} \right) \|u\|_{H^{r_i}(I_i, H^{r_1, \dots, r_d}(\Lambda_d^i))}. \tag{2.99}
\end{aligned}$$

Theorem 2.10.5. Let $1 \leq r_i$, $I = (0, T)$, $I_i = (a_i, b_i)$, $\Omega = I \times \left(\prod_{i=1}^d I_i \right)$, $\Lambda_k = \prod_{i=1}^k I_i$, $\Lambda_k^j = \prod_{\substack{i=1 \\ i \neq j}}^k I_i$ and $\frac{1}{2} < \nu_i < 1$ for $i = 1, \dots, d$. If $u \in \left(\bigcap_{i=1}^d H^{r_0}(I, H^{\nu_i}(I_i, H^{r_1, \dots, r_{i-1}, r_{i+1}, \dots, r_d}(\Lambda_d^i))) \right) \cap l H^\tau(I, H^{r_1, \dots, r_d}(\Lambda_d))$, then we have

$$\begin{aligned}
&\|u - \Pi_{r_0, \mathcal{N}}^{\tau} \Pi_d^h u\|_{\mathcal{B}^{\tau, \nu_1, \dots, \nu_d}(\Omega)} \\
&\leq \beta \left(\mathcal{N}^{\tau - r_0} \|u\|_{H^{r_0}(I, L^2(\Lambda_d))} + \sum_{j=1}^d \mathcal{N}^{\tau - r_0} \mathcal{M}_j^{-r_j} \|u\|_{H^{r_0}(I, H^{r_j}(I_j, L^2(\Lambda_d^j)))} + \cdots \right. \\
&\quad \left. + \mathcal{N}^{\tau - r_0} \left(\prod_{j=1}^d \mathcal{M}_j^{-r_j} \right) \|u\|_{H^{r_0}(I, H^{r_1, \dots, r_d}(\Lambda_d))} + \sum_{i=1}^d \left\{ \mathcal{M}_i^{\nu_i - r_i} \|u\|_{H^{r_i}(I_i, L^2(\Lambda_d^{i \times I}))} + \cdots \right. \right. \\
&\quad \left. \left. + \mathcal{M}_i^{\nu_i - r_i} \left(\prod_{\substack{j=1 \\ j \neq i, k}}^d \mathcal{M}_j^{-r_j} \right) \|u\|_{H^{r_i}(I_i, H^{r_1, \dots, r_d}(\Lambda_d^{i, L^2(I)}))} \right\} \right), \tag{2.100}
\end{aligned}$$

where $\Pi_d^h = \Pi_{r_1, \mathcal{M}_1}^{\nu_1} \cdots \Pi_{r_d, \mathcal{M}_d}^{\nu_d}$ and β is a real positive constant.

Proof. Directly from (2.41) we conclude that

$$\|u\|_{\mathcal{B}^{\tau, \nu_1, \dots, \nu_d}(\Omega)} \leq \beta \left(\|u\|_{lH^\tau(I, L^2(\Lambda_d))} + \sum_{i=1}^d \|u\|_{L^2(I, {}^cH^{\nu_i}(I_i, L^2(\Lambda_d^i)))} \right).$$

By Theorem 2.10.2 we obtain

$$\begin{aligned} \|u - \Pi_{r_0, \mathcal{N}}^{\tau} \Pi_d^h u\|_{lH^\tau(I, L^2(\Lambda_d))} &\leq \mathcal{N}^{\tau-r_0} \|u\|_{H^{r_0}(I, L^2(\Lambda_d))} \\ &+ \sum_{j=1}^d \mathcal{N}^{\tau-r_0} \mathcal{M}_j^{-r_j} \|u\|_{H^{r_0}(I, H^{r_j}(I_j, L^2(\Lambda_d)))} + \dots \\ &+ \mathcal{N}^{\tau-r_0} \left(\prod_{j=1}^d \mathcal{M}_j^{-r_j} \right) \|u\|_{H^{r_0}(I, H^{r_1, \dots, r_d}(\Lambda_d))}. \end{aligned} \quad (2.101)$$

Accordingly, the property of composite approximation to time-spatial (1+d)-dimensional space-time approximation operator in (2.100) is obtained immediately using (??) and (2.101).

Remark 2.10.6. Since the inf-sup condition holds (see Theorem 2.9.1), by the Banach-Nečas-Babuška theorem [118] and Lemma 2.5.1, the error in the numerical scheme is less than or equal to a constant times the projection error. Accordingly, we conclude the spectral accuracy of the scheme.

□

2.11 Numerical Tests

To study the convergence rate of the PG method in (2.48), we perform numerical simulations and consider the following relative errors in L^2 as

$$\|e\|_{L^2(\Omega)} = \frac{\|u - u^{ext}\|_{L^2(\Omega)}}{\|u^{ext}\|_{L^2(\Omega)}} \quad (2.102)$$

and in the energy norm as

$$\|e\|_{\mathcal{B}^{\tau, \nu_1}(\Omega)} = \frac{\|u - u^{ext}\|_{\mathcal{B}^{\tau, \nu_1}(\Omega)}}{\|u^{ext}\|_{\mathcal{B}^{\tau, \nu_1}(\Omega)}}, \quad (2.103)$$

where u^{ext} is presented in (2.105) and (2.106) in Case I and Case II respectively. Let $\Omega = (0, T) \times (-1, 1)$. Recalling that

$$\|\cdot\|_{\mathcal{B}^{\tau, \nu_1}(\Omega)} := \left\{ \|\cdot\|_{L^2(\Omega)}^2 + \|{}_0\mathcal{D}_t^\tau(\cdot)\|_{L^2(\Omega)}^2 + \|{}_{-1}\mathcal{D}_{x_1}^{\nu_1}(\cdot)\|_{L^2(\Omega)}^2 + \|{}_{x_1}\mathcal{D}_1^{\nu_1}(\cdot)\|_{L^2(\Omega)}^2 \right\}^{\frac{1}{2}}. \quad (2.104)$$

We particularly consider the time and space-fractional diffusion equation (i.e. $c_l = c_r = 0$ in (2.14)) in 2-D space-time as we have obtained similar results for advection-dispersion equation in higher dimensions.

Case I: We choose the exact solution to be

$$u^{ext}(t, x) = t^{p_1} \times [(1+x)^{p_2} - \epsilon(1+x)^{p_3}], \quad (2.105)$$

in (2.14), where $\epsilon = 2^{p_2-p_3}$. In (2.105), we take $p_1 = 5\frac{1}{20}$, $p_2 = 5\frac{3}{4}$ and $p_3 = 5\frac{1}{5}$.

Table 2.1: Convergence study of the PG spectral method for (1+1)-D diffusion problem, where $\kappa_{l_1} = \kappa_{r_1} = \frac{2}{10}$ and $T = 2$. Besides, $p_1 = 5\frac{1}{20}$, $p_2 = 5\frac{3}{4}$ and $p_3 = 5\frac{1}{5}$ in (2.105). Here, we denote by \bar{r}_0 the practical rate of the convergence, numerically achieved.

Case I-A: $\nu_1 = \frac{15}{20}$ fixed, where we consider the limit orders $\tau = \frac{1}{20}$ and $\tau = \frac{9}{20}$. Case I-B: $\tau = \frac{5}{20}$ fixed, where $\nu_1 = \frac{11}{20}$ and $\nu_1 = \frac{19}{20}$.

Temporal p -refinement Case I-A

$\tau = \frac{1}{20}$ and $\nu_1 = \frac{15}{20}$		$\tau = \frac{9}{20}$ and $\nu_1 = \frac{15}{20}$	
\mathcal{M}_t	$\ e\ _{\mathcal{B}^{\tau, \nu_1}(\Omega)}$	$\ e\ _{L^2(\Omega)}$	$\ e\ _{\mathcal{B}^{\tau, \nu_1}(\Omega)}$
($\bar{r}_0 = 12.81$)	($\bar{r}_0 = 14.09$)		($\bar{r}_0 = 13.32$)
3	0.48488	0.45541	0.65358
5	0.04176	0.04003	0.07529
7	3.44×10^{-5}	2.64×10^{-5}	0.00079
9	5.00×10^{-7}	2.81×10^{-7}	5.03×10^{-7}
11	4.82×10^{-8}	1.45×10^{-8}	4.81×10^{-8}
			2.59×10^{-7}
			6.61×10^{-9}

Spatial p -refinement Case I-B

$\nu_1 = \frac{11}{20}$ and $\tau = \frac{5}{20}$		$\nu_1 = \frac{19}{20}$ and $\tau = \frac{5}{20}$	
\mathcal{M}_s	$\ e\ _{\mathcal{B}^{\tau, \nu_1}(\Omega)}$	$\ e\ _{L^2(\Omega)}$	$\ e\ _{\mathcal{B}^{\tau, \nu_1}(\Omega)}$
($\bar{r}_1 = 9.18$)	($\bar{r}_1 = 9.36$)		($\bar{r}_1 = 8.51$)
3	0.45329	0.40578	0.55657
5	0.01738	0.01259	0.03097
7	4.68×10^{-5}	0.000029	3.08×10^{-5}
9	1.19×10^{-6}	6.96×10^{-7}	2.45×10^{-6}
11	7.09×10^{-8}	5.33×10^{-8}	5.42×10^{-7}
			6.63×10^{-7}
			1.56×10^{-7}

Temporal p -refinement: In Table 2.1 Case I-A, we study the spectral convergence of the method for the limit fractional orders of $\tau = \frac{1}{20}$ and $\frac{9}{20}$, while $\nu_1 = \frac{15}{20}$ fixed and $\kappa_{l_1} = \kappa_{r_1} = \frac{2}{10}$ in (2.14) for (1+1)-D diffusion problem. In the temporal p -refinement, we keep the spatial order of expansion fixed ($\mathcal{M}_s = 19$) such that the error in spatial direction approaches to the exact solution sufficiently and hence the rate of the convergence is a function of the minimum regularity in time direction. Theoretically, the rate of convergence is bounded by $\mathcal{M}_t^{\tau-r_0} \|u\|_{H^{r_0}(I, L^2(\Lambda_1))}$, where $r_0 = p_1 + \frac{1}{2} - \epsilon$ is the minimum regularity of the exact solution in time direction. In Table 2.1 we observe that \bar{r}_0 in $\|e\|_{L^2(\Omega)}$ and $\|e\|_{\mathcal{B}^{\tau, \nu_1}(\Omega)}$ are greater than $r_0 \approx 5\frac{11}{20}$. Accordingly, $\|e\|_{L^2(\Omega)} \leq \mathcal{M}_t^{-\tau} \|e\|_{\mathcal{B}^{\tau, \nu_1}(\Omega)} \leq \mathcal{M}_t^{-r_0} \|u\|_{H^{r_0}(I, L^2(\Lambda_1))}$.

Spatial p -refinement: We study the convergence rate of the PG method for the limit orders of $\nu_1 = \frac{11}{20}$ and $\frac{19}{20}$ while $\tau = \frac{5}{20}$ in Table 2.1 Case I-B. The temporal order of expansion is constant ($\mathcal{M}_t = 19$) to keep the solution sufficiently accurate in time direction. Similar to temporal p -refinement, we have $\|e\|_{L^2(\Omega)} \leq \mathcal{M}_s^{-\nu_1} \|e\|_{\mathcal{B}^{\tau, \nu_1}(\Omega)} \leq \mathcal{M}_s^{-r_1} \|u\|_{H^{r_1}(\Lambda_1, L^2(I))}$, where $r_1 = p_3 + \frac{1}{2} - \epsilon$ as the minimum regularity of the exact solution in spatial direction. In agreement with Theorem 2.10.5, the practical rates of convergence \bar{r}_1 in $\|e\|_{L^2(\Omega)}$ and in $\|e\|_{\mathcal{B}^{\tau, \nu_1}(\Omega)}$ are greater than $r_1 \approx 5\frac{7}{10}$. Further to the aforementioned cases, we have observed similar results for higher dimensional problems, including (1+2)-D time- and space-fractional diffusion equation as well.

Case II: We consider the smooth exact solution to be

$$u^{ext}(t, x) = t^{p_1} \times \left[\sin(n\pi(1+x)) \right], \quad (2.106)$$

in (2.14), where $p_1 = 5\frac{1}{20}$ and $n = 1$.

p -refinement: The convergence rate of the PG method for the limit orders of $\nu_1 = \frac{11}{20}$ and $\frac{19}{20}$ is investigated while $\tau = \frac{5}{20}$ in Table 2.2. The temporal order of expansion is chosen as ($\mathcal{M}_t = 19$) to keep the solution sufficiently accurate in time direction. The results in Table 2.2 show the expected exponential decay which verifies the PG method for different values of ν_1 .

Table 2.2: Here, we set $p_1 = 5 \frac{1}{20}$ and $n = 1$ in (2.106) to study the convergence of the PG spectral method for (1+1)-D diffusion problem, where $\kappa_{l_1} = \kappa_{r_1} = \frac{2}{10}$ and $T = 2$. Besides, the limit orders are $\nu_1 = \frac{11}{20}$ and $\nu_1 = \frac{19}{20}$, where $\tau = \frac{5}{20}$ is fixed.

<i>p</i> -refinement					
$\nu_1 = \frac{11}{20}$ and $\tau = \frac{5}{20}$			$\nu_1 = \frac{19}{20}$ and $\tau = \frac{5}{20}$		
\mathcal{M}_s	$\ e\ _{\mathcal{B}^{\tau, \nu_1}(\Omega)}$	$\ e\ _{L^2(\Omega)}$	\mathcal{M}_s	$\ e\ _{\mathcal{B}^{\tau, \nu_1}(\Omega)}$	$\ e\ _{L^2(\Omega)}$
5	0.04756	0.02655	5	0.05730	0.03147
9	2.89×10^{-5}	1.60×10^{-5}	9	2.72×10^{-4}	1.54×10^{-4}
13	4.44×10^{-9}	2.46×10^{-9}	13	4.32×10^{-8}	2.44×10^{-8}
17	4.10×10^{-11}	5.90×10^{-12}	17	8.88×10^{-11}	9.17×10^{-12}

CHAPTER 3

A UNIFIED PG METHOD FOR DISTRIBUTED-ORDER FPDES

3.1 Background

In many physical processes, which cannot be characterized with a certain single power-law scaling over the whole domain, distributed-order differential equations (DDEs) can serve as a framework for accommodating a distribution of power law behavior. More specifically, distributed order FPDEs are generating considerable interests in terms of accelerating superdiffusion, decelerating subdiffusion random processes in multi-physics anomalous phenomena. To model wave propagation in complex media like viscoelastic media, acoustics, and seismology, Bazhlekov and Bazhlekov [119] developed a subordination approach to multi-term time fractional diffusion-wave equations. Besides, Chechkin et al. [69] proposed distributed-order temporal fractional diffusion equation for describing the (retarding) sub-diffusion random processes which are subordinated to the Wiener process. A faithful description of such anomalous transport requires exploiting distributed-order derivatives, in which the derivative order has a distribution over a range of values. The reader is referred to [120, 64, 65, 114, 38, 63] and the references given therein for more details on the distributed-order fractional equations.

Numerical methods for FPDEs, which can exhibit history dependence and non-local features have been recently addressed by developing finite-element methods [121, 122], spectral/spectral-element methods [123, 124, 125, 126], and also finite-difference and finite-volume methods [127, 128, 129]. Distributed-order FPDEs impose further complications in numerical analysis by introducing distribution functions, which require compliant underlying function spaces, as well as efficient and accurate integration techniques over the order of the fractional derivatives. In [130, 131, 132, 133], numerical analysis of distributed-order FPDEs was extensively investigated. More recently, Liao et al. [134] studied simulation of a distributed subdiffusion equation, approximating the distributed order Caputo derivative using piecewise-linear and quadratic inter-

polating polynomials. Kharazmi and Zayernouri [135] developed a pseudo-spectral method of Petrov-Galerkin sense, employing nodal expansions in the weak formulation of distributed-order fractional PDEs. In [70], Kharazmi et al. also introduced *distributed Sobolev* space and developed two spectrally accurate schemes, namely, a Petrov–Galerkin spectral method and a spectral collocation method for distributed order fractional differential equations. Besides, Tomovski and Sandev [136] investigated the solution of generalized distributed-order diffusion equations with fractional time-derivative, using the Fourier-Laplace transform method.

The main purpose of this study is to develop and analyze a Petrov-Galerkin (PG) spectral method to solve a $(1 + d)$ -dimensional fully distributed-order FPDE with two-sided derivatives of the form

$$\begin{aligned} & \int_{\tau^{min}}^{\tau^{max}} \varphi(\tau) {}_0^C\mathcal{D}_t^{2\tau} u \, d\tau + \sum_{i=1}^d \int_{\mu_i^{min}}^{\mu_i^{max}} \varrho_i(\mu_i) [c_{l_i} {}_{a_i}^{RL}\mathcal{D}_{x_i}^{2\mu_i} u + c_{r_i} {}_{x_i}^{RL}\mathcal{D}_{b_i}^{2\mu_i} u] \, d\mu_i \\ &= \sum_{j=1}^d \int_{\nu_j^{min}}^{\nu_j^{max}} \rho_j(\nu_j) [\kappa_{l_j} {}_{a_j}^{RL}\mathcal{D}_{x_j}^{2\nu_j} u + \kappa_{r_j} {}_{x_j}^{RL}\mathcal{D}_{b_j}^{2\nu_j} u] \, d\nu_j - \gamma u + f, \end{aligned} \quad (3.1)$$

subject to homogeneous Dirichlet boundary conditions and zero initial condition, where for $i, j = 1, 2, \dots, d$

$$t \in [0, T], \quad x_j \in [a_j, b_j],$$

$$2\tau^{min} < 2\tau^{max} \in (0, 2], \quad 2\tau^{min} \neq 1, \quad 2\tau^{max} \neq 1,$$

$$2\mu_i^{min} < 2\mu_i^{max} \in (0, 1), \quad 2\nu_j^{min} < 2\nu_j^{max} \in (1, 2],$$

$$0 < \varphi(\tau) \in L^1((\tau^{min}, \tau^{max})), \quad 0 < \varrho_i(\mu_i) \in L^1((\mu_i^{min}, \mu_i^{max})), \quad 0 < \rho_j(\nu_j) \in L^1((\nu_j^{min}, \nu_j^{max})),$$

and the coefficients c_{l_i} , c_{r_i} , κ_{l_i} , κ_{r_i} , and γ are constant. We emphasize that (3.1) is reduced to fractional advection-dispersion-reaction equations when $\varphi(\tau)$, $\varrho_i(\mu_i)$, and $\rho_j(\nu_j)$ are chosen to be a Dirac delta function, where for $d = 1$ and $\rho_1(\nu_1) = \delta(\nu_1 - 1)$ the two-sided Riesz derivatives with proper coefficients recover the standard second order dispersion terms. We briefly highlight the main contributions of this study as follows:

- We consider fully distributed fractional PDEs as an extension of existing fractional PDEs in [60, 70] by replacing the fractional operators by their corresponding distributed order ones. We further derive the weak formulation of the problem.

- We construct the underlying function spaces by extending the *distributed Sobolev* space in [70] to higher dimensions in time and space, endowed with equivalent associated norms.
- We develop a Petrov-Galerkin spectral method, employing Legendre polynomials and Jacobi *poly-fractonomials* [56] as spatial and temporal basis/test functions, respectively. We also formulate a fast solver for the corresponding weak form of (3.1), which significantly reduces the computational expenses in high-dimensional problems.
- We establish well-posedness of the weak form of the problem in the underlying *distributed Sobolev* spaces respecting the analysis in chapter 2 and prove the stability of proposed numerical scheme. We additionally perform the corresponding error analysis, where the *distributed Sobolev* spaces enable us to obtain accurate error estimate of the scheme.

To examine the performance and convergence of the developed PG method in solving different cases, we also perform several numerical simulations.

This chapter is organized as follows: in Section 2, we introduce some preliminaries from fractional calculus. In Section 3, we present the mathematical framework of the bilinear form and carry out the corresponding well-posedness analysis. We construct the PG method for the discrete weak form problem and formulate the fast solver in Section 4. In Section 5, we perform the stability and error analysis in detail. In Section 6, we illustrate the convergence rate and the efficiency of method via numerical examples.

3.2 Preliminaries on Fractional Calculus

Recalling the definitions of the fractional derivatives and integrals from [56, 38], we denote by ${}^{RL}_a \mathcal{D}_x^\sigma g(x)$ and ${}^{RL}_x \mathcal{D}_b^\sigma g(x)$ the left-sided and the right-sided Riemann-Liouville fractional derivatives of order $\sigma > 0$,

$${}^{RL}_a \mathcal{D}_x^\sigma g(x) = \frac{1}{\Gamma(n-\sigma)} \frac{d^n}{dx^n} \int_a^x \frac{g(s)}{(x-s)^{\sigma+1-n}} ds, \quad x \in [a, b], \quad (3.2)$$

$${}^{RL}_x \mathcal{D}_b^\sigma g(x) = \frac{(-1)^n}{\Gamma(n-\sigma)} \frac{d^n}{dx^n} \int_x^b \frac{g(s)}{(s-x)^{\sigma+1-n}} ds, \quad x \in [a, b], \quad (3.3)$$

in which $g(x) \in L^1[a, b]$ and $\int_a^x \frac{g(s)}{(x-s)^{\sigma+1-n}} ds, \int_x^b \frac{g(s)}{(s-x)^{\sigma+1-n}} ds \in C^n[a, b]$, respectively, where $n = \lceil \sigma \rceil$. Besides, ${}_a^C\mathcal{D}_x^\sigma g(x)$ and ${}_x^C\mathcal{D}_b^\sigma g(x)$ represent the left-sided and the right-sided Caputo fractional derivatives, where

$${}_a^C\mathcal{D}_x^\sigma f(x) = \frac{1}{\Gamma(n-\sigma)} \int_a^x \frac{g^{(n)}(s)}{(x-s)^{\sigma+1-n}} ds, \quad x \in [a, b], \quad (3.4)$$

$${}_x^C\mathcal{D}_b^\sigma f(x) = \frac{(-1)^n}{\Gamma(n-\sigma)} \int_x^b \frac{g^{(n)}(s)}{(s-x)^{\sigma+1-n}} ds, \quad x \in [a, b]. \quad (3.5)$$

The relationship between the RL and the Caputo fractional derivatives is given by

$${}_{-1}^{RL}\mathcal{D}_x^\nu f(x) = \frac{f(a)}{\Gamma(1-\nu)(x-a)^\nu} + {}_a^C\mathcal{D}_x^\nu f(x) \quad (3.6)$$

$${}_{x}^{RL}\mathcal{D}_b^\nu f(x) = \frac{f(b)}{\Gamma(1-\nu)(b-x)^\nu} + {}_x^C\mathcal{D}_b^\nu f(x), \quad (3.7)$$

when $\lceil \nu \rceil = 1$, see e.g. (2.33) in [38]. In the case of homogeneous boundary conditions, we obtain

${}_{-1}^{RL}\mathcal{D}_x^\nu f(x) = {}_a^C\mathcal{D}_x^\nu f(x) := {}_a\mathcal{D}_x^\nu f(x)$ and ${}_{x}^{RL}\mathcal{D}_b^\nu f(x) = {}_x^C\mathcal{D}_b^\nu f(x) := {}_x\mathcal{D}_b^\nu f(x)$. The Reimann-Liouville fractional integrals of Jacobi *poly-fractonomials* are analytically obtained in [56, 55] in the standard domain $\xi \in [-1, 1]$ as

$${}_{-1}^{RL}\mathcal{I}_\xi^\sigma \{(1+\xi)^\beta P_n^{\alpha,\beta}(\xi)\} = \frac{\Gamma(n+\beta+1)}{\Gamma(n+\beta+\sigma+1)} (1+\xi)^{\beta+\sigma} P_n^{\alpha-\sigma,\beta+\sigma}(\xi), \quad (3.8)$$

and

$${}_\xi^{RL}\mathcal{I}_1^\sigma \{(1-\xi)^\alpha P_n^{\alpha,\beta}(\xi)\} = \frac{\Gamma(n+\alpha+1)}{\Gamma(n+\alpha+\sigma+1)} (1-\xi)^{\alpha+\sigma} P_n^{\alpha+\sigma,\beta-\sigma}(\xi), \quad (3.9)$$

where $0 < \sigma < 1, \alpha > -1, \beta > -1$, and $P_n^{\alpha,\beta}(\xi)$ denotes the standard Jacobi polynomials of order n and parameters α and β [137]. Accordingly,

$${}_{-1}^{RL}\mathcal{D}_\xi^\sigma P_n(\xi) = \frac{\Gamma(n+1)}{\Gamma(n-\sigma+1)} P_n^{\sigma,-\sigma}(\xi) (1+\xi)^{-\sigma} \quad (3.10)$$

and

$${}_\xi^{RL}\mathcal{D}_1^\sigma P_n(\xi) = \frac{\Gamma(n+1)}{\Gamma(n-\sigma+1)} P_n^{-\sigma,\sigma}(\xi) (1-\xi)^{-\sigma}, \quad (3.11)$$

where $P_n(\xi) := P_n^{0,0}(\xi)$ represents Legendre polynomial of degree n (see [137]).

Let define the distributed-order derivative as

$${}^D\mathcal{D}_t^\phi f(t, x) := \int_{\tau^{min}}^{\tau^{max}} \phi(\tau) {}_0\mathcal{D}_t^\tau f(t, x) d\tau, \quad (3.12)$$

where $\alpha \rightarrow \phi(\alpha)$ be a continuous mapping in $[\alpha^{min}, \alpha^{max}]$ [70] and $t > 0$. We note that by choosing the distribution function in the distributed-order derivatives to be the Dirac delta function $\delta(\tau - \tau_0)$, we recover a single (fixed) term fractional derivative, i.e.,

$$\int_{\tau^{min}}^{\tau^{max}} \delta(\tau - \tau_0) {}_0\mathcal{D}_t^\tau f(t, x) d\tau = {}_0\mathcal{D}_t^{\tau_0} f(t, x), \quad (3.13)$$

where $\tau_0 \in (\tau^{min}, \tau^{max})$.

3.3 Mathematical Formulation

We introduce the underlying solution and test spaces along with their proper norms, and also provide some useful lemmas to derive the corresponding bilinear form and thus, prove the well-posedness of problem.

3.3.1 Mathematical Framework

Let $C_0^\infty(\Lambda)$ represent the space of smooth functions with compact support in $\Lambda = (a, b)$. Recalling the definition of Sobolev space for real $\sigma \geq 0$ from [70, 107], the usual Sobolev space denoted by $H^\sigma(\Lambda)$ is the closure of $C_0^\infty(\Lambda)$ on the finite interval Λ , which is associated with the norm $\|\cdot\|_{H^\sigma(\Lambda)}$. For the real index $\sigma \geq 0$ and $\sigma \neq n - \frac{1}{2}$ on the bounded interval Λ the following norms are equivalent [109]

$$\|\cdot\|_{H^\sigma(\Lambda)} \cong \|\cdot\|_{l_{H^\sigma(\Lambda)}} \cong \|\cdot\|_{r_{H^\sigma(\Lambda)}} \cong |\cdot|_{H^\sigma(\Lambda)}^*, \quad (3.14)$$

where " \cong " denotes equivalence relation, $\|\cdot\|_{l_{H^\sigma(\Lambda)}} = \left(\|{}_a\mathcal{D}_x^\sigma(\cdot)\|_{L^2(\Lambda)}^2 + \|\cdot\|_{L^2(\Lambda)}^2 \right)^{\frac{1}{2}}$, $\|\cdot\|_{r_{H^\sigma(\Lambda)}} = \left(\|{}_x\mathcal{D}_b^\sigma(\cdot)\|_{L^2(\Lambda)}^2 + \|\cdot\|_{L^2(\Lambda)}^2 \right)^{\frac{1}{2}}$, and $|\cdot|_{H^\sigma(\Lambda)}^* = |({}_a\mathcal{D}_x^\sigma(\cdot), {}_x\mathcal{D}_b^\sigma(\cdot))_\Lambda|^{\frac{1}{2}}$. From Lemma 5.2 in [108], we have

$$|\cdot|_{l_{H^\sigma(\Lambda)}}^* \cong |\cdot|_{H^\sigma(\Lambda)}^{\frac{1}{2}} |\cdot|_{r_{H^\sigma(\Lambda)}}^{\frac{1}{2}} = \|{}_a\mathcal{D}_x^\sigma(\cdot)\|_{L^2(\Lambda)}^{\frac{1}{2}} \|{}_x\mathcal{D}_b^\sigma(\cdot)\|_{L^2(\Lambda)}^{\frac{1}{2}}, \quad (3.15)$$

where $|\cdot|_{lH^\sigma(\Lambda)} = \|{}_a\mathcal{D}_x^\sigma(\cdot)\|_{L^2(\Lambda)}$, and $|\cdot|_{rH^\sigma(\Lambda)} = \|{}_x\mathcal{D}_b^b(\cdot)\|_{L^2(\Lambda)}$. According to Lemma 3.1 in [61], the norms $\|\cdot\|_{lH^\sigma(\Lambda)}$ and $\|\cdot\|_{rH^\sigma(\Lambda)}$ are equivalent to $\|\cdot\|_{cH^\sigma(\Lambda)}$ in space $C_0^\infty(\Lambda)$, where

$$\|\cdot\|_{cH^\sigma(\Lambda)} = \left(\|{}_x\mathcal{D}_b^\sigma(\cdot)\|_{L^2(\Lambda)}^2 + \|{}_a\mathcal{D}_x^\sigma(\cdot)\|_{L^2(\Lambda)}^2 + \|\cdot\|_{L^2(\Lambda)}^2 \right)^{\frac{1}{2}}. \quad (3.16)$$

In the usual Sobolev space, for $u \in H^\sigma(\Lambda)$ we define

$$|u|_{H^\sigma(\Lambda)}^* = |({}_a\mathcal{D}_x^\sigma u, {}_x\mathcal{D}_b^\sigma v)_\Lambda|^{\frac{1}{2}} + |({}_x\mathcal{D}_b^\sigma u, {}_a\mathcal{D}_x^\sigma v)_\Lambda|^{\frac{1}{2}}, \quad \forall v \in H^\sigma(\Lambda),$$

where we assume $\sup_{u \in H^\sigma(\Lambda)} |({}_a\mathcal{D}_x^\sigma u, {}_x\mathcal{D}_b^\sigma v)_\Lambda|^{\frac{1}{2}} + |({}_x\mathcal{D}_b^\sigma u, {}_a\mathcal{D}_x^\sigma v)_\Lambda|^{\frac{1}{2}} > 0 \quad \forall v \in H^\sigma(\Lambda)$, which excludes the solutions to $|u|_{H^\sigma(\Lambda)}^* = 0$. Denoted by ${}^lH_0^\sigma(\Lambda)$ and ${}^rH_0^\sigma(\Lambda)$ are the closure of $C_0^\infty(\Lambda)$ with respect to the norms $\|\cdot\|_{lH^\sigma(\Lambda)}$ and $\|\cdot\|_{rH^\sigma(\Lambda)}$ in Λ , respectively.

Recalling from [70], ${}^\mathfrak{D}H^\varphi(\mathbb{R})$ represents the *distributed Sobolev* space on \mathbb{R} , which is associated with the following norm

$$\|\cdot\|_{{}^\mathfrak{D}H^\varphi(\mathbb{R})} = \left(\int_{\tau^{min}}^{\tau^{max}} \varphi(\tau) \| (1 + |\omega|^2)^{\frac{\tau}{2}} \mathcal{F}(\cdot)(\omega) \|_{L^2(\mathbb{R})}^2 d\tau \right)^{\frac{1}{2}}, \quad (3.17)$$

where $0 < \varphi(\tau) \in L^1([\tau^{min}, \tau^{max}])$, $0 < \tau^{min} < \tau^{max} < 1$ ($1 < \tau^{min} < \tau^{max} \leq 2$). Subsequently, we denote by ${}^\mathfrak{D}H^\varphi(I)$ the *distributed Sobolev* space on the bounded open interval $I = (0, T)$, which is defined as ${}^\mathfrak{D}H^\varphi(I) = \{v \in L^2(I) \mid \exists \tilde{v} \in {}^\mathfrak{D}H^\varphi(\mathbb{R}) \text{ s.t. } \tilde{v}|_I = v\}$ with the the equivalent norms $\|\cdot\|_{l, {}^\mathfrak{D}H^\varphi(I)}$ and $\|\cdot\|_{r, {}^\mathfrak{D}H^\varphi(I)}$ in [70], where

$$\|\cdot\|_{l, {}^\mathfrak{D}H^\varphi(I)} = \left(\|\cdot\|_{L^2(I)}^2 + \int_{\tau^{min}}^{\tau^{max}} \varphi(\tau) \| {}_0\mathcal{D}_t^\tau(\cdot) \|_{L^2(I)}^2 d\tau \right)^{\frac{1}{2}},$$

and

$$\|\cdot\|_{r, {}^\mathfrak{D}H^\varphi(I)} = \left(\|\cdot\|_{L^2(I)}^2 + \int_{\tau^{min}}^{\tau^{max}} \varphi(\tau) \| {}_t\mathcal{D}_T^\tau(\cdot) \|_{L^2(I)}^2 d\tau \right)^{\frac{1}{2}}.$$

In each realization of a physical process (e.g., sub- or super-diffusion), the distribution function $\varphi(\tau)$ can be obtained from experimental observations, while the theoretical setting of the problem remains invariant. More importantly, choice of *distributed Sobolev* space and the associated norms provide a sharper estimate for the accuracy of proposed PG method.

Let $\Lambda_1 = (a_1, b_1)$, $\Lambda_i = (a_i, b_i) \times \Lambda_{i-1}$ for $i = 2, \dots, d$. We define $\mathcal{X}_1 = {}^{\mathfrak{D}}H^{\rho_1}(\Lambda_1)$ with the associated norm $\|\cdot\|_{{}^{\mathfrak{D}}H^{\rho_1}(\Lambda_1)}$, where

$$\|\cdot\|_{{}^{\mathfrak{D}}H^{\rho_1}(\Lambda_1)} = \left(\|\cdot\|_{L^2(I)}^2 + \int_{v_1^{min}}^{v_1^{max}} \rho_1(v_1) \left(\|{}_{a_1} \mathcal{D}_{x_1}^{v_1}(\cdot)\|_{L^2(\Lambda_1)}^2 + \|{}_{x_1} \mathcal{D}_{b_1}^{v_1}(\cdot)\|_{L^2(\Lambda_1)}^2 \right) dv_1 \right)^{\frac{1}{2}}. \quad (3.18)$$

Subsequently, we construct \mathcal{X}_d such that

$$\begin{aligned} \mathcal{X}_2 &= {}^{\mathfrak{D}}H^{\rho_2}\left((a_2, b_2); L^2(\Lambda_1)\right) \cap L^2((a_2, b_2); \mathcal{X}_1), \\ &\vdots \\ \mathcal{X}_d &= {}^{\mathfrak{D}}H^{\rho_d}\left((a_d, b_d); L^2(\Lambda_{d-1})\right) \cap L^2((a_d, b_d); \mathcal{X}_{d-1}), \end{aligned} \quad (3.19)$$

associated with the norm

$$\|\cdot\|_{\mathcal{X}_d} = \left\{ \|\cdot\|_{{}^{\mathfrak{D}}H^{\rho_d}\left((a_d, b_d); L^2(\Lambda_{d-1})\right)}^2 + \|\cdot\|_{L^2\left((a_d, b_d); \mathcal{X}_{d-1}\right)}^2 \right\}^{\frac{1}{2}}. \quad (3.20)$$

Lemma 3.3.1. *Let $v_i > 0$ and $v_i \neq n - \frac{1}{2}$ for $i = 1, \dots, d$. Then*

$$\|\cdot\|_{\mathcal{X}_d} \cong \left\{ \sum_{i=1}^d \int_{v_i^{min}}^{v_i^{max}} \rho_i(v_i) \left(\|{}_{x_i} \mathcal{D}_{b_i}^{v_i}(\cdot)\|_{L^2(\Lambda_d)}^2 + \|{}_{a_i} \mathcal{D}_{x_i}^{v_i}(\cdot)\|_{L^2(\Lambda_d)}^2 \right) dv_i + \|\cdot\|_{L^2(\Lambda_d)}^2 \right\}^{\frac{1}{2}}. \quad (3.21)$$

Proof. Considering (3.18), \mathcal{X}_1 is endowed with $\|\cdot\|_{\mathcal{X}_1} \cong \|\cdot\|_{{}^{\mathfrak{D}}H^{\rho_1}(\Lambda_1)}$. \mathcal{X}_2 is associated with $\|\cdot\|_{\mathcal{X}_2} = \{\|\cdot\|_{{}^{\mathfrak{D}}H^{\rho_2}\left((a_2, b_2); L^2(\Lambda_1)\right)}^2 + \|\cdot\|_{L^2\left((a_2, b_2); \mathcal{X}_1\right)}^2\}^{\frac{1}{2}}$, which is proved to be

$$\begin{aligned} &\|u\|_{{}^{\mathfrak{D}}H^{\rho_2}\left((a_2, b_2); L^2(\Lambda_1)\right)}^2 \\ &= \int_{v_2^{min}}^{v_2^{max}} \rho_2(v_2) \int_{a_1}^{b_1} \left(\int_{a_2}^{b_2} |{}_{a_2} \mathcal{D}_{x_2}^{v_2} u|^2 dx_2 + \int_{a_2}^{b_2} |{}_{x_2} \mathcal{D}_{b_2}^{v_2} u|^2 dx_2 \right. \\ &\quad \left. + \int_{a_2}^{b_2} |u|^2 dx_2 \right) dx_1 dv_2 \\ &= \int_{v_2^{min}}^{v_2^{max}} \rho_2(v_2) \left(\|{}_{x_2} \mathcal{D}_{b_2}^{v_2}(u)\|_{L^2(\Lambda_2)}^2 + \|{}_{a_2} \mathcal{D}_{x_2}^{v_2}(u)\|_{L^2(\Lambda_2)}^2 \right) dv_2 + \|u\|_{L^2(\Lambda_2)}^2 \end{aligned} \quad (3.22)$$

and

$$\begin{aligned}
& \|u\|_{L^2((a_2, b_2); \mathcal{X}_1)}^2 \\
&= \int_{\nu_1^{\min}}^{\nu_1^{\max}} \rho_1(\nu_1) \int_{a_2}^{b_2} \left(\int_{a_1}^{b_1} |{}_{a_1} \mathcal{D}_{x_1}^{\nu_1} u|^2 dx_1 + \int_{a_1}^{b_1} |{}_{x_1} \mathcal{D}_{b_1}^{\nu_1} u|^2 dx_1 \right. \\
&\quad \left. + \int_{a_1}^{b_1} |u|^2 dx_1 \right) dx_2 d\nu_1 \\
&= \int_{\nu_1^{\min}}^{\nu_1^{\max}} \rho_1(\nu_1) \left(\|{}_{x_1} \mathcal{D}_{b_1}^{\nu_1} u\|_{L^2(\Lambda_2)}^2 + \|{}_{a_1} \mathcal{D}_{x_1}^{\nu_1} u\|_{L^2(\Lambda_2)}^2 \right) d\nu_1 + \|u\|_{L^2(\Lambda_2)}^2. \tag{3.23}
\end{aligned}$$

Next, providing that

$$\|\cdot\|_{\mathcal{X}_{d-1}} \cong \left\{ \sum_{i=1}^{d-1} \int_{\nu_i^{\min}}^{\nu_i^{\max}} \rho_i(\nu_i) \left(\|{}_{x_i} \mathcal{D}_{b_i}^{\nu_i} (\cdot)\|_{L^2(\Lambda_{d-1})}^2 + \|{}_{a_i} \mathcal{D}_{x_i}^{\nu_i} (\cdot)\|_{L^2(\Lambda_{d-1})}^2 \right) d\nu_i + \|\cdot\|_{L^2(\Lambda_{d-1})}^2 \right\}^{\frac{1}{2}},$$

then the inductive step is attained according to

$$\begin{aligned}
& \|u\|_{\mathfrak{D}_{H^{\rho_d}}((a_d, b_d); L^2(\Lambda_{d-1}))}^2 \\
&= \int_{\Lambda_{d-1}} \left(\int_{a_d}^{b_d} |u|^2 dx_d + \int_{a_d}^{b_d} \int_{\nu_d^{\min}}^{\nu_d^{\max}} \rho_d(\nu_d) (|{}_{a_d} \mathcal{D}_{x_d}^{\nu_d} u|^2 + |{}_{x_d} \mathcal{D}_{b_d}^{\nu_d} u|^2) d\nu_d dx_d \right) d\Lambda_{d-1} \\
&= \int_{\nu_d^{\min}}^{\nu_d^{\max}} \rho_d(\nu_d) \left(\|{}_{x_d} \mathcal{D}_{b_d}^{\nu_d} (u)\|_{L^2(\Lambda_d)}^2 + \|{}_{a_d} \mathcal{D}_{x_d}^{\nu_d} (u)\|_{L^2(\Lambda_d)}^2 \right) d\nu_d + \|u\|_{L^2(\Lambda_d)}^2, \tag{3.24}
\end{aligned}$$

and

$$\begin{aligned}
& \|u\|_{L^2((a_d, b_d); \mathcal{X}_{d-1})}^2 = \int_{a_d}^{b_d} \int_{\Lambda_{d-1}} \left(\sum_{i=1}^{d-1} \int_{\nu_i^{\min}}^{\nu_i^{\max}} \rho_i(\nu_i) (|{}_{a_i} \mathcal{D}_{x_i}^{\nu_i} u|^2 + |{}_{x_i} \mathcal{D}_{b_i}^{\nu_i} u|^2) d\nu_i \right) d\Lambda_{d-1} dx_d \\
&\quad + \int_{a_d}^{b_d} \int_{\Lambda_{d-1}} |u|^2 d\Lambda_{d-1} dx_d \\
&= \sum_{i=1}^{d-1} \int_{\nu_i^{\min}}^{\nu_i^{\max}} \rho_i(\nu_i) \left(\|{}_{x_i} \mathcal{D}_{b_i}^{\nu_i} u\|_{L^2(\Lambda_d)}^2 + \|{}_{a_i} \mathcal{D}_{x_i}^{\nu_i} u\|_{L^2(\Lambda_d)}^2 \right) d\nu_i \\
&\quad + \|u\|_{L^2(\Lambda_d)}^2. \tag{3.25}
\end{aligned}$$

Therefore, (3.21) arises from (3.22), (3.23), (3.24), and (3.25) by induction and the proof is complete. \square

The following assumptions allow us to prove the uniqueness of the bilinear form by excluding the solutions to $|(_{a_i} \mathcal{D}_{x_i}^{\nu_i} u, {}_{x_i} \mathcal{D}_{b_i}^{\nu_i} v)_{\Lambda_d}| + |({}_{x_i} \mathcal{D}_{b_i}^{\nu_i} u, {}_{a_i} \mathcal{D}_{x_i}^{\nu_i} v)_{\Lambda_d}| = 0$ for $i = 1, \dots, d$ and $|({}_0 \mathcal{D}_t^\tau u, {}_t \mathcal{D}_T^\tau v)_\Omega| = 0$.

Assumption 2. For $u \in X_d$

$$\sup_{u \in X_d} \int_{\nu_i^{\min}}^{\nu_i^{\max}} \rho_i(\nu_i) \left(|(_{a_i} \mathcal{D}_{x_i}^{\nu_i} u, {}_{x_i} \mathcal{D}_{b_i}^{\nu_i} v)_{\Lambda_d}| + |({}_{x_i} \mathcal{D}_{b_i}^{\nu_i} u, {}_{a_i} \mathcal{D}_{x_i}^{\nu_i} v)_{\Lambda_d}| \right) d\nu_i > 0, \quad \forall v \in X_d$$

when $i = 1, \dots, d$, and $\Lambda_d^i = \prod_{\substack{j=1 \\ j \neq i}}^d (a_j, b_j)$.

Assumption 3. For $u \in {}^{l,\mathfrak{D}} H^\varphi(I; L^2(\Lambda_d))$ $\sup_{0 \neq u \in {}^{l,\mathfrak{D}} H^\varphi(I; L^2(\Lambda_d))} \int_{\tau^{\min}}^{\tau^{\max}} \varphi(\tau) |({}_0 \mathcal{D}_t^\tau u, {}_t \mathcal{D}_T^\tau v)_\Omega| d\tau > 0 \quad \forall v \in {}^{r,\mathfrak{D}} H^\varphi(I; L^2(\Lambda_d))$.

In Lemma 2.4.3 in chapter 2, it is shown that if $1 < 2\nu_i < 2$ for $i = 1, \dots, d$ and $u, v \in X_d$, then $({}_{x_i} \mathcal{D}_{b_i}^{2\nu_i} u, v)_{\Lambda_d} = ({}_{x_i} \mathcal{D}_{b_i}^{\nu_i} u, {}_{a_i} \mathcal{D}_{x_i}^{\nu_i} v)_{\Lambda_d}$, and $({}_{a_i} \mathcal{D}_{x_i}^{2\nu_i} u, v)_{\Lambda_d} = ({}_{a_i} \mathcal{D}_{x_i}^{\nu_i} u, {}_{x_i} \mathcal{D}_{b_i}^{\nu_i} v)_{\Lambda_d}$. Consequently, we derive

$$\int_{\nu_i^{\min}}^{\nu_i^{\max}} \rho_i(\nu_i) ({}_{x_i} \mathcal{D}_{b_i}^{2\nu_i} u, v)_{\Lambda_d} d\nu_i = \int_{\nu_i^{\min}}^{\nu_i^{\max}} \rho_i(\nu_i) ({}_{x_i} \mathcal{D}_{b_i}^{\nu_i} u, {}_{a_i} \mathcal{D}_{x_i}^{\nu_i} v)_{\Lambda_d} d\nu_i \quad (3.26)$$

and

$$\int_{\nu_i^{\min}}^{\nu_i^{\max}} \rho_i(\nu_i) ({}_{a_i} \mathcal{D}_{x_i}^{2\nu_i} u, v)_{\Lambda_d} d\nu_i = \int_{\nu_i^{\min}}^{\nu_i^{\max}} \rho_i(\nu_i) ({}_{a_i} \mathcal{D}_{x_i}^{\nu_i} u, {}_{x_i} \mathcal{D}_{b_i}^{\nu_i} v)_{\Lambda_d} d\nu_i. \quad (3.27)$$

Additionally, in the light of chapter 2, we have

$$\begin{aligned} & \int_{\nu_i^{\min}}^{\nu_i^{\max}} \rho_i(\nu_i) \left(|(_{a_i} \mathcal{D}_{x_i}^{\nu_i} u, {}_{x_i} \mathcal{D}_{b_i}^{\nu_i} v)_{\Lambda_d}| + |({}_{x_i} \mathcal{D}_{b_i}^{\nu_i} u, {}_{a_i} \mathcal{D}_{x_i}^{\nu_i} v)_{\Lambda_d}| \right) d\nu_i \\ & \cong |u|_{{}_{\mathfrak{D} H^{\rho_i}((a_i, b_i); L^2(\Lambda_d^i))}}^{|v|} \end{aligned} \quad (3.28)$$

for $i = 1, \dots, d$, where Assumption 2 holds.

Next, we study the property of the fractional time-derivative in the following lemmas.

Lemma 3.3.2. If $0 < 2\tau^{\min} < 2\tau^{\max} < 1$ ($1 < 2\tau^{\min} < 2\tau^{\max} < 2$) and $u, v \in {}^{l,\mathfrak{D}}H^\varphi(I)$, when $u|_{t=0}(=\frac{du}{dt}|_{t=0}) = 0$, then

$$\int_{\tau^{\min}}^{\tau^{\max}} \varphi(\tau) ({}_0\mathcal{D}_t^{2\tau} u, v)_I d\tau = \int_{\tau^{\min}}^{\tau^{\max}} \varphi(\tau) ({}_0\mathcal{D}_t^\tau u, {}_t\mathcal{D}_T^\tau v)_I d\tau, \quad (3.29)$$

where $I = (0, T)$, $0 < \varphi(\tau) \in L^1([\tau^{\min}, \tau^{\max}])$.

Proof. It follows from [70] that for $u, v \in H^\tau(I)$, when $u|_{t=0}(=\frac{du}{dt}|_{t=0}) = 0$ and $v|_{t=T}(=\frac{dv}{dt}|_{t=T}) = 0$, we have

$$({}_0\mathcal{D}_t^{2\tau} u, v)_I = ({}_0\mathcal{D}_t^\tau u, {}_t\mathcal{D}_T^\tau v)_I. \quad (3.30)$$

Then (3.29) arises from (3.30). \square

Let $0 < 2\tau^{\min} < 2\tau^{\max} < 1$ ($1 < 2\tau^{\min} < 2\tau^{\max} \leq 2$), and $\Omega = I \times \Lambda_d$, where $I = (0, T)$ and $\Lambda_d = \prod_{i=1}^d (a_i, b_i)$. We define

$$\begin{aligned} & {}^{l,\mathfrak{D}}H^\varphi(I; L^2(\Lambda_d)) \\ &:= \left\{ u \mid \|u(t, \cdot)\|_{L^2(\Lambda_d)} \in {}^{l,\mathfrak{D}}H^\varphi(I), u|_{t=0}(=\frac{du}{dt}|_{t=0}) = u|_{x_i=a_i} = u|_{x_i=b_i} = 0, i = 1, \dots, d \right\}, \end{aligned} \quad (3.31)$$

which is endowed with the norm $\|\cdot\|_{{}^{l,\mathfrak{D}}H^\varphi(I; L^2(\Lambda_d))}$, where we have

$$\begin{aligned} \|u\|_{{}^{l,\mathfrak{D}}H^\varphi(I; L^2(\Lambda_d))} &= \left\| \|u(t, \cdot)\|_{L^2(\Lambda_d)} \right\|_{{}^{l,\mathfrak{D}}H^\varphi(I)} \\ &= \left(\int_{\tau^{\min}}^{\tau^{\max}} \varphi(\tau) \|{}_0\mathcal{D}_t^\tau(u)\|_{L^2(\Omega)}^2 d\tau + \|u\|_{L^2(\Omega)}^2 \right)^{\frac{1}{2}}. \end{aligned} \quad (3.32)$$

Similarly, we define

$$\begin{aligned} & {}^{r,\mathfrak{D}}H^\varphi(I; L^2(\Lambda_d)) \\ &:= \left\{ v \mid \|v(t, \cdot)\|_{L^2(\Lambda_d)} \in {}^{r,\mathfrak{D}}H^\varphi(I), v|_{t=T}(=\frac{dv}{dt}|_{t=0}) = v|_{x_i=a_i} = v|_{x_i=b_i} = 0, i = 1, \dots, d \right\}, \end{aligned} \quad (3.33)$$

which is equipped with the norm $\|\cdot\|_{{}^{r,\mathfrak{D}}H^\varphi(I; L^2(\Lambda_d))}$. Following (3.32),

$$\begin{aligned} \|v\|_{{}^{r,\mathfrak{D}}H^\varphi(I; L^2(\Lambda_d))} &= \left\| \|v(t, \cdot)\|_{L^2(\Lambda_d)} \right\|_{{}^{r,\mathfrak{D}}H^\varphi(I)} \\ &= \left(\int_{\tau^{\min}}^{\tau^{\max}} \varphi(\tau) \|{}_t\mathcal{D}_T^\tau(v)\|_{L^2(\Omega)}^2 d\tau + \|v\|_{L^2(\Omega)}^2 \right)^{\frac{1}{2}}. \end{aligned} \quad (3.34)$$

Lemma 3.3.3. For $u \in {}^{r,\mathfrak{D}}H^\varphi(I; L^2(\Lambda_d))$ and $0 < 2\tau^{\min} < 2\tau^{\max} < 1$ ($1 < 2\tau^{\min} < 2\tau^{\max} < 2$), $\int_{\tau^{\min}}^{\tau^{\max}} \varphi(\tau) |({}_0\mathcal{D}_t^\tau u, {}_t\mathcal{D}_T^\tau v)_\Omega| d\tau \leq \|u\|_{l,\mathfrak{D}H^\varphi(I; L^2(\Lambda_d))} \|v\|_{r,\mathfrak{D}H^\varphi(I; L^2(\Lambda_d))} \forall v \in {}^{r,\mathfrak{D}}H^\varphi(I; L^2(\Lambda_d))$.

Proof. From Lemma 2.4.7 in chapter 2 we have

$$|({}_0\mathcal{D}_t^\tau u, {}_t\mathcal{D}_T^\tau v)_\Omega| \leq \left(\|{}_0\mathcal{D}_t^\tau u\|_{L^2(\Omega)}^2 + \|u\|_{L^2(\Omega)}^2 \right)^{\frac{1}{2}} \left(\|{}_t\mathcal{D}_T^\tau v\|_{L^2(\Omega)}^2 + \|v\|_{L^2(\Omega)}^2 \right)^{\frac{1}{2}}.$$

Followingly, by Hölder inequality

$$\begin{aligned} & \int_{\tau^{\min}}^{\tau^{\max}} \varphi(\tau) |({}_0\mathcal{D}_t^\tau u, {}_t\mathcal{D}_T^\tau v)_\Omega| d\tau \\ &= \int_{\tau^{\min}}^{\tau^{\max}} \varphi(\tau) \int_{\Lambda_d} \int_0^T |{}_0\mathcal{D}_t^\tau u| |{}_t\mathcal{D}_T^\tau v| dt d\Lambda_d d\tau \\ &\leq \left(\int_{\tau^{\min}}^{\tau^{\max}} \int_{\Lambda_d} \int_0^T \varphi(\tau) |{}_0\mathcal{D}_t^\tau u|^2 dt d\Lambda_d d\tau \right)^{\frac{1}{2}} \left(\int_{\tau^{\min}}^{\tau^{\max}} \int_{\Lambda_d} \int_0^T \varphi(\tau) |{}_t\mathcal{D}_T^\tau v|^2 dt d\Lambda_d d\tau \right)^{\frac{1}{2}} \\ &= \left(\int_{\tau^{\min}}^{\tau^{\max}} \varphi(\tau) \|{}_0\mathcal{D}_t^\tau u\|_{L^2(\Omega)}^2 d\tau + \|u\|_{L^2(\Omega)}^2 \right)^{\frac{1}{2}} \\ &\quad \times \left(\int_{\tau^{\min}}^{\tau^{\max}} \varphi(\tau) \|{}_t\mathcal{D}_T^\tau v\|_{L^2(\Omega)}^2 d\tau + \|v\|_{L^2(\Omega)}^2 \right)^{\frac{1}{2}} \\ &= \|u\|_{r,\mathfrak{D}H^\varphi(I; L^2(\Lambda_d))} \|v\|_{r,\mathfrak{D}H^\varphi(I; L^2(\Lambda_d))}. \end{aligned} \tag{3.35}$$

□

Lemma 3.3.4. For any $u \in {}^{l,\mathfrak{D}}H^\varphi(I; L^2(\Lambda_d))$ and $0 < 2\tau^{\min} < 2\tau^{\max} < 1$ ($1 < 2\tau^{\min} < 2\tau^{\max} \leq 2$) there exists a constant $c > 0$ and independent of u such that

$$\sup_{0 \neq v \in {}^{r,\mathfrak{D}}H^\varphi(I; L^2(\Lambda_d))} \frac{\int_{\tau^{\min}}^{\tau^{\max}} \varphi(\tau) |({}_0\mathcal{D}_t^\tau u, {}_t\mathcal{D}_T^\tau v)_\Omega| d\tau}{\|v\|_{r,\mathfrak{D}H^\varphi(I; L^2(\Lambda_d))}} \geq c \|u\|_{l,\mathfrak{D}H^\varphi(I; L^2(\Lambda_d))}, \tag{3.36}$$

under Assumption 3.

Proof. Following Lemma 2.4 in [110] and Lemma 2.4.8 in chapter 2, for any $u \in {}^{l,\mathfrak{D}}H^\varphi(I; L^2(\Lambda_d))$ let $\mathcal{V}_u = H(t-T)(u - u|_{t=T})$ assuming that $\int_{\tau^{\min}}^{\tau^{\max}} \varphi(\tau) |({}_0\mathcal{D}_t^\tau u, {}_t\mathcal{D}_T^\tau u|_{t=T})_\Omega| > 0$, where $H(t)$

is the Heaviside function. Evidently, $\mathcal{V}_u \in {}^{r,\mathfrak{D}}H^\varphi(I; L^2(\Lambda_d))$. From Hölder inequality, we obtain

$$\begin{aligned}
& \| \mathcal{V}_u \|_{r,\mathfrak{D} H^\varphi(I; L^2(\Lambda_d))}^2 \\
&= \int_{\tau^{\min}}^{\tau^{\max}} \varphi(\tau) \| {}_t \mathcal{D}_T^\tau \left(H(t-T) (u - u|_{t=T}) \right) \|_{L^2(\Omega)}^2 d\tau \\
&= \int_{\tau^{\min}}^{\tau^{\max}} \varphi(\tau) \| {}^{RL}{}_t \mathcal{I}_T^{1-\tau} \frac{d}{dt} \left(H(t-T) (u - u|_{t=T}) \right) \|_{L^2(\Omega)}^2 d\tau \\
&= \int_{\tau^{\min}}^{\tau^{\max}} \varphi(\tau) \| {}^{RL}{}_t \mathcal{I}_T^{1-\tau} \left(\frac{d H(t-T)}{dt} (u - u|_{t=T}) + H(t-T) \frac{d(u - u|_{t=T})}{dt} \right) \|_{L^2(\Omega)}^2 d\tau \\
&= \int_{\tau^{\min}}^{\tau^{\max}} \varphi(\tau) \| {}^{RL}{}_t \mathcal{I}_T^{1-\tau} \left(H(t-T) \frac{d(u - u|_{t=T})}{dt} \right) \|_{L^2(\Omega)}^2 d\tau \\
&= \int_{\tau^{\min}}^{\tau^{\max}} \varphi(\tau) \| {}_t \mathcal{D}_T^\tau u \|_{L^2(\Omega)}^2 d\tau. \tag{3.37}
\end{aligned}$$

Regarding (12) in [61],

$$\| \mathcal{V}_u \|_{r,\mathfrak{D} H^\varphi(I; L^2(\Lambda_d))}^2 \cong \int_{\tau^{\min}}^{\tau^{\max}} \varphi(\tau) \| {}_0 \mathcal{D}_t^\tau u \|_{L^2(\Omega)}^2 d\tau = \| u \|_{l,\mathfrak{D} H^\varphi(I; L^2(\Lambda_d))}^2.$$

Hence, $\| {}_t \mathcal{D}_T^\tau \mathcal{V}_u \|_{L^2(\Omega)}^2 \cong \| {}_0 \mathcal{D}_t^\tau u \|_{L^2(\Omega)}^2$. Therefore,

$$\begin{aligned}
\int_{\tau^{\min}}^{\tau^{\max}} \varphi(\tau) |({}_0 \mathcal{D}_t^\tau u, {}_t \mathcal{D}_T^\tau \mathcal{V}_u)_\Omega| d\tau &= \int_{\tau^{\min}}^{\tau^{\max}} \varphi(\tau) \int_{\Lambda_d} \int_0^T |{}_0 \mathcal{D}_t^\tau u| |{}_t \mathcal{D}_T^\tau \mathcal{V}_u| dt d\Lambda_d d\tau \\
&\geq \tilde{\beta} \int_{\tau^{\min}}^{\tau^{\max}} \varphi(\tau) \int_{\Lambda_d} \int_0^T |{}_0 \mathcal{D}_t^\tau u|^2 dt d\Lambda_d d\tau \\
&= \| u \|_{l,\mathfrak{D} H^\varphi(I; L^2(\Lambda_d))}^2, \tag{3.38}
\end{aligned}$$

where $\tilde{\beta} > 0$ and independent of u . Considering (3.37) and (3.38), we obtain

$$\begin{aligned}
\sup_{0 \neq v \in {}^{r,\mathfrak{D}}H^\varphi(I; L^2(\Lambda_d))} \frac{\int_{\tau^{\min}}^{\tau^{\max}} \varphi(\tau) |({}_0 \mathcal{D}_t^\tau u, {}_t \mathcal{D}_T^\tau v)_\Omega| d\tau}{\| v \|_{r,\mathfrak{D} H^\varphi(I; L^2(\Lambda_d))}} &\geq \frac{\int_{\tau^{\min}}^{\tau^{\max}} \varphi(\tau) |({}_0 \mathcal{D}_t^\tau u, {}_t \mathcal{D}_T^\tau \mathcal{V}_u)_\Omega| d\tau}{\| \mathcal{V}_u \|_{r,\mathfrak{D} H^\varphi(I; L^2(\Lambda_d))}} \\
&\geq \tilde{\beta} \| u \|_{l,\mathfrak{D} H^\varphi(I; L^2(\Lambda_d))}. \tag{3.39}
\end{aligned}$$

□

Lemma 3.3.5. If $0 < 2\tau^{\min} < 2\tau^{\max} < 1$ ($1 < 2\tau^{\min} < 2\tau^{\max} \leq 2$) and $u, v \in {}^{l,\mathfrak{D}}H^\varphi(I; L^2(\Lambda_d))$,

then

$$\int_{\tau^{\min}}^{\tau^{\max}} \varphi(\tau) ({}_0 \mathcal{D}_t^{2\tau} u, v)_\Omega d\tau = \int_{\tau^{\min}}^{\tau^{\max}} \varphi(\tau) ({}_0 \mathcal{D}_t^\tau u, {}_t \mathcal{D}_T^\tau v)_\Omega d\tau, \tag{3.40}$$

where $0 < \varphi(\tau) \in L^1([\tau^{min}, \tau^{max}])$.

Proof. By Lemma 3.3.2,

$$\begin{aligned} & \int_{\tau^{min}}^{\tau^{max}} \varphi(\tau) (\mathcal{D}_t^{2\tau} u, v)_\Omega d\tau = \int_{\tau^{min}}^{\tau^{max}} \varphi(\tau) \int_{\Lambda_d} \int_0^T |\mathcal{D}_t^{2\tau} u| |v| dt d\Lambda_d d\tau \\ &= \int_{\Lambda_d} \int_{\tau^{min}}^{\tau^{max}} \varphi(\tau) \int_0^T |\mathcal{D}_t^\tau u| |\mathcal{D}_T^\tau v| dt d\tau d\Lambda_d = \int_{\tau^{min}}^{\tau^{max}} \varphi(\tau) (\mathcal{D}_t^\tau u, \mathcal{D}_T^\tau v)_\Omega d\tau. \end{aligned} \quad (3.41)$$

□

3.3.2 Solution and Test Function Spaces

Take $0 < 2\tau^{min} < 2\tau^{max} < 1$ ($1 < 2\tau^{min} < 2\tau^{max} \leq 2$) and $1 < 2\nu_i^{min} < 2\nu_i^{max} \leq 2$ for $i = 1, \dots, d$. We define the solution space

$$\mathcal{B}^{\varphi, \rho_1, \dots, \rho_d}(\Omega) := {}^{l, \mathfrak{D}} H^\varphi(I; L^2(\Lambda_d)) \cap L^2(I; \mathcal{X}_d), \quad (3.42)$$

associated with the norm

$$\|u\|_{\mathcal{B}^{\varphi, \rho_1, \dots, \rho_d}(\Omega)} = \left\{ \|u\|_{l, \mathfrak{D} H^\varphi(I; L^2(\Lambda_d))}^2 + \|u\|_{L^2(I; \mathcal{X}_d)}^2 \right\}^{\frac{1}{2}}. \quad (3.43)$$

Considering Lemma 3.3.1,

$$\begin{aligned} \|u\|_{L^2(I; \mathcal{X}_d)} &= \left\| \|u(t, \cdot)\|_{\mathcal{X}_d} \right\|_{L^2(I)} \\ &= \left\{ \sum_{i=1}^d \int_{\nu_i^{min}}^{\nu_i^{max}} \rho_i(\nu_i) \left(\|x_i \mathcal{D}_{b_i}^{\nu_i}(u)\|_{L^2(\Omega)}^2 + \|a_i \mathcal{D}_{x_i}^{\nu_i}(u)\|_{L^2(\Omega)}^2 \right) d\nu_i \right. \\ &\quad \left. + \|u\|_{L^2(\Lambda_d)}^2 \right\}^{\frac{1}{2}}. \end{aligned} \quad (3.44)$$

Therefore, from (3.32) and (3.44),

$$\begin{aligned} \|u\|_{\mathcal{B}^{\varphi, \rho_1, \dots, \rho_d}(\Omega)} &= \left\{ \|u\|_{L^2(\Omega)}^2 + \int_{\tau^{min}}^{\tau^{max}} \varphi(\tau) \|_0 \mathcal{D}_t^\tau(u)\|_{L^2(\Omega)}^2 d\tau \right. \\ &\quad \left. + \sum_{i=1}^d \int_{\nu_i^{min}}^{\nu_i^{max}} \rho_i(\nu_i) \left(\|x_i \mathcal{D}_{b_i}^{\nu_i}(u)\|_{L^2(\Omega)}^2 + \|a_i \mathcal{D}_{x_i}^{\nu_i}(u)\|_{L^2(\Omega)}^2 \right) d\nu_i \right\}^{\frac{1}{2}}. \end{aligned} \quad (3.45)$$

Similarly, we define the test space

$$\mathfrak{B}^{\varphi, \rho_1, \dots, \rho_d}(\Omega) := {}^{r, \mathfrak{D}} H^\varphi\left(I; L^2(\Lambda_d)\right) \cap L^2(I; \mathcal{X}_d), \quad (3.46)$$

equipped with the norm

$$\begin{aligned} \|v\|_{\mathfrak{B}^{\varphi, \rho_1, \dots, \rho_d}(\Omega)} &= \left\{ \|v\|_{r H^\varphi(I; L^2(\Lambda_d))}^2 + \|v\|_{L^2(I; \mathcal{X}_d)}^2 \right\}^{\frac{1}{2}} \\ &= \left\{ \|v\|_{L^2(\Omega)}^2 + \int_{\tau_{min}}^{\tau_{max}} \varphi(\tau) \|{}_t \mathcal{D}_T^\tau(v)\|_{L^2(\Omega)}^2 d\tau \right. \\ &\quad \left. + \sum_{i=1}^d \int_{\nu_i_{min}}^{\nu_i_{max}} \rho_i(\nu_i) \left(\|{}_{x_i} \mathcal{D}_{b_i}^{\nu_i}(v)\|_{L^2(\Omega)}^2 + \|{}_{a_i} \mathcal{D}_{x_i}^{\nu_i}(v)\|_{L^2(\Omega)}^2 \right) d\nu_i \right\}^{\frac{1}{2}} \end{aligned} \quad (3.47)$$

by Lemma (3.3.1) and (3.32). Take $\Omega = I \times \Lambda_d$ for a positive integer d . The Petrov-Galerkin spectral method reads as: find $u \in \mathfrak{B}^{\varphi, \rho_1, \dots, \rho_d}(\Omega)$ such that

$$a(u, v) = l(v), \quad \forall v \in \mathfrak{B}^{\varphi, \rho_1, \dots, \rho_d}(\Omega), \quad (3.48)$$

where the functional $l(v) = (f, v)_\Omega$ and

$$\begin{aligned} a(u, v) &= \int_{\tau_{min}}^{\tau_{max}} \varphi(\tau) ({}_0 \mathcal{D}_t^\tau u, {}_t \mathcal{D}_T^\tau v)_\Omega d\tau \\ &\quad + \sum_{i=1}^d \int_{\mu_i_{min}}^{\mu_i_{max}} \varrho_i(\mu_i) \left(c_{l_i} ({}_{a_i} \mathcal{D}_{x_i}^{\mu_i} u, {}_{x_i} \mathcal{D}_{b_i}^{\mu_i} v)_\Omega + c_{r_i} ({}_{a_i} \mathcal{D}_{x_i}^{\mu_i} v, {}_{x_i} \mathcal{D}_{b_i}^{\mu_i} u)_\Omega \right) d\mu_i \\ &\quad - \sum_{j=1}^d \int_{\nu_j_{min}}^{\nu_j_{max}} \rho_j(\nu_j) \left(k_{l_j} ({}_{a_j} \mathcal{D}_{x_j}^{\nu_j} u, {}_{x_j} \mathcal{D}_{b_j}^{\nu_j} v)_\Omega + k_{r_j} ({}_{a_j} \mathcal{D}_{x_j}^{\nu_j} v, {}_{x_j} \mathcal{D}_{b_j}^{\nu_j} u)_\Omega \right) d\nu_j \\ &\quad + \gamma(u, v)_\Omega \end{aligned} \quad (3.49)$$

following (3.26), (3.27) and Lemma 3.3.5 and $\gamma, c_{l_i}, c_{r_i}, \kappa_{l_i}$, and κ_{r_i} are all constant. Besides, $0 < 2\tau_{min} < 2\tau_{max} < 1$ ($1 < 2\tau_{min} < 2\tau_{max} \leq 2$), $0 < 2\mu_i_{min} < 2\mu_i_{max} < 1$ and $1 < 2\nu_j_{min} < 2\nu_j_{max} \leq 2$ for $i, j = 1, 2, \dots, d$.

Remark 3.3.6. In the case $\tau < \frac{1}{2}$, additional regularity assumptions are required to ensure equivalence between the weak and strong formulations, see [23] for more details.

U_N and V_N are chosen as the finite-dimensional subspaces of $\mathcal{B}^{\varphi, \rho_1, \dots, \rho_d}(\Omega)$ and $\mathfrak{B}^{\varphi, \rho_1, \dots, \rho_d}(\Omega)$, respectively. Then, the PG scheme reads as: find $u_N \in U_N$ such that

$$a(u_N, v_N) = l(v_N), \quad \forall v \in V_N, \quad (3.50)$$

where

$$\begin{aligned} a(u_N, v_N) &= \int_{\tau_{min}}^{\tau_{max}} \varphi(\tau) ({}_0\mathcal{D}_t^\tau u_N, {}_t\mathcal{D}_T^\tau v_N)_\Omega d\tau \\ &\quad + \sum_{i=1}^d \int_{\mu_i_{min}}^{\mu_i_{max}} \varrho_i(\mu_i) \left[c_{l_i} ({}_a\mathcal{D}_{x_i}^{\mu_i} u_N, {}_{x_i}\mathcal{D}_{b_i}^{\mu_i} v_N)_\Omega + c_{r_i} ({}_a\mathcal{D}_{x_i}^{\mu_i} u_N, {}_{x_i}\mathcal{D}_{b_i}^{\mu_i} v_N)_\Omega \right] d\mu_i \\ &\quad - \sum_{j=1}^d \int_{v_j_{min}}^{v_j_{max}} \rho_j(v_j) \left[k_{l_j} ({}_a\mathcal{D}_{x_j}^{v_j} u_N, {}_{x_j}\mathcal{D}_{b_j}^{v_j} v_N)_\Omega + k_{r_j} ({}_a\mathcal{D}_{x_j}^{v_j} u_N, {}_{x_j}\mathcal{D}_{b_j}^{v_j} v_N)_\Omega \right] dv_j \\ &\quad + \gamma(u_N, v_N)_\Omega. \end{aligned} \quad (3.51)$$

Representing u_N as a linear combination of elements in U_N , the finite-dimensional problem (3.51) leads to a linear system, known as Lyapunov system, introduced in Section 3.4.

3.3.3 Well-posedness Analysis

The following assumption permit us to prove uniqueness of the weak form in (3.48) in Theorem 3.3.9.

Assumption 4. For all $v \in \mathfrak{B}^{\varphi, \rho_1, \dots, \rho_d}(\Omega)$

$$\begin{aligned} &\sup_{u \in \mathcal{B}^{\varphi, \rho_1, \dots, \rho_d}(\Omega)} \int_{\tau_{min}}^{\tau_{max}} \varphi(\tau) |({}_0\mathcal{D}_t^\tau u, {}_t\mathcal{D}_T^\tau v)_\Omega| d\tau > 0, \\ &\sup_{u \in \mathcal{B}^{\varphi, \rho_1, \dots, \rho_d}(\Omega)} \int_{v_j_{min}}^{v_j_{max}} \rho_j(v_j) \left(|({}_a\mathcal{D}_{x_j}^{v_j} u, {}_{x_j}\mathcal{D}_{b_j}^{v_j} v)_\Omega| + |({}_{x_j}\mathcal{D}_{b_j}^{v_j} u, {}_a\mathcal{D}_{x_j}^{v_j} v)_\Omega| \right) dv_j > 0, \\ &\sup_{u \in \mathcal{B}^{\varphi, \rho_1, \dots, \rho_d}(\Omega)} |(u, v)_\Omega| > 0, \end{aligned}$$

when $j = 1, \dots, d$.

Lemma 3.3.7. (Continuity) Let Assumption 4 hold. The bilinear form in (3.49) is continuous, i.e., for $u \in \mathcal{B}^{\varphi, \rho_1, \dots, \rho_d}(\Omega)$,

$$\exists \beta > 0, \quad |a(u, v)| \leq \beta \|u\|_{\mathcal{B}^{\varphi, \rho_1, \dots, \rho_d}(\Omega)} \|v\|_{\mathfrak{B}^{\varphi, \rho_1, \dots, \rho_d}(\Omega)} \quad \forall v \in \mathfrak{B}^{\varphi, \rho_1, \dots, \rho_d}(\Omega). \quad (3.52)$$

Proof. It follows from (3.28) and Lemma 3.3.3. \square

Theorem 3.3.8. Let Assumption 4 holds. The inf-sup condition of the bilinear form (3.49) for any $d \geq 1$ holds with $\beta > 0$, i.e.,

$$\inf_{0 \neq u \in \mathcal{B}^{\varphi, \rho_1, \dots, \rho_d}(\Omega)} \sup_{0 \neq v \in \mathfrak{B}^{\varphi, \rho_1, \dots, \rho_d}(\Omega)} \frac{|a(u, v)|}{\|v\|_{\mathfrak{B}^{\varphi, \rho_1, \dots, \rho_d}(\Omega)} \|u\|_{\mathcal{B}^{\varphi, \rho_1, \dots, \rho_d}(\Omega)}} \geq \beta > 0, \quad (3.53)$$

where $\Omega = I \times \Lambda_d$.

Proof. For $u \in \mathcal{B}^{\varphi, \rho_1, \dots, \rho_d}(\Omega)$ and $v \in \mathfrak{B}^{\varphi, \rho_1, \dots, \rho_d}(\Omega)$ under Assumption 4,

$$\begin{aligned} |a(u, v)| &\cong |(u, v)_\Omega| + \int_{\tau_{min}}^{\tau_{max}} \varphi(\tau) |({}_0\mathcal{D}_t^\tau u, {}_t\mathcal{D}_T^\tau v)_\Omega| d\tau \\ &\quad + \sum_{i=1}^d \int_{\mu_i^{min}}^{\mu_i^{max}} \rho_i(\mu_i) \left(|({}_{a_i}\mathcal{D}_{x_i}^{\mu_i} u, {}_{x_i}\mathcal{D}_{b_i}^{\mu_i} v)_\Omega| + |({}_{x_i}\mathcal{D}_{a_i}^{\mu_i} u, {}_{a_i}\mathcal{D}_{x_i}^{\mu_i} v)_\Omega| \right) d\mu_i \\ &\quad + \sum_{j=1}^d \int_{\nu_j^{min}}^{\nu_j^{max}} \rho_j(\nu_j) \left(|({}_{a_j}\mathcal{D}_{x_j}^{\nu_j} u, {}_{x_j}\mathcal{D}_{b_j}^{\nu_j} v)_\Omega| + |({}_{x_j}\mathcal{D}_{b_j}^{\nu_j} u, {}_{a_j}\mathcal{D}_{x_j}^{\nu_j} v)_\Omega| \right) d\nu_j. \end{aligned} \quad (3.54)$$

Following (3.28) and Theorem 2.5.2 in chapter 2,

$$\begin{aligned} &\sum_{i=1}^d \int_{\nu_i^{min}}^{\nu_i^{max}} \rho_i(\nu_i) \left(|({}_{a_i}\mathcal{D}_{x_i}^{\nu_i} (u), {}_{x_i}\mathcal{D}_{b_i}^{\nu_i} (v))_\Omega| + |({}_{x_i}\mathcal{D}_{b_i}^{\nu_i} (u), {}_{a_i}\mathcal{D}_{x_i}^{\nu_i} (v))_\Omega| \right) \\ &\geq \tilde{C}_1 \sum_{i=1}^d \left[\int_{\nu_i^{min}}^{\nu_i^{max}} \rho_i(\nu_i) \left(\|{}_{a_i}\mathcal{D}_{x_i}^{\nu_i} (u)\|_{L^2(\Omega)} \right) d\nu_i \int_{\nu_i^{min}}^{\nu_i^{max}} \rho_i(\nu_i) \left(\|{}_{x_i}\mathcal{D}_{b_i}^{\nu_i} (v)\|_{L^2(\Omega)} \right) d\nu_i \right. \\ &\quad \left. + \int_{\nu_i^{min}}^{\nu_i^{max}} \rho_i(\nu_i) \left(\|{}_{x_i}\mathcal{D}_{b_i}^{\nu_i} (u)\|_{L^2(\Omega)} \right) d\nu_i \int_{\nu_i^{min}}^{\nu_i^{max}} \rho_i(\nu_i) \left(\|{}_{a_i}\mathcal{D}_{x_i}^{\nu_i} (v)\|_{L^2(\Omega)} \right) d\nu_i \right]. \end{aligned} \quad (3.55)$$

Thus,

$$\begin{aligned}
& \sum_{i=1}^d \int_{\nu_i^{\min}}^{\nu_i^{\max}} \rho_i(\nu_i) \left(|(a_i \mathcal{D}_{x_i}^{\nu_i}(u), {}_{x_i} \mathcal{D}_{b_i}^{\nu_i}(v))_{\Omega}| + |({}_{x_i} \mathcal{D}_{b_i}^{\nu_i}(u), a_i \mathcal{D}_{x_i}^{\nu_i}(v))_{\Omega}| \right) d\nu_i \\
& \geq \tilde{C}_1 \sum_{i=1}^d \int_{\nu_i^{\min}}^{\nu_i^{\max}} \rho_i(\nu_i) \left(\|a_i \mathcal{D}_{x_i}^{\nu_i}(u)\|_{L^2(\Omega)} + \|{}_{x_i} \mathcal{D}_{b_i}^{\nu_i}(u)\|_{L^2(\Omega)} \right) d\nu_i \\
& \times \sum_{j=1}^d \int_{\nu_j^{\min}}^{\nu_j^{\max}} \rho_j(\nu_j) \left(\|{}_{x_j} \mathcal{D}_{b_j}^{\nu_j}(v)\|_{L^2(\Omega)} + \|a_j \mathcal{D}_{x_j}^{\nu_j}(v)\|_{L^2(\Omega)} \right) d\nu_j \\
& = \tilde{C}_1 |u|_{L^2(I; \mathcal{X}_d)} |v|_{L^2(I; \mathcal{X}_d)}. \tag{3.56}
\end{aligned}$$

where \tilde{C}_1 is a positive constant and independent of u . Considering Lemma 3.3.4, there exists a positive constant $\tilde{C}_2 > 0$ and independent of u such that

$$\sup_{0 \neq v \in \mathfrak{B}^{\varphi, \rho_1, \dots, \rho_d}(\Omega)} \frac{\int_{\tau^{\min}}^{\tau^{\max}} \varphi(\tau) |({}_0 \mathcal{D}_t^{\tau}(u), {}_t \mathcal{D}_T^{\tau}(v))_{\Omega}| d\tau}{|v|_{r, \mathfrak{D}_{H^{\varphi}}(I; L^2(\Lambda_d))}} \geq \tilde{C}_2 |u|_{l, \mathfrak{D}_{H^{\varphi}}(I; L^2(\Lambda_d))}. \tag{3.57}$$

Furthermore, for $u \in \mathfrak{B}^{\varphi, \rho_1, \dots, \rho_d}(\Omega)$

$$\begin{aligned}
& \sup_{0 \neq v \in \mathfrak{B}^{\varphi, \dots, \rho_d}(\Omega)} \frac{\int_{\tau^{\min}}^{\tau^{\max}} \varphi(\tau) |({}_0 \mathcal{D}_t^{\tau}(u), {}_t \mathcal{D}_T^{\tau}(v))_{\Omega}| d\tau}{|v|_{r, \mathfrak{D}_{H^{\varphi}}(I; L^2(\Lambda_d))}} \cong \\
& \sup_{0 \neq v \in \mathfrak{B}^{\varphi, \dots, \rho_d}(\Omega)} \frac{\int_{\tau^{\min}}^{\tau^{\max}} \varphi(\tau) |({}_0 \mathcal{D}_t^{\tau}(u), {}_t \mathcal{D}_T^{\tau}(v))_{\Omega}| d\tau}{|v|_{\mathfrak{B}^{\varphi, \rho_1, \dots, \rho_d}(\Omega)}} \tag{3.58}
\end{aligned}$$

and

$$\begin{aligned}
& \sup_{0 \neq v \in \mathfrak{B}^{\varphi, \rho_1, \dots, \rho_d}(\Omega)} \frac{\sum_{j=1}^d \int_{\nu_j^{\min}}^{\nu_j^{\max}} \rho_j(\nu_j) \left(|({}_{x_j} \mathcal{D}_{b_j}^{\nu_j} u, {}_{x_j} \mathcal{D}_{b_j}^{\nu_j} v)_{\Omega}| \right.} {\|v\|_{L^2(I; \mathcal{X}_d)}} \\
& \quad \left. + \frac{|({}_{x_j} \mathcal{D}_{b_j}^{\nu_j} u, a_j \mathcal{D}_{x_j}^{\nu_j} v)_{\Omega}| \right) d\nu_j}{\|v\|_{L^2(I; \mathcal{X}_d)}} \\
& \cong \sup_{0 \neq v \in \mathfrak{B}^{\varphi, \rho_1, \dots, \rho_d}(\Omega)} \frac{\sum_{j=1}^d \int_{\nu_j^{\min}}^{\nu_j^{\max}} \rho_j(\nu_j) \left(|({}_{x_j} \mathcal{D}_{b_j}^{\nu_j} u, {}_{x_j} \mathcal{D}_{b_j}^{\nu_j} v)_{\Omega}| \right.} {\|v\|_{\mathfrak{B}^{\varphi, \rho_1, \dots, \rho_d}(\Omega)}} \\
& \quad \left. + \frac{|({}_{x_j} \mathcal{D}_{b_j}^{\nu_j} u, a_j \mathcal{D}_{x_j}^{\nu_j} v)_{\Omega}| \right) d\nu_j}{\|v\|_{\mathfrak{B}^{\varphi, \rho_1, \dots, \rho_d}(\Omega)}}. \tag{3.59}
\end{aligned}$$

Therefore, from (3.56), (3.57), (3.58), and (3.59) we have

$$\begin{aligned}
& \sup_{0 \neq v \in \mathcal{B}^{\varphi, \rho_1, \dots, \rho_d}(\Omega)} \frac{|a(u, v)|}{\|v\|_{\mathcal{B}^{\varphi, \rho_1, \dots, \rho_d}(\Omega)}} \\
& \geq \bar{\beta} \sup_{0 \neq v \in \mathcal{B}^{\varphi, \rho_1, \dots, \rho_d}(\Omega)} \frac{|(u, v)_\Omega| + \int_{\tau_{min}}^{\tau_{max}} \varphi(\tau) |(_0\mathcal{D}_t^\tau u, {}_t\mathcal{D}_T^\tau v)_\Omega| d\tau}{\|v\|_{\mathcal{B}^{\varphi, \rho_1, \dots, \rho_d}(\Omega)}} \\
& + \frac{\sum_{j=1}^d \int_{\nu_j^{min}}^{\nu_j^{max}} \rho_j(\nu_j) \left(|({}_{a_j}\mathcal{D}_{x_j}^{\nu_j} u, {}_{x_j}\mathcal{D}_{b_j}^{\nu_j} v)_\Omega| + |({}_{x_j}\mathcal{D}_{b_j}^{\nu_j} u, {}_{a_j}\mathcal{D}_{x_j}^{\nu_j} v)_\Omega| \right) d\nu_j}{\|v\|_{\mathcal{B}^{\varphi, \rho_1, \dots, \rho_d}(\Omega)}} \\
& \geq \bar{\beta} \bar{C} \left(\|u\|_{L^2(\Omega)} + |u|_{l, \mathfrak{D}_{H^\varphi(I; L^2(\Lambda_d))}} + |u|_{L^2(I; \mathcal{X}_d)} \right), \tag{3.60}
\end{aligned}$$

where $\bar{C} = \min\{\tilde{C}_2, \tilde{C}_1\}$. Accordingly,

$$\inf_{0 \neq u \in \mathcal{B}^{\varphi, \rho_1, \dots, \rho_d}(\Omega)} \sup_{0 \neq v \in \mathcal{B}^{\varphi, \rho_1, \dots, \rho_d}(\Omega)} \frac{|a(u, v)|}{\|v\|_{\mathcal{B}^{\varphi, \rho_1, \dots, \rho_d}(\Omega)}} \geq \beta \|u\|_{\mathcal{B}^{\varphi, \rho_1, \dots, \rho_d}(\Omega)}, \tag{3.61}$$

where $\beta = \bar{\beta} \bar{C}$ is a positive constant and independent. \square

Theorem 3.3.9. (Well-Posedness) For $0 < 2\tau_{min} < 2\tau_{max} < 1$ ($1 < 2\tau_{min} < 2\tau_{max} \leq 2$), $1 < 2\nu_i^{min} < 2\nu_i^{max} \leq 2$, and $i = 1, \dots, d$, there exists a unique solution to (3.50), which is continuously dependent on $f \in (\mathcal{B}^{\tau, \nu_1, \dots, \nu_d})^*(\Omega)$, where $(\mathcal{B}^{\tau, \nu_1, \dots, \nu_d})^*(\Omega)$ is the dual space of $\mathcal{B}^{\tau, \nu_1, \dots, \nu_d}(\Omega)$.

Proof. In virtue of the generalized Babuška-Lax-Milgram theorem [62], the well-posedness of the weak form in (3.48) in $(1+d)$ dimensions is guaranteed by the continuity and the *inf-sup* condition, which are proven in Lemma 3.3.7 and Theorem 3.3.8, respectively. \square

3.4 Petrov Galerkin Method

To construct a Petrov-Galerkin spectral method for the finite-dimensional weak form problem in (3.50), we first define the proper finite-dimensional basis/test spaces and then implement the numerical scheme.

3.4.1 Space of Basis (U_N) and Test (V_N) Functions

As discussed in chapter 2, we take the spatial basis, given in the standard domain $\xi \in [-1, 1]$ as $\phi_m(\xi) = \sigma_m(P_{m+1}(\xi) - P_{m-1}(\xi))$, $m = 1, 2, \dots$, where $P_m(\xi)$ is the Legendre polynomials of order m and $\sigma_m = 2 + (-1)^m$. Besides, employing Jacobi *poly-fractonomials* of the first kind [56, 101], the temporal basis functions are given in the standard domain $\eta \in [-1, 1]$ as $\psi_n^\tau(\eta) = \sigma_n(1 + \eta)^\tau P_{n-1}^{-\tau, \tau}(\eta)$, $n = 1, 2, \dots$.

We also let $\eta(t) = 2t/T - 1$ and $\xi_j(s) = 2\frac{s-a_j}{b_j-a_j} - 1$ to be temporal and spatial affine mappings from $t \in [0, T]$ and $x_j \in [a_j, b_j]$ to the standard domain $[-1, 1]$, respectively. Therefore,

$$U_N = \text{span}\left\{\left(\psi_n^\tau \circ \eta\right)(t) \prod_{j=1}^d \left(\phi_{m_j} \circ \xi_j\right)(x_j) : n = 1, 2, \dots, N, m_j = 1, 2, \dots, M_j\right\}.$$

Similarly, we employ Legendre polynomials and Jacobi *polyfractonomials* of second kind in the standard domain to construct the finite dimensional test space as

$$V_N = \text{span}\left\{\left(\Psi_r^\tau \circ \eta\right)(t) \prod_{j=1}^d \left(\Phi_{k_j} \circ \xi_j\right)(x_j) : r = 1, 2, \dots, R, k_j = 1, 2, \dots, M_j\right\},$$

where $\Psi_r^\tau(\eta) = \tilde{\sigma}_r(1 - \eta)^\tau P_{r-1}^{\tau, -\tau}(\eta)$, $r = 1, 2, \dots$ and $\Phi_k(\xi) = \tilde{\sigma}_k(P_{k+1}(\xi) - P_{k-1}(\xi))$, $k = 1, 2, \dots$. The coefficient $\tilde{\sigma}_k$ is defined as $\tilde{\sigma}_k = 2(-1)^k + 1$.

Since the univariate basis/test functions belong to the fractional Sobolev spaces (see [56]) and $0 < \varphi(\tau) \in L^1((\tau^{\min}, \tau^{\max}))$, $0 < \rho_j(\nu_j) \in L^1((\nu_j^{\min}, \nu_j^{\max}))$ for $j = 1, \dots, d$, then $U_N \subset \mathcal{B}^{\varphi, \rho_1, \dots, \rho_d}(\Omega)$ and $V_N \subset \mathfrak{B}^{\varphi, \rho_1, \dots, \rho_d}(\Omega)$. Accordingly, we approximate the solution in terms of a linear combination of elements in U_N , which satisfies initial and boundary conditions.

3.4.2 Implementation of the PG Spectral Method

The solution u_N of (3.50) can be represented as

$$u_N(x, t) = \sum_{n=1}^N \sum_{m_1=1}^{M_1} \dots \sum_{m_d=1}^{M_d} \hat{u}_{n, m_1, \dots, m_d} \left[\psi_n^\tau(t) \prod_{j=1}^d \phi_{m_j}(x_j) \right] \quad (3.62)$$

in Ω and also we take $v_N = \Psi_r^\tau(t) \prod_{j=1}^d \Phi_{k_j}(x_j)$, $r = 1, 2, \dots, N$, $k_j = 1, 2, \dots, M_j$. Accordingly, by replacing u_N and v_N in (3.50), we obtain the following Lyapunov system

$$\left(S_\tau^\varphi \otimes M_1 \otimes M_2 \cdots \otimes M_d + \sum_{j=1}^d [M_\tau \otimes M_1 \otimes \cdots \otimes M_{j-1} \otimes S_j^{Tot} \otimes M_{j+1} \cdots \otimes M_d] \right. \\ \left. + \gamma M_\tau \otimes M_1 \otimes M_2 \cdots \otimes M_d \right) \mathcal{U} = F, \quad (3.63)$$

in which \otimes represents the Kronecker product, F denotes the multi-dimensional load matrix whose entries are given as

$$F_{r,k_1,\dots,k_d} = \int_{\Omega} f(t, x_1, \dots, x_d) (\Psi_r^\tau \circ \eta)(t) \prod_{j=1}^d (\Phi_{k_j} \circ \xi_j)(x_j) d\Omega, \quad (3.64)$$

and $S_j^{Tot} = c_{l_j} S_l^{\varrho_j} + c_{r_j} S_r^{\varrho_j} - \kappa_{l_j} S_l^{\varrho_j} - \kappa_{r_j} S_r^{\varrho_j}$. The matrices S_τ^φ and M_τ denote the temporal stiffness and mass matrices, respectively; $S_l^{\varrho_j}$, $S_r^{\varrho_j}$, $S_l^{\rho_j}$, $S_r^{\rho_j}$, and M_j denote the spatial stiffness and mass matrices. The entries of spatial mass matrix M_j are computed analytically, while we employ proper quadrature rules to accurately compute the entries of temporal mass matrix M_τ as discussed in chapter 2. The entries of S_τ^φ are also computed based on Theorem 3.1 (spectrally/exponentially accurate quadrature rule in α -dimension) in [70]. Likewise, we present the computation of S_j^{Tot} in Lemma B.1.1 in Appendix B.

Remark 3.4.1. *The choices of coefficients in the construction of finite dimensional basis/test functions lead to symmetric mass/stiffness matrices, which help formulating the following fast solver.*

3.4.3 Unified Fast FPDE Solver

In order to formulate a closed-form solution to the Lyapunov system (3.63), we follow [55] and develop a fast solver in terms of the generalized eigen-solutions.

Theorem 3.4.2. *Take $\{\vec{e}_{m_j}^j, \lambda_{m_j}^j\}_{m_j=1}^{M_j}$ as the set of general eigen-solutions of the spatial stiffness matrix S_j^{Tot} with respect to the mass matrix M_j . Besides, let $\{\vec{e}_n^\tau, \lambda_n^\tau\}_{n=1}^N$ be the set of general*

eigen-solutions of the temporal mass matrix M_τ with respect to the stiffness matrix S_τ^φ . Then the unknown coefficients matrix \mathcal{U} is obtained as

$$\mathcal{U} = \sum_{n=1}^N \sum_{m_1=1}^{M_1} \cdots \sum_{m_d=1}^{M_d} \kappa_{n,m_1,\dots,m_d} \vec{e}_n^\tau \otimes \vec{e}_{m_1}^1 \otimes \cdots \otimes \vec{e}_{m_d}^d, \quad (3.65)$$

where

$$\kappa_{n,m_1,\dots,m_d} = \frac{(\vec{e}_n^\tau \vec{e}_{m_1}^1 \cdots \vec{e}_{m_d}^d)F}{\left[(\vec{e}_n^\tau)^T S_\tau^\varphi \vec{e}_n^\tau \right] \prod_{j=1}^d (\vec{e}_{m_j}^{jT} M_j \vec{e}_{m_j}^j) \Lambda_{n,m_1,\dots,m_d}}, \quad (3.66)$$

and

$$\Lambda_{n,m_1,\dots,m_d} = \left[(1 + \gamma \lambda_n^\tau) + \lambda_n^\tau \sum_{j=1}^d (\lambda_{m_j}^j) \right].$$

Proof. See theorem 2.8.1 in chapter 2. \square

Remark 3.4.3. The naive computation of all entries in (3.66) leads to a computational complexity of $O(N^{2+2d})$, including construction of stiffness and mass matrices. By performing sum-factorization [55], the operator counts can be reduced to $O(N^{2+d})$.

3.5 Stability and Error Analysis

The following theorems provide the finite dimensional stability and error analysis of the proposed scheme, based on the well-posedness analysis from Section 3.3.3.

3.5.1 Stability Analysis

Theorem 3.5.1. Let Assumption 4 hold. The Petrov-Galerkin spectral method for (3.51) is stable, i.e.,

$$\inf_{0 \neq u_N \in U_N} \sup_{0 \neq v \in V_N} \frac{|a(u_N, v_N)|}{\|v_N\|_{\mathcal{B}^{\varphi, \rho_1, \dots, \rho_d}(\Omega)} \|u_N\|_{\mathcal{B}^{\varphi, \rho_1, \dots, \rho_d}(\Omega)}} \geq \beta > 0, \quad (3.67)$$

holds with $\beta > 0$ and independent of N .

Proof. Regarding $U_N \subset \mathcal{B}^{\varphi, \rho_1, \dots, \rho_d}(\Omega)$ and $V_N \subset \mathfrak{B}^{\varphi, \rho_1, \dots, \rho_d}(\Omega)$, (3.67) follows directly from Theorem 3.3.8. \square

Remark 3.5.2. *The bilinear form (3.51) can be expanded in terms of the basis and test functions to obtain the lower limit of β , see [55].*

3.5.2 Error Analysis

Denoting by $P_{\mathcal{M}}(\Lambda)$ the space of all polynomials of degree $\leq \mathcal{M}$ on $\Lambda \subset \mathbb{R}$, $P_{\mathcal{M}}^{\varphi}(\Lambda) := P_{\mathcal{M}}(\Lambda) \cap {}^{\mathfrak{D}}H^{\varphi}(\Lambda)$, where $0 < \varphi(\tau) \in L^1((\tau^{\min}, \tau^{\max}))$ and ${}^{\mathfrak{D}}H^{\varphi}(\Lambda)$ is the *distributed Sobolev* space associated with the norm $\|\cdot\|_{{}^{\mathfrak{D}}H^{\varphi}(\Lambda)}$. In this section, we take $I_0 = (0, T)$, $I_i = (a_i, b_i)$ for $i = 1, \dots, d$, $\Lambda_i = I_i \times \Lambda_{i-1}$, and $\Lambda_i^j = \prod_{\substack{k=1 \\ k \neq j}}^i I_k$. Besides, $0 < 2\tau^{\min} < 2\tau^{\max} < 1$ ($1 < 2\tau^{\min} < 2\tau^{\max} \leq 2$), $1 < 2\nu_i^{\min} < 2\nu_i^{\max} \leq 2$ for $i = 1, \dots, d$. Where there is no confusion, the symbols I_i , Λ_i , and Λ_i^j and the intervals of $(\tau^{\min}, \tau^{\max})$ and $(\nu_i^{\min}, \nu_i^{\max})$ will be dropped from the notations.

Theorem 3.5.3. [115] *Let r_1 be a real number, where $r_1 \neq \mathcal{M}_1 + \frac{1}{2}$, and $1 \leq r_1$. There exists a projection operator $\Pi_{r_1, \mathcal{M}_1}^{\nu_1}$ from $H^{r_1}(\Lambda_1) \cap H_0^{\nu_1}(\Lambda_1)$ to $P_{\mathcal{M}_1}^{\nu_1}(\Lambda_1)$ such that for any $u \in H^{r_1}(\Lambda_1) \cap H_0^{\nu_1}(\Lambda_1)$, we have $\|u - \Pi_{r_1, \mathcal{M}_1}^{\nu_1} u\|_{cH^{\nu_1}(\Lambda_1)} \leq c_1 \mathcal{M}_1^{\nu_1 - r_1} \|u\|_{H^{r_1}(\Lambda_1)}$, where c_1 is a positive constant.*

Theorem 3.5.4. [70] *Let $r_0 \geq 1$, $r_0 \neq \mathcal{N} + \frac{1}{2}$. There exists an operator $\Pi_{r_0, \mathcal{N}}^{\varphi}$ from $H^{r_0}(I) \cap {}^l \mathfrak{D}H^{\varphi}(I)$ to $P_{\mathcal{N}}^{\varphi}(\Lambda_1)$ such that for any $u \in H^{r_0}(I) \cap {}^l \mathfrak{D}H^{\varphi}(I)$, we have*

$$\|u - \Pi_{r_0, \mathcal{N}}^{\varphi} u\|_{lH^{\varphi}(I)}^2 \leq c_0 \mathcal{N}^{-2r_0} \int_{\tau^{\min}}^{\tau^{\max}} \varphi(\tau) \mathcal{N}^{2\tau} \|u\|_{H^{r_0}(I)} d\tau,$$

where c_0 is a positive constant and $0 < \varphi(\tau) \in L^1((\tau^{\min}, \tau^{\max}))$.

In the following, employing Theorems 3.5.3 and 3.5.4 and also Theorem 2.10.3 in chapter 2, we study the properties of higher-dimensional approximation operators in the following Lemmas.

Theorem 3.5.5. *Let $r_1 \geq 1$, $r_1 \neq \mathcal{M}_1 + \frac{1}{2}$. There exists a projection operator $\Pi_{r_1, \mathcal{M}_1}^{\rho_1}(I_1)$ from $H^{r_1}(I_1) \cap {}^l \mathfrak{D}H^{\rho_1}(I_1)$ to $P_{\mathcal{M}_1}^{\rho_1}(I_1)$ such that for any $u \in H^{r_1}(I_1) \cap {}^l \mathfrak{D}H^{\rho_1}(I_1)$, we have*

$$\|u - \Pi_{r_1, \mathcal{M}_1}^{\rho_1} u\|_{l, \mathfrak{D}H^{\rho_1}(I_1)}^2 \leq \mathcal{M}_1^{-2r_1} \int_{\nu_1^{\min}}^{\nu_1^{\max}} \rho_1(\nu_1) \mathcal{M}_1^{2\nu_1} \|u\|_{H^{r_1}(I_1)} d\nu_1,$$

where $0 < \rho_1(\nu_1) \in L^1((\nu_1^{\min}, \nu_1^{\max}))$.

Proof. From Theorem 3.5.3 for $u \in H^{r_1} \cap {}^c H^{\nu_1}$ we have

$$\|u - \Pi_{r_1, M_1}^{\nu_1} u\|_{{}^c H^{\nu_1}(\Lambda_1)} \leq M_1^{\nu_1 - r_1} \|u\|_{H^{r_1}(\Lambda_1)}.$$

Therefore, for $u \in H^{r_1}(I_1) \cap {}^l H^{\rho_1}(I_1)$ we have

$$\begin{aligned} \|u - \Pi_{r_1, M_1}^{\rho_1} u\|_{{}^l \mathfrak{D} H^{\rho_1}(I_1)}^2 &= \int_{\nu_1^{\min}}^{\nu_1^{\max}} \rho_1(\nu_1) \|u - \Pi_{r_1, M_1}^{\nu_1} u\|_{{}^c H^{\nu_1}(\Lambda_1)}^2 d\nu_1 \\ &\leq \int_{\nu_1^{\min}}^{\nu_1^{\max}} \rho_1(\nu_1) M_1^{2\nu_1 - 2r_1} \|u\|_{H^{r_1}(\Lambda_1)}^2 d\nu_1 = M_1^{-2r_1} \int_{\nu_1^{\min}}^{\nu_1^{\max}} \rho_1(\nu_1) M_1^{2\nu_1} \|u\|_{H^{r_1}(I_1)} d\nu_1. \end{aligned}$$

□

Lemma 3.5.6. *Let the real-valued $1 \leq r_1, r_2$ and $\Omega = I_1 \times I_2$. If $u \in {}^l \mathfrak{D} H^{\rho_2}(I_2, H^{r_1}(I_1)) \cap H^{r_2}(I_2, {}^l \mathfrak{D} H_0^{\rho_1}(I_1))$, then*

$$\begin{aligned} &\|u - \Pi_{r_1, M_1}^{\rho_1} \Pi_{r_2, M_2}^{\rho_2} u\|_{{}^l \mathfrak{B}^{\rho_1, \rho_2}(\Omega)}^2 \leq \\ &M_2^{-2r_2} \int_{\nu_2^{\min}}^{\nu_2^{\max}} \rho_2(\nu_2) \left(M_2^{2\nu_2} \|u\|_{H^{r_2}(I_2, L^2(I_1))} + M_2^{2\nu_2} M_1^{-2r_1} \|u\|_{H^{r_2}(I_2, H^{r_1}(I_1))} \right) d\nu_2 \\ &+ M_1^{-2r_1} \int_{\nu_1^{\min}}^{\nu_1^{\max}} \rho_1(\nu_1) \left(M_1^{2\nu_1} \|u\|_{H^{r_1}(I_1, L^2(I_2))} + M_1^{2\nu_1} M_2^{-2r_2} \|u\|_{H^{r_1}(I_1, H^{r_2}(I_2))} \right) d\nu_1 \\ &+ M_2^{-2r_2} \|u\|_{{}^l \mathfrak{D} H^{\rho_1}(I_1, H^{r_2}(I_2))} + M_1^{-2r_1} \|u\|_{{}^l \mathfrak{D} H^{\rho_2}(I_2, H^{r_1}(I_1))}, \end{aligned} \quad (3.68)$$

where $\|\cdot\|_{{}^l \mathfrak{B}^{\rho_1, \rho_2}(\Omega)} = \{\|\cdot\|_{H^{\rho_1}(I_1, L^2(I_2))}^2 + \|\cdot\|_{H^{\rho_2}(I_2, L^2(I_1))}^2\}^{\frac{1}{2}}$, $0 < \rho_1(\nu_1) \in L^1([\nu_1^{\min}, \nu_1^{\max}])$, and $0 < \rho_2(\nu_2) \in L^1([\nu_2^{\min}, \nu_2^{\max}])$.

Proof. For $u \in {}^l \mathfrak{D} H^{\rho_2}(I_2, H^{r_1}(I_1)) \cap H^{r_2}(I_2, H^{\rho_1}(I_1))$, evidently $u \in H^{r_2}(I_2, H^{r_1}(I_1))$, $u \in H^{r_2}(I_2, L^2(I_1))$, and $u \in H^{r_1}(I_1, L^2(I_2))$. Besides, from the definition of $\|\cdot\|_{{}^l \mathfrak{B}^{\rho_1, \rho_2}(\Omega)}$ we have

$$\begin{aligned} &\|u - \Pi_{r_1, M_1}^{\rho_1} \Pi_{r_2, M_2}^{\rho_2} u\|_{{}^l \mathfrak{B}^{\rho_1, \rho_2}(\Omega)} \\ &= \{\|u - \Pi_{r_1, M_1}^{\rho_1} \Pi_{r_2, M_2}^{\rho_2} u\|_{{}^l \mathfrak{D} H^{\rho_1}(I_1, L^2(I_2))}^2 + \|u - \Pi_{r_1, M_1}^{\rho_1} \Pi_{r_2, M_2}^{\rho_2} u\|_{{}^l \mathfrak{D} H^{\rho_2}(I_2, L^2(I_1))}^2\}^{\frac{1}{2}}. \end{aligned}$$

Following Lemma 2.10.3 in chapter 2 and Theorem 3.5.5, $\|u - \Pi_{r_1, M_1}^{\rho_1} \Pi_{r_2, M_2}^{\rho_2} u\|_{\mathfrak{D} H^{\rho_2}(I_2, L^2(I_1))}^2$ can be simplified to

$$\begin{aligned}
& \|u - \Pi_{r_1, M_1}^{\rho_1} \Pi_{r_2, M_2}^{\rho_2} u\|_{\mathfrak{D} H^{\rho_2}(I_2, L^2(I_1))}^2 \\
&= \|u - \Pi_{r_2, M_2}^{\rho_2} u + \Pi_{r_2, M_2}^{\rho_2} u - \Pi_{r_1, M_1}^{\rho_1} \Pi_{r_2, M_2}^{\rho_2} u\|_{\mathfrak{D} H^{\rho_2}(I_2, L^2(I_1))}^2 \\
&\leq \|u - \Pi_{r_2, M_2}^{\rho_2} u\|_{\mathfrak{D} H^{\rho_2}(I_2, L^2(I_1))}^2 + \|\Pi_{r_2, M_2}^{\rho_2} u - \Pi_{r_1, M_1}^{\rho_1} \Pi_{r_2, M_2}^{\rho_2} u\|_{\mathfrak{D} H^{\rho_2}(I_2, L^2(I_1))}^2 \\
&\leq M_2^{-2r_2} \int_{v_2^{\min}}^{v_2^{\max}} \rho_2(v_2) M_2^{2v_2} \|u\|_{H^{r_2}(I_2, L^2(I_1))}^2 dv_2 \\
&\quad + \|(\Pi_{r_2, M_2}^{\rho_2} - \mathcal{I})(u - \Pi_{r_1, M_1}^{\rho_1} u)\|_{\mathfrak{D} H^{\rho_2}(I_2, L^2(I_1))}^2 + \|u - \Pi_{r_1, M_1}^{\rho_1} u\|_{\mathfrak{D} H^{\rho_2}(I_2, L^2(I_1))}^2 \\
&\leq M_2^{-2r_2} \int_{v_2^{\min}}^{v_2^{\max}} \rho_2(v_2) M_2^{2v_2} \|u\|_{H^{r_2}(I_2, L^2(I_1))}^2 dv_2
\end{aligned} \tag{3.69}$$

$$\begin{aligned}
& + M_2^{-2r_2} M_1^{-2r_1} \int_{v_2^{\min}}^{v_2^{\max}} \rho_2(v_2) M_2^{2v_2} \|u\|_{H^{r_2}(I_2, H^{r_1}(I_1))}^2 dv_2 + M_1^{-2r_1} \|u\|_{\mathfrak{D} H^{\rho_2}(I_2, H^{r_1}(I_1))}^2,
\end{aligned} \tag{3.70}$$

where \mathcal{I} is the identity operator. Furthermore,

$$\begin{aligned}
& \|u - \Pi_{r_1, M_1}^{\rho_1} \Pi_{r_2, M_2}^{\rho_2} u\|_{L^2(I_2, H^{\rho_1}(I_1))}^2 \\
&= \|u - \Pi_{r_1, M_1}^{\rho_1} u + \Pi_{r_1, M_1}^{\rho_1} u - \Pi_{r_1, M_1}^{\rho_1} \Pi_{r_2, M_2}^{\rho_2} u\|_{\mathfrak{D} H^{\rho_1}(I_1, L^2(I_2))}^2 \\
&\leq \|u - \Pi_{r_1, M_1}^{\rho_1} u\|_{\mathfrak{D} H^{\rho_1}(I_1, L^2(I_2))}^2 + \|\Pi_{r_1, M_1}^{\rho_1} u - \Pi_{r_1, M_1}^{\rho_1} \Pi_{r_2, M_2}^{\rho_2} u\|_{\mathfrak{D} H^{\rho_1}(I_1, L^2(I_2))}^2 \\
&\leq M_1^{-2r_1} \int_{v_1^{\min}}^{v_1^{\max}} \rho_1(v_1) M_1^{2v_1} \|u\|_{H^{r_1}(I_1, L^2(I_2))}^2 dv_1 \\
&\quad + \|(\Pi_{r_1, M_1}^{\rho_1} - \mathcal{I})(u - \Pi_{r_2, M_2}^{\rho_2} u)\|_{\mathfrak{D} H^{\rho_1}(I_1, L^2(I_2))}^2 + \|u - \Pi_{r_2, M_2}^{\rho_2} u\|_{\mathfrak{D} H^{\rho_1}(I_1, L^2(I_2))}^2 \\
&\leq M_1^{-2r_1} \int_{v_1^{\min}}^{v_1^{\max}} \rho_1(v_1) M_1^{2v_1} \|u\|_{H^{r_1}(I_1, L^2(I_2))}^2 dv_1 \\
&\quad + M_2^{-2r_2} M_1^{-2r_1} \int_{v_1^{\min}}^{v_1^{\max}} \rho_1(v_1) M_1^{2v_1} \|u\|_{H^{r_1}(I_1, H^{r_2}(I_2))}^2 dv_1 + M_2^{-2r_2} \|u\|_{\mathfrak{D} H^{\rho_1}(I_1, H^{r_2}(I_2))}^2.
\end{aligned} \tag{3.71}$$

Therefore, (3.68) can be derived immediately from (3.69) and (3.71). \square

Likewise, Lemma 3.5.5 can be easily extended to the d -dimensional approximation operator as

$$\begin{aligned}
& \|u - \Pi_d^h u\|_{\mathfrak{D} H^{\rho_i}(I_i, L^2(\Lambda_d^i))}^2 \\
& \leq \mathcal{M}_i^{-2r_i} \int_{\nu_i^{\min}}^{\nu_i^{\max}} \rho_i(\nu_i) \mathcal{M}_i^{2\nu_i} \|u\|_{H^{r_i}(I_i, L^2(\Lambda_d^i))}^2 d\nu_i + \sum_{\substack{j=1 \\ j \neq i}}^d \mathcal{M}_j^{-2r_j} \|u\|_{\mathfrak{D} H^{\rho_i}(I_i, H^{r_j}(I_j, L^2(\Lambda_d^{i,j})))}^2 \\
& + \mathcal{M}_i^{-2r_i} \int_{\nu_i^{\min}}^{\nu_i^{\max}} \rho_i(\nu_i) \mathcal{M}_i^{2\nu_i} \sum_{\substack{j=1 \\ j \neq i}}^d \mathcal{M}_j^{-2r_j} \|u\|_{H^{r_i}(I_i, H^{r_j}(I_j, L^2(\Lambda_d^{i,j})))}^2 d\nu_i \\
& + \sum_{\substack{k=1 \\ k \neq i}}^d \sum_{\substack{j=1 \\ j \neq i, k}}^d \mathcal{M}_j^{-2r_j} \mathcal{M}_k^{-2r_k} \|u\|_{\mathfrak{D} H^{\rho_i}(I_i, H^{r_k, r_j}(I_k \times I_j, L^2(\Lambda_d^{i,j,k})))}^2
\end{aligned} \tag{3.72}$$

$$+ \cdots + \mathcal{M}_i^{-2r_i} \int_{\nu_i^{\min}}^{\nu_i^{\max}} \rho_i(\nu_i) \mathcal{M}_i^{2\nu_i} \prod_{\substack{j=1 \\ j \neq i}}^d \mathcal{M}_j^{-r_j} \|u\|_{c H^{\nu_i}(I_i, H^{r_1, \dots, r_d}(\Lambda_d^i))}^2 d\nu_i, \tag{3.73}$$

where $\Pi_d^h = \Pi_{r_1, \mathcal{M}_1}^{\rho_1} \cdots \Pi_{r_d, \mathcal{M}_d}^{\rho_d}$.

Theorem 3.5.7. Let $1 \leq r_i$, $I_0 = (0, T)$, $I_i = (a_i, b_i)$, $\Omega = I_0 \times \left(\prod_{i=1}^d I_i \right)$, $\Lambda_k = \prod_{i=1}^k I_i$, $\Lambda_k^j = \prod_{\substack{i=1 \\ i \neq j}}^k I_i$ and $\frac{1}{2} < \nu_i^{\min} < \nu_i^{\max} \leq 1$ for $i = 1, \dots, d$. If

$$u \in \left(\bigcap_{i=1}^d H^{r_0}(I_0, \mathfrak{D} H^{\rho_i}(I_i, H^{r_1, \dots, r_{i-1}, r_{i+1}, \dots, r_d}(\Lambda_d^i))) \right) \cap {}^l \mathfrak{D} H^\varphi(I_0, H^{r_1, \dots, r_d}(\Lambda_d)),$$

then,

$$\begin{aligned}
& \|u - \Pi_{r_0, N}^\varphi \Pi_d^h u\|_{\mathcal{B}^{\tau, \nu_1, \dots, \nu_d}(\Omega)}^2 \\
& \leq N^{-2r_0} \int_{\tau^{min}}^{\tau^{max}} \varphi(\tau) N^{2\tau} \|u\|_{H^{r_0}(I_0, L^2(\Lambda_d))} d\tau \\
& + N^{-2r_0} \int_{\tau^{min}}^{\tau^{max}} \varphi(\tau) N^{2\tau} \sum_{j=1}^d \mathcal{M}_j^{-2r_j} \|u\|_{H^{r_0}(I_0, H^{r_j}(I_j, L^2(\Lambda_d^j)))}^2 d\tau + \dots \\
& + N^{-2r_0} \int_{\tau^{min}}^{\tau^{max}} \varphi(\tau) N^{2\tau} \left(\prod_{j=1}^d \mathcal{M}_j^{-2r_j} \right) \|u\|_{H^{r_0}(I_0, H^{r_1, \dots, r_d}(\Lambda_d)))} d\tau \\
& + \sum_{i=1}^d \int_{\nu_i^{min}}^{\nu_i^{max}} \rho_i(\nu_i) \left\{ \mathcal{M}_i^{2\nu_i - 2r_i} \|u\|_{H^{r_i}(I_i, L^2(\Lambda_d^i \times I_0))} + \dots \right. \\
& \quad \left. + \mathcal{M}_i^{2\nu_i - 2r_i} \left(\prod_{\substack{j=1 \\ j \neq i, k}}^d \mathcal{M}_j^{-2r_j} \right) \|u\|_{H^{r_i}(I_i, H^{r_1, \dots, r_d}(\Lambda_d^i, L^2(I_0)))} \right\} d\nu_i, \tag{3.74}
\end{aligned}$$

where $\Pi_d^h = \Pi_{r_1, \mathcal{M}_1}^{\rho_1} \cdots \Pi_{r_d, \mathcal{M}_d}^{\rho_d}$ and β is a real positive constant.

Proof. Directly from (3.45) we conclude that

$$\|u\|_{\mathcal{B}^{\tau, \nu_1, \dots, \nu_d}(\Omega)}^2 \leq \|u\|_{l^H(I_0, L^2(\Lambda_d))}^2 + \sum_{i=1}^d \|u\|_{L^2(I_0, \mathfrak{D}_{H^{\rho_i}}(I_i, L^2(\Lambda_d^i)))}^2.$$

Next, it follows from Theorem 3.5.4 that

$$\begin{aligned}
& \|u - \Pi_{r_0, N}^\varphi \Pi_d^h u\|_{l^H(I_0, L^2(\Lambda_d))}^2 \\
& \leq N^{-2r_0} \int_{\tau^{min}}^{\tau^{max}} \varphi(\tau) N^{2\tau} \left[\|u\|_{H^{r_0}(I_0, L^2(\Lambda_d))}^2 + \sum_{j=1}^d \mathcal{M}_j^{-r_j} \|u\|_{H^{r_0}(I_0, H^{r_j}(I_j, L^2(\Lambda_d)))}^2 + \dots \right. \\
& \quad \left. + \left(\prod_{j=1}^d \mathcal{M}_j^{-r_j} \right) \|u\|_{H^{r_0}(I_0, H^{r_1, \dots, r_d}(\Lambda_d)))}^2 \right] d\tau. \tag{3.75}
\end{aligned}$$

Therefore, (3.74) is obtained immediately from (3.72) and (3.75). \square

Remark 3.5.8. Since the inf-sup condition holds (see Theorem 3.5.1), by Lemma 3.3.7, the error in the numerical scheme is less than or equal to a constant times the projection error. Hence the results above imply the spectral accuracy of the scheme.

3.6 Numerical Tests

We provide several numerical examples to investigate the performance of the proposed scheme. We consider a $(1 + d)$ -dimensional fully distributed diffusion problem with left-sided derivative by letting $c_{l_i} = c_{r_i} = \kappa_{l_i} = 0$, $\kappa_{r_i} = 1$, $0 < 2\tau^{\min} < 2\tau^{\max} < 1$ and $1 < 2\nu_i^{\min} < 2\nu_i^{\max} \leq 2$ in (3.50) for $i = 1, \dots, d$, where the computational domain is $\Omega = (0, 2) \times \prod_{i=1}^{i=d} (-1, 1)$. We report the measured L^∞ error, $\|e\|_{L^\infty} = \|u_N - u^{ext}\|_{L^\infty}$ as the maximum bound of $\|e\|_{L^2}$.

In each of the following test cases, we use the method of fabricated solutions to construct the load vector, given an exact solution u^{ext} . Here, we assume $u^{ext} = u_t \times \prod_{i=1}^d u_{x_i}$. We project the spatial part in each dimension, u_{x_i} , on the spatial bases, and then, construct the load vector by plugging the projected exact solution into the weak form of problem. This helps us take the fractional derivative of exact solution more efficiently, while by truncating the projection with a sufficient number of terms, we make sure that the corresponding projection error does not dominantly propagate into the convergence analysis of numerical scheme.

Case I: We consider a smooth solution in space with finite regularity in time as

$$u^{ext} = t^{p_1+\alpha} \times ((1+x_1)^{p_2}(1-x_1)^{p_3}) \quad (3.76)$$

to investigate the spatial/temporal p -refinement. We allow the singularity to take order of $\alpha = 10^{-4}$, while p_1 , p_2 , and p_3 take some integer values. We show the L^∞ -error for different test cases in Fig.3.1, where by tuning the fractional parameter of the temporal basis, we can accurately capture the singularity of the exact solution, when the approximate solution converges as we increase the expansion order. In each case of spatial/temporal p -refinement, we choose sufficient number of bases in other directions to make sure their corresponding error is of machine precision order.

Considering $\alpha = 10^{-4}$, $p_1 = 2$, $p_2 = p_3 = 2$ in (3.76), and the temporal order of expansion being fixed ($N = 4$) in the spatial p -refinement, we get the rate of convergence as a function of the minimum regularity in the spatial direction. From Theorem 3.5.7, the rate of convergence is bounded by the spatial approximation error, i.e. $\|e\|_{L^2(\Omega)} \leq \|e\|_{L^\infty(\Omega)} \leq$

$\mathcal{M}_1^{-2r_1} \int_{\nu_1^{\min}}^{\nu_1^{\max}} \rho_1(\nu_1) \mathcal{M}_1^{2\nu_1} \|u\|_{H^{r_1}(I_1, L^2(I_0))} d\nu_1$, where $r_1 = p_2 + \frac{1}{2} - \epsilon$ is the minimum regularity of the exact solution in the spatial direction for $\epsilon < \frac{1}{2}$. Conforming to Theorem 3.5.7, the practical rate of convergence $\bar{r}_1 = 16.05$ in $\|e\|_{L^\infty(\Omega)}$ is greater than $r_1 \approx 2.50$.

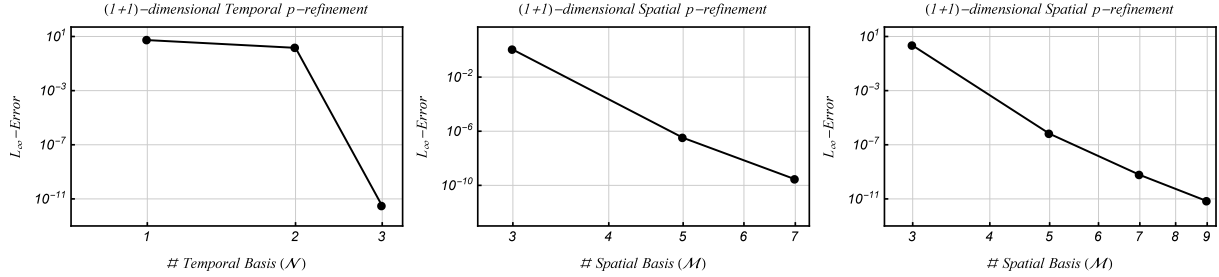


Figure 3.1: Temporal/Spatial p -refinement for case I with singularity of order $\alpha = 10^{-4}$. (Left): $p_1 = 3, p_2 = p_3 = 2$, and expansion order of $N \times 9$. (Middle): $p_1 = 2, p_2 = p_3 = 2$, and expansion order of $3 \times M$. (Right): $p_1 = 3, p_2 = p_3 = 2$, and expansion order of $4 \times M$.

Case II: We consider $u^{ext} = t^{p_1+\alpha} \sin(2\pi x_1)$, where $p_1 = 3$, and let $\alpha = 0.1$ and $\alpha = 0.9$. We set the number of temporal basis functions, $N = 4$, and show the convergence of approximate solution by increasing the number of spatial basis, M in Fig. 3.2. The main difficulty in this case is the construction of load vector. To accurately compute the integrals in the load vector, we project the spatial part of forcing function, $\sin(2\pi x_1)$, on the spatial bases. To make sure that the corresponding error is of machine-precision order and thus, not dominant, we truncate the projection at 25 terms, where there error is of order 10^{-16} . Therefore, the quadrature rule over derivative order should be performed for 25 terms rather than only a single $\sin(2\pi x_1)$ term. This will increase the computational cost.

Case III: (High-dimensional p -refinement) We consider the exact solution of the form

$$u^{ext} = t^{p_1+\alpha} \times \prod_{i=1}^3 (1+x_i)^{p_{2i}} (1-x_i)^{p_{2i+1}} \quad (3.77)$$

with singularity of order $\alpha = 10^{-4}$, where $p_1 = 3$, and $p_{2i} = p_{2i+1} = 1$. Similar to previous cases, we set the number of temporal bases, $N = 4$, and study convergence by uniformly increasing the number of spatial bases in all dimensions. Fig. 3.3 shows the results for $(1+2)$ -dimensional and $(1+3)$ -dimensional problems with expansion order of $N \times M_1 \times M_2$, and $N \times M_1 \times M_2 \times M_3$,

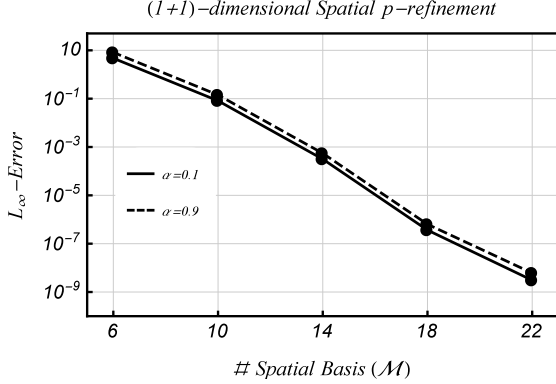


Figure 3.2: Spatial p -refinement for case II, $p_1 = 3$, $\alpha = 0.1$, and $\alpha = 0.9$.

respectively. Following Case I, the computed rate of convergence $\bar{r}_1 = \bar{r}_2 = \bar{r}_3 = 16.13$ in (3.77) for $\alpha = 10^{-4}$ is greater than the minimum regularity of the exact solution $r \approx 2.05$, which is in agreement with Theorem 3.5.7.

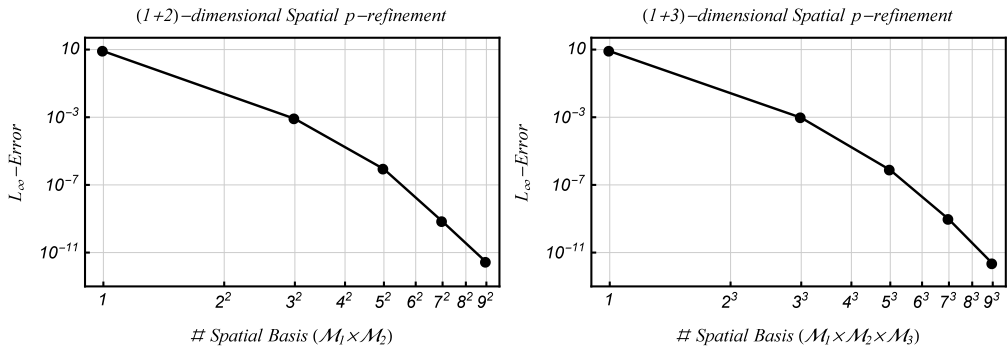


Figure 3.3: Spatial p -refinement for case III with singularity of order $\alpha = 10^{-4}$. (Left): (1 + 2)-dimensional, $p_1 = 3$, $p_{2i} = p_{2i+1} = 1$, where the expansion order is $\mathcal{N} \times \mathcal{M}_1 \times \mathcal{M}_2$. (Left): (1 + 3)-dimensional, $p_1 = 3$, $p_{2i} = p_{2i+1} = 1$, where the expansion order is $\mathcal{N} \times \mathcal{M}_1 \times \mathcal{M}_2 \times \mathcal{M}_3$.

In addition to the convergence study, we examine the efficiency of the developed method and fast solver by comparing the CPU times for (1 + 1)-, (1 + 2)-, and (1 + 3)-dimensional space-time hypercube domains in case III. The computed CPU times are obtained on an INTEL(XEON E52670) processor of 2.5 GHZ, and reported in Table 3.1.

Table 3.1: CPU time, PG spectral method for fully distributed (1+d)-dimensional diffusion problems. $u^{ext} = t^{p_1+\alpha} \times \prod_{i=1}^3 (1+x_i)^{p_{2i}} (1-x_i)^{p_{2i+1}}$, where $\alpha = 10^{-4}$, $p_1 = 3$, and the expansion order is 4×11^d .

	$p_{2i} = p_{2i+1} = 2$			$p_{2i} = p_{2i+1} = 3$		
	d=1	d=2	d=3	d=1	d=2	d=3
CPU Time [Sec]	1546.81	1735.03	2358.67	1596.16	1786.61	2407.22
$\ e\ _{L^\infty(\Omega)}$	6.84×10^{-12}	4.45×10^{-12}	3.27×10^{-12}	6.27×10^{-12}	3.86×10^{-12}	2.71×10^{-12}

CHAPTER 4

A FRACTIONAL SUBGRID-SCALE MODEL FOR TURBULENT FLOWS

4.1 Background

Due to the remarkable advancements in computational capabilities over the last decades, large eddy simulations (LES) have been introduced as a powerful approach in the computation of turbulent structures in [138, 139]. In modeling subgrid-scale (SGS) structures in LES of turbulent flows, spatially-filtered representation of a turbulent field is required for *a priori* and *a posteriori* analyses. As a key ingredient in the development of SGS models in turbulent flows, the statistical behavior of small scale motions and their cumulative effects on the evolution of the large scales should be incorporated. In comprehensive studies, including numerical and empirical approaches (see e.g., [31, 73, 74, 75, 76]), the intermittent statistical behavior of velocity gradients and the development of anomalously intense fluctuations were investigated. These studies confirmed the non-Gaussian statistics of SGS structures and the existence of intermittency in the inertial sub-range of turbulence. By measuring the Lagrangian velocity of tracer particles in a turbulent flow, Mordant et al. in [140] explored the intermittent statistics of probability distribution functions (PDF) of the velocity time increments, which is even more highlighted than the corresponding Eulerian spatial increments. Arnéodo et al. in [36] investigated the intermittency and universality properties of velocity temporal fluctuations in highly turbulent flows by quantitatively comparing experimental and numerical data. They described a stochastic phenomenological modelization in the entire range of scales, using a multifractal description, which links Eulerian and Lagrangian statistics. Recently, Buzzicotti et al. in [141] performed *a priori* analyses of statistical characteristics of resolved-to-subfilter scale (SFS) energy transfer. They quantified the intermittent scaling of the SFS energy transfer as a function of filtering type and described its non-trivial, anomalous deviations from the classical scaling as a function of cutoff scale. In fact, the anomalous behavior of turbulent small scales monotonically deviates from Gaussianity by enlarging the filter width (see e.g., [142, 143, 144, 145]). This means

that filtering a turbulent field incorporates nonlocal interactions of SGS motions into the resolved scales, which is reflected in heavy-tailed distributions of velocity increments.

Before any discussion on the various strategies of SGS modeling, the reader is referred to [146, 147, 148, 138, 81, 149, 150] for more history and background on LES of turbulent flows. The SGS modeling strategies are categorized into (I) functional and (II) structural modelings (see e.g., [147]). In the functional strategies, the closure problem can be expressed in the form of a mathematical operator, which is acting on the mean velocity field. Such turbulence models seek only to generate the net kinetic energy transfer from the resolved to small scales (see e.g., [151]). However, structural modeling strategies would approximate the SGS stresses in terms of the filtered velocity field, where the SGS structures and statistical properties are recovered from the resolved scale information. Multifractal modelings were introduced in [152, 153] as a structural approach to model the underlying intermittent cascading of energy. More specifically, in a study by Burton and Dahem [154], a new approach was presented on the multifractal modeling of subgrid-scale stresses in LES of turbulent flows motivated by *a priori* testing. Subsequently, Rasthofer and Gravemier in [155] proposed a new method of SGS modeling from a multifractal description of the vorticity field. Regarding the non-Gaussian statistics of small scale motions and nonlocal effects in turbulent flows, Hamilington and Dahem in [156] obtained a nonlocal closure modeling from a new derivation of the rapid pressure strain correlation. Recently, Maltba et al. [157] presented a new semi-local formulation employing a modified large eddy diffusivity (LED) approach, which retains the accuracy of a fully nonlocal approach. It turns out that in formulating SGS models, standard integer-order operators have commonly been used to mathematically represent the anomalous features of small scale motions.

In addition to the considerable progresses in developing nonlocal models using standard methods, fractional calculus appears to be a mathematical tractable tool to describe anomalous phenomena, manifesting in nonlocal interactions, self-similar structures, sharp peaks, and memory effects (see e.g., [42, 43]). It seamlessly generalizes the notion of standard integer-order calculus to its fractional-order counterpart, which leads to a broader class of mathematical models. Cushman

and Moroni in [158] developed a theory for modeling anomalous dispersion, which relied on the intermediate scattering function. In another experimental work in [159], they obtained the intermediate scattering function using the Lagrangian trajectories for a conservative tracer in a porous medium. Based on the anomalous characteristics of fluctuation processes in turbulence, several studies were conducted to explore the nonlocal modeling of turbulent flows. Chen in [160] proposed a fractional Laplacian stochastic equation to describe intermittent cascade of fully-developed turbulence. Furthermore, Churbanov and Vabishchevich presented a new fractional model to describe turbulent fluid flows in a rectangular duct, [161]. Recently, Egolf and Hutter [162] proposed nonlocal turbulent models in the form of fractional operators to generalize Reynolds shear stresses in local zero-equation models. Epps and Cushman-Roisin in [163] derived the Navier-Stokes (NS) equations with fractional Laplacian starting from the Boltzmann transport equation. In their study, they modeled large displacements of fluid particles by Lèvy α -stable distributions. Moreover, great progresses have been made towards the theories and numerical solutions to fractional partial differential equations (FPDEs). Samiee et al. [60, 61] developed a unified Petrov–Galerkin spectral method for a class of FPDEs with two-sided derivatives employing the so-called *Jacobi poly-fractonomials*. Zayernouri and Karniadakis in [56] introduced *Jacobi poly-fractonomials* as a new family of basis/test functions, which are the explicit eigenfunctions of fractional Strum-Liouville problems in bounded domains of the first and second kind. Zhou et al. developed two efficient first- and second-order implicit-explicit (IMEX) methods for accurate time-integration of stiff/nonlinear fractional differential equations with fractional order $\alpha \in (0, 1]$ in [164]. The reader is referred to [165, 21, 166, 18, 167, 22] and the references given therein for more details on fractional modeling of anomalous transport.

In comparison with the recent advances in SGS modeling of non-Gaussian features, the development of fractional transport modeling of turbulent structures is still at its very early stage. In the present work, we aim to open up a new perspective to functional modeling of the SGS stresses, employing the fractional calculus. This approach implies that we never question the correctness of Navier-Stokes (NS) subject to the Newtonian assumption. Starting from the Boltzmann transport

equation, we propose to approximate the filtered Maxwellian equilibrium distribution function of velocity with a *Lévy* α -stable distribution. Accordingly, we derive the filtered NS equations, in which the divergence of SGS stresses is approximated by the fractional Laplacian of filtered velocity field. From a physical point of view, (any generic) filtering the flow field in LES would further contribute to the nonlocal effects, which are rigorously modeled to appear as a fractional Laplacian term in the filtered NS equations. Certainly, by decreasing the filter width, the super-diffusive fractional operator gradually vanishes in compliance with the induced nonlocality. Here, we briefly highlight the main contributions of this work as follows:

- We develop a new functional approach to model the SGS stresses by employing the fractional Laplacian of the filtered velocity within the Boltzmann transport framework. The fractional exponent in the model arises from the heavy-tailed behavior of the SGS stresses.
- We show that the model is frame invariant and constrain it to a set of conditions to preserve the second-law of thermodynamics.
- We perform the *a priori* studies to assess performance of the model primarily by the correlation and regression coefficients utilizing the results of direct numerical simulation (DNS) for three-dimensional forced and decaying homogeneous isotropic turbulence (HIT) problems. We also investigate the nonlocality of proposed model, as a hallmark of fractional operators, in a range of filter widths.

The chapter is organized as follows: in section 2, we introduce some preliminaries on fractional calculus. We outline the problem and discuss the governing equations in section 3. In section 4, we develop the fractional model from the Boltzmann transport equation and study its mathematical and physical properties. In section 5, we provide the details of *a priori* analysis for three-dimensional forced and decaying HIT and study performance of the proposed fractional model.

4.2 Preliminaries on Fractional Laplacian

For modeling SGS stresses in isotropic turbulent flows, the heavy-tailed behavior of *Lévy* α -stable distributions are highly in demand due to their success in capturing singularities and

modeling anomalous phenomena (see e.g., [31]). From the stochastic point of view, the dynamics of the SGS features, which is modeled by an isotropic Lévy α -stable process at the microscopic level, can be upscaled by a fractional Laplacian operator. Such operator provides a rigorous tool for the mathematical modeling of nonlocal phenomena [168]. We denote by $(-\Delta)^\alpha$ the fractional Laplacian with $0 < \alpha \leq 1$,

$$\begin{aligned} (-\Delta)^\alpha u(\mathbf{x}) &= \frac{1}{(2\pi)^d} \int_{\mathbb{R}^d} |\xi|^{2\alpha} (u, e^{-i\xi \cdot \mathbf{x}})_{L^2} e^{i\xi \cdot \mathbf{x}} d\xi \\ &= \mathcal{F}^{-1} \left\{ |\xi|^{2\alpha} \mathcal{F}\{u\}(\xi) \right\}, \end{aligned} \quad (4.1)$$

where \mathcal{F} and \mathcal{F}^{-1} represent the Fourier and inverse Fourier transforms for a real-valued vector $\xi = \xi_j$, $j = 1, 2, 3$, respectively, and i denotes the imaginary unit. Moreover, $(\cdot, \cdot)_{L^2}$ denotes the L^2 -inner product on \mathbb{R}^d , $d = 1, 2, 3$. The Fourier transform of the fractional Laplacian is then obtained as

$$\mathcal{F} \left\{ (-\Delta)^\alpha u(\mathbf{x}) \right\} = |\xi|^{2\alpha} \mathcal{F}\{u\}(\xi). \quad (4.2)$$

It is worth noting that the integer-order Laplacian is recovered when $\alpha = 1$. Considering the definition of α -Riesz potential as

$$\mathcal{I}_\alpha u(\mathbf{x}) = C_{d,-\alpha} \int_{\mathbb{R}^d} \frac{u(\mathbf{x}) - u(\mathbf{s})}{|\mathbf{x} - \mathbf{s}|^{d-2\alpha}} ds, \quad (4.3)$$

the fractional Laplacian can also be expressed in the integral form as

$$(-\Delta)^\alpha u(\mathbf{x}) = C_{d,\alpha} \int_{\mathbb{R}^d} \frac{u(\mathbf{x}) - u(\mathbf{s})}{|\mathbf{x} - \mathbf{s}|^{2\alpha+d}} ds, \quad (4.4)$$

where $C_{d,\alpha} = \frac{2^{2\alpha} \Gamma(\alpha+d/2)}{\pi^{d/2} \Gamma(-\alpha)}$ for $2\alpha \in (0, d)$ and $\Gamma(\cdot)$ represents Gamma function (see [169]). The α -Riesz potential is also formulated in [170] as

$$\mathcal{I}_\alpha u(\mathbf{x}) = (-\Delta)^{-\alpha} u(\mathbf{x}) = \mathcal{F}^{-1} \left\{ |\xi|^{-2\alpha} \mathcal{F}\{u\}(\xi) \right\}. \quad (4.5)$$

Considering (4.5), the Riesz transform is then given by

$$\mathcal{R}_j u(\mathbf{x}) = \nabla_j \mathcal{I}_1 u(\mathbf{x}) = \mathcal{F}^{-1} \left\{ -\frac{i\xi_j}{|\xi|} \mathcal{F}\{u\}(\xi) \right\}, \quad (4.6)$$

which is dealt with in formulating the SGS stresses in section 4.3.3.

4.3 Governing Equations

In the mathematical description of incompressible turbulent flows, the primitive variables, including the velocity and the pressure fields are represented by $\mathbf{V}(\mathbf{x}, t) = (V_1, V_2, V_3)$ and $p(\mathbf{x}, t)$ for $\mathbf{x} = x_i$ and $i = 1, 2, 3$, respectively. In the following, the flow field variables are governed by the continuity and the Navier-Stokes (NS) equations, given as

$$\frac{\partial V_i}{\partial t} + \frac{\partial V_i V_j}{\partial x_j} = -\frac{1}{\rho} \frac{\partial p}{\partial x_i} + \frac{1}{\rho} \frac{\partial \sigma_{ij}}{\partial x_j}, \quad i, j = 1, 2, 3, \quad (4.7)$$

where ρ denotes the density and the viscous stress tensor σ_{ij} is defined as $\sigma_{ij} = \mu (\frac{\partial V_i}{\partial x_j} + \frac{\partial V_j}{\partial x_i})$, in which μ represents the dynamic viscosity for a Newtonian fluid.

In the LES of turbulent flows, the fluid motions are resolved down to some prescribed length scale, filter width (\mathcal{L}), which decomposes the velocity field, \mathbf{V} , into the filtered (resolved), $\bar{\mathbf{V}}$, and the residual, ν , components. The filtered velocity field is obtained by convolution, where $\bar{\mathbf{V}} = G * \mathbf{V}$ and $G = G(\mathbf{x})$ denotes the kernel of spatial filtering in the convolution (see [138, 139]). To produce the filtered velocity field and the true values of SGS stresses, we can adopt any generic isotropic filtering technique. Accordingly, the filtered NS equations in the index form are derived as

$$\frac{\partial \bar{V}_i}{\partial t} + \frac{\partial \bar{V}_i \bar{V}_j}{\partial x_j} = -\frac{1}{\rho} \frac{\partial \bar{p}}{\partial x_i} + \frac{\partial}{\partial x_j} (\nu \frac{\partial \bar{V}_i}{\partial x_j}) - \frac{\partial \mathcal{T}_{ij}^R}{\partial x_j}, \quad (4.8)$$

where the kinematic viscosity is represented by ν and the SGS stress tensor, $\mathcal{T}_{ij}^R = \overline{V_i V_j} - \bar{V}_i \bar{V}_j$, which must be closed in terms of the filtered flow variables. As the most popular eddy-viscosity closure, we exemplify the Smagorinsky model (SMG), introduced in [171]. The SGS stresses in the SMG are modeled by $\mathcal{T}_{ij}^R = -2\nu_{sgs} \bar{S}_{ij}$, where $\bar{S}_{ij} = \frac{\partial \bar{V}_i}{\partial x_j} + \frac{\partial \bar{V}_j}{\partial x_i}$, $\nu_{sgs} = (C_s \mathcal{L})^2 |\bar{\mathbf{S}}|$, and $|\bar{\mathbf{S}}| = \sqrt{2\bar{S}_{ij}\bar{S}_{ij}}$.

4.3.1 Boltzmann Transport Equation (BTE)

The kinetic theory aims to describe the motion of particles in a gas from a microscopic point of view. The state of the gas is obtained by a distribution function $f(t, \mathbf{x}, \mathbf{u})$ in the particle phase space

such that $f(t, \mathbf{x}, \mathbf{u}) d\mathbf{x} d\mathbf{u}$ is defined as the mass of gas particles in phase space within volume $d\mathbf{x} d\mathbf{u}$ centered on \mathbf{x}, \mathbf{u} at time t , where \mathbf{x} and \mathbf{u} represent gas particle's location and speed, respectively. We note that \mathbf{x} , \mathbf{u} , and t are independent variables. Let $f = f(t, \mathbf{x}, \mathbf{u}) : \mathbb{R}^+ \times \mathbb{R}^d \times \mathbb{R}^d \rightarrow \mathbb{R}$ (see e.g., [163, 77]). Without loss of generality, we take $d = 3$. Then ensemble-averaged macroscopic flow variables are given by:

$$\rho = \int_{\mathbb{R}^d} f(t, \mathbf{x}, \mathbf{u}) d\mathbf{u}, \quad (4.9)$$

$$V_i = \frac{1}{\rho} \int_{\mathbb{R}^d} u_i f(t, \mathbf{x}, \mathbf{u}) d\mathbf{u}, \quad i = 1, 2, 3, \quad (4.10)$$

where ρ and V_i denote the fluid density and the i -th component of flow velocity field in the NS equations, respectively. The accurate description of non-reacting ideal gas particles is governed by the Boltzmann transport equation [77, 78], which is written as

$$\frac{\partial f}{\partial t} + \mathbf{u} \cdot \nabla f = \left(\frac{\partial f}{\partial t} \right)_{coll} \equiv -\frac{f - f^{eq}}{\tau}, \quad (4.11)$$

where $f^{eq} = f^{eq}(t, \mathbf{x}, \mathbf{u})$ represents the equilibrium distribution function and τ is the relaxation time, which is the required time for fluid particles to reach equilibrium state. The left-hand side of (4.11) represents the streaming of *non-interacting* particles and the right-hand side expresses the collision term due to two-particle interactions [77]. Assuming that the system of gaseous particles is in thermodynamic equilibrium, the equilibrium distribution is given by the Maxwell distribution [79],

$$f^{eq}(\Delta) = \frac{\rho}{U^3} F(\Delta), \quad (4.12)$$

where $F(\Delta) = e^{-\Delta/2}$, $\Delta = \frac{|\mathbf{u}-\mathbf{V}|^2}{U^2}$ and U denotes the agitation speed. For instance, for air at the room-temperature $T = 15^\circ C$, we get $U = \sqrt{3k_B T / m} = 502 \text{ m/s}$, in which k_B , T , and m represent the Boltzmann constant, room temperature, and the molecular weight of air [163], respectively. It should be pointed out that $F(\Delta)$ is an isotropic function with respect to the velocity variables. Moreover, we define L as the macroscopic characteristic length, l as the microscopic characteristic length associated with the Kolmogorov length scale, and λ as the mean-free path, which is the average distance, traveled by a particle between successive collisions. Let take \mathbf{x}' the location of

particles before scattering, where \mathbf{x} is the current location. Then, $\mathbf{x}' = \mathbf{x} - \delta\mathbf{x}$ and $\delta\mathbf{x} = (t - t')\mathbf{u}$, in which we assume that \mathbf{u} remains constant during $t - t'$. As discussed in [163], the analytical solution for the mass probability distribution function is

$$f(t, \mathbf{x}, \mathbf{u}) = \int_0^\infty e^{-s} f^{eq}(t - s\tau, \mathbf{x} - s\tau\mathbf{u}, \mathbf{u}) ds = \int_0^\infty e^{-s} f_{s,s}^{eq}(\Delta) ds, \quad (4.13)$$

where $s \equiv \frac{t-t'}{\tau}$ and $f_{s,s}^{eq}(\Delta) = f^{eq}(t - s\tau, \mathbf{x} - s\tau\mathbf{u}, \mathbf{u})$. To establish a mathematical framework for deriving the NS equations from the Boltzmann equation in (4.11), we restrain our attention to some necessary assumptions, following [163].

Assumption 5. *The underlying assumptions for deriving the NS equations from BTE are:*

- The density, ρ , and the thermal agitation, U , speed are constant,
- $s \sim O(1)$,
- The mean flow velocity is less than the thermal agitation speed, i.e., $|V| \ll U$,
- $\lambda \ll l \ll L$ and $\tau \ll \frac{L}{|V|}$.

4.3.2 Filtered Boltzmann Transport Equation (FBTE)

To proceed for the LES of a turbulent flow, we can decompose f to the filtered (resolved) and the residual (unresolved) values as $f = \bar{f} + f'$. Recalling from section 3 that overbar represents the spatial isotropic filtering, i.e. $\bar{f} = G * f$, where G is the kernel of spatial filtering with the filter width, \mathcal{L} . Then, we formulate the filtered BTE (FBTE) according to

$$\frac{\partial \bar{f}}{\partial t} + \mathbf{u} \cdot \nabla \bar{f} = -\frac{\bar{f} - \overline{f^{eq}(\Delta)}}{\tau}. \quad (4.14)$$

We also define $\bar{\Delta} := \frac{|\mathbf{u} - \bar{V}|^2}{U^2}$. Following (4.13), we obtain the corresponding analytical solution to (4.14) in terms of $\overline{f^{eq}(\Delta)}$ as

$$\bar{f}(t, \mathbf{x}, \mathbf{u}) = \int_0^\infty e^{-s} \overline{f_{s,s}^{eq}(\Delta)} ds, \quad (4.15)$$

where $\overline{f_{s,s}^{eq}(\Delta)} = \overline{f^{eq}(\Delta(t - s\tau, \mathbf{x} - s\tau\mathbf{u}, \mathbf{u}))}$.

It is well-known that the nonlinear term is responsible for the transfer of kinetic energy in the cascade of turbulent kinetic energy from large to small scale turbulent motions. In principle, the SGS stresses originate from the convection term in the NS equations. It accordingly appears natural to recognize the advection term, $\mathbf{u} \cdot \nabla f$, in (4.11) as the resource of turbulent motions. Considering (4.15), the streaming and collision terms in (4.14) can be revised in terms of $\overline{f_{s,s}^{eq}(\Delta)}$, which plays a key role in the development of a model for the SGS stresses. More specifically, the effects of highly vortical flow field on the filtered shifted equilibrium, $\overline{f_{s,s}^{eq}(\Delta)}$, is manifesting in the advection term in (4.14), which gives rise to the SGS stresses. Clearly, the way we treat $\overline{f_{s,s}^{eq}(\Delta)}$ can lead us to the development of a closure model in the LES of turbulent flows. It is very important to note that $\overline{f^{eq}(\Delta)}$ is not equal to the Gaussian distribution of $\bar{\Delta}$, i.e.,

$$\overline{f^{eq}(\Delta)} = \frac{\rho}{U^3} \overline{e^{-\Delta/2}} \neq \frac{\rho}{U^3} e^{-\bar{\Delta}/2} = f^{eq}(\bar{\Delta}). \quad (4.16)$$

A common practice in dealing with $\overline{f^{eq}(\Delta)}$ is to follow the eddy-viscosity approach (see e.g., [172, 173, 174]). Generally, the residual scale motions can be modeled by approximating the collision term through a modified relaxation time, τ^\star . In an analogy with the standard Smagorinsky SGS model, the Boltzmann equation with the modeled collision term [172, 175] can be proposed as

$$\frac{\partial \bar{f}}{\partial t} + \mathbf{u} \cdot \nabla \bar{f} = -\frac{\bar{f} - f^{eq}(\bar{\Delta})}{\tau^\star}, \quad (4.17)$$

where τ^\star accounts for the difference between $\overline{f^{eq}(\Delta)}$ and $f^{eq}(\bar{\Delta})$. Interestingly, τ^\star is inherently associated with the turbulent viscosity in the Smagorinsky model.

Here, we outline a new framework to develop an LES modeling strategy from the BTE using a non-Gaussian stochastic process. Without loss of generality, we consider $G(\mathbf{r}) = \frac{1}{\mathcal{L}} H(\frac{1}{2}\mathcal{L} - |\mathbf{r}|)$ as the convolution kernel of box filtering, where $H(\cdot)$ denotes a Heaviside step function. Therefore,

$$\overline{f^{eq}(\Delta)} = G * f^{eq}(\Delta(t, \mathbf{u}, \mathbf{x})) = \int_{R_f} G(\mathbf{r}) f^{eq}(\Delta(t, \mathbf{u}, \mathbf{x} - \mathbf{r})) d\mathbf{r}, \quad (4.18)$$

where $R_f = [-\frac{\mathcal{L}}{2}, \frac{\mathcal{L}}{2}]^3$. Technically, $\overline{f^{eq}(\Delta)}$ represents a summation of exponential functions, which leads to its multi-exponential characteristics especially when \mathcal{L} gets increased. That is,

by enlarging \mathcal{L} , we are incorporating more information into $\overline{f^{eq}(\Delta)}$ according to (4.18), which essentially induces more heaviness to the statistical behavior of $\overline{f^{eq}(\Delta)}$. Thus, $\overline{f^{eq}(\Delta)}$ deviates more and more from the Gaussianity of $f^{eq}(\Delta)$ (see e.g., [141, 176, 142]). It should be noted that we are permitted to employ any generic type of filtering.

For the purpose of modeling $\overline{f^{eq}(\Delta)}$, it is understood from [177, 178] that the multi-exponential distributions can be fitted with a power-law model, in which the discrepancy between the model and true values can be reduced by increasing the number of exponential functions. Accordingly, we propose to model $\overline{f^{eq}(\Delta)} - f^{eq}(\bar{\Delta})$ with a power-law distribution, which follows as

$$\overline{f^{eq}(\Delta)} - f^{eq}(\bar{\Delta}) \simeq f^{Model}(\bar{\Delta}) = \mathfrak{C}_\beta f^\beta(\bar{\Delta}), \quad (4.19)$$

where $f^\beta(\bar{\Delta}) = \frac{\rho}{U^3} F^\beta(\Delta)$, in which $F^\beta(\Delta)$ denotes an isotropic Lévy β -stable distribution. We assume \mathfrak{C}_β is a real-valued constant number. Moreover, we consider $\beta \in (\frac{d}{2}, 1 + \frac{d}{2})$ and $d = 3$ represents the dimension of physical domain.

Remark 4.3.1. *Unlike the fractional exponent in [163], β relies not only on the thermodynamic properties and boundary conditions, but also it is a function of Taylor Reynolds number, Re_λ (defined further in Table 4.1), and \mathcal{L} . It is also worth mentioning that the power-law distribution can be well-suited in the modeling of multi-exponential functions if the filter width is chosen large enough to incorporate nonlocal interactions.*

Therefore, we propose to model $\overline{f^{eq}(\Delta)}$ in the collision term by using an isotropic Lévy β -stable distribution. Therefore, the FBTE is approximated by

$$\frac{\partial \bar{f}}{\partial t} + \mathbf{u} \cdot \nabla \bar{f} = -\frac{\bar{f} - f^{eq}(\bar{\Delta}) + f^{eq}(\bar{\Delta}) - \overline{f^{eq}(\Delta)}}{\tau} \simeq -\frac{\bar{f} - f^{eq}(\bar{\Delta}) - f^{Model}(\bar{\Delta})}{\tau}. \quad (4.20)$$

For the sake of simplicity, we take $f^*(\bar{\Delta}) = f^{eq}(\bar{\Delta}) + f^{Model}(\bar{\Delta})$. In comparison to the eddy-viscosity models, we approximate the collision term by replacing $\overline{f^{eq}(\Delta)}$ by $f^*(\bar{\Delta})$ rather than modifying τ , which leverages incorporating nonlocal interactions in turbulent flows.

4.3.3 Derivation of the FSGS model

The macroscopic continuum variables, associated with (4.8), can be expressed in terms of filtered distribution function in (4.20) as

$$\bar{\rho} = \int_{\mathbb{R}^d} \bar{f}(t, \mathbf{x}, \mathbf{u}) d\mathbf{u}, \quad (4.21)$$

$$\bar{V}_i = \frac{1}{\rho} \int_{\mathbb{R}^d} u_i \bar{f}(t, \mathbf{x}, \mathbf{u}) d\mathbf{u}, \quad i = 1, 2, 3, \quad (4.22)$$

where $\rho = \bar{\rho}$ for an incompressible flow. It follows from [163, 179] that by multiplying both sides of (4.20) by a collisional invariant $X = X(\mathbf{u})$ and then integrating over the kinetic momentum, we attain

$$\int_{\mathbb{R}^d} X \left(\frac{\partial \bar{f}}{\partial t} + \mathbf{u} \cdot \nabla \bar{f} \right) d\mathbf{u} = - \int_{\mathbb{R}^d} X \left(\frac{\bar{f} - f^*(\bar{\Delta})}{\tau} \right) d\mathbf{u}, \quad (4.23)$$

where the choices of $X = 1, \mathbf{u}$ lead to the conservation of mass and momentum equations, respectively. As noted in [180], due to the microscopic reversibility of the particles (the collisions are taken to be elastic), $\int_{\mathbb{R}^d} X \left(\frac{\bar{f} - f^*(\bar{\Delta})}{\tau} \right) d\mathbf{u} = 0$. This allows (4.23) to be found as

$$\int_{\mathbb{R}^d} \left(\frac{\partial \bar{f}}{\partial t} + \nabla \cdot (\mathbf{u} \bar{f}) \right) d\mathbf{u} = 0 \implies \frac{\partial \rho}{\partial t} + \nabla \cdot (\rho \bar{V}) = 0, \quad (4.24)$$

$$\int_{\mathbb{R}^d} \left(\mathbf{u} \frac{\partial \bar{f}}{\partial t} + \nabla \cdot (\mathbf{u}^2 \bar{f}) \right) d\mathbf{u} = 0 \implies \rho \frac{\partial \bar{V}}{\partial t} + \nabla \cdot \int_{\mathbb{R}^d} \mathbf{u}^2 \bar{f} d\mathbf{u} = 0, \quad (4.25)$$

in which \mathbf{u} is independent of t and \mathbf{x} . Reminding that the filter convolution kernel, $G = G(\mathbf{x})$, is independent of t and \mathbf{u} and thereby, Assumption 5 still holds. In (4.25), by adding and subtracting $\bar{V}\bar{V}$, the advection term, \mathbf{u}^2 , is evaluated as

$$\begin{aligned} \int_{\mathbb{R}^d} \mathbf{u}^2 \bar{f} d\mathbf{u} &= \int_{\mathbb{R}^d} (\mathbf{u} - \bar{V})(\mathbf{u} - \bar{V}) \bar{f} d\mathbf{u} + \int_{\mathbb{R}^d} \bar{V}\bar{V} \bar{f} d\mathbf{u} \\ &= \int_{\mathbb{R}^d} (\mathbf{u} - \bar{V})(\mathbf{u} - \bar{V}) \bar{f} d\mathbf{u} + \rho \bar{V}^2. \end{aligned} \quad (4.26)$$

Plugging (4.26) into (4.25), we obtain

$$\rho \left(\frac{\partial \bar{V}}{\partial t} + \nabla \cdot \bar{V}^2 \right) = -\nabla \cdot \boldsymbol{\varsigma}, \quad (4.27)$$

where

$$\boldsymbol{\varsigma}_{ij} = \int_{\mathbb{R}^d} (u_i - \bar{V}_i)(u_j - \bar{V}_j) \bar{f} d\mathbf{u}. \quad (4.28)$$

It is worth mentioning that the Cauchy and filtered SGS stresses arise from ς_{ij} . Considering (4.15), we formulate ς_{ij} in (4.28) as

$$\varsigma_{ij} = \int_{\mathbb{R}^d} \int_0^\infty e^{-s} (u_i - \bar{V}_i)(u_j - \bar{V}_j) f_{s,s}^*(\bar{\Delta}) ds d\mathbf{u}, \quad (4.29)$$

where $f_{s,s}^{Model} := f^{Model}(\bar{\Delta}(t - s\tau, \mathbf{x} - s\tau\mathbf{u}, \mathbf{u}))$, $f_{s,s}^{eq} := f^{eq}(\bar{\Delta}(t - s\tau, \mathbf{x} - s\tau\mathbf{u}, \mathbf{u}))$, thus, $f_{s,s}^* := f^*(\bar{\Delta}(t - s\tau, \mathbf{x} - s\tau\mathbf{u}, \mathbf{u}))$. In Appendix C, we prove that the temporal shift can be dropped from (4.29) following the derivations of fractional NS equations in [163]. Consequently, ς_{ij} in (4.29) can be simplified to

$$\begin{aligned} \varsigma_{ij} &= \int_{\mathbb{R}^d} \int_0^\infty e^{-s} (u_i - \bar{V}_i)(u_j - \bar{V}_j) f_s^{eq}(\bar{\Delta}) ds d\mathbf{u} \\ &\quad + \int_{\mathbb{R}^d} \int_0^\infty e^{-s} (u_i - \bar{V}_i)(u_j - \bar{V}_j) f_s^{Model}(\bar{\Delta}) ds d\mathbf{u}. \end{aligned} \quad (4.30)$$

According to the kinetic definition of static pressure, $p = \rho U^2$, we decouple ς_{ij} as

$$\varsigma_{ij} = -\bar{p}\delta_{ij} + \mathcal{T}_{ij}, \quad (4.31)$$

where

$$-\bar{p}\delta_{ij} = \int_{\mathbb{R}^d} (u_i - \bar{V}_i)(u_j - \bar{V}_j) f^*(\bar{\Delta}) d\mathbf{u} \int_0^\infty e^{-s} ds \quad (4.32)$$

and $\mathcal{T}_{ij} = \mathcal{T}_{ij}^{Shear} + \mathcal{T}_{ij}^R$ denotes the sum of shear stress tensor, \mathcal{T}_{ij}^{Shear} , and the SGS stress tensor, \mathcal{T}_{ij}^R . It is worth noting that in (4.32) when $i \neq j$, $(u_i - \bar{V}_i)(u_j - \bar{V}_j)f^*(\bar{\Delta})$ represents an odd function of u_i and u_j ; consequently, $\int_{\mathbb{R}^d} (u_i - \bar{V}_i)(u_j - \bar{V}_j) f^*(\bar{\Delta}) d\mathbf{u} = 0$. Considering $f_s^*(\bar{\Delta}) = f^*(\bar{\Delta}) + (f_s^*(\bar{\Delta}) - f^*(\bar{\Delta}))$, \mathcal{T}_{ij} is then obtained as

$$\mathcal{T}_{ij} = \int_0^\infty \int_{\mathbb{R}^d} (u_i - \bar{V}_i)(u_j - \bar{V}_j) (f_s^*(\bar{\Delta}) - f^*(\bar{\Delta})) e^{-s} d\mathbf{u} ds. \quad (4.33)$$

By ascribing the Gaussian distribution $f^{eq}(\bar{\Delta})$ to \mathcal{T}_{ij}^{Shear} and the isotropic Lévy β -stable distribution, $f^{Model}(\bar{\Delta})$, to \mathcal{T}_{ij}^R , \mathcal{T}_{ij} in (4.33) is decomposed to

$$\mathcal{T}_{ij}^{Shear} = \int_0^\infty \int_{\mathbb{R}^d} (u_i - \bar{V}_i)(u_j - \bar{V}_j) (f_s^{eq}(\bar{\Delta}) - f^{eq}(\bar{\Delta})) e^{-s} d\mathbf{u} ds, \quad (4.34)$$

$$\begin{aligned} \mathcal{T}_{ij}^R &= \int_0^\infty \int_{\mathbb{R}^d} (u_i - \bar{V}_i)(u_j - \bar{V}_j) (f_s^{Model}(\bar{\Delta}) - f^{Model}(\bar{\Delta})) e^{-s} d\mathbf{u} ds \\ &= \int_0^\infty \int_{\mathbb{R}^d} (u_i - \bar{V}_i)(u_j - \bar{V}_j) (f_s^\beta(\bar{\Delta}) - f^\beta(\bar{\Delta})) e^{-s} d\mathbf{u} ds. \end{aligned} \quad (4.35)$$

In Appendix C, we discuss the evaluations of \mathcal{T}_{ij}^{Shear} and \mathcal{T}_{ij}^R in terms of the macroscopic quantities, including ρ and \bar{V} . Eventually, the shear stresses are given by

$$\mathcal{T}_{ij}^{Shear} = \mu \left(\frac{\partial \bar{V}_i}{\partial x_j} + \frac{\partial \bar{V}_j}{\partial x_i} \right), \quad (4.36)$$

where $\mu = \rho U^2 \tau$ denotes the kinematic viscosity. Furthermore, we formulate the divergence of SGS stress tensor as

$$(\nabla \cdot \mathcal{T}^R)_i = \frac{\rho(U\tau)^{2\alpha}}{\tau} \Gamma(2\alpha + 1) C_\alpha \int_{\mathbb{R}^d} \frac{\bar{V}_i(\mathbf{x}') - \bar{V}_i(\mathbf{x})}{|\mathbf{x}' - \mathbf{x}|^{2\alpha+d}} d\mathbf{x}', \quad (4.37)$$

where $\alpha = -\beta - d/2$. Regarding the definition of fractional Laplacian given in (4.4), we can rewrite equation (4.37) as

$$(\nabla \cdot \mathcal{T}^R)_i = \mu_\alpha (-\Delta)^\alpha \bar{V}_i, \quad (4.38)$$

in which $\mu_\alpha = \frac{\rho(U\tau)^{2\alpha}}{\tau} \Gamma(2\alpha + 1) C_\alpha$ and $C_\alpha = \frac{2^{2\alpha} \Gamma(\alpha+d/2)}{\pi^{d/2} \Gamma(-\alpha)} \mathfrak{C}_\alpha$ and \mathfrak{C}_α is a real-valued constant.

Therefore, the filtered NS equations, developed from the filtered kinetic transport equation, is described by

$$\frac{\partial \bar{V}_i}{\partial t} + \frac{\partial \bar{V}_i}{\partial x_j} \bar{V}_j = -\frac{1}{\rho} \frac{\partial \bar{p}}{\partial x_i} + \nu \Delta \bar{V}_i - \nu_\alpha (-\Delta)^\alpha \bar{V}_i, \quad (4.39)$$

where $\alpha \in (0, 1]$, $\nu_\alpha = \frac{\mu_\alpha}{\rho}$. With a proper choice of $\alpha = \alpha(Re_\lambda, \mathcal{L})$, in which $\alpha|_{\mathcal{L}=0} = 1$, the FSGS model is able to capture the heavy-tailed distribution of the SGS quantities and predict the corresponding high-order statistical moments. By setting $\mathcal{L} = 0$, we obtain $\nu_{\alpha=1} = 0$, and hence $\nu_\alpha (-\Delta)^\alpha \bar{V}_i = 0$, which evidently recovers the exact NS equations, given in (4.7).

Remark 4.3.2. In [163], Epps and Cushman-Roisin evaluated the fractional NS equations from the BTE by replacing $f^{eq}(\Delta)$ as a Gaussian distribution with a Lévy β -stable distribution and splitting the jumps of particles into small and large scales. From this perspective, the fractional exponent, α , in the fractional NS equations is introduced only as a function of fluid properties and boundary conditions. Unlike that, we developed the proposed fractional SGS model from the FBTE by approximating $\overline{f^{eq}(\Delta)} - f^{eq}(\bar{\Delta})$ with a Lévy- β stable distribution, in which $\overline{f^{eq}(\Delta)} = G * f^{eq}(\Delta)$ and $G = G(\mathbf{x})$. Besides, we found that the fractional exponent depends on the flow properties, Re_λ , and also \mathcal{L} . Therefore, by setting $\mathcal{L} = 0$ we recover the standard NS equations at any Re_λ .

From the Fourier definition of fractional Laplacian and the Riesz transform in Section 4.2, it is straightforward to verify that

$$\mathcal{F}\left\{(-\Delta)^\alpha \bar{V}_j\right\} = i\xi_i \left(-\frac{i\xi_i}{|\xi|} \right) (|\xi|^2)^{\alpha-\frac{1}{2}} \mathcal{F}\left\{\bar{V}_j\right\}, \quad (4.40)$$

which leads to

$$(-\Delta)^\alpha \bar{V} = \nabla_j (\mathcal{R}_j (-\Delta)^{\alpha-\frac{1}{2}} \bar{V}). \quad (4.41)$$

Therefore, we obtain

$$\nabla \cdot \mathcal{T}^R = \nabla \cdot (\mathcal{R}(-\Delta)^{\alpha-\frac{1}{2}} \bar{V}). \quad (4.42)$$

Using (4.42), we can find the equivalent form of the SGS stress tensor as

$$\mathcal{T}_{ij}^* = \mathcal{T}_{ij}^R + C = \frac{1}{2} (\mathcal{R}_j (-\Delta)^{\alpha-\frac{1}{2}} \bar{V}_i + \mathcal{R}_i (-\Delta)^{\alpha-\frac{1}{2}} \bar{V}_j), \quad (4.43)$$

where C is a real-valued constant. \mathcal{T}_{ij}^* is dealt with later in section 4.4 in the computation of the correlation coefficients .

Remark 4.3.3. As described earlier in (4.2), $\mathcal{F}\left\{(-\Delta)^\alpha \bar{V}\right\} = |\xi|^{2\alpha} \mathcal{F}\{\bar{V}\}$. Similar to the eddy-viscosity models, $\nabla \cdot \mathcal{T}^R$ can be explicitly derived in the Fourier domain, hence maintaining the high-order accuracy of scheme.

4.3.4 Physical Properties

In order to ensure that the developed FSGS model is physically and mathematically consistent with the filtered NS equations, we introduce a mild condition for the model in accordance with the second law of thermodynamics and also examine the frame invariant modeling as follows.

4.3.4.1 Second-law of Thermodynamics

The contribution of filtered momentum equation in the entropy production rate is formulated in [181] as

$$\dot{S}_{prod} = \frac{1}{T} (\mathcal{T}^{Shear} : \nabla \bar{V} + \mathcal{T}^R : \nabla \bar{V}), \quad (4.44)$$

where T represents the temperature of flow and “ $:$ ” denotes a double dot product operator. In thermodynamic analysis of the exact NS equations, discussed in [182], it is proven that $\mu > 0$, in the description of $\mathcal{T}_{ij}^{Shear} = \mu \left(\frac{\partial \bar{V}_i}{\partial x_j} + \frac{\partial \bar{V}_j}{\partial x_i} \right)$. Regarding $\mu > 0$ and $\mathcal{T}^R = \mathcal{R}(-\Delta)^{\alpha-\frac{1}{2}} \bar{V}$ in (4.42), the underlying coefficient in the FSGS model, μ_α , should satisfy

$$\mu_\alpha \leq \mu \min \left| \frac{\nabla \bar{V} : \nabla \bar{V}}{(\mathcal{R}(-\Delta)^{\alpha-\frac{1}{2}} \bar{V}) : \nabla \bar{V}} \right|, \quad (4.45)$$

to ensure the positivity of entropy generation rate.

4.3.4.2 Frame Invariance

The SGS stresses and their divergence are separately proven to be frame invariant [183, 184], which contribute to invariant characteristics of the NS equations. In order to reproduce all local and nonlocal turbulent solutions in the LES of turbulence, SGS models should undergo certain restrictions to follow such invariant properties; otherwise, the value of turbulent stresses may change with any frame movement.

It is apparent that in the FSGS model, μ_α is frame invariant. Additionally, as a generator of Lévy-stable processes, the fractional Laplacian operator is proven to be rotationally and Galilean invariant (see [185, 186]); therefore, we do not need to impose any additional constraint on the FSGS model.

4.4 A Priori Analysis of the Fractional SGS Model

We perform *a priori* tests using DNS database to study the performance and capability of the proposed model in capturing anomalous behavior of SGS quantities. To pursue the *a priori* evaluations, we introduce two primary cases: three-dimensional forced and decaying homogeneous isotropic turbulent flows with periodic boundary conditions as follows.

Table 4.1: Computational parameters and statistical features of a forced HIT problem, provided by JHTDB [2]

$Re_\lambda = \frac{u'_{rms}\lambda}{\nu}$	$u'_{rms} = \sqrt{\frac{2}{3}E_{tot}}$	$E_{tot} = \langle v'_i v'_i \rangle$	ν	$\varepsilon = 2\nu \langle \bar{S}_{ij} \bar{S}_{ij} \rangle$
(m/sec)	(m ² /sec ²)	(m ² /sec)	(m ² /sec)	(m ² /sec ³)
437	0.686	0.93	1.85×10^{-4}	9.28×10^{-2}

Case (I): Forced HIT

Forced HIT is a canonical benchmark in studying the performance of subgrid-scale models. This test case has the obvious advantage of allowing the statistical features to be approximately stationary. Here, the corresponding computational domain is specified as $\Omega = [0, 2\pi]^3$, which is uniformly discretized on a Cartesian grid using 1024^3 grid points. The Johns Hopkins Turbulence Databases (JHTDB)¹ has provided public access to DNS database of a forced isotropic homogeneous turbulent flow, which is characterized by the micro-scale statistical properties presented in Table 4.1. For more information, the reader is referred to [2, 187].

In the *a priori* assessments of the FSGS model, the filtered velocity fields are obtained from the DNS data by using a three-dimensional box filtering, in which we set $\mathcal{L}_\delta = \frac{\mathcal{L}}{2^\delta} = 2^j$ for $j = 0, \dots, 5$, where \mathcal{L} and δ represent filter and grid widths, respectively.

Case (II): Decaying HIT

In terms of *a priori* tests, the DNS of decaying HIT set the ground to evaluate the modeling capabilities of FSGS while Re_λ experiences a decaying process. Furthermore, the DNS dataset of decaying HIT gives us the opportunity to conduct a series of *a priori* tests to evaluate the performance of the proposed model for a wider range of Reynolds numbers.

Similar to **Case (I)**, the computational domain is chosen to be the cube of $\Omega = [0, 2\pi]^3$ with the periodic boundary conditions. We start from a three-dimensional fully-developed HIT as the initial condition, which was previously obtained from the DNS of a forced HIT. The skewness and

¹<http://turbulence.pha.jhu.edu>

Table 4.2: Micro-scale statistical characteristics of turbulence for the applied initial condition in DNS of decaying HIT.

Re_λ	u'_{rms}	K	ν	ε	\mathcal{L}	$\tau_{\mathcal{L}}$
	(m/sec)	(m^2/sec^2)	(m^2/sec)	(m^2/sec^3)	(m)	(sec)
66	0.186	0.052	0.001	4.17×10^{-3}	0.275	1.478

flatness of the velocity derivatives for the initial condition data are approximately -0.5 and 4.0 , respectively. Table 4.2 shows the micro-scale statistical properties of the initial condition, which are described in Table 4.1. It should be mentioned that \mathcal{L} and $\tau_{\mathcal{L}}$ represent the integral length scale and the eddy turnover time, respectively.

Furthermore, we conduct the numerical simulation of decaying HIT using the incompressible Navier-Stokes solver of NEKTAR++, which is an open-source spectral/ hp element framework [188, 189]. Using a C^0 -continuous Galerkin projection, the discretized domain consists of 64^3 uniform tetrahedral elements and the fifth-order modified polynomials, $p = 5$, as the basis functions within each element. In other words, our computational domain would be a uniformly discretized cube with 256^3 grid points. The applied solver works based on the velocity-correction method and for time integration we use the second-order IMEX scheme. Let k_{max} and $\eta = (\nu^3/\varepsilon)^{1/4}$ denote the maximum wave number of turbulence and the Kolmogorov length scale, respectively. As a measure of accuracy, we evaluate $k_{max}\eta > 2.6$, which ensures that Kolmogorov scale motions are well-resolved. Figure 4.1 depicts the time evolution of normalized turbulent kinetic energy, $K(t')/K_0$, normalized dissipation rate, $\varepsilon(t')/\varepsilon_0$, and $Re_\lambda(t')$, where $t' = t/\tau_{\mathcal{L}}$ is the dimensionless time and $K_0 = K(t' = 0)$, $\varepsilon_0 = \varepsilon(t' = 0)$, and $\tau_{\mathcal{L}}$ are the values reported in Table 4.2. The kinetic energy is monotonically decaying in Figure 4.1 while the dissipation rate first experiences an increase up to approximately two large eddy turnover times, $t' \approx 2$, and later monotonically decays. The decay of dissipation rate occurs when the energy spectrum starts to completely decay at the entire wavenumbers, which is consistent with the physics of decaying HIT problems [138]. To conduct the *a priori* analysis of **Case (II)**, we collect the velocity field data, starting from $t' \approx 2$, where $Re_\lambda \approx 45$, and we set $\mathcal{L}_\delta = j$ for $j = 1, \dots, 15$.

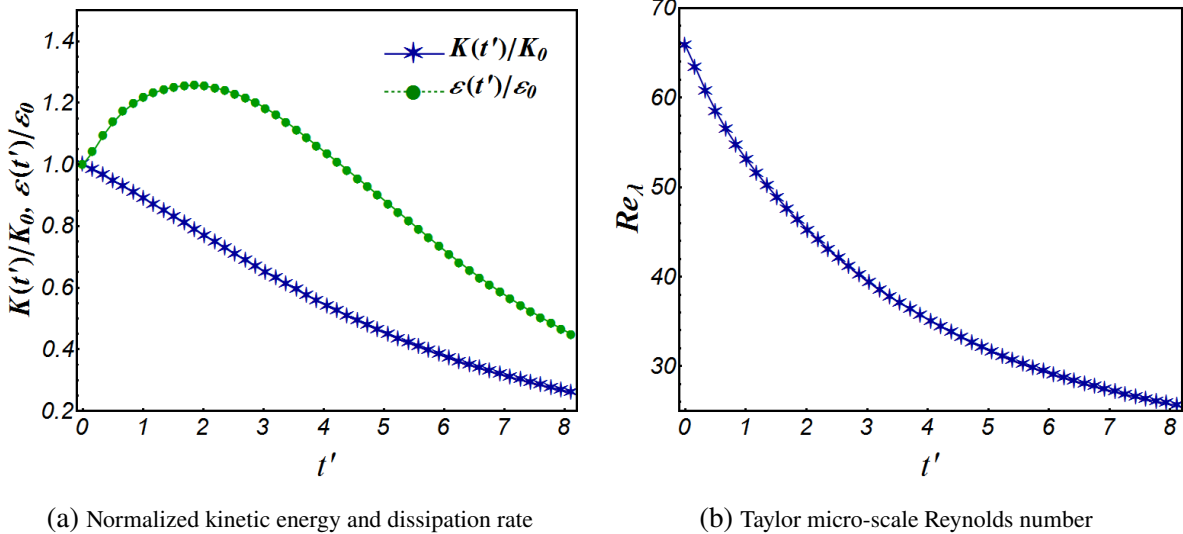


Figure 4.1: Time evolution of $K(t')/K_0$, $\varepsilon(t')/\varepsilon_0$, and $Re_\lambda(t')$ during the DNS of decaying HIT

4.4.1 Estimation of Fractional Exponent α

To achieve a high degree of accuracy and performance in the FSGS model, the model parameters are considered to be a function of \mathcal{L}_δ and Re_λ . By assuming \mathfrak{C}_α as a real-valued function of α in (4.19), there is only one adjustable model parameter, α , given in (4.39). Conventionally, the correlation and regression coefficients are known as the primary tools in *a priori* tests for tuning the parameters associated with an SGS model. Following [190], we denote by $\varrho_i \in [-1, 1]$ and \mathcal{R}_i for $i = 1, 2, 3$ the correlation and regression coefficients between $[\nabla \cdot \mathcal{T}^R]_i^{DNS}$ from the filtered DNS data and $[\nabla \cdot \mathcal{T}^R]_i^{FSGS}$ from the FSGS model, respectively. Moreover, the correlation coefficient associated with a component of SGS stresses, \mathcal{T}_{ij}^R , is indicated by ϱ_{ij} with dual subscripts, where $i, j = 1, 2, 3$. Since the FSGS model is strictly limited to access the straight form of SGS stresses, we employ the equivalent SGS stresses, \mathcal{T}_{ij}^* , given in (4.43) to attain ϱ_{ij} . Therefore, $\varrho_{ij} = \varrho(\mathcal{T}_{ij}^*, \mathcal{T}_{ij}^{DNS}) = \varrho(\mathcal{T}_{ij}^R, \mathcal{T}_{ij}^{DNS})$, where \mathcal{T}_{ij}^{DNS} denotes the SGS stress tensor obtained from the DNS data.

Technically, the proper choice of α can be made by looking at a range of α , in which we obtain the relatively largest values of ϱ_i while the corresponding \mathcal{R}_i is around 1. As a rule of thumb, \mathfrak{C}_α should be designed such that $\mathcal{R}_i \approx 1$ occurs, where the values of ϱ_i are relatively maximum. With

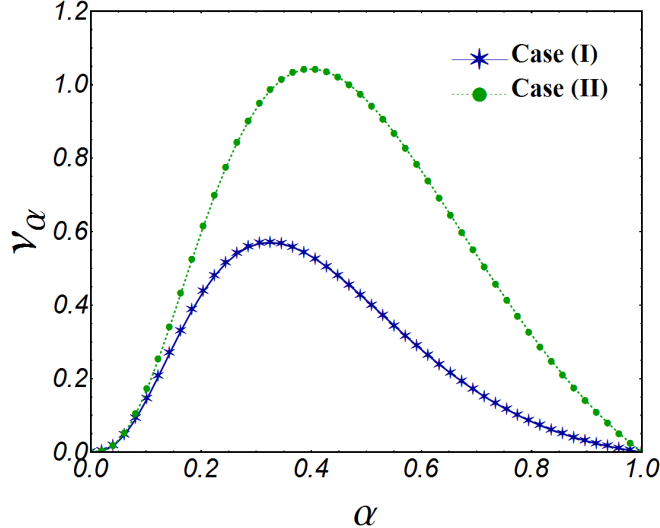


Figure 4.2: v_α versus α for $\nu = 1.85 \times 10^{-4}$ in **Case (I)** and $\nu = 10^{-3}$ in **Case (II)**

this in mind, we adopt $\mathfrak{C}_\alpha = \bar{c}\alpha^2$, where $\bar{c} = 1500$. Figure 4.2 illustrates the variation of v_α versus $\alpha \in [0, 1]$ for the specified properties of **Case (I)** and **Case (II)** in Tables 4.1 and 4.2 at room temperature.

To estimate the optimal fractional exponent, α^{opt} , in the case of forced HIT problem (**Case (I)**), we perform a comparative study of ϱ_i and R_i versus \mathcal{L}_δ by carrying out several *a priori* tests. In Figure 4.3a, we illustrate ϱ_i and R_i for uniformly distributed $\alpha \in [0, 1]$ at the specific $\mathcal{L}_\delta = 8$ for $i = 1, 2, 3$. It is important to note that the values of α^{opt} , obtained from the evaluations in each direction, can be approximately represented by the same value. Accordingly, we reduce the evaluation of α^{opt} to only the first direction as presented in Figure 4.3b. After running enough test cases, we show the variations of α^{opt} versus \mathcal{L}_δ in Figure 4.4. It reveals that enlarging \mathcal{L}_δ accelerates the reduction of α^{opt} toward the smaller values. Recall that Re_λ remains approximately unchanged over time in forced HIT problems, hence, α^{opt} is primarily relying on \mathcal{L}_δ .

In a similar fashion, we perform *a priori* tests of the FSGS model using the dataset of **Case (II)** for the purpose of calibrating α^{opt} to well-describe the non-Gaussian features of the SGS stresses. Such analysis also provides a platform for studying the statistical behavior of the FSGS model regarding a range of Re_λ . Using the Kriging method [191, 192, 193] from 135 direct evaluations, we approximate a high-resolution surrogate of α^{opt} , which is presented as a function of \mathcal{L}_δ and Re_λ

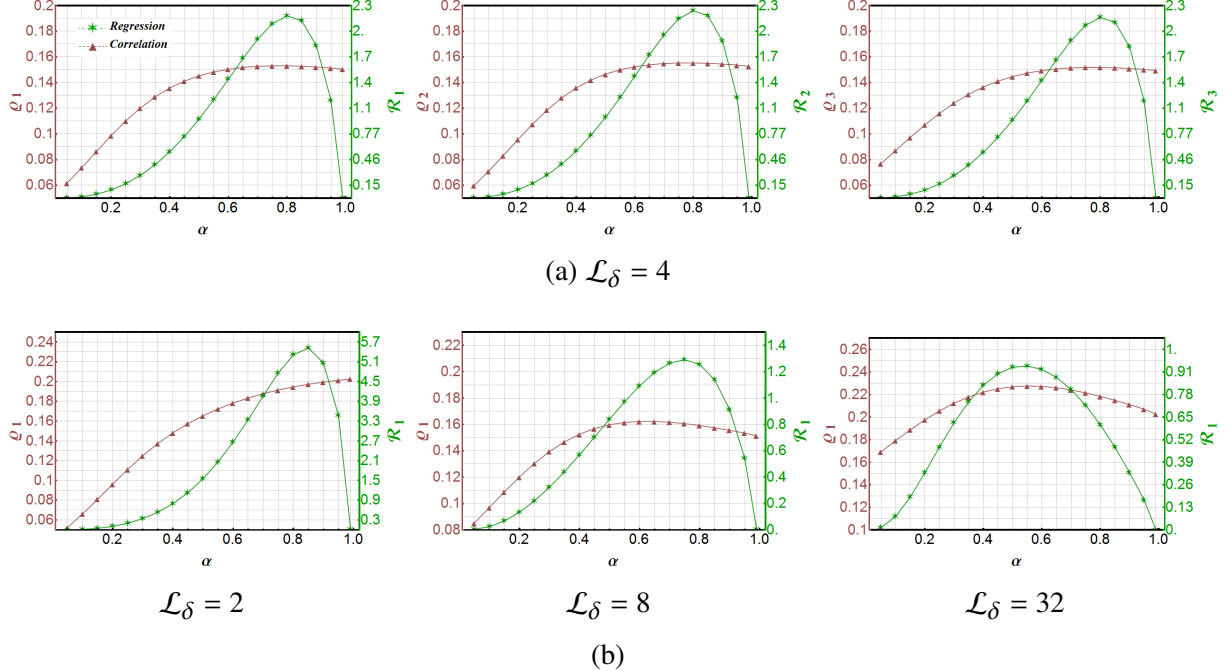


Figure 4.3: Variation of the correlation coefficient, ρ_i , and the regression coefficient, β_i , in terms of the fractional exponent, $\alpha \in (0, 1)$ using the DNS database of **Case (I)** for (a) $i = 1, 2, 3$ at $\mathcal{L}_\delta = 4$, and (b) $i = 1$ at $\mathcal{L}_\delta = 2, 8, 32$

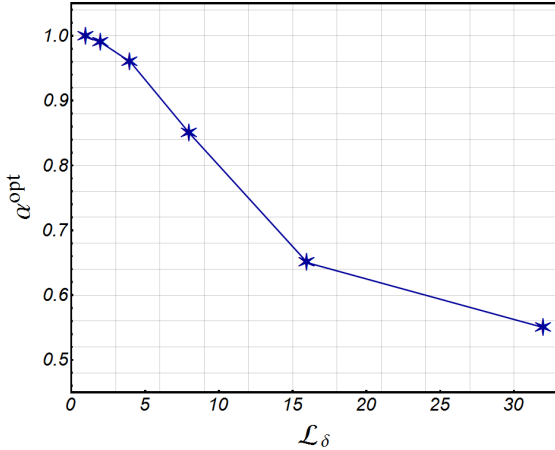


Figure 4.4: α^{opt} versus \mathcal{L}_δ for the **Case (I)**, of properties are given in Table 4.1

in Figure 4.5a. For three specific Re_λ , we also show the curves of α^{opt} versus \mathcal{L}_δ in Figure 4.5b. Similar to the corresponding Figure in **Case (I)**, α^{opt} shows a substantial reduction by enlarging \mathcal{L}_δ . Additionally, Figure 4.5b confirms that, when Re_λ decreases in a decaying process, α^{opt} exhibits a sharp reduction in a more limited span of \mathcal{L}_δ . In further discussions, we elaborate on the results and the nonlocality effects induced by larger Re_λ on α^{opt} .

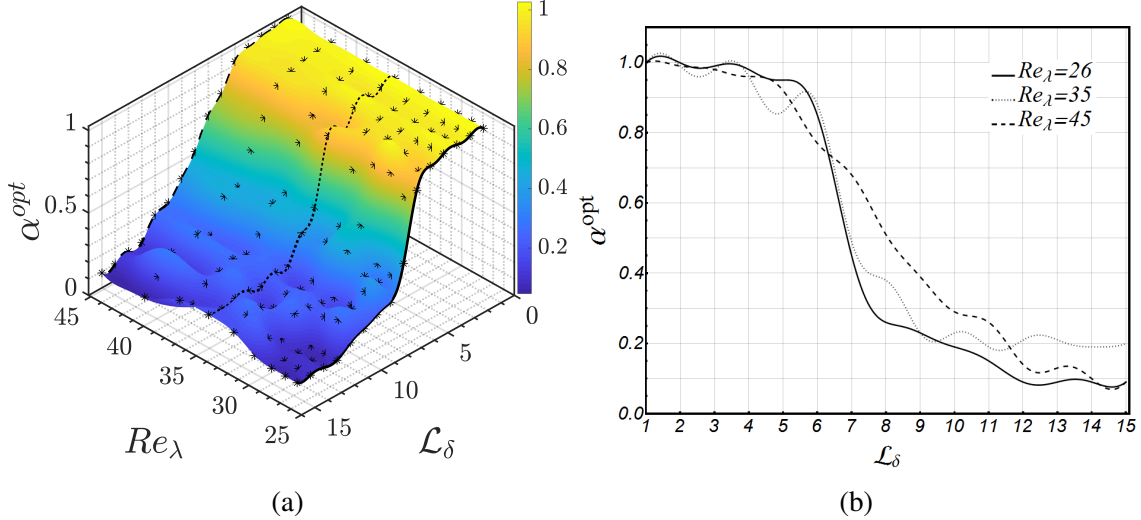


Figure 4.5: (a) The surface of α^{opt} , obtained by the Kriging method, versus \mathcal{L}_δ and Re_λ using the data points, denoted by \star , which are estimated by the *a priori* tests of FSGS model for **Case (II)** and (b) comparison between the curves of α^{opt} versus \mathcal{L}_δ , which are designated by $Re_\lambda \approx 26, 35, 45$

4.4.2 Analysis of the Model Performance

Following the evaluation of α^{opt} , we perform a comparative study of performance for the FSGS model employing the introduced correlation coefficients, i.e., ϱ_i and ϱ_{ij} . Using the high resolution turbulent fields of **Case (I)**, we compare the variation of ϱ_i obtained from the FSGS and SMG models in terms of \mathcal{L}_δ in Figure 4.6. Seemingly, the FSGS model shows acceptable correlations with the true values obtained from the DNS data, which is the notion of adequate magnitude and phase agreement. More significantly, by intensifying nonlocality in the filtered velocity field through increasing \mathcal{L}_δ , the FSGS model works relatively better in terms of capturing heavy-tailed behavior of the SGS stresses in all directions. In Figure 4.7, we present the scatter plot analysis on the values of $(\nabla \cdot \mathcal{T}^R)_i$ for $i = 1, 2, 3$, attained by the FSGS model and the filtered DNS data, for $\mathcal{L}_\delta = 8, 64$. The results confirm that, with a proper selection of α^{opt} in the FSGS model, we can achieve an approximate unit regression, which represents the same level of magnitudes in the scatter plots. In order to study the influence of Re_λ on the performance, we reiterate the evaluation of correlation coefficients at other instantaneous realization of DNS database for **Case (I)** by imposing the same α^{opt} . The outcomes in Table 4.4 are seemingly in an acceptable agreement with the

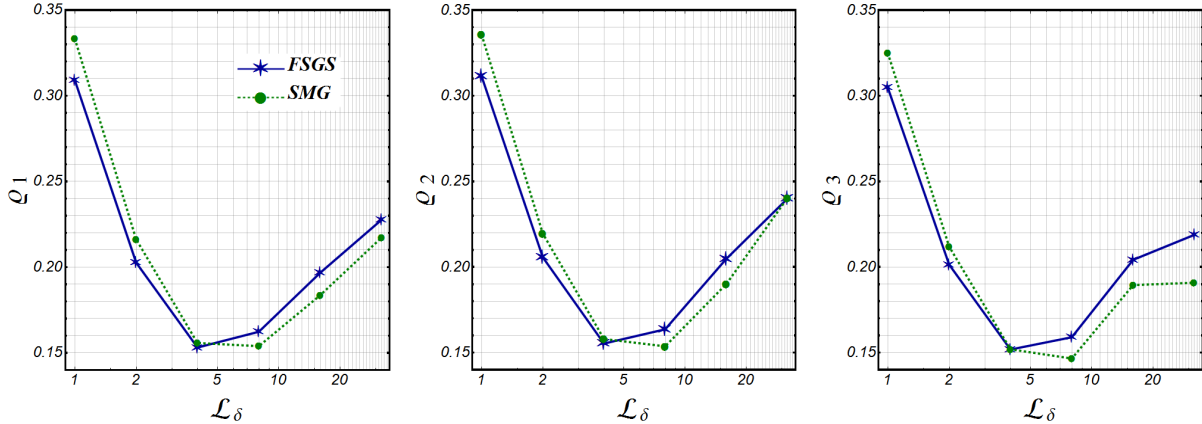


Figure 4.6: Comparing the correlation coefficients, ϱ_i , from the FSGS model using the optimum fractional exponent, with the corresponding ones implied by the Smagorinsky model

Table 4.3: *A priori* results for the correlation coefficients, ϱ_{ij} , of SGS stresses obtained from the FSGS and SMG models at two different Reynolds numbers, \mathcal{L}_δ

$\mathcal{L}_\delta = 16$						$\mathcal{L}_\delta = 32$							
	ϱ_{11}	ϱ_{12}	ϱ_{13}	ϱ_{22}	ϱ_{23}	ϱ_{33}		ϱ_{11}	ϱ_{12}	ϱ_{13}	ϱ_{22}	ϱ_{23}	ϱ_{33}
FSGS	0.17	0.29	0.30	0.13	0.30	0.23		0.18	0.36	0.33	0.13	0.33	0.27
SMG	0.16	0.29	0.28	0.12	0.31	0.23		0.17	0.33	0.32	0.11	0.32	0.27

results shown in Figure 4.6. Therefore, in the LES of forced HIT problems, α^{opt} can be dealt with as a constant parameter since \mathcal{L}_δ is considered as a constant value.

Despite the limitations of fractional approaches in approximating the SGS stresses, our findings explicitly formulate ϱ_{ij} by evaluating \mathcal{T}_{ij}^* in (4.43) on the filtered velocity field. Consistent with the results discussed previously, Table 4.3 reports the correlations of the components of SGS stress tensor, ϱ_{ij} , for $\mathcal{L}_\delta = 16$ and 32. More clearly, the results support compatible behavior of the FSGS model with the SMG model in the description of SGS stresses.

In the LES of decaying HIT problems, α^{opt} retains Re_λ dependence since Re_λ as a macro-scale property undergoes a temporal decay. Employing α^{opt} in Figure 4.5, we study the accuracy of the FSGS model in a broader framework, as shown in Figure 4.8. Similar to **Case (I)**, the FSGS model shows better correlations at a wide range of Re_λ by enlarging \mathcal{L}_δ . Taken together, the FSGS model seems to be in a relatively favorable agreement with the filtered DNS database yet not comparable with structural models.

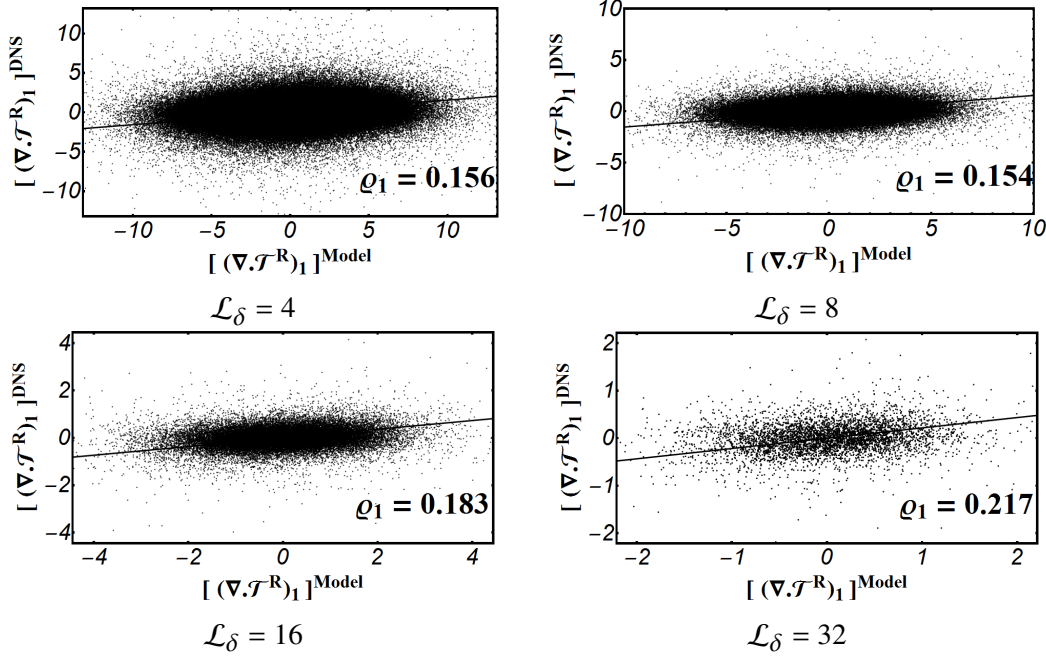


Figure 4.7: *A priori* results for the correlation between the true and model values for the components of $\nabla \cdot \mathcal{T}^R$, where $[\nabla \cdot \mathcal{T}^R]^{FSGS} = \mu_\alpha (-\Delta)^\alpha \bar{\mathbf{V}}|_{\alpha=\alpha^{opt}}$, yielding the correlation coefficients, as shown

Table 4.4: Study of FSGS model in terms of \mathcal{L} through *a priori* analysis at other time instants of **Case (I)**

\mathcal{L}_δ	$Re_\lambda = 427$		$Re_\lambda = 437$		$Re_\lambda = 421$	
	4	16	4	16	4	16
ϱ_1	0.15	0.20	0.15	0.20	0.15	0.20
ϱ_2	0.16	0.21	0.15	0.21	0.15	0.22
ϱ_3	0.16	0.20	0.15	0.20	0.15	0.21

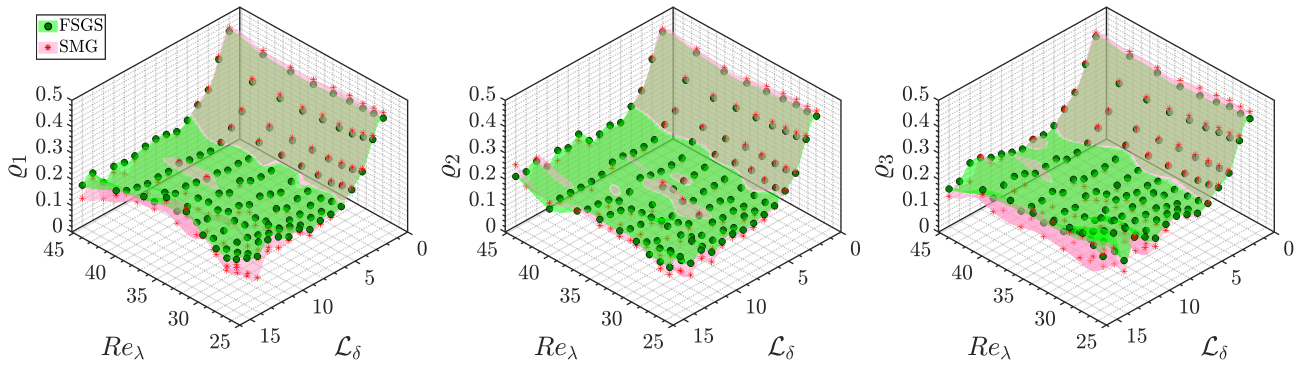


Figure 4.8: Comparison of Kriging-constructed surfaces of ϱ_i for $i = 1, 2, 3$, obtained from *a priori* study of the FSGS and the SMG models, versus \mathcal{L}_δ and Re_λ on **Case (II)**

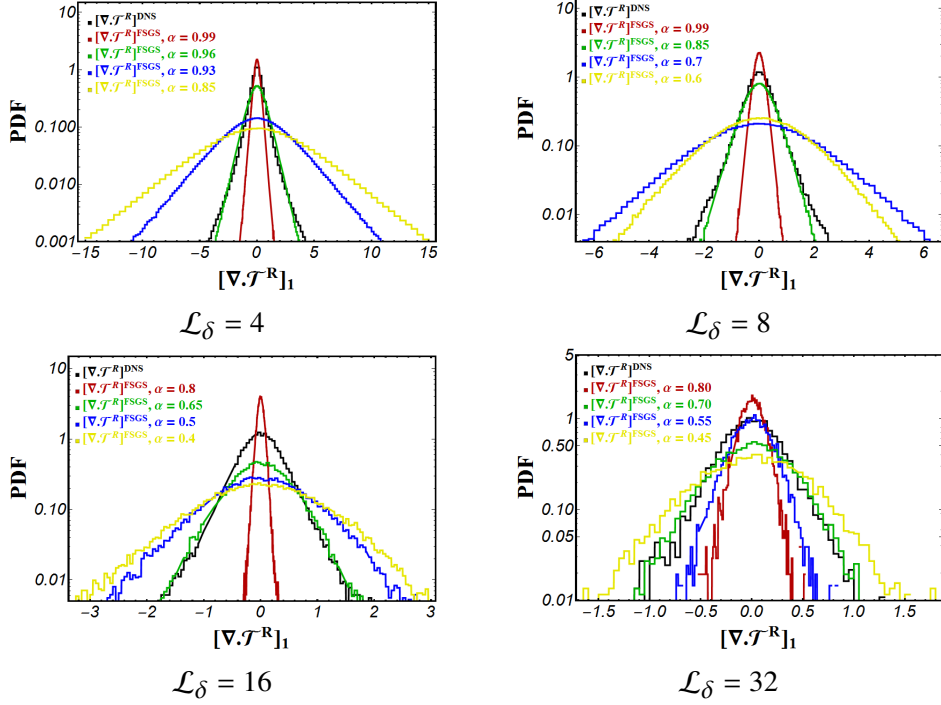


Figure 4.9: *A priori* results for the PDF of the true and modeled $(\nabla \cdot \mathcal{T}^R)_1$ regarding α variations at each \mathcal{L}_δ

4.4.3 Towards Modeling Nonlocal Effects

As pointed out previously, performance of the proposed model relies strictly on the selection of α^{opt} as a function of Re_λ and \mathcal{L}_δ . Regarding the connection between small scale turbulent motions in the NS and BT equations in section 4.3.2, we explore the influence of nonlocal interactions on the model's performance at the microscopic level. Within the Boltzmann transport framework, $\overline{f^{eq}(\Delta)}$ demonstrates increasingly multi-exponential behavior by enlarging \mathcal{L} . Practically, when we increase \mathcal{L} in the filtered NS equations, more nonlocalities are incorporated into ω_{ij} in (4.30) through $\overline{f^{eq}(\Delta)}$. From a physical point of view, vortices in turbulent flows tend to live longer than their turnover time. During the formation of coherent structures, the mutual advection and filamentation of vortices render nonlocal flow structures in isotropic turbulent flows. Filtering the flow field variables integrates such nonlocalities in a single numerical grid point, which intensifies the heavy-tailed characteristics of $\overline{f^{eq}(\Delta)}$.

In the proposed framework, the multi-exponential behavior of $\overline{f^{eq}(\Delta)}$ is readily modeled by

a Lévy β -stable distribution described in (4.19), in which the tail heaviness is indicated directly by \mathcal{L}_δ . The multi-exponential pattern suggests that the heavy-tailed characteristics of $\overline{f^{eq}(\Delta)}$ get more intensified if we increase \mathcal{L}_δ . Interestingly, as we decrease β , the Lévy β -stable distribution exhibits more fat-tailed behavior, which is provably in demand for the best-description of $\overline{f^{eq}(\Delta)}$. Extending this argument to the macroscopic level, the FSGS model inherently moves from the diffusion toward the advection to precisely represent the heavy-tailed behavior of SGS statistics by choosing the smaller values of α in (4.14). This argument accounts for the abrupt reduction of α^{opt} versus \mathcal{L}_δ , presented in Figures 4.4 and 4.5. For $\alpha < \alpha^{opt}$, the FSGS model is subject to overfit the heavy-tailed behavior of $\overline{f^{eq}(\Delta)}$, thereby losing the correlation.

On such a background, the FSGS model can be dealt with as a new framework to capture anomalous features of SGS statistics at large values of \mathcal{L}_δ . As shown in Figures 4.6 and 4.8, the correlations associated with the FSGS model offer an improvement compared to the SMG model. Moreover, we proceed to perform qualitative assessment of the FSGS model in predicting the PDF of $(\nabla \cdot \mathcal{T}^R)_i$ depicted in Figure 4.9 for different values of \mathcal{L}_δ in **Case (I)**. We should note that the presented results are confined to $i = 1$ due to the similarities in other directions. It appears that by employing the proper choice of α^{opt} , the PDF obtained by the FSGS model fits into the heavy-tailed distribution of true SGS values while with $\alpha < \alpha^{opt}$ the PDF is overpredicted. This argument emphasizes the reliability of the FSGS model on the selection α^{opt} as a function of \mathcal{L}_δ and Re_λ .

Inevitably, due to the approximation we made in modeling $\overline{f^{eq}(\Delta)}$ in the filtered Boltzmann equation, there are some discrepancies between the results obtained from the fractional model and the filtered DNS data. We believe that this new framework has the advantage of allowing us to promote the accuracy of the model by involving more compatible options for approximating $\overline{f^{eq}(\Delta)}$ in (4.14).

CHAPTER 5

A TEMPERED FRACTIONAL APPROACH TO LES OF TURBULENT FLOWS

5.1 Background

With the recent notable developments in computer technologies and, by extension, in the computational mechanics, there is a rapidly growing interest toward using large eddy simulations (LES) in a wide range of applications. Over the past decade, LES modeling has received an increasing attraction from scientific communities as a powerful and promising tool in connection with turbulence phenomena [194, 195]. In LES, one resolves the large energy-containing eddies by modeling the interplay between large and subgrid scale motions. Due to the tendency of small scales to homogeneous and universal dynamics, LES offers more accurate predictions comparing with the results of resolving the Reynolds-averaged Navier-Stokes (RANS) equations [196, 197]. Furthermore, it lightens the burden of computational costs imposed by accurately capturing the dissipative scales, which renders LES more affordable than direct numerical simulations (DNS).

Concurrent with the recent computational advancements, a marked shift occurred toward using artificial intelligence (AI) as an effective and tractable tool in turbulence modeling due to their significant capabilities in discovering anomalous structures and reproducing nonlocal statistical properties [198, 199]. In this paradigm, turbulence modeling comes into two divisions:

Machine learning based approaches: They introduce advancements in prediction capabilities and reconstructing turbulence structures. Several assorted machine learning (ML) algorithms were proposed for turbulence closure problems including kernel regression and a deep neural network [200, 201, 202]. Essentially, pure machine learning-based approaches are limited by the representativeness training dataset though they appear to be simpler for implementation. Moreover, to pinpoint complex patterns, large volumes of data are required for the algorithms to learn physical constraints (e.g., frame invariance) and statistical properties, which secondarily makes further complications like optimizing of data compression [203]. This reveals the significance of physics

based models in mentoring the AI approaches and pushing hybrid models as a new direction, which exploit ML algorithms with a significant reduction in the required input data [see e.g., 204, 205, 206, 207, 208].

Physics based approaches: As a catch-all phrase for a spectrum of physics based techniques, they introduce a mathematical representation of physical structures through a number of parameters with a sufficient amount of information. Contrary to ML based approaches, physics based models do not involve large volumes of data although they are inherently limited by the model incompleteness or the complexity of parameterizing physical structures [203]. Accordingly, it is markedly essential to entail the underlying statistical properties in formulating and inferring an optimum model in a numerically rigorous framework, which links a variety of research disciplines like turbulence, numerical and statistical analysis, and data science. This approach employs principles of physics and borrows insights from the statistical analysis to form a model for real phenomena, which can also be used to guide the ML algorithms [see e.g., 209, 210, 211].

Establishment of such a physically-consistent LES model ties strongly with characterization of nonlocal turbulence mechanisms and a better understanding of *anomalous* structures. As a puzzling feature, the non-Gaussian behavior of turbulent dynamics is linked to the spatial intermittency of small-scale motions, which is embodied in the form of very thin and elongated vortices [212, 213]. Technically, the nonlocal closure of Navier-Stokes (NS) equations, originated from the Green's function of the Laplacian operator for solving Poisson pressure equation, induces long-range interactions (nonlocal triadic structures) in spectral space of homogeneous turbulence [82]. In a preliminary investigation of isotropic turbulence [214], the significant role of highly vortical structures, typically tube-like, was disclosed on generating nonlocal dynamics and coherence of turbulence. Supported by Laval et al. [213], nonlocality as a crucial element in generating intermittent structures has tendency to prevail the local interactions by orders of magnitude. She and Leveque attempted to express self-similar structures in terms of a sequence of moment ratios for the energy dissipation field [215]. Recently, Mishra and Girimaji in [216] studied the role of pressure on nonlocal mechanisms in incompressible turbulent flows and identified the intercomponent of

energy transfer by the rapid pressure strain correlation. For more information, the reader is referred to [217, 218, 219, 220].

From this perspective, an ideal subgrid-scale (SGS) model represent correctly statistics of the filtered real turbulence at the resolved levels. Given the dependence of an ideal model on an infinite-dimensional set of multi-point statistics, it would be more practical to define a weaker set of conditions in study of SGS parameterization [82]. As one of the earliest studies on statistical analysis of LES, Meneveau in [76] derived a closed set of necessary, yet mild, conditions to fulfill *a priori* consistency in SGS quantities. More generally, the Karman-Howarth (KH) theorem for anisotropic turbulent flows were studied in [221] by eliminating pressure velocity correlations to determine the two-point structure function equations. By proposing a hyper-eddy viscosity term in [81], SGS dissipation spectrum were measured in locally isotropic turbulence to assess ability of classical two-point closures in prediction of the mean energy transfer. Recently, some of the prevailed challenges in developing an optimal LES model was reviewed succinctly by [80]. This review presents a clear set of statistical characteristics in performing an *a priori* analysis and providing adequate information for optimizing SGS models.

Statistical descriptions of an ideal closure model derive a desire for developing nonlocal approaches in terms of two-point high-order structure functions in a rigorous mathematical framework. The eddy damped quasi-normal Markovian (EDQNM) approach, described in [222], undertakes closing of SGS motions in spectral space by involving high-order statistical moments. As a functional approach, direct interaction approximation pushes the non-Markovanized stochastic models to the direction of turbulence closure problem, whose solutions are constructed in a fraction form [223]. Furthermore, multifractal models [e.g., 152, 224] suggest a potential realizable strategy to accurately capture anomalous scaling exponents, observed in turbulent velocity increments. Recently, Charalampopoulos and Sapsis [225] developed a new data-driven approach in closure modeling of temporal and spatial nonlocalities for a two-dimensional jet flow. In addressing statistical local and nonlocal interactions, this progress proceeds with modeling turbulent effects at the kinetic level. Premnath in [173] developed a framework for applying dynamic procedure in

the lattice-Boltzmann method for LES of inhomogeneous and anisotropic turbulent flows. A new collision approach were proposed by [226] for LES of weakly compressible flows using two forms of the modified Bhatanagar-Gross-Krook (BGK) collision operators. For more comprehensive review of the literature, we refer the reader to [227, 175].

Focusing on the key ideas of (*i*) describing of anomalous structures in turbulence and (*ii*) nonlocal closure modeling, fractional calculus appears to be a tractable mathematical tool due to their power-law or logarithmic types of kernel. As an alternative approach to standard methods, they leverage their inherent potentials in representing long-range interactions, self-similar structures, sharp peaks, and memory effects in a variety of application [see 228, 229]. Egolf and Hutter in [162] generalized Reynolds shear stresses in local zero-equation to the fractional counterparts. Furthermore, Epps and Cushman-Roisin derived fractional NS equations from the Boltzmann transport equation in [163], which supply profound understanding of turbulent nonlocal effects at the kinetic level. For more information, Egolf and Hutter [230] provided a comprehensive overview of fractional and nonlocal turbulence, spanning from coherent structures to state-of-the-art ideas on closure modeling in canonical flows. Recently, Di Leoni et al. [231] contributed in fractional LES modeling by developing a two-point correlation based model in a robust physically-meaning framework.

In the class of nonlocal models, Samiee et al. [232] laid out a mathematical framework for developing fractional models, which starts treating turbulence effects at the kinetic level. In a precise derivation, the proposed distribution function in the closed form of filtered collision operator, turns into a fractional model in the LES equations. Throughout a data-driven approach, Akhavan-safaei in [211] extended the fractional modeling to the LES of scalar turbulence using two-point correlation functions between the SGS scalar flux and filtered scalar gradient.

In the specific case of isotropic turbulent flows, cascading of energy from large to small scales expresses a self-similar behavior in the inertial range, and then it falls exponentially into the dissipation range. Inspired by such real physics phenomena, we focus on developing a nonlocal model by employing a tempered heavy-tailed distribution within the proposed fractional framework,

which contributes in tempered fractional SGS (TFSGS) modeling. Such a tractable fractional operator offers a great flexibility in characterizing nonlocal structures in the turbulent inertial and dissipation ranges through fractional and tempering parameters. To achieve the enhanced performance of the proposed model, we also present an optimization algorithm, involving two-point structure functions. Regarding the best approximation of an ideal physics based model, the optimized TFSGS model restores many essential statistical properties of SGS stresses and presents an *a priori* consistency in the dissipation spectrum.

This chapter is organized as follows. In section 5.2, we introduce some preliminaries of tempered fractional calculus. We outline a mathematical framework in section 5.3 to develop the tempered fractional model from the Boltzmann transport equation and derive the corresponding forms for SGS quantities. Within a statistical framework, we present a two-point structure based algorithm to infer the optimal behavior of the tempered fractional model in section 5.4. Using the DNS database of an stationary isotropic turbulent flow, we evaluate the statistical *a priori* analysis and perform a comparative study on the two-point structure functions in section 5.5. Next, we carry out an *a posteriori* investigation in section 5.6 by tracking turbulent kinetic energy.

5.2 Preliminaries on Tempered Fractional Calculus

Fractional calculus introduces well-established mathematical tools for an accurate description of anomalous phenomena, ubiquitous in a wide range of applications from biotissues [166, 49] and material science [233, 234, 235] to vibration [167], porous media [236, 237, 238] and turbulence [211, 231, 163]. As alternative approaches to the standard nonlinear models, fractional models offer a great potential in capturing heavy-tailed distributions, self-similar structures, nonlocal interactions, and memory effects. This potential is substantially indicated by power-law or logarithmic kernels of convolution type in the corresponding fractional operators. From the stochastic point of view, fractional transport models arise from the heavy-tailed distribution functions in modeling the underlying super- or sub-diffusive motions of particles in complex heterogeneous systems at the microscopic level [60, 61, 72, 71]. Nevertheless, common patterns in nature follow finite variance

dynamics, which urges the role of tempered fractional calculus as a more sophisticated approach in representing natural cut-offs in real applications and retaining their finite statistical properties.

Recalling from [239, 101], we begin by the definitions of the left- and right-sided tempered fractional derivatives respectively as

$$\mathcal{D}_{\pm x}^{\alpha, \lambda} u(x) = \frac{\alpha}{\Gamma(1-\alpha)} \int_0^\infty \frac{u(x) - u(x \mp s)}{s^{\alpha+1} e^{\lambda s}} ds, \quad (5.1)$$

where the fractional derivative order, $\alpha \in (0, 1)$, and the tempering parameter, $\lambda > 0$. Also, $\Gamma(\cdot)$ represents a Gamma function. For $\alpha \in (1, 2)$, the corresponding fractional derivatives are given by:

$$\mathcal{D}_{\pm x}^{\alpha, \lambda} u(x) = \frac{\alpha(\alpha-1)}{\Gamma(2-\alpha)} \int_0^\infty \frac{u(x \mp s) - u(x) \pm s \frac{du(x)}{dx}}{s^{\alpha+1} e^{\lambda s}} ds. \quad (5.2)$$

The link between the derivatives in (5.2) and (5.3) and their counterparts in the Riemann-Liouville sense are described by

$${}^{RL}\mathcal{D}_{\pm x}^{\alpha, \lambda} u(x) = \mathcal{D}_{\pm x}^{\alpha, \lambda} u(x) + \lambda^\alpha u(x) \quad (5.3)$$

$${}^{RL}\mathcal{D}_{\pm x}^{\alpha, \lambda} u(x) = \mathcal{D}_{\pm x}^{\alpha, \lambda} u(x) + \lambda^\alpha u(x) \pm \alpha \lambda^{\alpha-1} \frac{du(x)}{dx}. \quad (5.4)$$

In particular, for $n \geq 0$ the tempered integer-order derivatives are reduced as

$${}^{RL}\mathcal{D}_{+x}^{n, \lambda} u(x) = e^{-\lambda x} \frac{d^n (e^{\lambda x} u(x))}{dx^n}, \quad (5.5)$$

which recover the classic integer-order derivatives as $\lambda \rightarrow 0$.

Let $\mathcal{F}[u](\xi)$ denote the Fourier transform of u , where ξ is the Fourier numbers. Then, we obtain

$$\mathcal{F}\left[{}^{RL}\mathcal{D}_{\pm x}^{\alpha, \lambda} u(x)\right] = (\lambda \pm i\xi)^\alpha \mathcal{F}[u](\xi).$$

In this context, the corresponding Fourier transform of the left- and right-sided tempered fractional integrals are given by

$$\mathcal{F}\left[{}^{RL}\mathcal{I}_{\pm x}^{\alpha, \lambda} u(x)\right](\xi) = (\lambda \pm i\xi)^{-\alpha} \mathcal{F}[u](\xi).$$

Evidently, tempered integrals and derivatives functions as inverse operators when u possesses sufficient regularity [see 240, 239]. Moreover, tempered fractional operators preserve semi-group property, which prepares a useful and rigorous framework for further numerical considerations.

5.2.1 Tempered fractional Laplacian

Denoted by $(\Delta + \lambda)^\alpha(\cdot)$, we define the tempered fractional Laplacian of the integral form as

$$(\Delta + \lambda)^\alpha u(\mathbf{x}) = C_{d,\alpha} \text{P.V.} \int_{\mathbb{R}^d} \frac{u(\mathbf{x}) - u(\mathbf{s})}{e^{\lambda|\mathbf{x}-\mathbf{s}|} |\mathbf{x} - \mathbf{s}|^{2\alpha+d}} ds, \quad (5.6)$$

where $C_{d,\alpha} = \frac{-\Gamma(\frac{d}{2})}{2\pi^{\frac{d}{2}} \Gamma(-2\alpha)} \frac{1}{2F_1(-\alpha, \frac{d+2\alpha-1}{2}; \frac{d}{2}; 1)}$ for $\alpha \in (0, 1)$ and $\alpha \neq \frac{1}{2}$. In particular, for $d = 1$ $(\Delta + \lambda)^\alpha$ is reduced to the so-called *Riesz* fractional form, described by

$$\begin{aligned} (\Delta + \lambda)^\alpha u(x) &= (-1)^{\lfloor 2\alpha \rfloor + 1} \frac{RL\mathcal{D}_{+x}^{\alpha,\lambda} u(x) + RL\mathcal{D}_{-x}^{\alpha,\lambda} u(x)}{2} \\ &= C_\alpha \text{P.V.} \int_{\mathbb{R}} \frac{u(x) - u(s)}{e^{\lambda|x-s|} |x - s|^{2\alpha+1}} ds, \end{aligned}$$

where $C_\alpha = \frac{-\Gamma(\frac{1}{2})}{2\pi^{\frac{1}{2}} \Gamma(-2\alpha)} \frac{1}{\cos(\pi\alpha)}$ [see 240]. In Appendix D.1, we detail the derivation of the Fourier transform of $(\Delta + \lambda)^\alpha u(\mathbf{x})$, formulated as

$$\begin{aligned} \mathcal{F}[(\Delta + \lambda)^\alpha u(\mathbf{x})](\xi) &= \mathfrak{C}_{d,\alpha} \times \\ &\quad \left(\lambda^{2\alpha} - (\lambda^2 + \xi^2)^\alpha 2F_1(-\alpha, \frac{d+2\alpha-1}{2}; \frac{d}{2}; \frac{\xi^2}{\xi^2 + \lambda^2}) \right) \mathcal{F}[u](\xi), \end{aligned} \quad (5.7)$$

in which $\mathfrak{C}_{d,\alpha} = \frac{1}{2F_1(-\alpha, \frac{d+2\alpha-1}{2}; \frac{d}{2}; 1)}$ and $\xi = |\xi|$. For $d = 3$, we define $\mathfrak{C}_\alpha = \frac{1}{2F_1(-\alpha, \frac{2+2\alpha}{2}; \frac{3}{2}; 1)}$. It is worth noting that when λ approaches 0, we recover the usual fractional Laplacian in both integral or Fourier forms.

5.3 Boltzmannian Framework

The kinetic Boltzmann transport (BT) is a formal framework for describing fluid particle motions over a wide range of flow physics (e.g., rarefied gas flows and turbulence). This framework offers a great potential for statistical description of turbulent small-scales towards a better understanding

of coherent structures in turbulence yet at the kinetic level. As an alternative approach in turbulent closure modeling, reconciling SGS terms in the BT and the Navier-Stokes (NS) equations can conceivably give rise to a rigorous physics-based model at the continuum level.

Within the BT framework proposed in chapter 4, we develop a SGS model, respecting the statistical and physical properties of turbulent motions.

5.3.1 A review on the subgrid-scale modeling

In the description of incompressible turbulent flows, we consider large eddy simulation (LES) equations [138], governing the dynamics of the resolved-scale flow variables,

$$\frac{\partial \bar{V}}{\partial t} + \bar{V} \cdot \nabla \bar{V} = -\frac{1}{\rho} \nabla \bar{p} + \nu \nabla \cdot \bar{S} - \nabla \cdot \mathbf{T}^R, \quad (5.8)$$

where in the index form $\bar{V}(\mathbf{x}, t) = \bar{V}_i$ and $\bar{p}(\mathbf{x}, t)$ represent the velocity and the pressure fields for $i = 1, 2, 3$ and $\mathbf{x} = x_i$. Moreover, ν and ρ denote the kinematic viscosity and the density, respectively. Considering \mathcal{L} as the filter width, the filtered field is obtained in the form of $\bar{V} = G * V$, where $G = G(\mathbf{x})$ denotes the kernel of a spatial isotropic filtering type and $*$ is the convolution operator. By implementing the filtering operation, we decomposes the velocity field, V , into the filtered (resolved), \bar{V} , and the residual, v , components. In (5.8), the filtered strain rate, \bar{S} , and the SGS stress tensor, \mathbf{T}^R , are defined by $\bar{S}_{ij} = \frac{1}{2} (\frac{\partial V_i}{\partial x_j} + \frac{\partial V_j}{\partial x_i})$ and $T_{ij}^R = \overline{V_i V_j} - \bar{V}_i \bar{V}_j$.

Since the filtering operator cannot commute with the nonlinear terms in the NS equations, SGS stresses must be modeled in terms of the resolved velocity field. As a common yet reliable approach, Smagorinsky [171] offered modeling the SGS stresses borrowing the Boussinesq approximation from the kinetic theory such that $\mathbf{T}^R = -2\nu_R \bar{S}$ and ν_R is indicated by $\nu_R = (C_s \mathcal{L})^2 |\bar{S}|$, where $|\bar{S}| = \sqrt{2\bar{S}_{ij}\bar{S}_{ij}}$ and C_s is the Smagorinsky (SMG) constant.

5.3.2 The BGK equation and the closure problem

Starting from the Boltzmann kinetic theory [77], the evolution of mass distribution function f is governed by the Boltzmann transport (BT) equation as

$$\frac{\partial f}{\partial t} + \mathbf{u} \cdot \nabla f = \Omega(f), \quad (5.9)$$

in which $f(t, \mathbf{x}, \mathbf{u}) d\mathbf{x}d\mathbf{u}$ represent the probability of finding mass of particles, located within volume $d\mathbf{x}d\mathbf{u}$ centered on a specific location, \mathbf{x} , and speed, \mathbf{u} , at time t . It is worth noting that in the particle phase space \mathbf{x} , \mathbf{u} , and t are independent variables. Technically, the left-hand side of (5.9) concerns the streaming of non-reacting particles in absence of any body force and the right-hand side represent the collision operator. The most common form of $\Omega(f)$ with a single collision is the so-called BGK approximation [77, 79], given by

$$\Omega(f) = -\frac{f - f^{eq}}{\tau}, \quad (5.10)$$

where τ represent the single relaxation time. In the case of incompressible flows with roughly constant temperature, τ is assumed to be independent of macroscopic flow field velocity and pressure. Moreover, under the circumstances of thermodynamic equilibrium of particles, $f^{eq}(\Delta)$ serves as

$$f^{eq}(\Delta) = \frac{\rho}{U^3} F(\Delta), \quad (5.11)$$

where $F(\Delta) = e^{-\Delta/2}$, $\Delta = \frac{|\mathbf{u}-\mathbf{V}|^2}{U^2}$ as an isotropic Maxwellian distribution and U denotes the agitation speed. More specifically, $U = \sqrt{3k_B T/m}$, in which k_B , T , and m represent the Boltzmann constant, room temperature, and the molecular weight of air.

By recalling the basics of BT equation from [163, 232], we introduce the following quantities: L as the macroscopic length scale, l_s as the microscopic characteristic length associated with the Kolmogorov length scale, l_m as the average distance, traveled by a particle between successive collisions. Furthermore, we define \mathbf{x}' as the location of particles before scattering, where \mathbf{x} is the current location. Thus, $\mathbf{x}' = \mathbf{x} - (t - t')\mathbf{u}$, where \mathbf{u} is assumed to be constant during $t - t'$. The

analytical solution of (5.9) and (5.10) in [163] is given by

$$\begin{aligned} f(t, \mathbf{x}, \mathbf{u}) &= \int_0^\infty e^{-s} f^{eq}(t - s\tau, \mathbf{x} - s\tau\mathbf{u}, \mathbf{u}) ds \\ &= \int_0^\infty e^{-s} f_{s,s}^{eq}(\Delta) ds, \end{aligned} \quad (5.12)$$

where $s \equiv \frac{t-t'}{\tau}$ and $f_{s,s}^{eq}(\Delta) = f^{eq}(t - s\tau, \mathbf{x} - s\tau\mathbf{u}, \mathbf{u})$.

Remark 5.3.1. In order to develop an LES model within the kinetic transport framework, we constrain our attention to the BT equation with the BGK collision approximation, involving a single relaxation time. Moreover, we follow Assumption 1 in [232, pp. 4] in the further derivations to establish a physical connection between the collision operator and the convective terms at the continuum level.

In description of turbulence effects at the kinetic level, we decompose f into the filtered, \bar{f} , and residual values, f' , where $\bar{f} = G * f$. As defined previously, G represents the kernel of any generic spatial isotropic filtering type. Then, the filtered kinetic transport for \bar{f} suffices:

$$\frac{\partial \bar{f}}{\partial t} + \mathbf{u} \cdot \nabla \bar{f} = -\frac{\bar{f} - \overline{f^{eq}(\Delta)}}{\tau}, \quad (5.13)$$

in which \mathbf{u} is independent of t and \mathbf{x} . Ensuing (5.12), the analytical solution of (5.13) is described by

$$\bar{f}(t, \mathbf{x}, \mathbf{u}) = \int_0^\infty e^{-s} \overline{f_{s,s}^{eq}(\Delta)} ds, \quad (5.14)$$

where $\overline{f_{s,s}^{eq}(\Delta)} = \overline{f^{eq}(\Delta(t - s\tau, \mathbf{x} - s\tau\mathbf{u}, \mathbf{u}))}$. Let define $\bar{\Delta} := \frac{|\mathbf{u} - \bar{\mathbf{V}}|^2}{U^2}$. Due to the nonlinear character of the collision operator [172], the filtering operation does not commute with Ω , which yields the following inequality as

$$\overline{f^{eq}(\Delta)} = \frac{\rho}{U^3} e^{-\Delta/2} \neq \frac{\rho}{U^3} e^{-\bar{\Delta}/2} = f^{eq}(\bar{\Delta}). \quad (5.15)$$

This inequality gives rise to the so-called turbulence *closure problem* at the kinetic level. From the mathematical standpoint, the SGS motions stem from the convective nonlinear terms in the NS equations, which resembles with the corresponding advective term of the BT equation. Therefore,

it seems natural to recognize $\mathbf{u} \cdot \nabla f$ responsible for the unresolved turbulence effects in the BT equation, they manifest implicitly via the filtered collision operator though. That is, the filtered collision term in the right-side of (5.13) undertakes not only molecular collisions, but also the embedded SGS motions. By emphasizing on the importance of modeling $\overline{f^{eq}(\Delta)}$ in the filtered collision operator, we review some different approaches in treating nonlinear effects.

Classical approaches: As a common practice in modeling the SGS closures, the attentions were directed toward with eddy-viscosity approximations by employing a modified relaxation time, τ^* , in the BT equation [e.g., 175]. Therefore, the proposed filtered BT equation reads as

$$\frac{\partial \bar{f}}{\partial t} + \mathbf{u} \cdot \nabla \bar{f} = -\frac{\bar{f} - f^{eq}(\bar{\Delta})}{\tau^*}. \quad (5.16)$$

In this approach, the inequality in (5.15) is disregarded through using τ^* , which renders the SGS model inappropriate for reproducing many features of the SGS motions. Nevertheless, there some non-eddy viscosity models within the lattice Boltzmann framework, which make use of (5.15) to propose more consistent SGS model. For more details, the reader is referred to [241, 173, 242].

Fractional approach: In the proposed framework in [232], the modeling of turbulence nonlinear effects begins with closing the filtered collision operator, where the multi-exponential behavior of $\overline{f^{eq}(\Delta)}$ is approximated properly by a heavy-tailed distribution function. Therefore, the $\overline{f^{eq}(\Delta)}$ in (5.13) is described by

$$\overline{f^{eq}(\Delta)} - f^{eq}(\bar{\Delta}) \simeq f^\beta(\bar{\Delta}), \quad (5.17)$$

where $f^\beta(\bar{\Delta}) = \frac{\rho}{U^3} F^\beta(\bar{\Delta})$ and $F^\beta(\bar{\Delta})$ denotes an isotropic Lévy β -stable distribution. By taking the first moment of (5.13), one derives the corresponding fractional Laplacian operator, called FSGS model, at the continuum level, where

$$(\nabla \cdot \mathbf{T}^R) = \mu_\alpha (-\Delta)^\alpha \bar{\mathbf{V}}, \quad (5.18)$$

where $\mu_\alpha = \frac{\rho(U\tau)^{2\alpha}\Gamma(2\alpha+1)}{\tau} \frac{2^{2\alpha}\Gamma(\alpha+d/2)}{\pi^{d/2}\Gamma(-\alpha)} c_\alpha$ for $\alpha \in (0, 1)$ and c_α is a real-valued constant. In principle, the choice of distribution function in (5.17) gives rise to a nonlocal operator of the resolved flow field in (5.8) as an SGS model.

Despite the notable potentials of the FSGS model in maintaining some important physical and mathematical properties of the SGS stresses, it suffers from a shortcoming by lacking a finite second-order statistical moment. To control this statistical barrier in the FSGS model and to achieve more congruence between both sides of (5.17), we seek a finite variance alternative for the *Lévy* β -stable distribution by employing the tempered counterpart and thereby a more flexible and predictive fractional operator in the LES equations in the following subsection.

5.3.3 Tempered fractional SGS modeling

In a more accurate study, multi-exponential functions express a power-law behavior in the moderate range of distribution and eventually relaxes into an exponential decay [see 243]. By engaging more exponential terms to a multi-exponential function, the corresponding power-law behavior extends toward long ranges; however, it is bound to vanish exponentially at the tail of the distribution, enforced by nature of the physical phenomenon. As a rich class of stochastic functions for fitting into realistic phenomena, tempered stable distributions [239] resemble a sheer power-law at the moderate range and then converge to an exponential decay.

Inspired by this argument, we propose to model $\overline{f^{eq}(\Delta)}$ with a coefficient of tempered *Lévy* β -stable distribution, denoted by $f^{\beta,\lambda}(\bar{\Delta})$, within the proposed fractional framework as

$$\overline{f^{eq}(\Delta)} - f^{eq}(\bar{\Delta}) \simeq f^{Model}(\bar{\Delta}) = c_{\beta,\lambda} f^{\beta,\lambda}(\bar{\Delta}), \quad (5.19)$$

where $c_{\beta,\lambda}$ is a real-valued constant number. Moreover, we consider $\beta \in (-1 - \frac{d}{2}, -\frac{d}{2})$, $\lambda > 0$ and $d = 3$ represents dimension of the physical domain. Therefore the filtered BT equation reads as

$$\begin{aligned} \frac{\partial \bar{f}}{\partial t} + \mathbf{u} \cdot \nabla \bar{f} &= -\frac{\bar{f} - f^{eq}(\bar{\Delta}) + f^{eq}(\bar{\Delta}) - \overline{f^{eq}(\Delta)}}{\tau} \\ &\simeq -\frac{\bar{f} - f^{eq}(\bar{\Delta}) - f^{Model}(\bar{\Delta})}{\tau}. \end{aligned} \quad (5.20)$$

For the sake of simplicity, we take $f^*(\bar{\Delta}) = f^{eq}(\bar{\Delta}) + f^{Model}(\bar{\Delta})$. The approximation in (5.20) conceivably provides a good fit into the filtered collision operator by maintaining the significant statistical features of $\overline{f^{eq}(\Delta)}$ and sets a physically-richer starting point for developing a nonlocal LES model at the continuum level.

In this regard, the macroscopic variables associated with the flow field can be reconstructed according to

$$\bar{\rho} = \int_{\mathbb{R}^d} \bar{f}(t, \mathbf{x}, \mathbf{u}) d\mathbf{u}, \quad (5.21)$$

$$\bar{V}_i = \frac{1}{\rho} \int_{\mathbb{R}^d} u_i \bar{f}(t, \mathbf{x}, \mathbf{u}) d\mathbf{u}, \quad i = 1, 2, 3, \quad (5.22)$$

where $\bar{\rho} = \rho$ for an incompressible flow. To establish the connection between the kinetic description and the filtered NS equation, we proceed with deriving the macroscopic form of (5.20) by multiplying it with \mathbf{u} , and integrating over the kinetic momentum, which yields

$$\int_{\mathbb{R}^d} \left(\mathbf{u} \frac{\partial \bar{f}}{\partial t} + \nabla \cdot (\mathbf{u}^2 \bar{f}) \right) d\mathbf{u} = 0 \implies \rho \frac{\partial \bar{V}}{\partial t} + \nabla \cdot \int_{\mathbb{R}^d} \mathbf{u}^2 \bar{f} d\mathbf{u} = 0. \quad (5.23)$$

Recalling the assumptions in Remark 5.3.1 that $\int_{\mathbb{R}^d} \mathbf{u} \left(\frac{\bar{f} - f^*(\bar{\Delta})}{\tau} \right) d\mathbf{u} = 0$ due to microscopic reversibility of the particle collisions. Following the derivations in [232, pp. 5-6], we add and subtract $\bar{V}\bar{V}$ to the advection term and accordingly, (5.23) is found to be

$$\rho \left(\frac{\partial \bar{V}}{\partial t} + \nabla \cdot \bar{V}\bar{V} \right) = -\nabla \cdot \boldsymbol{\varsigma}, \quad (5.24)$$

where $\boldsymbol{\varsigma}$ in the index form is expressed as

$$\varsigma_{ij} = \int_{\mathbb{R}^d} (u_i - \bar{V}_i)(u_j - \bar{V}_j) \bar{f} d\mathbf{u}. \quad (5.25)$$

Comparing (5.8) and (5.24), it turns out that pressure term, viscous and SGS stresses all trace back to $\nabla \cdot \boldsymbol{\varsigma}$, where $\varsigma_{ij} = -\bar{p}\delta_{ij} + T_{ij}^{shear} + T_{ij}^R$. By plugging (5.14) into the kinetic definitions of each term in ς_{ij} , we obtain

$$\bar{p}\delta_{ij} = - \int_{\mathbb{R}^d} (u_i - \bar{V}_i)(u_j - \bar{V}_j) f^*(\bar{\Delta}) d\mathbf{u} \int_0^\infty e^{-s} ds, \quad (5.26)$$

$$T_{ij}^{shear} = \int_0^\infty \int_{\mathbb{R}^d} (u_i - \bar{V}_i)(u_j - \bar{V}_j) \times (f_{s,s}^{eq}(\bar{\Delta}) - f^{eq}(\bar{\Delta})) e^{-s} d\mathbf{u} ds = 2\mu \bar{S}_{ij}, \quad (5.27)$$

where $\mu = \rho U^2 \tau$. Similarly, by employing f^{Model} in (5.19), we attain

$$\begin{aligned} T_{ij}^R &= c_{\beta,\lambda} \int_0^\infty \int_{\mathbb{R}^d} (u_i - \bar{V}_i)(u_j - \bar{V}_j) (f_{s,s}^{\beta,\lambda}(\bar{\Delta}) - f^{\beta,\lambda}(\bar{\Delta})) e^{-s} d\mathbf{u} ds \\ &= \frac{\rho c_{\beta,\lambda}}{U^3} \int_0^\infty \int_{\mathbb{R}^d} (u_i - \bar{V}_i)(u_j - \bar{V}_j) (F^{\beta,\lambda}(\bar{\Delta}_{s,s}) - F^{\beta,\lambda}(\bar{\Delta})) e^{-s} d\mathbf{u} ds, \end{aligned} \quad (5.28)$$

in which $\bar{\Delta}_{s,s} = \bar{\Delta}(t - s\tau, \mathbf{x} - s\tau\mathbf{u}, \mathbf{u})$. As discussed in Appendix C, the temporal shift can be detached from $f_{s,s}^{\beta,\lambda}(\bar{\Delta})$ and then $\bar{\Delta}_{s,s}$ is simplified to $\bar{\Delta}_s = \bar{\Delta}(t, \mathbf{x} - s\tau\mathbf{u}, \mathbf{u})$. Therefore,

$$\mathbf{T}_{ij}^R = \frac{\rho c_{\beta,\lambda}}{U^3} \int_0^\infty \int_{\mathbb{R}^d} (u_i - \bar{V}_i)(u_j - \bar{V}_j) (F^{\beta,\lambda}(\bar{\Delta}_s) - F^{\beta,\lambda}(\bar{\Delta})) e^{-s} d\mathbf{u} ds. \quad (5.29)$$

The strategy to evaluate \mathbf{T}_{ij}^R is to decouple the particle speed into time and displacement by employing $\mathbf{u} = \frac{\mathbf{x}' - \mathbf{x}}{s\tau}$ and approximate the asymptotic behavior of $F^{\beta,\lambda}(\bar{\Delta})$ with a tempered power-law distribution. In a detailed discussion in Appendix D, we show that

$$\mathbf{T}_{ij}^R = c_{\alpha,\lambda} \bar{v}_\alpha \sum_{k=0}^K \bar{\phi}_k^{\mathcal{K}}(\alpha) \int_{\mathbb{R}^d} (x_i - x'_i)(x_j - x'_j) \frac{(\mathbf{x} - \mathbf{x}') \cdot (\bar{\mathbf{V}} - \bar{\mathbf{V}}')}{|\mathbf{x} - \mathbf{x}'|^{2\alpha+5} e^{\bar{\lambda}_k |\mathbf{x} - \mathbf{x}'|}} d\mathbf{x}', \quad (5.30)$$

in which $\bar{v}_\alpha = (2\alpha + 3)(\rho C_\alpha \tau^{2\alpha-1} U^{2\alpha})$ for $\alpha \in (0, \frac{1}{2}) \cup (\frac{1}{2}, 1)$ and recalling $\bar{\lambda}_k = \frac{k}{\tau U} \lambda$. Moreover, $\bar{\phi}_k^{\mathcal{K}}(\alpha)$ is indicated in (D.12). Eventually, we disclose the integral form of $\nabla \cdot \mathbf{T}^R$ as

$$(\nabla \cdot \mathbf{T}^R)_j = c_{\alpha,\lambda} \bar{v}_\alpha \sum_{k=0}^K \frac{(2\alpha + \bar{\lambda}_k)}{(2\alpha + 3)} \bar{\phi}_k^{\mathcal{K}}(\alpha) \int_{\mathbb{R}^d} \frac{(\bar{V}_j - \bar{V}')}{|\mathbf{x} - \mathbf{x}'|^{2\alpha+3} e^{\bar{\lambda}_k |\mathbf{x} - \mathbf{x}'|}} d\mathbf{x}', \quad (5.31)$$

where $v_\alpha = c_{\alpha,\lambda} \bar{v}_\alpha$. Reminding the integral representation of a tempered fractional Laplacian in (5.6), we formulate the divergence of the SGS stresses as follows

$$(\nabla \cdot \mathbf{T}^R)_j = v_\alpha \sum_{k=0}^K \phi_k^{\mathcal{K}}(\alpha, \lambda) (\Delta + \bar{\lambda}_k)^\alpha \bar{V}_j, \quad (5.32)$$

where $\phi_k^{\mathcal{K}}(\alpha, \lambda) = \frac{(2\alpha + \bar{\lambda}_k)}{(2\alpha + 3)} \bar{\phi}_k^{\mathcal{K}}(\alpha)$. Evidently, by setting $\mathcal{K} = 0$, we find $\bar{\phi}_k^{\mathcal{K}}(\alpha) = \Gamma(2\alpha)$ and the new operator in (5.32) reduces to a fractional Laplacian, which recovers the FSGS model.

Inferring from (5.32), our choice in the kinetic description of turbulent effects reflects in the form of a tempered fractional operator through a rigorous connection between the filtered BT and NS equations. More specifically, we adopt $\mathcal{K} = 1$ and hence the tempered fractional SGS (TFSGS) model can be formulated as

$$\nabla \cdot \mathbf{T}^R = v_\alpha [\phi_0^1(\alpha) (-(-\Delta)^\alpha) \bar{V} + \phi_1^1(\alpha) (\Delta + \bar{\lambda}_1)^\alpha \bar{V}], \quad (5.33)$$

where $\phi_0^1(\alpha) = \frac{1}{(2\alpha+3)} (\Gamma(2\alpha+1) - \Gamma(2\alpha))$ and $\phi_1^1(\alpha, \lambda) = \frac{(2\alpha+\lambda)}{(2\alpha+3)} \Gamma(2\alpha-1)$. Accordingly, the governing LES equations read as

$$\frac{\partial \bar{V}_i}{\partial t} + \frac{\partial \bar{V}_i}{\partial x_j} \bar{V}_j = -\frac{1}{\rho} \frac{\partial \bar{p}}{\partial x_i} + v \Delta \bar{V}_i - v_\alpha \sum_{k=0}^1 \phi_k^1(\alpha, \lambda) (\Delta + \bar{\lambda}_k)^\alpha \bar{V}_i, \quad (5.34)$$

where $\alpha \in (0, \frac{1}{2}) \cup (\frac{1}{2}, 1)$, $\lambda > 0$, and $v_\alpha = \frac{\mu_\alpha}{\rho}$.

Remark 5.3.2. As a generator of tempered Lévy stable processes, the tempered fractional Laplacian is proven to be rotationally and Galilean invariant [see 244, 245]. Therefore, by having v_α and ϕ_k^1 as real-valued functions of α and λ , the TFSGS model adopts the frame invariance property in a consistent fashion with the SGS stresses.

5.3.4 TFSGS formulations for the SGS stresses

To study the key role of tempering fractional operators in recovering turbulent statistical structures, it is essential to establish a straightforward form of the modeled SGS stresses. Due to some numerical complications in evaluating the integral in (5.31), we settle to proceed with the Fourier representation of the TFSGS model. Employing the definition of \mathcal{I}^α (α -Riesz potential) from [170], it is possible to verify that

$$\nabla \cdot \mathbf{T}^R = (\Delta + \lambda)^\alpha \bar{\mathbf{V}} = \nabla \cdot \nabla \mathcal{I}^{\alpha=1} \left[v_\alpha \sum_{k=0}^1 \phi_k^1(\alpha, \lambda) (\Delta + \bar{\lambda}_k)^\alpha \bar{\mathbf{V}} \right]. \quad (5.35)$$

Inspired by (5.35), we introduce $\mathcal{R}_j^{\alpha, \lambda}(\cdot) = \nabla_j \mathcal{I}^{\alpha=1}(\Delta + \lambda)^\alpha(\cdot)$ as a tempered fractional operator such that

$$\mathbf{T}_{ij}^R = \frac{v_\alpha}{2} \sum_{k=0}^1 \phi_k^1(\alpha, \lambda) [\mathcal{R}_j^{\alpha, \bar{\lambda}_k} \bar{V}_i + \mathcal{R}_i^{\alpha, \bar{\lambda}_k} \bar{V}_j], \quad (5.36)$$

where $\mathcal{F}[I^{\alpha=1}] = \frac{1}{\xi^2}$ and $\mathcal{F}[\nabla_j](\xi) = -i\xi_j$ and i denotes an imaginary unite. Following (5.7) into (5.36), we find the Fourier form of $\mathcal{R}_j^{\alpha, \lambda}$ as

$$\mathcal{F}[\mathcal{R}_j^{\alpha, \lambda}](\xi) = \mathfrak{C}_\alpha \frac{-i\xi_j}{\xi^2} (\lambda^{2\alpha} - (\lambda^2 + \xi^2)^\alpha {}_2F_1(-\alpha, 1 + \alpha; \frac{3}{2}; \frac{\xi^2}{\xi^2 + \lambda^2})). \quad (5.37)$$

5.4 Statistical Analysis

In pursuit of an ideal SGS model, nonlinearity induced by the convective terms and nonlocality imparted by the pressure term in the NS equations contribute to a synthetic hierarchy of transport equations and multi-point descriptions of SGS terms, as shown in [82]. The infinitely-extended

hierarchical triangle of nonlinearity and nonlocality brings up the idea of indicating a set of weaker, and yet significant, statistical conditions and make the ideal LES model more attainable, as endorsed by [80]. To identify such statistical features, Menevuela in [76] developed a rigorous framework via a statistical *a priori* analysis and formulated some sufficient conditions for the assessment of LES models. As one of the candidates for evaluating SGS models, we give a brief review of the argued formulations in [76] and introduce an optimization strategy, which enables the TFSGS model to correctly generate the requisite statistical conditions.

Hereafter, we consider the following notations in study of the SGS fields. Let $\mathbf{T}^{R,D}$ and $\mathbf{T}^{R,*}$ denote the SGS stresses, implied by the true DNS data and the SGS model, respectively. We also take \mathbf{r} as the displacement vector between two points in the correlation functions and \mathbf{e} denotes the unit vectors of the axes in the Cartesian coordinates. Then, $r = |\mathbf{r}|$. As discussed in [76], performing an ensemble-average of the filtered NS equations offers a set of necessary conditions for an LES simulation to ensure the equality of mean velocity profiles and the second-order moments, listed as:

- (a) $\langle \mathbf{T}_{ij}^{R,D} \rangle = \langle \mathbf{T}_{ij}^{R,*} \rangle,$
- (b) $\langle \bar{V}_i \mathbf{T}_{ij}^{R,D} \rangle = \langle \bar{V}_i \mathbf{T}_{ij}^{R,*} \rangle,$
- (c) $\langle \bar{\mathbf{S}}_{ij} \mathbf{T}_{ij}^{R,D} \rangle = \langle \bar{\mathbf{S}}_{ij} \mathbf{T}_{ij}^{R,*} \rangle,$

in which conditions (b) and (c) are inferred from the ensemble-averaged SGS transport equation.

Focusing on the nonlocality axis of the closure triangle for a homogeneous isotropic turbulent (HIT) flow, one obtains the so-called Karman-Howarth (KH) equation as

$$\left[\frac{\partial}{\partial t} - 2\nu \left(\frac{\partial^2}{\partial r^2} + \frac{4}{r} \frac{\partial}{\partial r} \right) \right] B_{LL}(r, t) - \left(\frac{\partial}{\partial r} + \frac{4}{r} \right) B_{LLL}(r, t) = \left(\frac{\partial}{\partial r} + \frac{4}{r} \right) G_{LLL}(r, t), \quad (5.38)$$

for sufficiently large $\mathcal{L} \gg \eta$, where L represents the longitudinal direction. Additionally, we denote by $B_{LL}(r, t) = \langle \bar{V}_L(\mathbf{x}, t) \bar{V}_L(\mathbf{x} + \mathbf{r} \cdot \mathbf{e}, t) \rangle$ and $B_{LLL}(r, t) = \langle \bar{V}_L(\mathbf{x}, t)^2 \bar{V}_L(\mathbf{x} + \mathbf{r} \cdot \mathbf{e}, t) \rangle$ the second- and third-order velocity correlation functions, respectively and $G_{LLL}(r, t) = \langle \mathbf{T}_{LL}^R(\mathbf{x}, t) \bar{V}_L(\mathbf{x} + \mathbf{r} \cdot \mathbf{e}, t) \rangle$

refers to the stress-strain correlation function. Technically, the third-order correlation function in (5.38) is subdivided into B_{LLL} stemming from the resolved velocity field and $G_{LLL}(r, t)$ coming from the SGS stresses. It turns out from (5.38) that the SGS model should undergo a correct prediction of $G_{LLL}(r, t)$ to re-generate B_{LL} and B_{LLL} accurately. Referring to [76, pp. 819-820], we arrive at the following equation

$$\langle [\bar{V}_L(\mathbf{x} + \mathbf{r} \cdot \mathbf{e}, t) - \bar{V}_L(\mathbf{x}, t)]^3 \rangle + 6 G_{LLL}(r, t) = 6 \langle \bar{S}_{LL} \mathbf{T}_{LL}^R \rangle r, \quad (5.39)$$

which exhibits the only sufficient condition for modeling third-order structure in an HIT flow. Therefore, by satisfying the equality of SGS dissipation via conditions (c), modeling G_{LLL} remains the only requisite for capturing the third-order structure functions.

This finding reveals the significance of condition (c), which intrinsically ties with the stress-strain correlation function, represented by $D_{LL}(r, t) = \langle \bar{S}_{LL}(\mathbf{x} + \mathbf{r} \cdot \mathbf{e}, t) \mathbf{T}_{LL}^R \rangle$. Using the conversation in [81, pp. 317], D_{LL} is derived in terms of G_{LLL} as

$$D_{LL}(r, t) = \frac{7}{2} \frac{dG_{LLL}(r, t)}{dr} + \frac{4G_{LLL}(r, t)}{r} + \frac{r}{2} \frac{d^2G_{LLL}(r, t)}{dr^2}. \quad (5.40)$$

Emphasizing the role of tempering parameter in modulating the turbulent dissipation range, we therefore adopt $D_{LL}(r, t)$ as a key quantity in optimizing the TFSGS model to address condition (c) and capture the nonlocal structures in (5.39). It must be noted that in evaluating the aforementioned conditions and high-order structures, \mathbf{T}^R represents either $\mathbf{T}^{R,D}$, obtained by filtering the instant DNS database, or $\mathbf{T}^{R,*}$, implied by implementing the model to the true resolved velocity field.

5.4.1 Optimization strategy

Devising a robust optimization framework is an inevitable element in predictive fractional and tempered fractional modeling [see 228, 218]. Regarding the given set of conditions for the closure problem, we find conditions (a) and (c) practically crucial in developing an approach for estimating the parameters and coefficient associated with the TFSGS model while condition (b) can be substantially recovered by imposing (5.39), where $G_{LLL}(r, t)|_{r=0} = \langle \bar{V}_i \mathbf{T}_{ij}^R \rangle$. As we learn from

the one-point correlation analysis in [232] and the further section, correlation between the SGS stresses, obtained by the DNS data and the model, highly relies on α and λ in the TFSGS model rather plays a central role in capturing the SGS dissipation energy and nonlocal structure functions. This approach provides the basis for an optimal estimation of the fractional exponents (α and λ) by employing the normalized D_{LL} and ϱ_i , defined in Algorithm 5.1.

Algorithm 5.1 Estimation of the optimal model parameters for a specific \mathcal{L}

[INPUT]: $\bar{V}_i, T_{ij}^{R,D}, \bar{V}_L(\mathbf{x} + \mathbf{r} \cdot \mathbf{e}, t)$

OUTPUT: $\alpha^{opt}, \lambda^{opt}, c_{\alpha,\lambda}$

PROCESS: Find α^{opt} where the maximum of $\varrho_{ii} = \left\langle \varrho \left[T_{ii}^{R,D}, T_{ii}^{R,TF} \right] \right\rangle$ occurs. Find λ^{opt} where $\left[\frac{D_{LL}(r,t)}{D_{LL}(0,t)} \right]^{TF}$ fits into $\left[\frac{D_{LL}(r,t)}{D_{LL}(0,t)} \right]^D$ for the inferred α^{opt} . Quantify the model constant such that $c_{\alpha,\lambda} = \frac{\langle \bar{S}_{ij} T_{ij}^{R,D} \rangle}{\langle \bar{S}_{ij} T_{ij}^{R,N} \rangle}$, given α^{opt} and λ^{opt} .

VALIDATION ANALYSIS:

1. Evaluate $G_{LLL}(r)$ for the modeled and true SGS stresses to check if (5.39) is validated.
 2. Perform a comparative study on the PDFs of $\langle \bar{S}_{ij} T_{ij}^R \rangle$ and $\langle T_{ii}^R \rangle$.
-

By fixing the values of fractional exponents, it is possible to accurately quantify the model coefficient and thereby re-producing the third-order structure in (5.39) via modeling G_{LLL} . In Algorithm 5.1, we schematically present the proposed method for optimizing the parameters associated with the TFSGS model at a given flow Reynolds number (Re) and a specific \mathcal{L} . It must be noted that in step 3, we define

$$T_{ij}^{R,N} = \frac{T_{ij}^{R,TF}}{c_{\alpha,\lambda}} = \frac{\bar{v}_\alpha}{2} \sum_{k=0}^1 \phi_k^1(\alpha, \lambda) [\mathcal{R}_j^{\alpha, \bar{\lambda}_k} V_i + \mathcal{R}_i^{\alpha, \bar{\lambda}_k} V_j]. \quad (5.41)$$

Moreover, superscripts “ D ” and “ TF ” represent the values obtained by filtering the true DNS data and the SGS model, respectively.

5.5 A Priori Study

As discussed in previous sections, the TFSGS model inherits the potentials of a tempered power-law distribution at the kinetic level, which account for the interplay between the resolved

and small-scale motions. To attain the optimal behavior of the TFSGS model, we follow the steps in Algorithm 5.1 by performing an *a priori* analysis and evaluate the capabilities of the TFSGS model in generating the statistical features of turbulent flows.

5.5.1 DNS Database and LES Platform

In terms of *a priori* tests, we conduct the numerical simulation of a forced HIT flow employing the open-source pseudo-spectral NS solver for a triply periodic domain the code of which is presented at [246]. It should be noted that in the next section, the LES solver is successfully prepared using the DNS code and the presented stationary dataset as initial conditions for the final *a posteriori* assessments.

Using the NS solver, we performed DNS of a stationary HIT flow with 320^3 resolution for a periodic computation domain as $\Omega = [0, 2\pi]^3$ and the large scale forcing occurs at $0 < |\xi| \leq 2$ to maintain turbulence statistics stationary. Here, ξ represents the vector of Fourier wave numbers and $\xi_{max} = 2N\sqrt{2}/3$ is the maximum wave number solved numerically, where $N = 320$ is the number of grid points. In this case, $\xi_{max}\eta_k = 1.6 > 1$ certifies that all the scales of motion are well-resolved, where η_k refers to the Kolmogorov length scale. We detail the flow parameters and some of the statistical properties at Table 5.1, in which ε and K_{tot} denote the expected values of dissipation rate and turbulent kinetic energy, respectively. Moreover, $Re_\lambda = \frac{u'_{rms}l_\lambda}{\nu}$ and $l_\lambda = \sqrt{15\nu u'^2_{rms}/\varepsilon}$ represent the Taylor Reynolds number and micro-scale length, respectively, where $u'_{rms} = \sqrt{2K_{tot}/3}$. The simulation undergoes running for 30 eddy turn-over times, $\tau_{\mathcal{L}}$, to construct 40 sample snapshots as our database. Due to the incumbent homogeneity and isotropy in the HIT flow, we find the database adequate for obtaining the required statistics in the further analysis. The kurtosis and skewness values of the diagonal velocity gradients are also presented in Table 5.1, supporting non-Gaussianity of turbulent structures.

For the purpose of crunching heavy DNS database and overcoming the burden of timely filtering process in the two-point correlation analysis, we develop a scalable multi-threaded filtering code using `Numpy`, `threading`, and `astropy.convolution`. The described platform is publicly acces-

Table 5.1: Flow parameters and statistical properties in the DNS of a forced HIT flow.

Re_λ	u'_{rms}	K_{tot}	ν	ε	$\tau_{\mathcal{L}}$	skewness	kurtosis
	(m/sec)	(m ² /sec ²)	(m ² /sec)	(m ² /sec ³)	(sec)		
190	0.67	0.68	0.001	0.1	4.2	-0.5	6.5

sible through (<https://github.com/FMATH-Group>) and (<https://github.com/samieeme/Dissertation>).

5.5.2 Optimal estimation of fractional parameters

In order to optimize the efficiency of the TFSGS model, we developed a multi-step strategy in Algorithm 5.1. The proposed algorithm is equipped with verification and validation mechanisms through conventional correlation coefficients and two-point structure functions. Recalling from section 5.4.1 that $T_{ij}^{R,D}$ denotes the true SGS stresses obtained by filtering the well-resolved DNS data. Moreover, $T_{ij}^{R,*}$ represents the general form of modeled SGS values, where * can be replaced by *TF* or *SM* in the TFSGS or SMG models, respectively.

The first step in Algorithm 5.1 concerns detecting optimum value of fractional exponent, α^{opt} , where the maximum of ensemble-averaged correlation between $T_{ii}^{R,D}$ and $T_{ii}^{R,TF}$, denoted by ϱ_{ii} , occurs. Our premise is that the tempering parameter, λ , does not make any noticeable changes in ϱ_{ii} , namely less than 3 percents, which is endorsed by the results of Table 5.2. In the absence of λ , we plot the variations of ϱ_{ii} versus α^{opt} in Figure 5.1 for $i = 1, 2, 3$, in which each dashed box specifies the interval of α yielding the maximum of ϱ_{ii} . Without any loss of accuracy, we adopt $\alpha^{opt} = 0.76, 0.58, 0.51$ as the corresponding minimum value in each specified interval for $\mathcal{L}_\delta = \frac{\mathcal{L}}{2\delta x} = 4, 8, 12$, respectively, where $\delta x = \frac{2\pi}{N}$ represents the computational grid size.

From the kinetic perspective, by enlarging \mathcal{L}_δ , $\overline{f^{eq}(\Delta)}$ in (5.13) demonstrates an increasingly multi-exponential pattern, which can be better described by a power-law distribution function. This argument accounts for the prediction enhancement in Figure 5.1, achieved by the TFSGS model and the abduct reduction of α^{opt} versus \mathcal{L}_δ , which is extensively discussed in [232, page

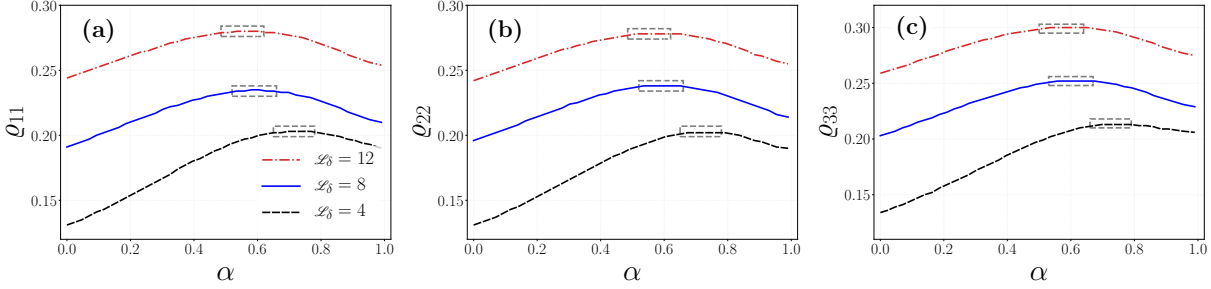


Figure 5.1: variation of the correlation coefficients **(a)** ϱ_{11} , **(b)** ϱ_{22} , and **(c)** ϱ_{33} versus $\alpha \in (0, 1)$ for $\mathcal{L}_\delta = 4, 8, 12$ by setting $\lambda \approx 0$ in (5.41). The maximum values lie in the dashed boxes.

Table 5.2: The ensemble-averaged correlation coefficients (ϱ_{ii}) between SGS stresses obtained by the filtered DNS data ($T_{ii}^{R,D}$) and the TFSGS model ($T_{ii}^{R,TF}$) for $i = 1, 2, 3$. In the fractional models, α^{opt} is set as 0.76, 0.58, and 0.51 for $\mathcal{L}_\delta = 4, 8, 12$ respectively.

		$\mathcal{L}_\delta = 4$			$\mathcal{L}_\delta = 8$			
λ	FSGS	TFSGS		SMG	FSGS	TFSGS		SMG
		0	0.1	4		0	0.35	5
ϱ_{11}	0.21	0.20	0.19	0.20	0.23	0.24	0.22	0.22
ϱ_{22}	0.21	0.20	0.20	0.21	0.24	0.24	0.23	0.23
ϱ_{33}	0.22	0.21	0.21	0.21	0.25	0.25	0.24	0.23
$\mathcal{L}_\delta = 12$								
λ	FSGS	TFSGS		SMG	FSGS	TFSGS		SMG
		0	0.45	5		0.28	0.26	0.26
ϱ_{11}	0.29	0.28	0.26	0.26	0.29	0.30	0.29	0.28
ϱ_{22}	0.29	0.28	0.26	0.26	0.29	0.30	0.29	0.28
ϱ_{33}	0.30	0.30	0.29	0.28	0.30	0.30	0.29	0.28

10]. Theoretically, the tempered power-law distribution can resemble a power-law or a Gaussian distribution by letting λ go to 0 or ∞ , respectively. This grounds for the TFSGS model to span the gap between the FSGS model, representing self-similar behavior of the inertial range, and the SMG model, renowned for its dissipative characteristics. The results in Table 5.2 support this line of reasoning by a row of correlation quantities for the given filter widths, particularly at $\mathcal{L}_\delta = 12$.

On this background, we proceed with the second step in Algorithm 5.1 to indicate λ^{opt} through a comparative study of the normalized strain-stress correlation function, defined as $S_\Delta = \frac{D_{LL}(r,t)}{D_{LL}(0,t)}$. With the knowledge of $D_{LL}(r,t)$, we extend the two-point correlation analysis to the spectral space by evaluating the instantaneous radial dissipation spectrum, given by $\tilde{\mathcal{D}}(\xi) = \mathcal{F}[D_{LL}(r,t)](\xi)$.

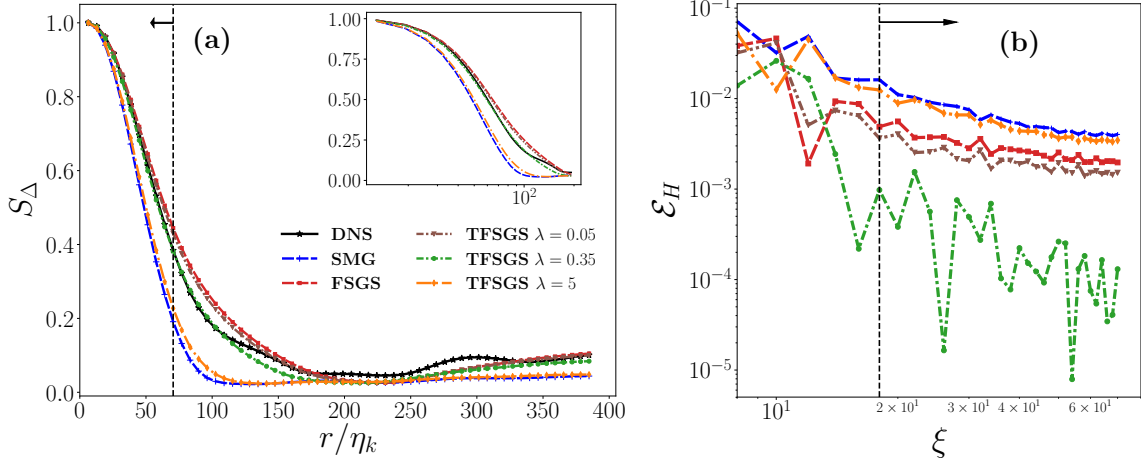


Figure 5.2: (a) Comparing results of the normalized two-point stress-strain rate correlation functions (S_Δ) and (b) error analysis of the longitudinal dissipation spectrum (\mathcal{E}_H) for fractional SGS and Smagorinsky models, where $\mathcal{L}_\delta = 8$ and ξ represents the radius of Fourier wave numbers. In both plots, the arrows point to the dissipation range.

To evaluate the error between the dissipation spectrum, obtained by the true DNS data and the LES models at high wave numbers, we define

$$\mathcal{E}_H = \frac{\left| [\tilde{\mathcal{D}}(\xi)]^* - [\tilde{\mathcal{D}}(\xi)]^D \right|}{\left| [\tilde{\mathcal{D}}(\xi)]^D \right|},$$

where $|\cdot|$ represents norm of the vector. Figure 5.2 (a) displays S_Δ versus the spatial shift, r , for a logarithmic sequence of λ spanning three orders of magnitude in the TFSGS model, where $\mathcal{L}_\delta = 8$. As stated earlier, the proposed model can take a journey from the FSGS to the SMG models by tuning λ . Evidently, the true quantities of S_Δ , colored by black, are well-predicted by the proposed model with $\lambda^{opt} = 0.45$, where $\alpha^{opt} = 0.58$ is fixed. Figure 5.2 (b) confirms our findings quantitatively in a plot of \mathcal{E}_H versus radius of wave numbers, ξ , with log-scale axes. In fact, this plot implies accuracy of the TFSGS model in capturing the two-point structure function at the dissipation range, pointed by an arrow.

Employing the same analysis for $\mathcal{L}_\delta = 4, 12$, we infer the optimal behavior of the TFSGS model, evaluated for a logarithmic range of λ with a fixed α^{opt} , in Figure 5.3. The inset plots show \mathcal{E}_H versus ξ using log-scale on both axes to magnify the dissipation range at high wave numbers. Interestingly, at $\mathcal{L}_\delta = 4$ the FSGS model is dissipative enough to outperform the tempered model

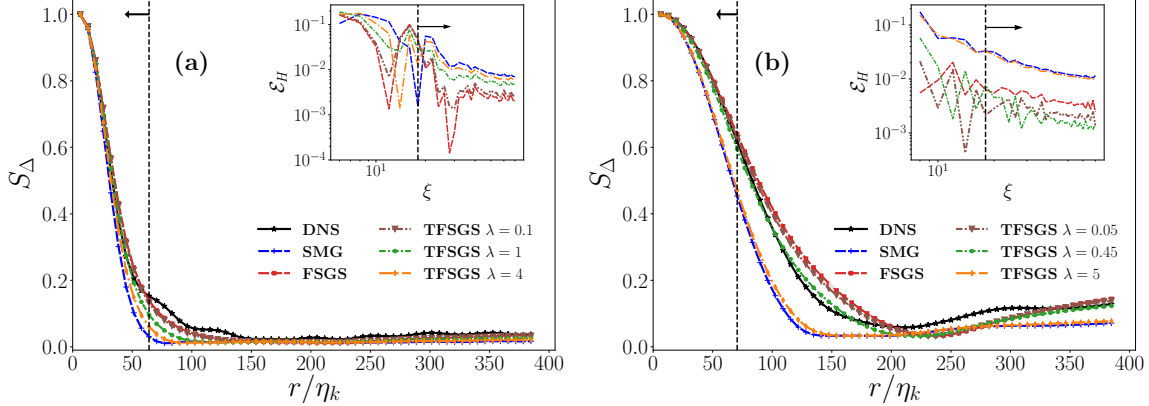


Figure 5.3: Comparing results of the normalized two-point stress-strain rate correlation functions for (a) $\mathcal{L}_\delta = 4$ and (b) $\mathcal{L}_\delta = 12$. The inset plots illustrate the scaled error of longitudinal dissipation spectrum (\mathcal{E}_H) versus the radius of Fourier wave numbers (ξ). The arrows point to the dissipation range.

in capturing the true S_Δ in Figure 5.3 (a). With all this in mind, these results certify the importance of tempering in correct regeneration of two-point correlation functions particularly at larger filter widths ($\mathcal{L}_\delta = 8, 12$). Moreover, the SMG model, resembling the TFSGS with $\lambda \sim 5$, exhibits a relatively steeper slope at the dissipation range, which is rooted in the diffusive form of its operator. In this context, tempering plays a crucial role in characterizing dissipation structures by comparing the widening gaps between the asymptotic cases ($\lambda = 0.01$ and 5) in Figure 5.3 (b). This brings up the TFSGS model as superior physics based model regarding the counterparts, i.e., the SMG and the FSGS models.

Given the values of α^{opt} and λ^{opt} , we proceed lastly with quantifying $c_{\alpha,\lambda}$ as prescribed in Algorithm 5.1. Under statistically stationary circumstances of the flow field, $c_{\alpha,\lambda}$ remains fairly unchanged for each \mathcal{L}_δ of interest, as reported in Table 5.3. It should be noted that $c_{\alpha,\lambda}$ is only part of the fractional coefficient, described in (5.41), in order to scale up the model in a constant Re_λ and \mathcal{L}_δ .

5.5.3 Interpretation of two-point structure functions

The third-order structure functions, arising from the KH equations, provide insights about the statistics of unresolved scales and their strong interactions with large scale motions. As discussed

Table 5.3: Optimized parameters associated with the TFSGS model in terms of Algorithm 5.1 for differing filter widths.

$\mathcal{L}_\delta = 4$			$\mathcal{L}_\delta = 8$			$\mathcal{L}_\delta = 12$		
α	λ	$c_{\alpha,\lambda}$	α	λ	$c_{\alpha,\lambda}$	α	λ	$c_{\alpha,\lambda}$
0.76	$\simeq 0$	2.08	0.58	0.35	0.88	0.51	0.45	0.048

previously in section 5.4, $G_\Delta = \frac{G_{LLL}}{\epsilon \mathcal{L}}$, representing the scaled two-point velocity-stress correlation function, is introduced as a sufficient condition for precise regeneration of third-order structure functions and an *a priori* consistency in LES modeling. Following the derivation of the longitudinal Taylor maicroscale in [138, chapter 6], $D_{LL}(r)$ seems to be directly connected to the first-order derivative of $G_{LLL}(r)$ at the dissipation range. This offers the capability of the optimum edition of TFSGS model in capturing G_Δ and thereby fulfilling the essential conditions in (5.39).

In the first stage of the statistical analysis, we perform a comprehensive study on G_Δ in Figure 5.4 (a) for $\mathcal{L}_\delta = 8$, in which the dissipation and inertial ranges are magnified in Figure 5.4 (b) with semi-logarithmic scale on the x-axis and Figure 5.4 (c) with logarithmic scale on both axes, respectively. The balance regions (BR), including extremum points, are thickened up in all the graphs in Figure 5.4 (a). BR also indicates the transitional zone between dissipation and inertial ranges. Aligned with the right side of the (5.39), the trend of G_Δ at small-scale interactions appear to be a linear function of spatial displacement, r , suggested by [76, Figure 2]. The results in Figure 5.4 (a) and more accurately in Figure 5.4 (b) offer that the optimum TFSGS model well-predict the true DNS quantities at the left side of BR, not only the slope of G_Δ but also the maximum of G_Δ occurring at a relatively close r . This spotlights the importance of step three of Algorithm 5.1 in tuning slope of G_Δ at the dissipation range and effective role of the tempering parameter in fitting the BR, associated with the filtered DNS data. In practice, increasing λ pushes BR toward the left side to preserve the increasing linear correlation as a notion of more dissipative behavior. These findings are endorsed qualitatively for the other filter widths in Figure 5.5, considering λ^{opt} in Table 5.3.

In analysis of G_Δ at the inertial range, the graph, associated with λ^{opt} , shows a favorable match

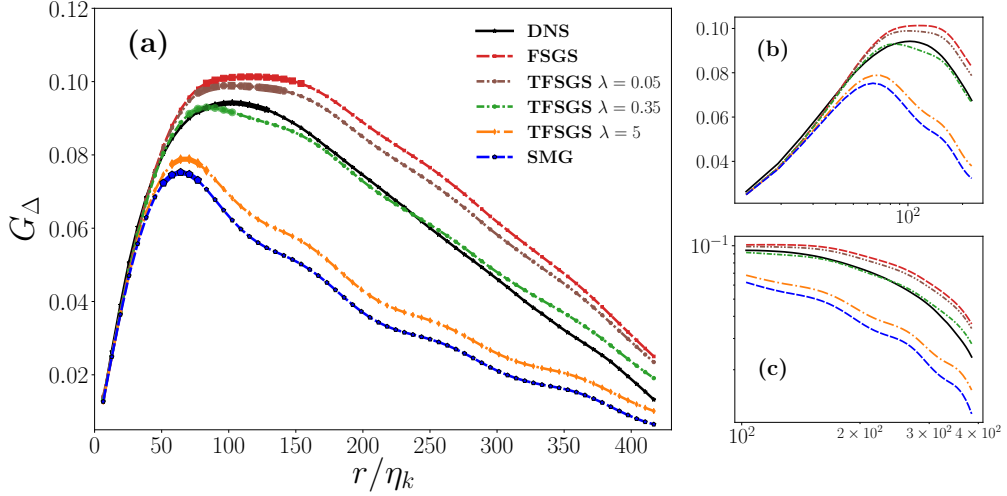


Figure 5.4: Two-point velocity-stress correlation function in a stationary HIT flow for $\mathcal{L}_\delta = 8$ using box filtering. The segment of balance region (BR) has been thickened up in **(a)** for all the graphs. The dissipation and the inertial ranges have been enlarged in plots **(b)** with semi-logarithmic scale on the x-axis and **(c)** with logarithmic scale on the both axes, respectively.

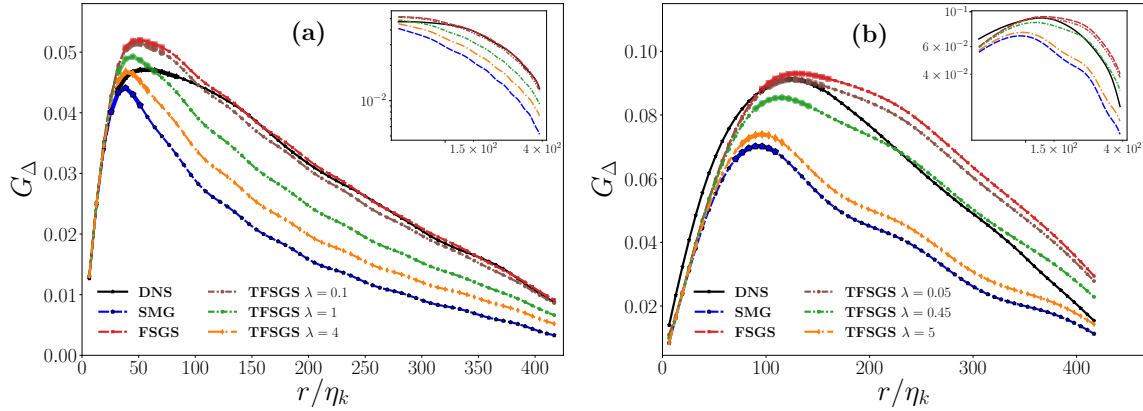


Figure 5.5: Two-point velocity-stress correlation function in a stationary HIT flow for **(a)** $\mathcal{L}_\delta = 4$ and **(b)** $\mathcal{L}_\delta = 12$ using box filtering. The inertial range has been enlarged in the inset plots with logarithmic scale on the both axes.

with true points, colored by black, in Figures 5.4 and 5.5. For the purpose of clarity, the inertial ranges are magnified in log-log scale plots in Figure 5.4 (c) for $\mathcal{L}_\delta = 8$ and the inset plots in Figure 5.5 for $\mathcal{L}_\delta = 4, 12$, respectively. Motivated by these results, tempered fractional modeling seems to be faithful in fitting structures at the dissipation and the inertial ranges and also estimating the correct value of r , associated with the extremum points. Inevitably, enlarging \mathcal{L}_δ accounts for inaccuracies in fitting the tail of graphs as observed in 5.5 (b). Notwithstanding, the mid-range interactions are acceptably predicted by the optimized TFSGS model.

With an overview of the present results, the TFSGS model stands out as a structure-based approach, which reasonably covers the gap between the FSGS and the SMG models. In $\mathcal{L}_\delta = 4$, λ^{opt} is found to be very close to zero, which renders tempering nonessential in capturing two-point structures. As we increase \mathcal{L}_δ , this gap starts widening up and tempering mechanism acts more dynamically in finding the true BR and fitting the dissipation structures. This argument confirms that the tempered fractional approach displays a great potential for parameterizing structure function especially at larger filter widths while retaining fairly acceptable accuracy.

5.5.4 PDF of SGS stresses

Within the proposed statistical framework, the last step in Algorithm 5.1 focuses on the PDFs of filtered DNS data. The key idea is to assess the performance of models and verify if the proposed model maintains the true statistics. In this context, we present the scatter plots of $T_{ii}^{R,D}$ against $T_{ii}^{R,TF}$ in Figure 5.6 for three given filter widths and $i = 3$. We should note that the present results are confined to $i = 3$ due to the similarities in other directions. The slope in each plot is indicated by the corresponding correlation coefficients in Table 5.2. The most noticeable specific about these results is that the data points are bounded within a same order of magnitude on both axes. As a matter of fact, we achieve a roughly unit regression coefficient between $T_{ii}^{R,D}$ and $T_{ii}^{R,TF}$, where our optimization strategy targets for correct estimation of the SGS dissipation. This analysis can be extended to the PDF plots in Figure 5.7. With nearly the same correlation coefficients, the SMG model fails to reproduce the true statistics, while the optimum TFSGS model offers a great

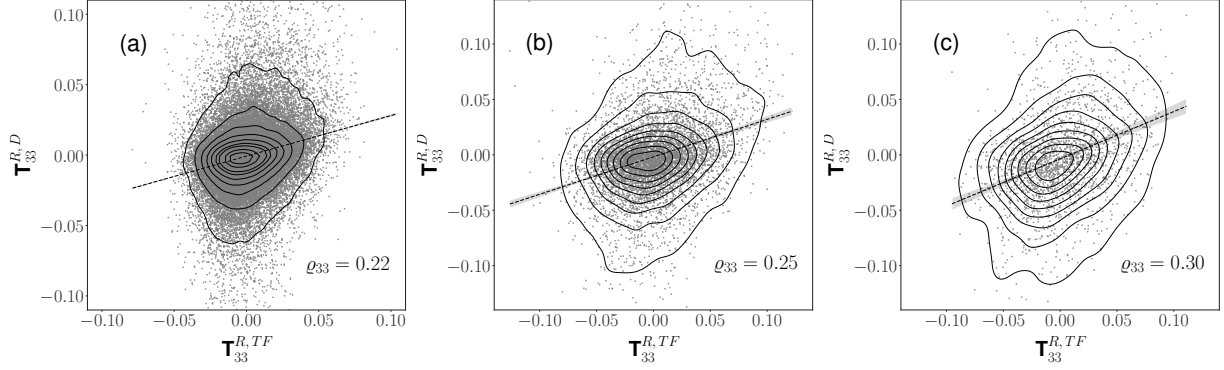


Figure 5.6: Scatter plots of the SGS stresses obtained by the filtered DNS data ($T_{33}^{R,D}$) versus the modeled stresses ($T_{33}^{R,TF}$) using optimized parameters in Table 5.3 for (a) $\mathcal{L}_\delta = 4$, (b) $\mathcal{L}_\delta = 8$, and (c) $\mathcal{L}_\delta = 12$.

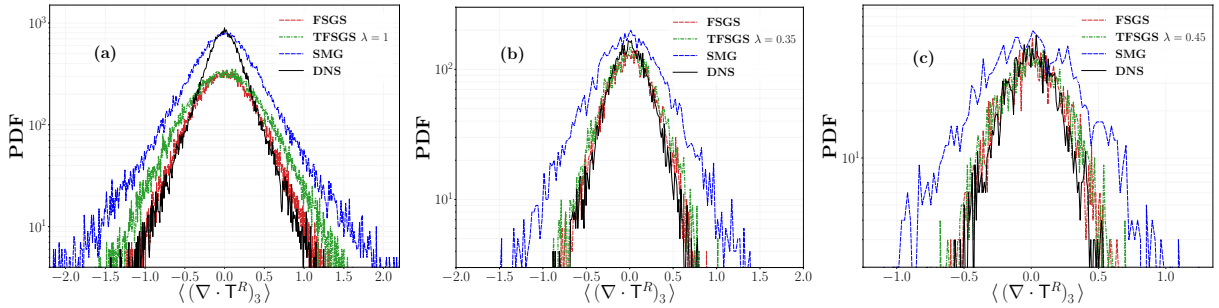


Figure 5.7: PDF of the ensemble-averaged $(\nabla \cdot \mathbf{T})_{i=3}$ for the optimized (tempered) fractional and the SMG models at (a) $\mathcal{L}_\delta = 4$, (b) $\mathcal{L}_\delta = 8$, and (c) $\mathcal{L}_\delta = 12$.

match with the true graphs. As pointed out previously, in $\mathcal{L}_\delta = 4$ the FSGS model represents the equivalent form of the TFSGS with $\alpha^{opt} = 0.76$ and $\lambda^{opt} \approx 0$.

From the understanding of energy cascading in turbulent flows, the SGS dissipation, ϵ , is considered as an external parameter in two-point structure equations for describing small-scale motions. In the statistical sense, we compare the PDFs of ϵ , implied by the models, with the true PDFs, obtained by the filtered DNS data for $\mathcal{L}_\delta = 4, 8, 12$. As shown in Figure 5.8, the fractional models accurately predict the forward scattering, associated with the positive dissipation, ϵ^+ , while the SMG model appears to be too dissipative due to its positive eddy viscosity. Furthermore, the TFSGS model presents an under-prediction of the backward scattering by producing a slim amount of negative dissipation, ϵ^- . On the side of numerical analysis, this limitation results in preserving numerical stability by minimizing negative dissipation error. In next section, we provide

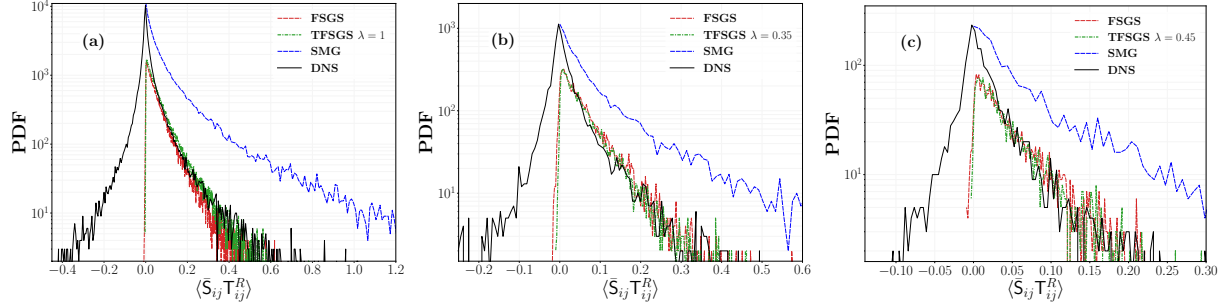


Figure 5.8: PDF of the ensemble-averaged SGS dissipation for the optimized (tempered) fractional and the SMG models at (a) $\mathcal{L}_\delta = 4$, (b) $\mathcal{L}_\delta = 8$, and (c) $\mathcal{L}_\delta = 12$.

an extensive discussion in terms of an *a posteriori* analysis.

5.6 A Posteriori Analysis

With a focus on numerical stability, we extend the statistical *a priori* assessments to an *a posteriori* analysis in order to evaluate the performance of proposed models in time. To outline the *a posteriori* framework, we employ the flow solver, described in section 5.5.1, on 40^3 and 20^3 grids for the corresponding $\mathcal{L}_\delta = 4, 8$, respectively. The simulations are initiated with an instantaneous flow field, given from the filtered DNS of the stationary HIT flow. This analysis also allows for structural comparisons between the fractional models with the filtered DNS data through the resolved turbulent kinetic energy, $\bar{K}_{tot}(t) = \langle \frac{\bar{V}_i \bar{V}_i}{2} \rangle_s$, and the enstrophy, $\bar{\mathcal{E}}(t) = \langle \frac{\bar{\omega}_i \bar{\omega}_i}{2} \rangle_s$, where $\bar{\omega}_i(t, x_i)$ denotes the i th component of the instantaneous filtered vorticity field. It should be noted that in this section $\langle \cdot \rangle_s$ denotes the spatial averaging over the entire domain.

Figure 5.9 displays the decay of kinetic energy in the subgrid-scale level, which verifies the computational stability for the fractional model. In most LES approaches, fidelity in representing spatial structures is essentially compromised to preserve numerical stability by inducing the excessive amount of energy dissipation. Nevertheless, the present results verify our findings in section 5.4 that the TFSGS model provides stable LES solutions while preserving high-order structure functions in the *a priori* tests. Comparing the results in Figure 5.9, the fractional model also exhibits an acceptable performance in predicting the time-evolution of kinetic energy after one or two eddy turn-over times, $\tau_{\mathcal{L}}$, for both resolutions.

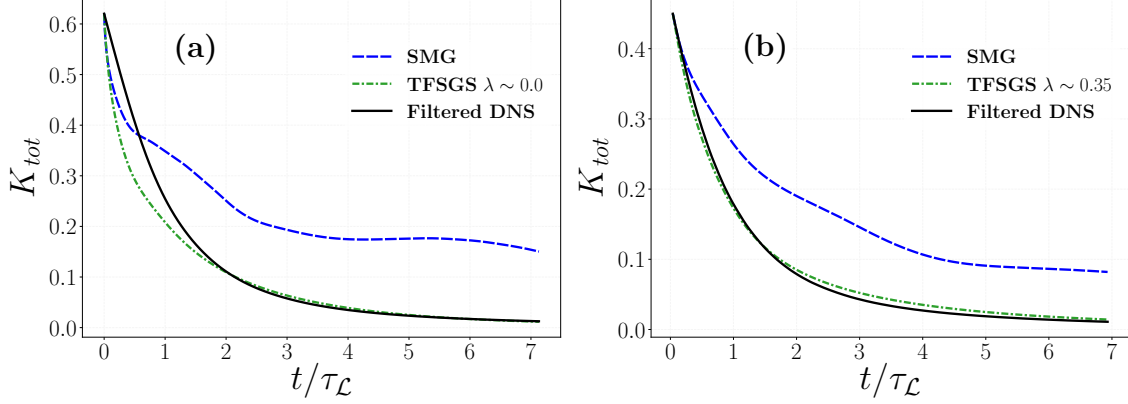


Figure 5.9: Decaying of the resolved turbulent kinetic energy, \bar{K}_{tot} , for the optimized TFSGS and the SMG models with (a) 40^3 and (b) 20^3 grid points.

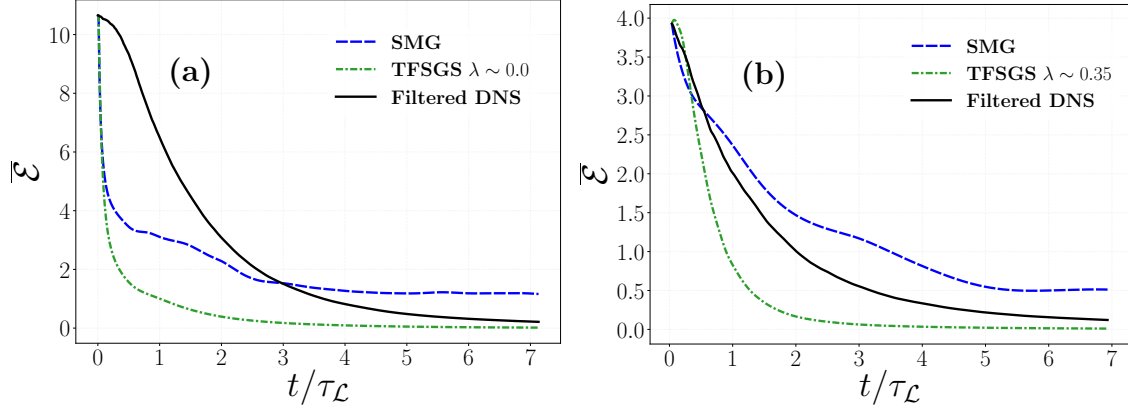


Figure 5.10: Time-evolution of the resolved enstrophy, $\bar{\mathcal{E}}$, for the optimized TFSGS and the SMG models with (a) 40^3 and (b) 20^3 grid points.

Given the analysis in section 5.4, third-order structure functions in (5.39) are connected to the third-order moment of filtered velocity derivatives and thereby the enstrophy balance as described in [76]. Interestingly, based on the analysis of two-point structures in subsection 5.5.1, the TFSGS model presents fulfilling the essential conditions in Algorithm 5.1 and accordingly, maintaining the equilibrium between the production and the dissipation of enstrophy at the resolved and the subgrid-scale levels. Figure 5.10 demonstrates performance of the LES models in estimating this equilibrium in time. It seems that enforcing a constant coefficient, $c_{\alpha,\lambda}$, into the LES solver causes the under-prediction of the enstrophy decaying rate in Figure 5.10. However, these results confirm numerical stability of the proposed models for both resolutions.

CHAPTER 6

SUMMARY AND FUTURE WORKS

The main objective of this study was to develop a robust mathematical framework for fractional modeling of anomalous phenomena, starting from the kinetic level. In the context of modeling scalar dispersion in underground waters, we developed a fast and accurate numerical method for the proposed fractional model and performed a comprehensive theoretical and numerical analysis, as the essential components of the framework. Inspired by the nonlocal triad interactions between large and small scale motions, we also extended the framework to turbulent flows by developing a SGS model using fractional operators. This framework offers the advantage of allowing us to develop more physically-consistent SGS models, which suitably capture the anomalous features of turbulent flows.

6.1 Concluding Remarks

- In **chapter 2**, we developed a new unified PG spectral method for a class of fractional partial differential equations with constant coefficients in a $(1+d)$ -dimensional *space-time* hypercube, $d = 1, 2, 3$, etc, subject to homogeneous Dirichlet initial/boundary conditions. We employed Jacobi *poly-fractonomials*, as temporal basis/test functions, and the Legendre polynomials as spatial basis/test functions, yielding spatial mass matrices being independent of the spatial fractional orders. Additionally, we formulated the novel unified fast linear solver for the resulting high-dimensional linear system, which reduces the computational cost significantly. In fact, the main idea of the study was to formulate a closed-form solution for the high-dimensional Lyapunov equation in terms of the eigensolutions up to the precision accuracy of computationally obtained eigensolutions. Moreover, we proved the corresponding well-posedness and discrete stability analysis. We obtained the theoretical error estimates, proving that the method converges spectrally fast under certain conditions. Finally, several numerical test cases, including finite regularity and smooth solutions, have been performed to show the

spectral accuracy of the method.

- In **chapter 3**, we developed a unified PG spectral method for fully distributed-order PDEs with constant coefficients on a $(1+d)$ -dimensional *space-time* hypercube, subject to homogeneous Dirichlet initial/boundary conditions. We obtained the weak formulation of the problem, and proved the well-posedness by defining the proper underlying *distributed Sobolev* spaces and the associated norms. We then formulated the numerical scheme, exploiting Jacobi *poly-fractonomials* as temporal basis/test functions, and Legendre polynomials as spatial basis/test functions. In order to improve efficiency of the proposed method in higher-dimensions, we constructed a unified fast linear solver employing certain properties of the stiffness/mass matrices, which significantly reduced the computation time. Moreover, we proved stability of the developed scheme and carried out the error analysis. Finally, via several numerical test cases, we examined the practical performance of proposed method and illustrated the spectral accuracy.
- More broadly, this study presented a new framework in **chapter 4** to the functional modeling of SGS stresses in the LES of turbulent flows, starting from the kinetic theory. Within the proposed framework, we began with modeling the filtered equilibrium distribution function as a key term to consider the power-law scaling of SGS motions in the filtered BTE. Due to the multi-exponential behavior of the filtered equilibrium distribution function, we proposed to approximate it with a Lévy-stable distribution, where the associated fractional parameter strictly relied on the filter width. Subsequently, we derived the filtered NS equations from the approximated filtered BTE, in which the divergence of SGS stresses was modeled via a fractional Laplacian operator, $(-\Delta)^\alpha(\cdot)$ for $\alpha \in (0, 1]$. In general, we established a framework, which permitted us to treat the source of turbulent motions at the kinetic level by employing a compatible choice of distribution function and derive the corresponding fractional operator in the filtered NS equations as an SGS model. Therefore, the proposed framework, termed “FSGS modeling”, could potentially recover the non-Gaussian statistics

of SGS motions precisely. Next, we studied the physical and mathematical properties of the proposed model and introduced a set of mild conditions to preserve the second law of thermodynamics. Eventually, we carried out *a priori* evaluations of the FSGS model based on the DNS database of forced and decaying HIT problems. In light of the analysis, there was a relatively great agreement between the modeled and true SGS values in terms of the correlation and regression coefficients. The performance of the FSGS model depended rigorously on the choice of fractional exponent, α , as a function of filter width, \mathcal{L} , and flow Reynolds number, Re_λ . We showed that, by enlarging \mathcal{L} , the heavy-tailed characteristics of the SGS motions could become more intensified, which were conceivably well-described by the FSGS model with smaller values of α . With all this in mind, FSGS model provided a new perspective, which respected the non-Gaussian behavior of SGS stresses by exploiting fractional calculus within the Boltzmann transport framework.

- Motivated by the semi-power-law behavior of energy cascading phenomenon in turbulent flows, we focus on developing a nonlocal model by employing a tempered heavy-tailed distribution within the described fractional framework in **chapter 5**. To approximate multi-exponential behaviors of the filtered equilibrium distribution in the collision operator, we employed a tempered Lévy-stable distribution function, which presents a power-law at a moderate range and then converges to an exponential decay. By ensemble-averaging of the approximated Boltzmann transport, we derived the LES equations, in which the divergence of SGS stresses emerged as a summation of tempered fractional Laplacian, $(\Delta + \lambda)^\alpha(\cdot)$, where $\alpha \in (0, 1)$ and $\lambda > 0$. Interestingly, the FSGS is found to be a particular form of the TFSGS model when λ approaches 0. Moreover, we formulated the SGS stresses straightforwardly in terms of a combination of integer and fractional operators, which gives the advantage of being feasible and quite easy to implement in the Fourier space. The corollary on frame invariant property of the FSGS model were also extended to the current model, showing its physical and mathematical consistency. In a statistical framework, we constructed a structure based algorithm for optimizing the fractional models, which involved the closed essential conditions

for a weaker sense of an ideal LES model. Following the optimization strategy, we inferred the optimum tempering parameter through a comparative study of two-point strain-stress correlation functions while the fractional exponent was fixed for maintaining reasonable values of correlation coefficients. Regarding the KH equation, the optimum TFSGS model presented a great match with the true values of two-point velocity-stress correlation functions, which ensures the accurate prediction of third-order structure functions. The success of tempering mechanism in capturing structure correlation functions, particularly at larger \mathcal{L}_δ , originated from the capabilities of our choice in fitting semi-heavy-tailed behavior of the filtered equilibrium distribution at the kinetic level. The inspection of statistical results also supported accuracy of the fractional model in keeping unit regression and capturing the corresponding PDF tails. As a notion of numerical stability, we demonstrated that the optimized TFSGS model well-predicted the true forward scattering in a statistical sense without generating any significant negative dissipation. Lastly, the TFSGS model underwent the ultimate *a posteriori* analysis, which verified numerically stable performance of the fractional model through tracking turbulent kinetic energy

6.2 Future Works

Despite the theoretical and statistical achievements, we believe that this framework, as a viable and promising direction toward nonlocal modelings, can be upgraded for the purpose of studying more complex turbulent regimes. On the theoretical side, the current framework deserves a careful mathematical attention to be extended to anisotropic and inhomogeneous flows employing proper forms of distributions at the kinetic level. Moreover, further works should be undertaken to generalize the fractional model to a data-driven representation of spatial and temporal structures in more complex turbulent regimes.

APPENDICES

APPENDIX A

DERIVATIONS IN CHAPTER 2

Here, we provide the force function based on the exact solutions.

A.1 Force term of test case (I)

Let take the exact solution as

$$u^{exact} = t^{p_1} \times \left((1+x)^{p_2} - \epsilon (1+x)^{p_3} \right), \quad (\text{A.1})$$

where $t \in [0, 2]$ and $x \in [-1, 1]$. To obtain f in (2.14) based on (A.1), first we need to calculate all fractional derivatives of u^{ext} . To satisfy the corresponding boundary conditions, $\epsilon_i = 2^{p_{2i}-p_{2i+1}}$. Take $X^T = t^{p_1}$ and $X_i^S = (1 + \zeta_i)^{p_{2i}} - \epsilon_i (1 + \zeta_i)^{p_{2i+1}}$, where $\zeta_i = 2^{\frac{x_i-a_i}{b_i-a_i}} - 1$ and $\zeta_i \in [-1, 1]$.

Considering (2.2),

$${}_0\mathcal{D}_t^{2\tau} X^T = \frac{\Gamma[p_1+1]}{\Gamma[p_1+1-2\tau]} t^{p_1-2\tau} = \left(\frac{T}{2}\right)^{p_1-2\tau} \frac{\Gamma[p_1+1]}{\Gamma[p_1+1-2\tau]} (1 + \eta(t))^{p_1-2\tau}, \quad (\text{A.2})$$

where $\eta(t) = 2\left(\frac{t}{T}\right) - 1$. Similarly,

$$\begin{aligned} {}_{a_i}\mathcal{D}_{x_i}^{2\mu_i} X_i^S &= \left(\frac{b_i-a_i}{2}\right)^{-2\mu_i} \left[\frac{\Gamma[p_{2i}+1]}{\Gamma[p_{2i}+1-2\mu_i]} (1 + \zeta_{2i}(x_i))^{p_{2i}-2\mu_i} - \right. \\ &\quad \left. \epsilon_i \frac{\Gamma[p_{2i+1}+1]}{\Gamma[p_{2i+1}+1-2\mu_i]} (1 + \zeta_{2i}(x_i))^{p_{2i+1}-2\mu_i} \right], \end{aligned} \quad (\text{A.3})$$

and

$$\begin{aligned} {}_{a_i}\mathcal{D}_{x_i}^{2\nu_i} X_i^S &= \left(\frac{b_i-a_i}{2}\right)^{-2\nu_i-2} \left[\frac{\Gamma[p_{2i}+1]}{\Gamma[p_{2i}+1-2\nu_i]} (1 + \zeta_{2i}(x_i))^{p_{2i}-2\nu_i} - \right. \\ &\quad \left. \epsilon_i \frac{\Gamma[p_{2i+1}+1]}{\Gamma[p_{2i+1}+1-2\nu_i]} (1 + \zeta_{2i}(x_i))^{p_{2i+1}-2\nu_i} \right]. \end{aligned} \quad (\text{A.4})$$

Therefore,

$$\begin{aligned}
f = & \left(\frac{T}{2} \right)^{p_1-2\tau} \frac{\Gamma[p_1+1]}{\Gamma[p_1+1-2\tau]} (1+\eta)^{p_1-2\tau} \prod_{i=1}^d (1+\zeta_i)^{p_{2i}} - \epsilon_i (1+\zeta_i)^{p_{2i+1}} \\
& + \sum_{i=1} \left(\frac{T}{2} \right)^{p_1} (1+\eta)^{p_1} \left(c_{l_i} \left(\frac{b_i-a_i}{2} \right)^{-2\mu_i} \left[\frac{\Gamma[p_{2i}+1]}{\Gamma[p_{2i}+1-2\mu_i]} (1+\zeta_{2i})^{p_{2i}-2\mu_i} \right. \right. \right. \\
& - \left. \left. \left. \epsilon_i \frac{\Gamma[p_{2i+1}+1]}{\Gamma[p_{2i+1}+1-2\mu_i]} (1+\zeta_{2i})^{p_{2i+1}-2\mu_i} \right] \prod_{j=1, j \neq i}^d [(1+\zeta_j)^{p_{2j}} - \epsilon_j (1+\zeta_j)^{p_{2j+1}}] \right) \\
& - \sum_{i=1} \left(\frac{T}{2} \right)^{p_1} (1+\eta)^{p_1} \left(\kappa_{l_i} \left(\frac{b_i-a_i}{2} \right)^{-2\nu_i-2} \left[\frac{\Gamma[p_{2i}+1]}{\Gamma[p_{2i}+1-2\nu_i]} (1+\zeta_{2i})^{p_{2i}-2\nu_i} \right. \right. \\
& - \left. \left. \left. \epsilon_i \frac{\Gamma[p_{2i+1}+1]}{\Gamma[p_{2i+1}+1-2\nu_i]} (1+\zeta_{2i})^{p_{2i+1}-2\nu_i} \right] \prod_{j=1, j \neq i}^d [(1+\zeta_j)^{p_{2j}} - \epsilon_j (1+\zeta_j)^{p_{2j+1}}] \right). \quad (\text{A.5})
\end{aligned}$$

A.2 Force term of test case (II)

Take $X^T = t^{p_1}$ and $X^S = \sin(n\pi\zeta_1)$. Here, we approximate X^S as

$$X^S = \sum_{j=1}^{N_s} (-1)^{2j-1} \frac{(n\pi\zeta_1)^{2j-1}}{(2j-1)!}, \quad (\text{A.6})$$

where N_s controls the level of approximation error. Taking the same steps of (A.5), we obtain

$$\begin{aligned}
f = & \left(\frac{T}{2} \right)^{p_1-2\tau} \frac{\Gamma[p_1+1]}{\Gamma[p_1+1-2\tau]} (1+\eta)^{p_1-2\tau} \sum_{j=1}^{N_s} (-1)^{2j-1} \frac{(n\pi\zeta_1)^{2j-1}}{(2j-1)!} \\
& + \left(\frac{T}{2} \right)^{p_1} (1+\eta)^{p_1} \left[(c_{l_1}) \left(\frac{b_1-a_1}{2} \right)^{-2\mu_1} \sum_{j=1}^{N_s} (-1)^{2j-1} \frac{(n\pi\zeta_1)^{2j-1}}{(2j-1)!} \frac{\Gamma[2j]}{\Gamma[2j-2\mu_1]} \zeta^{2j-2\mu_1} \right. \\
& - \left. (c_{l_1}) \left(\frac{b_1-a_1}{2} \right)^{-2\nu_1-2} \sum_{j=1}^{N_s} (-1)^{2j-1} \frac{(n\pi\zeta_1)^{2j-1}}{(2j-1)!} \frac{\Gamma[2j]}{\Gamma[2j-2\nu_1]} \zeta^{2j-2\nu_1} \right]. \quad (\text{A.7})
\end{aligned}$$

A.3 Proof of Lemma 2.4.1

Proof. In Lemma 2.1 in [109] and also in [108], it is shown that $\|\cdot\|_{l_{H^\sigma}(\Lambda)}$ and $\|\cdot\|_{r_{H^\sigma}(\Lambda)}$ are equivalent. Therefore, for $u \in H^\sigma(\Lambda)$, there exist positive constants C_1 and C_2 such that

$$\begin{aligned}
\|u\|_{H^\sigma(\Lambda)} &\leq C_1 \|u\|_{l_{H^\sigma}(\Lambda)}, \\
\|u\|_{H^\sigma(\Lambda)} &\leq C_2 \|u\|_{r_{H^\sigma}(\Lambda)}, \quad (\text{A.8})
\end{aligned}$$

which leads to

$$\begin{aligned}
\|u\|_{H^\sigma(\Lambda)}^2 &\leq C_1^2 \|u\|_{l H^\sigma(\Lambda)}^2 + C_2^2 \|u\|_{r H^\sigma(\Lambda)}^2 \\
&= C_1^2 \|{}_a \mathcal{D}_x^\sigma(u)\|_{L^2(\Lambda)}^2 + C_2^2 \|{}_x \mathcal{D}_b^\sigma(u)\|_{L^2(\Lambda)}^2 + (C_1^2 + C_2^2) \|u\|_{L^2(\Lambda)}^2 \\
&\leq \tilde{C}_1 \|u\|_{c H^\sigma(\Lambda)}^2,
\end{aligned} \tag{A.9}$$

where \tilde{C}_1 is a positive constant. Similarly, we can show that

$$\|u\|_{c H^\sigma(\Lambda)}^2 \leq \tilde{C}_2 \|u\|_{H^\sigma(\Lambda)}, \tag{A.10}$$

where \tilde{C}_2 is a positive constant. This equivalency and (2.19) conclude the proof. \square

A.4 Proof of Lemma 2.4.4

Proof. Let $\Lambda_d = \prod_{i=1}^d (a_i, b_i)$. According to [70], we have ${}_a \mathcal{D}_{x_i}^{2\nu_i} u = {}_{a_i} \mathcal{D}_{x_i}^{\nu_i} ({}_{a_i} \mathcal{D}_{x_i}^{\nu_i} u)$ and ${}_{x_i} \mathcal{D}_{b_i}^{\nu_i} u = {}_{x_i} \mathcal{D}_{b_i}^{\nu_i} ({}_{x_i} \mathcal{D}_{b_i}^{\nu_i} u)$. Let $\bar{u} = {}_{a_i} \mathcal{D}_{x_i}^{\nu_i} u$. Then,

$$\begin{aligned}
({}_{a_i} \mathcal{D}_{x_i}^{2\nu_i} u, v)_{\Lambda_d} &= ({}_{a_i} \mathcal{D}_{x_i}^{\nu_i} \bar{u}, v)_{\Lambda_d} = \int_{\Lambda_d} \frac{1}{\Gamma(1-\nu_i)} \left[\frac{d}{dx_i} \int_{a_i}^{x_i} \frac{\bar{u}(s) ds}{(x_i-s)^{\nu_i}} \right] v d\Lambda_d \\
&= \int_{\Lambda_d} \left\{ \frac{v}{\Gamma(1-\nu_i)} \int_{a_i}^{x_i} \frac{\bar{u} ds}{(x_i-s)^{\nu_i}} \right\}_{x_i=a_i}^{b_i} d\Lambda_d \\
&\quad - \int_{\Lambda_d} \frac{1}{\Gamma(1-\nu_i)} \int_{a_i}^{x_i} \frac{\bar{u}(s) ds}{(x_i-s)^{\nu_i}} \frac{dv}{dx_i} d\Lambda_d,
\end{aligned} \tag{A.11}$$

where $\Lambda_d^i = \prod_{j=1, j \neq i}^d (a_j, b_j)$. Then, we have $\int_{\Lambda_d^i} \left\{ \frac{v}{\Gamma(1-\nu_i)} \int_{a_i}^{x_i} \frac{\bar{u} ds}{(x_i-s)^{\nu_i}} \right\}_{x_i=a_i}^{b_i} d\Lambda_d^i = 0$ due to the homogeneous boundary conditions. Therefore,

$$({}_{a_i} \mathcal{D}_{x_i}^{2\nu_i} u, v)_{\Lambda_d} = - \int_{\Lambda_d^i} \int_{a_i}^{b_i} \frac{1}{\Gamma(1-\nu_i)} \int_{a_i}^{x_i} \frac{\bar{u}(s) ds}{(x_i-s)^{\nu_i}} \frac{dv}{dx_i} dx_i d\Lambda_d^i. \tag{A.12}$$

Moreover, we find that

$$\begin{aligned}
\frac{d}{ds} \int_s^{b_i} \frac{v}{(x_i-s)^{\nu_i}} dx_i &= \frac{d}{ds} \left\{ \left\{ \frac{v (x_i-s)^{1-\nu_i}}{1-\nu_i} \right\}_{x_i=s}^{b_i} - \frac{1}{1-\nu_i} \int_s^{b_i} \frac{dv}{dx_i} (x_i-s)^{1-\nu_i} dx_i \right\} \\
&= - \frac{d}{ds} \frac{1}{1-\nu_i} \int_s^{b_i} \frac{dv}{dx_i} (x_i-s)^{1-\nu_i} dx_i = \int_s^{b_i} \frac{\frac{dv}{dx_i}}{(x_i-s)^{\nu_i}} dx_i.
\end{aligned} \tag{A.13}$$

Therefore, we get

$$({}_{a_i} \mathcal{D}_{x_i}^{\nu_i} \bar{u}, v)_{\Lambda_d} = - \int_{\Lambda_d} \frac{1}{\Gamma(1-\nu)_i} \bar{u}(s) \left(\frac{d}{ds} \int_s^{b_i} \frac{\nu}{(x_i - s)^{\nu_i}} dx_i \right) ds d\Lambda_d = (\bar{u}, {}_{x_i} \mathcal{D}_{b_i}^{\nu_i} v)_{\Lambda_d}.$$

□

A.5 Proof of Lemma 2.10.4

Proof. Let $i = 1, j = 2$, and $k = 3$. We have

$$\begin{aligned} & \|u - \Pi_{r_1, \mathcal{M}_1}^{\nu_1} \Pi_{r_2, \mathcal{M}_2}^{\nu_2} \Pi_{r_3, \mathcal{M}_3}^{\nu_3} u\|_{cH^{\nu_1}(I_1, L^2(\Lambda_3^1))} \\ &= \|u - \Pi_{r_1, \mathcal{M}_1}^{\nu_1} u + \Pi_{r_1, \mathcal{M}_1}^{\nu_1} u - \Pi_{r_1, \mathcal{M}_1}^{\nu_1} \Pi_{r_2, \mathcal{M}_2}^{\nu_2} u + \Pi_{r_1, \mathcal{M}_1}^{\nu_1} \Pi_{r_2, \mathcal{M}_2}^{\nu_2} u \\ &\quad - \Pi_{r_1, \mathcal{M}_1}^{\nu_1} \Pi_{r_2, \mathcal{M}_2}^{\nu_2} \Pi_{r_3, \mathcal{M}_3}^{\nu_3} u\|_{cH^{\nu_1}(I_1, L^2(\Lambda_3^1))} \\ &\leq \|u - \Pi_{r_1, \mathcal{M}_1}^{\nu_1} u\|_{cH^{\nu_1}(I_1, L^2(\Lambda_3^1))} + \|\Pi_{r_1, \mathcal{M}_1}^{\nu_1} u - \Pi_{r_1, \mathcal{M}_1}^{\nu_1} \Pi_{r_2, \mathcal{M}_2}^{\nu_2} u\|_{cH^{\nu_1}(I_1, L^2(\Lambda_3^1))} \\ &\quad + \|\Pi_{r_1, \mathcal{M}_1}^{\nu_1} \Pi_{r_2, \mathcal{M}_2}^{\nu_2} u - \Pi_{r_1, \mathcal{M}_1}^{\nu_1} \Pi_{r_2, \mathcal{M}_2}^{\nu_2} \Pi_{r_3, \mathcal{M}_3}^{\nu_3} u\|_{cH^{\nu_1}(I_1, L^2(\Lambda_3^1))}, \end{aligned} \tag{A.14}$$

where by Theorem 2.10.1

$$\|\Pi_{r_1, \mathcal{M}_1}^{\nu_1} u\|_{cH^{\nu_1}(I_1, L^2(\Lambda_3^1))} \leq \mathcal{M}_1^{\nu_1 - r_1} \|u\|_{H^{r_1}(I_1, L^2(\Lambda_3^1))}. \tag{A.15}$$

Furthermore,

$$\begin{aligned} & \|\Pi_{r_1, \mathcal{M}_1}^{\nu_1} u - \Pi_{r_1, \mathcal{M}_1}^{\nu_1} \Pi_{r_2, \mathcal{M}_2}^{\nu_2} u\|_{cH^{\nu_1}(I_1, L^2(\Lambda_3^1))} \\ &\leq \|(\Pi_{r_1, \mathcal{M}_1}^{\nu_1} - \mathcal{I})(u - \Pi_{r_2, \mathcal{M}_2}^{\nu_2} u)\|_{cH^{\nu_1}(I_1, L^2(\Lambda_3^1))} + \|u - \Pi_{r_2, \mathcal{M}_2}^{\nu_2} u\|_{cH^{\nu_1}(I_1, L^2(\Lambda_3^1))} \\ &\leq \mathcal{M}_1^{\nu_1 - r_1} \|u - \Pi_{r_2, \mathcal{M}_2}^{\nu_2} u\|_{H^{r_1}(I_1, L^2(\Lambda_3^1))} + \|u - \Pi_{r_2, \mathcal{M}_2}^{\nu_2} u\|_{cH^{\nu_1}(I_1, L^2(\Lambda_3^1))} \\ &\leq \mathcal{M}_1^{\nu_1 - r_1} \mathcal{M}_2^{-r_2} \|u\|_{H^{r_1, r_2}(\Lambda_2, L^2(I_3))} + \mathcal{M}_2^{-r_2} \|u\|_{H^{\nu_1}(I_1, H^{r_2}(I_2, L^2(I_3)))}. \end{aligned} \tag{A.16}$$

Similarly,

$$\begin{aligned}
& \|\Pi_{r_1, \mathcal{M}_1}^{\nu_1} \Pi_{r_2, \mathcal{M}_2}^{\nu_2} u - \Pi_{r_1, \mathcal{M}_1}^{\nu_1} \Pi_{r_2, \mathcal{M}_2}^{\nu_2} \Pi_{r_3, \mathcal{M}_3}^{\nu_3} u\|_{cH^{\nu_1}(I_1, L^2(\Lambda_3^1))} \\
&= \|\Pi_{r_1, \mathcal{M}_1}^{\nu_1} \Pi_{r_2, \mathcal{M}_2}^{\nu_2} u - \Pi_{r_1, \mathcal{M}_1}^{\nu_1} \Pi_{r_2, \mathcal{M}_2}^{\nu_2} \Pi_{r_3, \mathcal{M}_3}^{\nu_3} u - \Pi_{r_2, \mathcal{M}_2}^{\nu_2} u + \Pi_{r_2, \mathcal{M}_2}^{\nu_2} \Pi_{r_3, \mathcal{M}_3}^{\nu_3} u \\
&\quad + \Pi_{r_2, \mathcal{M}_2}^{\nu_2} u - \Pi_{r_2, \mathcal{M}_2}^{\nu_2} \Pi_{r_3, \mathcal{M}_3}^{\nu_3} u\|_{cH^{\nu_1}(I_1, L^2(\Lambda_3^1))} \\
&\leq \|(\Pi_{r_1, \mathcal{M}_1}^{\nu_1} - \mathcal{I})(\Pi_{r_2, \mathcal{M}_2}^{\nu_2} u - \Pi_{r_2, \mathcal{M}_2}^{\nu_2} \Pi_{r_3, \mathcal{M}_3}^{\nu_3} u)\|_{cH^{\nu_1}(I_1, L^2(\Lambda_3^1))} \\
&\quad + \|\Pi_{r_2, \mathcal{M}_2}^{\nu_2} u - \Pi_{r_2, \mathcal{M}_2}^{\nu_2} \Pi_{r_3, \mathcal{M}_3}^{\nu_3} u\|_{cH^{\nu_1}(I_1, L^2(\Lambda_3^1))} \\
&\leq \mathcal{M}_1^{\nu_1-r_1} (\|(\Pi_{r_2, \mathcal{M}_2}^{\nu_2} - \mathcal{I})(u - \Pi_{r_3, \mathcal{M}_3}^{\nu_3} u)\|_{H^{r_1}(I_1, L^2(\Lambda_3^1))} + \|u - \Pi_{r_3, \mathcal{M}_3}^{\nu_3} u\|_{H^{r_1}(I_1, L^2(\Lambda_3^1))}) \\
&\quad + \|(\Pi_{r_2, \mathcal{M}_2}^{\nu_2} - \mathcal{I})(u - \Pi_{r_3, \mathcal{M}_3}^{\nu_3} u)\|_{cH^{\nu_1}(I_1, L^2(\Lambda_3^1))} + \|u - \Pi_{r_3, \mathcal{M}_3}^{\nu_3} u\|_{cH^{\nu_1}(I_1, L^2(\Lambda_3^1))} \\
&\leq \mathcal{M}_1^{\nu_1-r_1} \mathcal{M}_2^{-r_2} \|u - \Pi_{r_3, \mathcal{M}_3}^{\nu_3} u\|_{H^{r_1, r_2}(\Lambda_2, L^2(I_3)))} + \mathcal{M}_1^{\nu_1-r_1} \mathcal{M}_3^{-r_3} \|u\|_{H^{r_1, r_3}(\Lambda_3^2, L^2(I_2)))} \\
&\quad + \mathcal{M}_2^{-r_2} \|u - \Pi_{r_3, \mathcal{M}_3}^{\nu_3} u\|_{cH^{\nu_1}(I_1, H^{r_2}(I_2, L^2(I_3)))} + \mathcal{M}_3^{-r_3} \|u\|_{cH^{\nu_1}(I_1, H^{r_3}(I_3, L^2(I_2)))} \\
&\leq \mathcal{M}_1^{\nu_1-r_1} \mathcal{M}_2^{-r_2} \mathcal{M}_3^{-r_3} \|u\|_{H^{r_1, r_2, r_3}(\Lambda_3))} + \mathcal{M}_1^{\nu_1-r_1} \mathcal{M}_3^{-r_3} \|u\|_{H^{r_1, r_3}(\Lambda_3^2, L^2(I_2)))} \\
&\quad + \mathcal{M}_2^{-r_2} \mathcal{M}_3^{-r_3} \|u\|_{cH^{\nu_1}(I_1, H^{r_2, r_3}(\Lambda_3^1))} + \mathcal{M}_3^{-r_3} \|u\|_{cH^{\nu_1}(I_1, H^{r_3}(I_3, L^2(I_2)))}. \tag{A.17}
\end{aligned}$$

Therefore,

$$\begin{aligned}
& \|u - \Pi_{r_1, \mathcal{M}_1}^{\nu_1} \Pi_{r_2, \mathcal{M}_2}^{\nu_2} \Pi_{r_3, \mathcal{M}_3}^{\nu_3} u\|_{cH^{\nu_1}(I_1, L^2(\Lambda_3^1))} \\
&\leq \mathcal{M}_1^{\nu_1-r_1} \|u\|_{H^{r_1}(I_1, L^2(\Lambda_3^1))} + \mathcal{M}_1^{\nu_1-r_1} \mathcal{M}_2^{-r_2} \|u\|_{H^{r_1, r_2}(\Lambda_2, L^2(I_3)))} \\
&\quad + \mathcal{M}_2^{-r_2} \|u\|_{cH^{\nu_1}(I_1, H^{r_2}(I_2, L^2(I_3)))} + \mathcal{M}_1^{\nu_1-r_1} \mathcal{M}_2^{-r_2} \mathcal{M}_3^{-r_3} \|u\|_{H^{r_1, r_2, r_3}(\Lambda_3))} \\
&\quad + \mathcal{M}_1^{\nu_1-r_1} \mathcal{M}_3^{-r_3} \|u\|_{H^{r_1, r_3}(\Lambda_3^2, L^2(I_2)))} + \mathcal{M}_2^{-r_2} \mathcal{M}_3^{-r_3} \|u\|_{cH^{\nu_1}(I_1, H^{r_2, r_3}(\Lambda_3^1))} \\
&\quad + \mathcal{M}_3^{-r_3} \|u\|_{cH^{\nu_1}(I_1, H^{r_3}(I_3, L^2(I_2)))}. \tag{A.18}
\end{aligned}$$

Following the same steps, we get

$$\begin{aligned}
& \|u - \Pi_{r_1, \mathcal{M}_1}^{\nu_1} \Pi_{r_2, \mathcal{M}_2}^{\nu_2} \Pi_{r_3, \mathcal{M}_3}^{\nu_3} u\|_{cH^{\nu_2}(I_2, L^2(\Lambda_3^2))} \\
&\leq \mathcal{M}_2^{\nu_2-r_2} \|u\|_{H^{r_2}(I_2, L^2(\Lambda_3^2))} + \mathcal{M}_2^{\nu_2-r_2} \mathcal{M}_1^{-r_1} \|u\|_{H^{r_2, r_1}(\Lambda_2, L^2(I_3)))} \\
&\quad + \mathcal{M}_1^{-r_1} \|u\|_{cH^{\nu_2}(I_2, H^{r_1}(I_1, L^2(I_3)))} + \mathcal{M}_2^{\nu_2-r_2} \mathcal{M}_1^{-r_1} \mathcal{M}_3^{-r_3} \|u\|_{H^{r_2, r_1, r_3}(\Lambda_3))} \\
&\quad + \mathcal{M}_2^{\nu_2-r_2} \mathcal{M}_3^{-r_3} \|u\|_{H^{r_2, r_3}(\Lambda_3^1, L^2(I_1)))} + \mathcal{M}_2^{-r_1} \mathcal{M}_3^{-r_3} \|u\|_{cH^{\nu_2}(I_2, H^{r_1, r_3}(\Lambda_3^2))} \\
&\quad + \mathcal{M}_3^{-r_3} \|u\|_{cH^{\nu_2}(I_2, H^{r_3}(I_3, L^2(I_1)))} \tag{A.19}
\end{aligned}$$

and

$$\begin{aligned}
& \|u - \Pi_{r_1, \mathcal{M}_1}^{\nu_1} \Pi_{r_2, \mathcal{M}_2}^{\nu_2} \Pi_{r_3, \mathcal{M}_3}^{\nu_3} u\|_{cH^{\nu_3}(I_3, L^2(\Lambda_2))} \\
& \leq \mathcal{M}_3^{\nu_3 - r_3} \|u\|_{H^{r_3}(I_3, L^2(\Lambda_2))} + \mathcal{M}_3^{\nu_3 - r_3} \mathcal{M}_1^{-r_1} \|u\|_{H^{r_3, r_1}(\Lambda_3^2, L^2(I_2)))} \\
& \quad + \mathcal{M}_1^{-r_1} \|u\|_{cH^{\nu_3}(I_3, H^{r_1}(I_1, L^2(I_2)))} + \mathcal{M}_3^{\nu_3 - r_3} \mathcal{M}_1^{-r_1} \mathcal{M}_2^{-r_2} \|u\|_{H^{r_3, r_1, r_2}(\Lambda_3))} \\
& \quad + \mathcal{M}_3^{\nu_3 - r_3} \mathcal{M}_2^{-r_2} \|u\|_{H^{r_3, r_2}(\Lambda_3^1, L^2(I_1))} + \mathcal{M}_1^{-r_1} \mathcal{M}_2^{-r_2} \|u\|_{cH^{\nu_3}(I_3, H^{r_1, r_2}(\Lambda_2))} \\
& \quad + \mathcal{M}_2^{-r_2} \|u\|_{cH^{\nu_3}(I_3, H^{r_2}(I_2, L^2(I_1)))}. \tag{A.20}
\end{aligned}$$

□

APPENDIX B

DERIVATIONS IN CHAPTER 3

B.1 Entries of Spatial Stiffness Matrix

Here, we provide the computation of entries of the spatial stiffness matrix by performing an affine mapping ϑ from the standard domain $\mu_j^{stn} \in [-1, 1]$ to $\mu_j \in [\mu_j^{\max}, \mu_j^{\min}]$.

Lemma B.1.1. *The total spatial stiffness matrix S_j^{Tot} is symmetric and its entries can be exactly computed as:*

$$S_j^{Tot} = c_{l_j} \times S_l^{\varrho j} + c_{r_j} \times S_r^{\varrho j} - \kappa_{l_j} \times S_l^{\varrho j} - \kappa_{r_j} \times S_r^{\varrho j}, \quad (\text{B.1})$$

where $j = 1, 2, \dots, d$.

Proof. Regarding the definition of stiffness matrix, we have

$$\begin{aligned} \{S_l^{\varrho j}\}_{r,n} &= \int_{-1}^1 \int_{\mu_j^{\min}}^{\mu_j^{\max}} \varrho_j(\mu_j) {}_{-1}\mathcal{D}_{\xi_j}^{\mu_j} (\phi_n(x_j)) {}_{\xi_j} \mathcal{D}_1^{\mu_j} (\Phi_r(x_j)) dx_j, \\ &= \beta_1 \int_{-1}^1 \int_{-1}^1 \varrho_j(\vartheta(\mu_j^{stn})) {}_{-1}\mathcal{D}_{\xi_j}^{\mu_j^{stn}} (P_{n+1}(\xi_j) - P_{n-1}(\xi_j)) \\ &\quad \times {}_{\xi_j} \mathcal{D}_1^{\mu_j^{stn}} (P_{k+1}(\xi_j) - P_{k-1}(\xi_j)) d\xi_j, \\ &= \beta_1 \left[\tilde{S}_{r+1,n+1}^{\varrho j} - \tilde{S}_{r+1,n-1}^{\varrho j} - \tilde{S}_{r-1,n+1}^{\varrho j} + \tilde{S}_{r-1,n-1}^{\varrho j} \right], \end{aligned} \quad (\text{B.2})$$

where $\beta_1 = \tilde{\sigma}_r \sigma_n \left(\frac{\mu_j^{\max} - \mu_j^{\min}}{2} \right)$ and

$$\begin{aligned} \tilde{S}_{r,n}^{\varrho j} &= \int_{-1}^1 \int_{-1}^1 \varrho_j(\vartheta(\mu_j^{stn})) {}_{-1}\mathcal{D}_{\xi_j}^{\mu_j^{stn}} (P_n(\xi_j)) {}_{\xi_j} \mathcal{D}_1^{\mu_j^{stn}} (P_r(\xi_j)) d\xi_j d\mu_j^{stn} \\ &= \int_{-1}^1 \varrho_j(\vartheta(\mu_j^{stn})) \frac{\Gamma(r+1)}{\Gamma(r - \mu_j^{stn} + 1)} \frac{\Gamma(n+1)}{\Gamma(n - \mu_j^{stn} + 1)} \\ &\quad \times \int_{-1}^1 (1 - \xi_j^2)^{-\mu_j^{stn}} P_r^{-\mu_j^{stn}, \mu_j^{stn}} P_n^{\mu_j^{stn}, -\mu_j^{stn}} d\xi_j d\mu_j^{stn}. \end{aligned}$$

$\tilde{S}_{r,n}^{\varrho_j}$ can be computed accurately using Gauss-Legendre (GL) quadrature rules as

$$\begin{aligned}\tilde{S}_{r,n}^{\varrho_j} &= \sum_{q=1}^Q \frac{\Gamma(r+1)}{\Gamma(r-\mu_j^{stn}|_q+1)} \frac{\Gamma(n+1)}{\Gamma(n-\mu_j^{stn}|_q+1)} \varrho_j|_q w_q \times \\ &\quad \int_{-1}^1 (1-\xi_j^2)^{-\mu_j^{stn}|_q} P_r^{-\mu_j^{stn}|_q, \mu_j^{stn}|_q}(\xi_j) P_n^{\mu_j^{stn}|_q, -\mu_j^{stn}|_q}(\xi_j) d\xi_j, \end{aligned}\quad (\text{B.3})$$

in which $Q \geq M_j + 2$ represents the minimum number of GL quadrature points $\{\mu_j^{stn}|_q\}_{q=1}^Q$ for exact quadrature, and $\{w_q\}_{q=1}^Q$ are the corresponding quadrature weights. Exploiting the property of the Jacobi polynomials where $P_n^{\alpha, \beta}(-\xi_j) = (-1)^n P_n^{\beta, \alpha}(\xi_j)$, we have $\tilde{S}_{r,n}^{\varrho_j} = (-1)^{(r+n)} \tilde{S}_{n,r}^{\varrho_j}$. Following chapter 2, $\tilde{\sigma}_r$ and σ_n are chosen such that $(-1)^{(n+r)}$ is canceled. Accordingly, $\{S_l^{\varrho_j}\}_{n,r} = \{S_l^{\varrho_j}\}_{r,n} = \{S_r^{\varrho_j}\}_{r,n} = \{S_r^{\varrho_j}\}_{r,n}$ due to the symmetry of $S_l^{\varrho_j}$ and $S_r^{\varrho_j}$. Similarly, we get $\{S_l^{\varrho_j}\}_{n,r} = \{S_l^{\varrho_j}\}_{r,n} = \{S_r^{\varrho_j}\}_{n,r} = \{S_r^{\varrho_j}\}_{r,n}$. Eventually, we conclude that the stiffness matrix $S_l^{\varrho_j}, S_r^{\varrho_j}, S_l^{\rho_j}, S_r^{\rho_j}$, and thereby $\{S_j^{Tot}\}_{n,r}$ as the sum of symmetric matrices is symmetric. \square

APPENDIX C

DERIVATIONS IN CHAPTER 4

In this chapter, we follow the derivations of fractional NS equations in [163] to evaluate the shear and SGS stresses in (4.36) and (4.37).

C.1 Temporal Shift

Recalling from the Assumption 5 that $s \sim O(1)$, we take the temporal Taylor expansion of f^* as follows:

$$\begin{aligned} f_{s,s}^* = f^*(\bar{\Delta}(t - s\tau, \mathbf{x} - s\tau\mathbf{u}, \mathbf{u})) &= f_s^*(\bar{\Delta}) + \frac{\partial f_s^*}{\partial \bar{\Delta}} \frac{\partial \bar{\Delta}}{\partial t} \delta t + O(\delta t^2) \\ &= f_s^*(\bar{\Delta}) + \frac{\partial f_s^*}{\partial \bar{\Delta}} \frac{\partial \bar{\Delta}}{\partial t} (-s\tau) + O(\tau^2), \end{aligned} \quad (\text{C.1})$$

where $f_s^*(\bar{\Delta}) = f^*(\bar{\Delta}(t, \mathbf{x} - s\tau\mathbf{u}, \mathbf{u}))$, $\delta t = -s\tau$ and

$$\frac{\partial \bar{\Delta}}{\partial t} = \frac{-2}{U^2} \sum_{k=1}^3 (u_k - \bar{V}_k) \frac{\partial \bar{V}_k}{\partial t}. \quad (\text{C.2})$$

Considering (C.1), we can approximate (4.29) according to

$$\begin{aligned} \varsigma_{ij} &\approx \int_0^\infty e^{-s} \int_{\mathbb{R}^d} (u_i - \bar{V}_i)(u_j - \bar{V}_j) \left(f_s^*(\bar{\Delta}) + \frac{\partial f_s^*}{\partial \bar{\Delta}} \frac{\partial \bar{\Delta}}{\partial t} (s\tau) \right) d\mathbf{u} ds, \\ &= \int_0^\infty e^{-s} \int_{\mathbb{R}^d} (u_i - \bar{V}_i)(u_j - \bar{V}_j) \left[f_s^*(\bar{\Delta}) + \frac{2}{U^2} \frac{\partial f_s^*}{\partial \bar{\Delta}} \left(\sum_{k=1}^3 (u_k - \bar{V}_k) \frac{\partial \bar{V}_k}{\partial t} \right) (s\tau) \right] d\mathbf{u} ds. \end{aligned} \quad (\text{C.3})$$

Since $\bar{\Delta}$ is an even function of $(u_k - \bar{V}_k)$ for $k = 1, \dots, 3$, $f^{eq}(\bar{\Delta})$ and $f^{Model}(\bar{\Delta})$ and also their corresponding first derivatives $\frac{\partial f_s^{eq}}{\partial \bar{\Delta}}$ and $\frac{\partial f_s^{Model}}{\partial \bar{\Delta}}$ are even functions of $(u_k - \bar{V}_k)$. Subsequently, there is an odd power of either $(u_i - \bar{V}_i)$ or $(u_j - \bar{V}_j)$, which makes

$$\int_{\mathbb{R}^d} (u_i - \bar{V}_i)(u_j - \bar{V}_j) \left[\frac{\partial f_s^*}{\partial \bar{\Delta}} \left(\sum_{k=1}^3 (u_k - \bar{V}_k) \frac{\partial \bar{V}_k}{\partial t} \right) (s\tau) \right] d\mathbf{u} = 0.$$

Therefore,

$$\begin{aligned} \varsigma_{ij} &\approx \int_0^\infty e^{-s} \int_{\mathbb{R}^d} (u_i - \bar{V}_i)(u_j - \bar{V}_j) f_s^*(\bar{\Delta}) d\mathbf{u} ds \\ &= \int_{\mathbb{R}^d} \int_0^\infty e^{-s} (u_i - \bar{V}_i)(u_j - \bar{V}_j) f_s^*(\bar{\Delta}) ds d\mathbf{u}. \end{aligned} \quad (\text{C.4})$$

C.2 Shear Stresses

Regarding (4.34), the shear stress tensors are described according to

$$\mathcal{T}_{ij}^{Shear} = \int_0^\infty \int_{\mathbb{R}^d} (u_i - \bar{V}_i)(u_j - \bar{V}_j)(f_s^{eq}(\bar{\Delta}) - f^{eq}(\bar{\Delta}))e^{-s} d\mathbf{u} ds,$$

in which $f_s^{eq}(\bar{\Delta}) = f^{eq}(\bar{\Delta}(t, \mathbf{x} - s\tau\mathbf{u}, \mathbf{u}))$. The spatial shift $\delta x = s\tau|\mathbf{u}|$ can be decomposed into small $\delta x \leq l$ and large $\delta x > l$ displacements, which are associated with $\bar{\Delta} \leq 1$ and $\bar{\Delta} > 1$, respectively. Therefore,

$$\begin{aligned} \mathcal{T}_{ij}^{Shear} &= \int_0^\infty \int_{\delta x \leq l} (u_i - \bar{V}_i)(u_j - \bar{V}_j)(f_s^{eq}(\bar{\Delta}) - f^{eq}(\bar{\Delta}))e^{-s} d\mathbf{u} ds \\ &\quad + \int_0^\infty \int_{\delta x > l} (u_i - \bar{V}_i)(u_j - \bar{V}_j)(f_s^{eq}(\bar{\Delta}) - f^{eq}(\bar{\Delta}))e^{-s} d\mathbf{u} ds. \end{aligned} \quad (\text{C.5})$$

Since $f^{eq}(\bar{\Delta})$ belongs to C^∞ , which denotes the space of infinitely differentiable functions, we can perform the local linear approximation of $f_s^{eq}(\bar{\Delta})$, which yields in

$$f_s^{eq}(\bar{\Delta}) \approx f^{eq}(\bar{\Delta}) + \frac{\partial f^{eq}}{\partial \bar{\Delta}}(\bar{\Delta}_s - \bar{\Delta}), \quad (\text{C.6})$$

where $\frac{\partial f^{eq}}{\partial \bar{\Delta}} = -\frac{\rho}{2U^3} e^{-\bar{\Delta}/2}$ and $\bar{\Delta}_s = \bar{\Delta}(t, \mathbf{x} - s\tau\mathbf{u}, \mathbf{u})$. Due to the exponential behavior of $f_s^{eq}(\bar{\Delta}) - f^{eq}(\bar{\Delta})$, we obtain

$$\int_0^\infty \int_{\delta x > l} (u_i - \bar{V}_i)(u_j - \bar{V}_j)(f_s^{eq}(\bar{\Delta}) - f^{eq}(\bar{\Delta}))e^{-s} d\mathbf{u} ds \approx 0 \quad (\text{C.7})$$

and thereby

$$\mathcal{T}_{ij}^{Shear} \approx \int_0^\infty \int_{\delta x \leq l} (u_i - \bar{V}_i)(u_j - \bar{V}_j)(f_s^{eq}(\bar{\Delta}) - f^{eq}(\bar{\Delta}))e^{-s} d\mathbf{u} ds. \quad (\text{C.8})$$

Moreover, it is permissible to use the Taylor expansion of $\bar{\Delta}_s$ for $\delta x \leq l$, which is formulated as

$$\bar{\Delta}_s = \bar{\Delta} + \frac{\partial \bar{\Delta}}{\partial x_k} \delta x_k + \mathcal{O}(|\delta x|^2),$$

where

$$\frac{\partial \bar{\Delta}}{\partial x_k} = \frac{-2}{U^2} \sum_{m=1}^3 (u_m - \bar{V}_m) \frac{\partial \bar{V}_m}{\partial x_k}. \quad (\text{C.9})$$

Therefore,

$$\begin{aligned} f_s^{eq} = f^{eq}(\bar{\Delta}(t, \mathbf{x} - s\tau\mathbf{u}, \mathbf{u})) &= f^{eq}(\bar{\Delta}) + \frac{\partial f^{eq}}{\partial \bar{\Delta}} \frac{\partial \bar{\Delta}}{\partial x_k} \delta x_k + O(|\delta x|^2) \\ &= f^{eq}(\bar{\Delta}) + \frac{\partial f^{eq}}{\partial \bar{\Delta}} \frac{\partial \bar{\Delta}}{\partial x_k} (-s\tau u_k) + O((s\tau|\mathbf{u}|)^2). \end{aligned} \quad (\text{C.10})$$

Plugging (C.10) and (C.9) into (4.34), we attain

$$\begin{aligned} \mathcal{T}_{ij}^{Shear} &\approx - \int_0^\infty \int_{\delta x \leq l} (u_i - \bar{V}_i)(u_j - \bar{V}_j) \left(\frac{\partial f^{eq}}{\partial \bar{\Delta}} \frac{\partial \bar{\Delta}}{\partial x_k} (s\tau u_k) \right) e^{-s} d\mathbf{u} ds \\ &= - \frac{2\rho}{U^5} \int_0^\infty \int_{\delta x \leq l} (u_i - \bar{V}_i)(u_j - \bar{V}_j) \left(e^{-\Delta} \sum_{m=1}^3 (u_m - \bar{V}_m) \frac{\partial \bar{V}_m}{\partial x_k} \right) (s\tau u_k) e^{-s} d\mathbf{u} ds. \end{aligned}$$

We should note that the limits of integral in (C.11) can be extended to \mathbb{R}^3 due to (C.7). Following every steps in the derivation of shear stresses from (4.33) to (4.36) in [163], we can formulate $\mathcal{T}_{ij}^{Shear} = \mu \left(\frac{\partial \bar{V}_i}{\partial x_j} + \frac{\partial \bar{V}_j}{\partial x_i} \right)$ in (4.36) from (C.11), in which we obtain $\mu = \frac{-2\rho\tau}{U^5} \int_0^\infty I_0 s e^{-s} ds = \rho U^2 \tau$ and $I_0 = \frac{4\pi}{15} \int_0^\infty r^6 e^{-\Delta} dr$, where $\Delta = \frac{r^2}{U^2}$ and $r = |\mathbf{u} - \bar{\mathbf{V}}|$.

C.3 SGS Stresses

The SGS stresses are given by

$$\mathcal{T}_{ij}^R = \int_0^\infty \int_{\mathbb{R}^d} (u_i - \bar{V}_i)(u_j - \bar{V}_j)(f_s^\beta(\bar{\Delta}) - f^\beta(\bar{\Delta})) e^{-s} d\mathbf{u} ds \quad (\text{C.11})$$

in (4.35), where $f^\beta(\bar{\Delta}) = \frac{\rho}{U^3} F^\beta(\bar{\Delta})$ and $F^\beta(\bar{\Delta})$ denotes the isotropic Lévy- β stable distribution.

Therefore,

$$\mathcal{T}_{ij}^R = - \frac{\rho}{U^3} \int_0^\infty \int_{\mathbb{R}^d} (u_i - \bar{V}_i)(u_j - \bar{V}_j)(F_s^\beta(\bar{\Delta}) - F^\beta(\bar{\Delta})) e^{-s} d\mathbf{u} ds. \quad (\text{C.12})$$

Asymptotically, $F^\beta(\bar{\Delta})$ behaves like a power-law distribution when $\bar{\Delta} > 1$, i.e., $F^\beta(\bar{\Delta}) \sim \tilde{C}_\beta \bar{\Delta}^\beta = \frac{C_\alpha}{\bar{\Delta}^{-\alpha+d/2}}$, where $\beta = -\alpha - \frac{d}{2}$ and $C_\alpha = \frac{2^{2\alpha}\Gamma(\alpha+d/2)}{\pi^{d/2}\Gamma(-\alpha)}$. It is worth mentioning that $\overline{f^{eq}(\Delta)}$ demonstrates a heavy-tailed behavior at $\bar{\Delta} > 1$, it keeps the exponential trait for $\bar{\Delta} < 1$ though. Regarding the exponential behavior of $f^{eq}(\bar{\Delta})$, $\overline{f^{eq}(\Delta)} - f^{eq}(\bar{\Delta})$ can be fitted by a heavy-tailed distribution like $F^\beta(\bar{\Delta})$, in which $F^\beta(\bar{\Delta})$ reduces exponentially in a close proximity of $\bar{\Delta} = 0$.

Therefore, we can simplify (C.12) to

$$\mathcal{T}_{ij}^R \approx -\frac{\rho C_\alpha}{U^3} \int_0^\infty \int_{\mathbb{R}^d - B_\epsilon} (u_i - \bar{V}_i)(u_j - \bar{V}_j)(\bar{\Delta}_s^{-\alpha+d/2} - \bar{\Delta}^{-\alpha+d/2}) e^{-s} d\mathbf{u} ds, \quad (\text{C.13})$$

where $d = 3$ and $B_\epsilon = \{\mathbf{u} \in \mathbb{R}^d \text{ s.t. } |\bar{\Delta}| < \epsilon\}$, which is associated with $\bar{\Delta} \ll 1$. Due to the fact that $F^\beta(\bar{\Delta})$ is continuously differentiable for $|\mathbf{u}| \in \mathbb{R}^d - B_\epsilon$, we perform the Taylor expansion of $F_s^\beta(\bar{\Delta})$ as follows:

$$F_s^\beta(\bar{\Delta}) - F^\beta(\bar{\Delta}) \approx \frac{\partial F^\beta(\bar{\Delta})}{\partial \bar{\Delta}}(\bar{\Delta}_s - \bar{\Delta}) = (\alpha + \frac{3}{2}) \frac{\rho C_\alpha}{U^3} \frac{(\bar{\Delta}_s - \bar{\Delta})}{\bar{\Delta}^{\alpha+5/2}}.$$

Under Assumption 5, in which $s \sim O(1)$, we obtain

$$\delta x = s|\mathbf{u}|\tau > O(l) \rightarrow |\mathbf{u}| > O(\frac{l}{\tau}) = O(\frac{l}{\lambda/U}) > O(U)$$

at large $\delta x > l$, which yields in $\bar{\Delta} = \frac{|\mathbf{u} - \bar{\mathbf{V}}|^2}{U^2} \approx \frac{|\mathbf{u}|^2}{U^2} \gg 1$ and $u_i - \bar{V}_i \approx u_i$. In virtue of (4.50-51) in [163], we also conclude that

$$\bar{\Delta}_s - \bar{\Delta} \approx -2 \sum_{k=1}^3 \frac{u_k(\bar{V}_k(\mathbf{x}) - \bar{V}_k(\mathbf{x}'))}{U^2}. \quad (\text{C.14})$$

Utilizing the definition of $\mathbf{u} = \frac{\mathbf{x} - \mathbf{x}'}{s\tau}$ in Section 4.3.1 and (C.14), we reformulate (C.13) as

$$\begin{aligned} \mathcal{T}_{ij}^R &\approx (\alpha + \frac{3}{2}) \frac{\rho C_\alpha}{U^3} \int_0^\infty \int_{\mathbb{R}^d - B_\epsilon} \left(\frac{x_i - x'_i}{s\tau} \right) \left(\frac{x_j - x'_j}{s\tau} \right) \frac{(\bar{\Delta}_s - \bar{\Delta})}{(\frac{|\mathbf{x} - \mathbf{x}'|}{s\tau U})^{2\alpha+5}} \frac{d\mathbf{x}'}{(s\tau)^3} e^{-s} ds, \\ &= (2\alpha + 3)(\rho C_\alpha \tau^{2\alpha-1} U^{2\alpha}) \int_0^\infty \frac{e^{-s}}{s^{1-2\alpha}} ds \times \\ &\quad \int_{\mathbb{R}^d - B_\epsilon} (x_i - x'_i)(x_j - x'_j) \frac{(\mathbf{x} - \mathbf{x}') \cdot (\bar{\mathbf{V}}(\mathbf{x}) - \bar{\mathbf{V}}(\mathbf{x}'))}{|\mathbf{x} - \mathbf{x}'|^{2\alpha+5}} d\mathbf{x}', \end{aligned} \quad (\text{C.15})$$

which corresponds to (4.58) in [163]. Therefore, we can proceed the same derivations as discussed in (4.58) to (4.64) in [163] to obtain

$$\begin{aligned} (\nabla \cdot \mathcal{T}^R)_i &= \frac{\rho(U\tau)^{2\alpha}}{\tau} \Gamma(2\alpha + 1) C_\alpha \int_{\mathbb{R}^d - B_\epsilon} \frac{\bar{V}_i(\mathbf{x}') - \bar{V}_i(\mathbf{x})}{|\mathbf{x}' - \mathbf{x}|^{2\alpha+d}} d\mathbf{x}' \\ &= p.v. \frac{\rho(U\tau)^{2\alpha}}{\tau} \Gamma(2\alpha + 1) C_\alpha \int_{\mathbb{R}^d} \frac{\bar{V}_i(\mathbf{x}') - \bar{V}_i(\mathbf{x})}{|\mathbf{x}' - \mathbf{x}|^{2\alpha+d}} d\mathbf{x}' \end{aligned} \quad (\text{C.16})$$

in which "p.v." denotes the principal value of the integral.

APPENDIX D

DERIVATIONS IN CHAPTER 5

D.1 Fourier Transform of Tempered Fractional Laplacian

As noted in [247, 248], the tempered fractional Laplacian operator can be represented in various equivalent forms, i.e.,

$$\begin{aligned} (\Delta + \lambda)^\alpha u(\mathbf{x}) &= -C_{d,\alpha} \text{P.V.} \int_{\mathbb{R}^d} \frac{u(\mathbf{x}) - u(\mathbf{s})}{e^{\lambda|\mathbf{x}-\mathbf{s}|} |\mathbf{x} - \mathbf{s}|^{2\alpha+d}} d\mathbf{s} \\ &= \frac{C_{d,\alpha}}{2} \text{P.V.} \int_{\mathbb{R}^d} \frac{u(\mathbf{x} + \mathbf{s}) + u(\mathbf{x} - \mathbf{s}) - 2u(\mathbf{x})}{e^{\lambda s} s^{2\alpha+d}} d\mathbf{s}, \end{aligned} \quad (\text{D.1})$$

where $s = |\mathbf{s}|$, $\alpha \in (0, \frac{1}{2}) \cup (\frac{1}{2}, 1)$, and $\lambda > 0$. By performing the Fourier transform of (D.1), we get

$$\begin{aligned} \mathcal{F}[(\Delta + \lambda)^\alpha u(\mathbf{x})](\xi) &= \frac{C_{d,\alpha}}{2} \int_{\mathbb{R}^d} \frac{e^{\xi \cdot \mathbf{s}} + e^{-\xi \cdot \mathbf{s}} - 2}{e^{\lambda s} s^{2\alpha+d}} d\mathbf{s} \\ &= -C_{d,\alpha} \int_{\mathbb{R}^d} \frac{1 - \cos(\xi \cdot \mathbf{s})}{e^{\lambda s} s^{n+2\alpha}} d\mathbf{s} \mathcal{F}[u(\mathbf{x})](\xi), \end{aligned} \quad (\text{D.2})$$

in which ξ denotes the Fourier numbers. For the sake of simplicity, we define

$$I(\xi) = - \int_{\mathbb{R}^d} \frac{1 - \cos(\xi \cdot \mathbf{s})}{e^{\lambda s} s^{n+2\alpha}} d\mathbf{s},$$

which appears to be rotationally invariant. Moreover, we introduce $\xi = |\xi|$ and $s_\theta = s \cos(\theta)$. Without loss of generality, θ can be chosen such that $s \cos(\theta)$ is aligned with the first primary direction. Therefore, $I(\xi)$ can be re-expressed by

$$I(\xi) = \int_{\mathbb{R}^d} \frac{\cos(\xi \cdot \mathbf{s}) - 1}{e^{\lambda s} s^{n+2\alpha}} d\mathbf{s} = \int_{\mathbb{R}^d} \frac{\cos(\eta_\theta) - 1}{e^{\lambda \eta / \xi} (\eta / \xi)^{n+2\alpha}} \frac{d\boldsymbol{\eta}}{\xi^n} = \xi^{2\alpha} \int_{\mathbb{R}^d} \frac{\cos(\eta_\theta) - 1}{e^{\lambda \eta / \xi} (\eta)^{n+2\alpha}} d\boldsymbol{\eta}, \quad (\text{D.3})$$

where $\boldsymbol{\eta} = \xi \mathbf{s}$, $\eta = |\boldsymbol{\eta}|$, and $\eta_\theta = \xi s_\theta$. Due to the invariant properties of $I(\xi)$, we proceed the derivations with transforming (D.3) into the corresponding spherical coordinate, $(r, \phi_1, \dots, \phi_{d-1})$.

In terms of the transformation, we let $\eta = |\boldsymbol{\eta}| = r$ and $\eta_\theta = \eta \cos(\theta) = r \cos(\phi_1)$. Then, in a general case for $d > 1$, $d\boldsymbol{\eta}$ follows

$$d\boldsymbol{\eta} = \mathcal{J}(r, \phi_1, \dots, \phi_{d-1}) dr d\phi_1 \cdots d\phi_{d-1},$$

where

$$\mathcal{J}(r, \phi_1, \dots, \phi_{d-1}) = \left| \det \frac{\partial x_i}{\partial(r\phi_j)} \right| = r^{d-1} \sin^{d-2}(\phi_1) \sin^{d-3}(\phi_2) \cdots \sin(\phi_{d-2})$$

for $i = 1, \dots, d$ and $j = 1, \dots, d-1$ [see 249]. Therefore, we find the general form of $I(\xi)$ as

$$I(\xi) = \xi^{2\alpha} \bar{c} \int_0^\infty \int_0^{2\pi} \frac{\cos(r \cos(\phi_1)) - 1}{e^{\lambda r/\xi}} r^{d-1} \sin^{d-2}(\phi_1) d\phi_1 dr, \quad (\text{D.4})$$

where $\bar{c} = \int_0^\pi \sin^{d-3}(\phi_2) d\phi_2 \cdots \int_0^\pi \sin(\phi_{d-1}) d\phi_{d-1} = \frac{2\pi^{(d-1)/2}}{\Gamma(\frac{d-1}{2})}$. It is shown by [247] that

$$\begin{aligned} I(\xi) &= \bar{c} \xi^{2\alpha} \int_0^\infty \frac{e^{-\lambda r/\xi}}{r^{\beta+1}} \int_0^{2\pi} [\cos(r \cos(\phi_1)) - 1] \sin^{d-2}(\phi_1) d\phi_1 dr \\ &= \frac{\bar{c} \Gamma(-2\alpha) \pi^{1/2} \Gamma(\frac{d-1}{2})}{\Gamma(\frac{d}{2})} \left[\lambda^2 - (\lambda^2 + \xi^2)^\alpha {}_2F_1(-\alpha, \frac{d+2\alpha-1}{2}; \frac{d}{2}; \frac{\xi^2}{\xi^2 + \lambda^2}) \right], \end{aligned}$$

where ${}_2F_1$ denotes a Gaussian hypergeometric function. Therefore,

$$\mathcal{F}[(\Delta + \lambda)^\alpha u(\mathbf{x})](\xi) = \mathfrak{C}_{d,\alpha} \times \left[\lambda^2 - (\lambda^2 + \xi^2)^\alpha {}_2F_1(-\alpha, \frac{d+2\alpha-1}{2}; \frac{d}{2}; \frac{\xi^2}{\xi^2 + \lambda^2}) \right], \quad (\text{D.5})$$

$$\text{where } \mathfrak{C}_{d,\alpha} = C_{d,\alpha} \bar{c} \Gamma(-2\alpha) \frac{\pi^{1/2} \Gamma(\frac{d-1}{2})}{\Gamma(d/2)} = \frac{1}{{}_2F_1(-\alpha, \frac{d+2\alpha-1}{2}; \frac{d}{2}; 1)}.$$

D.2 Tempered Fractional Modeling of SGS Stresses

As we discussed in subsection 5.3.3, the SGS stresses are described by

$$T_{ij}^R = \frac{\rho c_{\beta,\lambda}}{U^3} \int_0^\infty \int_{\mathbb{R}^3} (u_i - \bar{V}_i)(u_j - \bar{V}_j) (F^{\beta,\lambda}(\bar{\Delta}_s) - F^{\beta,\lambda}(\bar{\Delta})) e^{-s} d\mathbf{u} ds \quad (\text{D.6})$$

where $F^{\beta,\lambda}(\bar{\Delta})$ represents a tempered Lévy β -stable distribution. Let consider $\beta = -\alpha - \frac{3}{2}$ for $\alpha \in (0, \frac{1}{2}) \cup (\frac{1}{2}, 1)$. Regarding the equivalent Pareto-like behavior of Lévy distributions [250] at $\bar{\Delta} > 1$, we decompose the domain of kinetic momentum such that $\mathbb{R}^3 = \mathcal{I}_\epsilon \cup (\mathbb{R}^3 \setminus \mathcal{I}_\epsilon)$, where $\mathcal{I}_\epsilon = \{u \in \mathbb{R}^d \text{ s.t. } |\bar{\Delta}| < \epsilon\}$ and $\epsilon \ll 1$. This allows for the following approximation as

$$F^{\alpha,\lambda}(\bar{\Delta}) \simeq C_\alpha \begin{cases} 0, & \mathbf{u} \in \mathcal{I}_\epsilon \\ e^{-\lambda \bar{\Delta}^{\frac{1}{2}}} \bar{\Delta}^{-(\alpha+\frac{3}{2})}, & \mathbf{u} \in \mathbb{R}^3 \setminus \mathcal{I}_\epsilon \end{cases} \quad (\text{D.7})$$

where $C_\alpha = \frac{-\Gamma(\frac{3}{2})}{2\pi^{\frac{3}{2}}\Gamma(-2\alpha)} \frac{1}{{}_2F_1(-\alpha, 1+\alpha; \frac{3}{2}; 1)}$. It is worth mentioning that $F^{\alpha, \lambda}(\bar{\Delta})$ reduces exponentially in a close proximity of $\bar{\Delta} = 0$. With all this in mind, the approximated function of $F^{\alpha, \lambda}(\bar{\Delta})$ in (D.7) can properly capture the heavy-tailed behavior of the filtered collision term. Evidently, by replacing $e^{-\lambda\bar{\Delta}_s^{\frac{1}{2}}}$ with $e^{-\lambda\bar{\Delta}^{\frac{1}{2}}}$ for $\bar{\Delta} > 1$, we arrive at the following expression

$$F^{\alpha, \lambda}(\bar{\Delta}_s) - F^{\alpha, \lambda}(\bar{\Delta}) = C_\alpha \left(\frac{e^{-\lambda\bar{\Delta}_s^{\frac{1}{2}}}}{\bar{\Delta}_s^{(\alpha+\frac{3}{2})}} - \frac{e^{-\lambda\bar{\Delta}^{\frac{1}{2}}}}{\bar{\Delta}^{(\alpha+\frac{3}{2})}} \right) \simeq C_\alpha e^{-\lambda\bar{\Delta}^{\frac{1}{2}}} \left(\frac{1}{\bar{\Delta}_s^{(\alpha+\frac{3}{2})}} - \frac{1}{\bar{\Delta}^{(\alpha+\frac{3}{2})}} \right),$$

and accordingly,

$$\mathbf{T}_{ij}^R = \frac{\rho c_{\alpha, \lambda}}{U^3} C_\alpha \int_0^\infty \int_{\mathbb{R}^3 \setminus \mathcal{I}_\Delta} (u_i - \bar{V}_i)(u_j - \bar{V}_j) e^{-\lambda\bar{\Delta}^{\frac{1}{2}}} \left(\frac{1}{\bar{\Delta}_s^{(\alpha+\frac{3}{2})}} - \frac{1}{\bar{\Delta}^{(\alpha+\frac{3}{2})}} \right) e^{-s} d\mathbf{u} ds, \quad (\text{D.8})$$

where $c_{\alpha, \lambda}$ is a real-valued constant. As a continuous differentiable function for $\bar{\Delta} > 1$, we proceed with the Taylor expansion of $\bar{\Delta}_s^{-(\alpha+\frac{3}{2})}$ according to

$$\bar{\Delta}_s^{-(\alpha+\frac{3}{2})} - \bar{\Delta}^{-(\alpha+\frac{3}{2})} \approx \frac{\partial \bar{\Delta}^{-(\alpha+\frac{3}{2})}}{\partial \bar{\Delta}} (\bar{\Delta}_s - \bar{\Delta}) = -(\alpha + \frac{3}{2}) C_\alpha \frac{(\bar{\Delta}_s - \bar{\Delta})}{\bar{\Delta}^{\alpha+5/2}}.$$

In terms of the assumptions in remark 5.3.1, we use the same argument, presented by [232, Appendix], on approximating $\bar{\Delta}_s - \bar{\Delta}$ for $\bar{\Delta} \gg 1$, which allows for $u_i - \bar{V}_i \approx u_i$ and thus

$$\bar{\Delta}_s - \bar{\Delta} \approx 2 \sum_{k=1}^3 \frac{u_k(\bar{V}_k(\mathbf{x}') - \bar{V}_k(\mathbf{x}))}{U^2}. \quad (\text{D.9})$$

Reminding the definition of $\mathbf{u} = \frac{\mathbf{x}-\mathbf{x}'}{s\tau}$ from section 5.3.2, we plug (D.9) into (D.8) and obtain

$$\begin{aligned} \mathbf{T}_{ij}^R &= (2\alpha + 3)(\rho c_{\alpha, \lambda} C_\alpha \tau^{2\alpha-1} U^{2\alpha}) \times \\ &\quad \int_0^\infty \frac{e^{-s}}{s^{1-2\alpha}} \int_{\mathbb{R}^3 \setminus \mathcal{I}_\Delta} (x_i - x'_i)(x_j - x'_j) \frac{(\mathbf{x} - \mathbf{x}') \cdot (\bar{\mathbf{V}}(\mathbf{x}) - \bar{\mathbf{V}}(\mathbf{x}'))}{|\mathbf{x} - \mathbf{x}'|^{2\alpha+5} e^{\lambda \frac{|\mathbf{x}-\mathbf{x}'|}{s\tau U}}} d\mathbf{x}' ds. \end{aligned} \quad (\text{D.10})$$

In order to evaluate the outer integral in D.10 and find the corresponding coefficient, our approach is to dissociate the temporal element by employing the binomial series of $e^{\lambda \frac{|\mathbf{x}-\mathbf{x}'|}{s\tau U}}$ as

follows:

$$\begin{aligned}
e^{-\frac{\lambda|\mathbf{x}-\mathbf{x}'|}{s\tau U}} &= (1 - 1 + e^{-\frac{\lambda|\mathbf{x}-\mathbf{x}'|}{s\tau U}})^{\frac{1}{s}} = \sum_{k=0}^{\infty} \binom{\frac{1}{s}}{k} (e^{\bar{\lambda}|\mathbf{x}-\mathbf{x}'|} - 1) \\
&= 1 + \frac{1}{s} (e^{\bar{\lambda}|\mathbf{x}-\mathbf{x}'|} - 1) + \frac{\frac{1}{s}(\frac{1}{s} - 1)}{2!} (e^{\bar{\lambda}|\mathbf{x}-\mathbf{x}'|} - 1) + \dots \\
&= \sum_{k=0}^{\infty} W_{k,\infty}(s) e^{-\bar{\lambda}_k |\mathbf{x}-\mathbf{x}'|} \\
&\simeq \sum_{k=0}^{\mathcal{K}} W_{k,\mathcal{K}}(s) e^{-\bar{\lambda}_k |\mathbf{x}-\mathbf{x}'|}, \tag{D.11}
\end{aligned}$$

where $\bar{\lambda} = \frac{\lambda}{\tau U}$ and $\bar{\lambda}_k = \bar{\lambda}$. Under the assumption of $\lambda > 0.01$, we can approximate the binomial series with the first two leading terms, which yields $W_{0,1} = 1 - \frac{1}{s}$ and $W_{1,1} = \frac{1}{s}$ for $\mathcal{K} = 1$.

Accordingly, by defining $\bar{v}_\alpha = (2\alpha + 3)(\rho C_\alpha \tau^{2\alpha-1} U^{2\alpha})$ and

$$\bar{\phi}_k^\mathcal{K}(\alpha) = \int_0^\infty \frac{e^{-s}}{s^{1-2\alpha}} W_{k,\mathcal{K}}(s) ds, \tag{D.12}$$

we obtain the closed form of T_{ij}^R as

$$T_{ij}^R = c_{\alpha,\lambda} \bar{v}_\alpha \sum_{k=0}^{\mathcal{K}} \bar{\phi}_k^\mathcal{K}(\alpha) \underbrace{\int_{\mathbb{R}^d - B_\epsilon} (x_i - x'_i) (x_j - x'_j) \frac{(\mathbf{x} - \mathbf{x}') \cdot (\bar{\mathbf{V}} - \bar{\mathbf{V}}')}{|\mathbf{x} - \mathbf{x}'|^{2\alpha+5} e^{\bar{\lambda}_k |\mathbf{x}-\mathbf{x}'|}} d\mathbf{x}'}_{\mathcal{I}_{ij}}. \tag{D.13}$$

To ensure the proper form of the SGS stresses in the filtered NS equations, we take the derivative of \mathcal{I}_{ij} term by term, which yields

$$\begin{aligned}
\frac{\partial \mathcal{I}_{ij}}{\partial x_i} &= \int_{\mathbb{R}^d - B_\epsilon} \sum_{i=1}^3 \left\{ \begin{aligned} &-(x_j - x'_j) \frac{(\mathbf{x} - \mathbf{x}') \cdot (\bar{\mathbf{V}} - \bar{\mathbf{V}}')}{|\mathbf{x} - \mathbf{x}'|^{2\alpha+5} e^{\bar{\lambda}_k |\mathbf{x}-\mathbf{x}'|}} \\ &-(x_i - x'_i) \delta_{ij} \frac{(\mathbf{x} - \mathbf{x}') \cdot (\bar{\mathbf{V}} - \bar{\mathbf{V}}')}{|\mathbf{x} - \mathbf{x}'|^{2\alpha+5} e^{\bar{\lambda}_k |\mathbf{x}-\mathbf{x}'|}} \\ &-\frac{(x_j - x'_j)(x_j - x'_j)(\bar{V}_i - \bar{V}'_i)}{|\mathbf{x} - \mathbf{x}'|^{2\alpha+5} e^{\bar{\lambda}_k |\mathbf{x}-\mathbf{x}'|}} \\ &-(x_i - x'_i)(x_j - x'_j)(x_k - x'_k) \frac{\partial \bar{V}_k}{\partial x_i} \frac{e^{-\bar{\lambda}_k |\mathbf{x}-\mathbf{x}'|}}{|\mathbf{x} - \mathbf{x}'|^{2\alpha+5}} \\ &(2\alpha + 5)(x_i - x'_i)^2 (x_j - x'_j) \frac{(\mathbf{x} - \mathbf{x}') \cdot (\bar{\mathbf{V}} - \bar{\mathbf{V}}')}{|\mathbf{x} - \mathbf{x}'|^{2\alpha+5} e^{\bar{\lambda}_k |\mathbf{x}-\mathbf{x}'|}} \\ &+\bar{\lambda}_k (x_i - x'_i)(x_j - x'_j) \frac{(\mathbf{x} - \mathbf{x}') \cdot (\bar{\mathbf{V}} - \bar{\mathbf{V}}')}{|\mathbf{x} - \mathbf{x}'|^{2\alpha+5} e^{\bar{\lambda}_k |\mathbf{x}-\mathbf{x}'|}} \end{aligned} \right\} d\mathbf{x}', \end{aligned}$$

which is clearly simplified to

$$\frac{\partial \mathcal{I}_{ij}}{\partial x_i} = (\bar{\lambda}_k + 2\alpha + 5 - 3 - 1 - 1) \int_{\mathbb{R}^d - B_\epsilon} (x_j - x'_j) \frac{(\mathbf{x} - \mathbf{x}') \cdot (\bar{\mathbf{V}} - \bar{\mathbf{V}}')}{|\mathbf{x} - \mathbf{x}'|^{2\alpha+5} e^{\bar{\lambda}_k |\mathbf{x} - \mathbf{x}'|}} d\mathbf{x}'. \quad (\text{D.14})$$

Following the derivations in [232, 163], (D.14) can be formulated in the form of a tempered fractional Laplacian by performing the technique of integration-by-parts for (D.14) as $\int A dB = AB - \int B dA$. We consider

$$A = (x_j - x'_j)(\bar{V}_k - \bar{V}'_k)e^{-\bar{\lambda}_k |\mathbf{x} - \mathbf{x}'|}, \quad dB = \frac{(x_k - x'_k)}{|\mathbf{x} - \mathbf{x}'|^{2\alpha+5}} d\mathbf{x}', \quad (\text{D.15})$$

which directly leads to $AB|_{u \in \mathbb{R}^3} \simeq 0$. Therefore, we get $\int A dB = - \int B dA$, in which

$$\begin{aligned} B &= \frac{-1}{(2\alpha + 3)|\mathbf{x} - \mathbf{x}'|^{2\alpha+3}}, \\ dA &= \delta_{jk}(\bar{V}_k - \bar{V}'_k)e^{-\bar{\lambda}_k |\mathbf{x} - \mathbf{x}'|} + (x_j - x'_j)\left(\frac{\partial \bar{V}_k}{\partial x_k}\right)e^{-\bar{\lambda}_k |\mathbf{x} - \mathbf{x}'|} - \bar{\lambda}_k(x_j - x'_j)(\bar{V}_k - \bar{V}'_k)e^{-\bar{\lambda}_k |\mathbf{x} - \mathbf{x}'|} d\mathbf{x}'. \end{aligned}$$

We can make even more simplifications by eliminating the second term of dA due to the incompressibility assumption, i.e., $\frac{\partial \bar{V}_k}{\partial x_k} = 0$. Moreover, by evaluating $\int B dA$ the last term vanishes since it represents an odd function of \mathbf{x}' . Therefore, the ultimate form of the TFSGS model is found to be

$$\begin{aligned} (\nabla \cdot \mathbf{T}^{\mathcal{R}})_j &= c_{\alpha, \lambda} \bar{v}_\alpha \sum_{k=0}^K \frac{(2\alpha + \bar{\lambda}_k)}{(2\alpha + 3)} \bar{\phi}_k^{\mathcal{K}}(\alpha) \int_{\mathbb{R}^d - B_\epsilon} \frac{(\bar{V}_j - \bar{V}'_j)}{|\mathbf{x} - \mathbf{x}'|^{2\alpha+3} e^{\bar{\lambda}_k |\mathbf{x} - \mathbf{x}'|}} d\mathbf{x}', \\ &= v_\alpha \sum_{k=0}^K \bar{\phi}_k^{\mathcal{K}}(\alpha, \bar{\lambda}_k) (\Delta + \bar{\lambda}_k)^\alpha \bar{V}_j, \end{aligned} \quad (\text{D.16})$$

where $v_\alpha = c_{\alpha, \lambda} \bar{v}_\alpha$.

BIBLIOGRAPHY

BIBLIOGRAPHY

- [1] Ralf Metzler, Jae-Hyung Jeon, Andrey G Cherstvy, and Eli Barkai. Anomalous diffusion models and their properties: non-stationarity, non-ergodicity, and ageing at the centenary of single particle tracking. *Physical Chemistry Chemical Physics*, 16(44):24128–24164, 2014.
- [2] Yi Li, Eric Perlman, Minping Wan, Yunke Yang, Charles Meneveau, Randal Burns, Shiyi Chen, Alexander Szalay, and Gregory Eyink. A public turbulence database cluster and applications to study lagrangian evolution of velocity increments in turbulence. *Journal of Turbulence*, 9:N31, 2008.
- [3] Peter Dieterich, Rainer Klages, Roland Preuss, and Albrecht Schwab. Anomalous dynamics of cell migration. *Proceedings of the National Academy of Sciences*, 105(2):459–463, 2008.
- [4] Tatjana Sentjabrskaja, Emanuela Zaccarelli, Cristiano De Michele, Francesco Sciortino, Piero Tartaglia, Thomas Voigtmann, Stefan U Egelhaaf, and Marco Laurati. Anomalous dynamics of intruders in a crowded environment of mobile obstacles. *Nature communications*, 7:11133, 2016.
- [5] Dirk Brockmann. Anomalous diffusion and the structure of human transportation networks. *The European Physical Journal Special Topics*, 157(1):173–189, 2008.
- [6] Pietro De Anna, Tanguy Le Borgne, Marco Dentz, Alexandre M Tartakovsky, Diogo Bolster, and Philippe Davy. Flow intermittency, dispersion, and correlated continuous time random walks in porous media. *Physical review letters*, 110(18):184502, 2013.
- [7] Kartik P Iyer, Jörg Schumacher, Katepalli R Sreenivasan, and PK Yeung. Steep cliffs and saturated exponents in three-dimensional scalar turbulence. *Physical review letters*, 121(26):264501, 2018.
- [8] Boris I Shraiman and Eric D Siggia. Scalar turbulence. *Nature*, 405(6787):639–646, 2000.
- [9] Takahiro Iwayama, Shinya Murakami, and Takeshi Watanabe. Anomalous eddy viscosity for two-dimensional turbulence. *Physics of Fluids*, 27(4):045104, 2015.
- [10] Aijie Cheng, Hong Wang, and Kaixin Wang. A eulerian–lagrangian control volume method for solute transport with anomalous diffusion. *Numerical Methods for Partial Differential Equations*, 31(1):253–267, 2015.
- [11] Alina Tyukhova, Marco Dentz, Wolfgang Kinzelbach, and Matthias Willmann. Mechanisms of anomalous dispersion in flow through heterogeneous porous media. *Physical Review Fluids*, 1(7):074002, 2016.
- [12] Abbas Ghasempour Ardakani. Investigation of brewster anomalies in one-dimensional disordered media having lévy-type distribution. *The European Physical Journal B*, 89(3):76, 2016.

- [13] Yong Zhang, Mark M Meerschaert, and Roseanna M Neupauer. Backward fractional advection dispersion model for contaminant source prediction. *Water Resources Research*, 52(4):2462–2473, 2016.
- [14] Yaniv Edery, Ishai Dror, Harvey Scher, and Brian Berkowitz. Anomalous reactive transport in porous media: Experiments and modeling. *Physical Review E*, 91(5):052130, 2015.
- [15] Yong Zhang, Mark M Meerschaert, Boris Baeumer, and Eric M LaBolle. Modeling mixed retention and early arrivals in multidimensional heterogeneous media using an explicit lagrangian scheme. *Water Resources Research*, 51(8):6311–6337, 2015.
- [16] D. A. Benson, S. W. Wheatcraft, and M. M. Meerschaert. Application of a fractional advection-dispersion equation. *Water Resources Research*, 36(6):1403–1412, 2000.
- [17] Kyle C Armour, John Marshall, Jeffery R Scott, Aaron Donohoe, and Emily R Newsom. Southern ocean warming delayed by circumpolar upwelling and equatorward transport. *Nature Geoscience*, 9(7):549–554, 2016.
- [18] Maryam Naghibolhosseini and Glenis R Long. Fractional-order modelling and simulation of human ear. *International Journal of Computer Mathematics*, pages 1–17, 2017.
- [19] Paris Perdikaris and George Em Karniadakis. Fractional-order viscoelasticity in one-dimensional blood flow models. *Annals of biomedical engineering*, 42(5):1012–1023, 2014.
- [20] Benjamin Michael Regner. Randomness in biological transport. 2014.
- [21] Jorge L Suzuki and Mohsen Zayernouri. An automated singularity-capturing scheme for fractional differential equations. *arXiv preprint arXiv:1810.12219*, 2018.
- [22] JL Suzuki, M Zayernouri, ML Bittencourt, and GE Karniadakis. Fractional-order uniaxial visco-elasto-plastic models for structural analysis. *Computer Methods in Applied Mechanics and Engineering*, 308:443–467, 2016.
- [23] Igor Goychuk. Anomalous transport of subdiffusing cargos by single kinesin motors: the role of mechano–chemical coupling and anharmonicity of tether. *Physical biology*, 12(1):016013, 2015.
- [24] RA Mashelkar and G Marrucci. Anomalous transport phenomena in rapid external flows of viscoelastic fluids. *Rheologica Acta*, 19(4):426–431, 1980.
- [25] R. Klages, G. Radons, and I. M. Sokolov. *Anomalous Transport: Foundations and Applications*. Wiley-VCH, 2008.
- [26] Xiao-Rong Yang and Yan Wang. Ubiquity of anomalous transport in porous media: Numerical evidence, continuous time random walk modelling, and hydrodynamic interpretation. *Scientific reports*, 9(1):4601, 2019.
- [27] Peter K Kang, Pietro de Anna, Joao P Nunes, Branko Bijeljic, Martin J Blunt, and Ruben Juanes. Pore-scale intermittent velocity structure underpinning anomalous transport through 3-d porous media. *Geophysical Research Letters*, 41(17):6184–6190, 2014.

- [28] Yaniv Edery, Alberto Guadagnini, Harvey Scher, and Brian Berkowitz. Origins of anomalous transport in heterogeneous media: Structural and dynamic controls. *Water Resources Research*, 50(2):1490–1505, 2014.
- [29] Michael Wilczek, Dimitar G Vlaykov, and Cristian C Lalescu. Emergence of non-gaussianity in turbulence. In *Progress in Turbulence VII*, pages 3–9. Springer, 2017.
- [30] Laura J Lukassen and Michael Wilczek. Lagrangian intermittency based on an ensemble of gaussian velocity time series. In *Progress in Turbulence VII*, pages 23–29. Springer, 2017.
- [31] Francois G Schmitt and Yongxiang Huang. *Stochastic analysis of scaling time series: from turbulence theory to applications*. Cambridge University Press, 2016.
- [32] YI Li and Charles Meneveau. Intermittency trends and lagrangian evolution of non-gaussian statistics in turbulent flow and scalar transport. *Journal of Fluid Mechanics*, 558:133–142, 2006.
- [33] R Camussi and R Verzicco. Anomalous scaling exponents and coherent structures in high re fluid turbulence. *Physics of Fluids*, 12(3):676–687, 2000.
- [34] Carlos Rosales and Charles Meneveau. A minimal multiscale lagrangian map approach to synthesize non-gaussian turbulent vector fields. *Physics of Fluids*, 18(7):075104, 2006.
- [35] Carlos Rosales and Charles Meneveau. Anomalous scaling and intermittency in three-dimensional synthetic turbulence. *Physical Review E*, 78(1):016313, 2008.
- [36] Alain Arnéodo, Roberto Benzi, Jacob Berg, Luca Biferale, Eberhard Bodenschatz, A Busse, Enrico Calzavarini, Bernard Castaing, Massimo Cencini, Laurent Chevillard, et al. Universal intermittent properties of particle trajectories in highly turbulent flows. *Physical Review Letters*, 100(25):254504, 2008.
- [37] Igor Podlubny. *Fractional differential equations: an introduction to fractional derivatives, fractional differential equations, to methods of their solution and some of their applications*, volume 198. Academic press, 1998.
- [38] Mark M Meerschaert and Alla Sikorskii. *Stochastic models for fractional calculus*, volume 43. Walter de Gruyter, 2012.
- [39] Boling Guo, Xueke Pu, and Fenghui Huang. *Fractional partial differential equations and their numerical solutions*. World Scientific, 2015.
- [40] Stefan G Samko, Anatoly A Kilbas, and Oleg I Marichev. *Fractional integrals and derivatives. Theory and Applications*, Gordon and Breach, Yverdon, 1993, 1993.
- [41] Alberto Carpinteri and Francesco Mainardi. *Fractals and fractional calculus in continuum mechanics*, volume 378. Springer, 2014.
- [42] Hong Wang and Xiangcheng Zheng. Wellposedness and regularity of the variable-order time-fractional diffusion equations. *Journal of Mathematical Analysis and Applications*, 475(2):1778–1802, 2019.

- [43] Mark M Meerschaert and Alla Sikorskii. Stochastic models for fractional calculus, volume 43. Walter de Gruyter, 2011.
- [44] Wojciech Sumelka and Marcin Nowak. Non-normality and induced plastic anisotropy under fractional plastic flow rule: a numerical study. International Journal for Numerical and Analytical Methods in Geomechanics, 40(5):651–675, 2016.
- [45] Wojciech Sumelka. Application of fractional continuum mechanics to rate independent plasticity. Acta Mechanica, 225(11):3247–3264, 2014.
- [46] Wojciech Sumelka and Marcin Nowak. On a general numerical scheme for the fractional plastic flow rule. Mechanics of Materials, 116:120–129, 2018.
- [47] Goran Lazović, Zoran Vosika, Mihailo Lazarević, Jovana Simić-Krstić, and Đuro Koruga. Modeling of bioimpedance for human skin based on fractional distributed-order modified cole model. FME Transactions, 42(1):74–81, 2014.
- [48] D Baleanu, A Jajarmi, SS Sajjadi, and D Mozyrska. A new fractional model and optimal control of a tumor-immune surveillance with non-singular derivative operator. Chaos: An Interdisciplinary Journal of Nonlinear Science, 29(8):083127, 2019.
- [49] C Ionescu, A Lopes, Dana Copot, JA Tenreiro Machado, and JHT Bates. The role of fractional calculus in modeling biological phenomena: A review. Communications in Nonlinear Science and Numerical Simulation, 51:141–159, 2017.
- [50] Yong Zhang, David A Benson, and Donald M Reeves. Time and space nonlocalities underlying fractional-derivative models: Distinction and literature review of field applications. Advances in Water Resources, 32(4):561–581, 2009.
- [51] Kaixin Wang and Hong Wang. A fast characteristic finite difference method for fractional advection–diffusion equations. Advances in water resources, 34(7):810–816, 2011.
- [52] Anna Suzuki, Sergei A Fomin, Vladimir A Chugunov, Yuichi Niibori, and Toshiyuki Hashida. Fractional diffusion modeling of heat transfer in porous and fractured media. International Journal of Heat and Mass Transfer, 103:611–618, 2016.
- [53] A Sapora, P Cornetti, B Chiaia, EK Lenzi, and LR Evangelista. Nonlocal diffusion in porous media: a spatial fractional approach. Journal of Engineering Mechanics, 143(5):D4016007, 2017.
- [54] FDA Aarao Reis, D Bolster, and Vaughan R Voller. Anomalous behaviors during infiltration into heterogeneous porous media. Advances in water resources, 113:180–188, 2018.
- [55] Mohsen Zayernouri, Mark Ainsworth, and George Em Karniadakis. A unified petrov–galerkin spectral method for fractional pdes. Computer Methods in Applied Mechanics and Engineering, 283:1545–1569, 2015.
- [56] Mohsen Zayernouri and George Em Karniadakis. Fractional sturm–liouville eigen-problems: theory and numerical approximation. Journal of Computational Physics, 252:495–517, 2013.

- [57] J. Fitch R. Askey. Integral representations for jacobi polynomials and some applications. *Journal of Mathematical Analysis and Applications*, 26, 1969.
- [58] Heidi Christiansen Barlebo, Mary C Hill, and Dan Rosbjerg. Investigating the macrodispersion experiment (made) site in columbus, mississippi, using a three-dimensional inverse flow and transport model. *Water Resources Research*, 40(4), 2004.
- [59] Boris Baeumer, Tomasz Luks, and Mark M Meerschaert. Space-time fractional dirichlet problems. *arXiv preprint arXiv:1604.06421*, 2016.
- [60] Mehdi Samiee, Mohsen Zayernouri, and Mark M Meerschaert. A unified spectral method for fpdes with two-sided derivatives; part i: a fast solver. *Journal of Computational Physics*, 385:225–243, 2019.
- [61] Mehdi Samiee, Mohsen Zayernouri, and Mark M Meerschaert. A unified spectral method for fpdes with two-sided derivatives; part ii: Stability, and error analysis. *Journal of Computational Physics*, 385:244–261, 2019.
- [62] Jie Shen, Tao Tang, and Li-Lian Wang. *Spectral methods: algorithms, analysis and applications*, volume 41. Springer Science & Business Media, 2011.
- [63] IM Sokolov, AV Chechkin, and J Klafter. Distributed-order fractional kinetics. *arXiv preprint cond-mat/0401146*, 2004.
- [64] Jun-Sheng Duan and Dumitru Baleanu. Steady periodic response for a vibration system with distributed order derivatives to periodic excitation. *Journal of Vibration and Control*, page 1077546317700989.
- [65] Sanja Konjik, Ljubica Oparnica, and Dusan Zorica. Distributed order fractional constitutive stress-strain relation in wave propagation modeling. *arXiv preprint arXiv:1709.01339*, 2017.
- [66] C.H. Eab and S.C. Lim. Fractional langevin equations of distributed order. *Physical Review E*, 83(3):031136, 2011.
- [67] Francesco Mainardi, Antonio Mura, Gianni Pagnini, and Rudolf Gorenflo. Time-fractional diffusion of distributed order. *Journal of Vibration and Control*, 14(9-10):1267–1290, 2008.
- [68] Francesco Mainardi, Antonio Mura, Rudolf Gorenflo, and Mirjana Stojanović. The two forms of fractional relaxation of distributed order. *Journal of Vibration and Control*, 13(9-10):1249–1268, 2007.
- [69] AV Chechkin, Rudolf Gorenflo, and IM Sokolov. Retarding subdiffusion and accelerating superdiffusion governed by distributed-order fractional diffusion equations. *Physical Review E*, 66(4):046129, 2002.
- [70] Ehsan Kharazmi, Mohsen Zayernouri, and George Em Karniadakis. Petrov–galerkin and spectral collocation methods for distributed order differential equations. *SIAM Journal on Scientific Computing*, 39(3):A1003–A1037, 2017.

- [71] Mehdi Samiee, Ehsan Kharazmi, Mohsen Zayernouri, and Mark M Meerschaert. Petrov-galerkin method for fully distributed-order fractional partial differential equations. *arXiv preprint arXiv:1805.08242*, 2018.
- [72] Mehdi Samiee, Ehsan Kharazmi, and Mohsen Zayernouri. Fast spectral methods for temporally-distributed fractional pdes. In *Spectral and High Order Methods for Partial Differential Equations ICOSAHOM 2016*, pages 651–667. Springer, 2017.
- [73] Laurent Chevillard, Bernard Castaing, Emmanuel Lévéque, and Alain Arnéodo. Unified multifractal description of velocity increments statistics in turbulence: Intermittency and skewness. *Physica D: Nonlinear Phenomena*, 218(1):77–82, 2006.
- [74] FA Jaberi, RS Miller, CK Madnia, and P Givi. Non-gaussian scalar statistics in homogeneous turbulence. *Journal of Fluid Mechanics*, 313:241–282, 1996.
- [75] O Cardoso, B Gluckmann, O Parcollet, and P Tabeling. Dispersion in a quasi-two-dimensional-turbulent flow: An experimental study. *Physics of Fluids*, 8(1):209–214, 1996.
- [76] Charles Meneveau. Statistics of turbulence subgrid-scale stresses: Necessary conditions and experimental tests. *Physics of Fluids*, 6(2):815–833, 1994.
- [77] Rodrigo Soto. *Kinetic theory and transport phenomena*, volume 25. Oxford University Press, 2016.
- [78] Sauro Succi and Sauro Succi. *The lattice Boltzmann equation: for fluid dynamics and beyond*. Oxford university press, 2001.
- [79] Yoshio Sone. *Kinetic theory and fluid dynamics*. Springer Science & Business Media, 2012.
- [80] Robert D Moser, Sigfried W Haering, and Gopal R Yalla. Statistical properties of subgrid-scale turbulence models. *Annual Review of Fluid Mechanics*, 53, 2021.
- [81] Stefano Cerutti, Charles Meneveau, and Omar M Knio. Spectral and hyper eddy viscosity in high-Reynolds-number turbulence. *Journal of Fluid Mechanics*, 421:307–338, 2000.
- [82] Pierre Sagaut and Claude Cambon. *Homogeneous turbulence dynamics*, volume 10. Springer, 2008.
- [83] Ch Lubich. Discretized fractional calculus. *SIAM Journal on Mathematical Analysis*, 17(3):704–719, 1986.
- [84] N Sugimoto. Burgers equation with a fractional derivative; hereditary effects on nonlinear acoustic waves. *Journal of fluid mechanics*, 225:631–653, 1991.
- [85] N Sugimoto. Generalized burgers equations and fractional calculus. *Nonlinear wave motion*, 408:162–179, 1989.
- [86] Mark M Meerschaert and Charles Tadjeran. Finite difference approximations for fractional advection-dispersion flow equations. *Journal of Computational and Applied Mathematics*, 172(1):65–77, 2004.

- [87] Charles Tadjeran and Mark M Meerschaert. A second-order accurate numerical method for the two-dimensional fractional diffusion equation. *Journal of Computational Physics*, 220(2):813–823, 2007.
- [88] Hala Hejazi, Timothy Moroney, and Fawang Liu. A finite volume method for solving the two-sided time-space fractional advection-dispersion equation. *Open Physics*, 11(10):1275–1283, 2013.
- [89] Minghua Chen and Weihua Deng. A second-order numerical method for two-dimensional two-sided space fractional convection diffusion equation. *Applied Mathematical Modelling*, 38(13):3244–3259, 2014.
- [90] Fanhai Zeng, Changpin Li, Fawang Liu, and Ian Turner. Numerical algorithms for time-fractional subdiffusion equation with second-order accuracy. *SIAM Journal on Scientific Computing*, 37(1):A55–A78, 2015.
- [91] Xuan Zhao, Zhi-zhong Sun, and George Em Karniadakis. Second-order approximations for variable order fractional derivatives: algorithms and applications. *Journal of Computational Physics*, 293:184–200, 2015.
- [92] Dongfang Li, Chengjian Zhang, and Maohua Ran. A linear finite difference scheme for generalized time fractional burgers equation. *Applied Mathematical Modelling*, 40(11):6069–6081, 2016.
- [93] LB Feng, P Zhuang, F Liu, I Turner, and J Li. High-order numerical methods for the riesz space fractional advection–dispersion equations. *Computers & Mathematics with Applications*, 2016.
- [94] Mohsen Zayernouri and Anastasios Matzavinos. Fractional adams–bashforth/moulton methods: An application to the fractional keller–segel chemotaxis system. *Journal of Computational Physics*, 317:1–14, 2016.
- [95] Jie Shen and Li-Lian Wang. Fourierization of the legendre–galerkin method and a new space–time spectral method. *Applied numerical mathematics*, 57(5):710–720, 2007.
- [96] NH Sweilam, MM Khader, and M Adel. Chebyshev pseudo-spectral method for solving fractional advection-dispersion equation. *Applied Mathematics*, 5(19):3240, 2014.
- [97] Feng Chen, Qinwu Xu, and Jan S Hesthaven. A multi-domain spectral method for time-fractional differential equations. *Journal of Computational Physics*, 293:157–172, 2015.
- [98] P Mokhtary. Discrete galerkin method for fractional integro-differential equations. *Acta Mathematica Scientia*, 36(2):560–578, 2016.
- [99] Ehsan Kharazmi and Mohsen Zayernouri. Fractional pseudo-spectral methods for distributed-order fractional pdes. *International Journal of Computer Mathematics*, (in press):1–22, 2017.

- [100] Anna Lischke, Mohsen Zayernouri, and George Em Karniadakis. A petrov–galerkin spectral method of linear complexity for fractional multiterm odes on the half line. *SIAM Journal on Scientific Computing*, 39(3):A922–A946, 2017.
- [101] Mohsen Zayernouri, Mark Ainsworth, and George Em Karniadakis. Tempered fractional sturm–liouville eigenproblems. *SIAM Journal on Scientific Computing*, 37(4):A1777–A1800, 2015.
- [102] Mohsen Zayernouri and George Em Karniadakis. Exponentially accurate spectral and spectral element methods for fractional odes. *Journal of Computational Physics*, 257:460–480, 2014.
- [103] Mohsen Zayernouri and George Em Karniadakis. Fractional spectral collocation method. *SIAM Journal on Scientific Computing*, 36(1):A40–A62, 2014.
- [104] Lijing Zhao, Weihua Deng, and Jan S. Hesthaven. Spectral methods for tempered fractional differential equations. *Mathematics of Computation*, 2016.
- [105] Sheng Chen, Jie Shen, and Li-Lian Wang. Generalized jacobi functions and their applications to fractional differential equations. *Mathematics of Computation*, 85(300):1603–1638, 2016.
- [106] Zhiping Mao and Jie Shen. Efficient spectral–galerkin methods for fractional partial differential equations with variable coefficients. *Journal of Computational Physics*, 307:243–261, 2016.
- [107] Xianjuan Li and Chuanju Xu. A space-time spectral method for the time fractional diffusion equation. *SIAM Journal on Numerical Analysis*, 47(3):2108–2131, 2009.
- [108] Vincent J Ervin and John Paul Roop. Variational solution of fractional advection dispersion equations on bounded domains in rd. *Numerical Methods for Partial Differential Equations*, 23(2):256, 2007.
- [109] Xianjuan Li and Chuanju Xu. Existence and uniqueness of the weak solution of the space-time fractional diffusion equation and a spectral method approximation. *Communications in Computational Physics*, 8(5):1016, 2010.
- [110] Beiping Duan, Bangti Jin, Raytcho Lazarov, Joseph Pasciak, and Zhi Zhou. Space-time petrov–galerkin fem for fractional diffusion problems. *Computational Methods in Applied Mathematics* (2017), 2017.
- [111] Bangti Jin, Raytcho Lazarov, and Zhi Zhou. A petrov–galerkin finite element method for fractional convection-diffusion equations. *SIAM Journal on Numerical Analysis*, 54(1):481–503, 2016.
- [112] Roman Wituła, Edyta Hetmaniok, and Damian Słota. A stronger version of the second mean value theorem for integrals. *Computers & Mathematics with Applications*, 64(6):1612–1615, 2012.

- [113] H Zhang, Fawang Liu, and Vo Anh. Galerkin finite element approximation of symmetric space-fractional partial differential equations. *Applied Mathematics and Computation*, 217(6):2534–2545, 2010.
- [114] Rudolf Gorenflo, Yuri Luchko, and Masahiro Yamamoto. Time-fractional diffusion equation in the fractional sobolev spaces. *Fractional Calculus and Applied Analysis*, 18(3):799–820, 2015.
- [115] Y Maday. Analysis of spectral projectors in one-dimensional domains. *mathematics of computation*, 55(192):537–562, 1990.
- [116] C Canuto and A Quarteroni. Approximation results for orthogonal polynomials in sobolev spaces. *Mathematics of Computation*, 38(157):67–86, 1982.
- [117] Christine Bernardi, Yvon Maday, and Brigitte Métivet. Spectral approximation of the periodic-nonperiodic navier-stokes equations. *Numerische Mathematik*, 51(6):655–700, 1987.
- [118] Alexandre Ern and Jean-Luc Guermond. *Theory and practice of finite elements*, volume 159. Springer Science & Business Media, 2013.
- [119] Emilia Bazhlekova and Ivan Bazhlekov. Subordination approach to multi-term time-fractional diffusion–wave equations. *Journal of Computational and Applied Mathematics*, 339:179–192, 2018.
- [120] Živorad Tomovski and Trifce Sandev. Distributed-order wave equations with composite time fractional derivative. *International Journal of Computer Mathematics*, 95(6-7):1100–1113, 2018.
- [121] Bangti Jin, Raytcho Lazarov, Vidar Thomée, and Zhi Zhou. On nonnegativity preservation in finite element methods for subdiffusion equations. *Mathematics of Computation*, 86(307):2239–2260, 2017.
- [122] Mark Ainsworth and Christian Glusa. Aspects of an adaptive finite element method for the fractional laplacian: a priori and a posteriori error estimates, efficient implementation and multigrid solver. *Computer Methods in Applied Mechanics and Engineering*, 327:4–35, 2017.
- [123] Masahiro Yamamoto. Weak solutions to non-homogeneous boundary value problems for time-fractional diffusion equations. *Journal of Mathematical Analysis and Applications*, 460(1):365–381, 2018.
- [124] Sheng Chen, Jie Shen, and Li-Lian Wang. Laguerre functions and their applications to tempered fractional differential equations on infinite intervals. *Journal of Scientific Computing*, pages 1–28, 2017.
- [125] Zhiping Mao and Jie Shen. Spectral element method with geometric mesh for two-sided fractional differential equations. *Advances in Computational Mathematics*, pages 1–27, 2017.

- [126] Ehsan Kharazmi, Mohsen Zayernouri, and George Em Karniadakis. A petrov–galerkin spectral element method for fractional elliptic problems. *Computer Methods in Applied Mechanics and Engineering*, 324:512–536, 2017.
- [127] A Coronel-Escamilla, JF Gómez-Aguilar, L Torres, and RF Escobar-Jiménez. A numerical solution for a variable-order reaction–diffusion model by using fractional derivatives with non-local and non-singular kernel. *Physica A: Statistical Mechanics and its Applications*, 491:406–424, 2018.
- [128] JE Macías-Díaz. An explicit dissipation-preserving method for riesz space-fractional non-linear wave equations in multiple dimensions. *Communications in Nonlinear Science and Numerical Simulation*, 59:67–87, 2018.
- [129] Moulay Rchid Sidi Ammi and Ismail Jamiai. Finite difference and legendre spectral method for a time-fractinal diffusion-convection equation for image restoration. *Discrete & Continuous Dynamical Systems-Series S*, 11(1), 2018.
- [130] Xiaoli Li and Hongxing Rui. Two temporal second-order h1-galerkin mixed finite element schemes for distributed-order fractional sub-diffusion equations. *Numerical Algorithms*, page (in press), 2018.
- [131] Wenping Fan and Fawang Liu. A numerical method for solving the two-dimensional distributed order space-fractional diffusion equation on an irregular convex domain. *Applied Mathematics Letters*, 77:114–121, 2018.
- [132] WenYi Tian, Han Zhou, and Weihua Deng. A class of second order difference approximations for solving space fractional diffusion equations. *Mathematics of Computation*, 84(294):1703–1727, 2015.
- [133] Bangti Jin, Raytcho Lazarov, Dongwoo Sheen, and Zhi Zhou. Error estimates for approximations of distributed order time fractional diffusion with nonsmooth data. *Fractional Calculus and Applied Analysis*, 19(1):69–93, 2016.
- [134] Hong-lin Liao, Pin Lyu, Seakweng Vong, and Ying Zhao. Stability of fully discrete schemes with interpolation-type fractional formulas for distributed-order subdiffusion equations. *Numerical Algorithms*, 75(4):845–878, 2017.
- [135] Ehsan Kharazmi and Mohsen Zayernouri. Fractional pseudo-spectral methods for distributed-order fractional pdes. *International Journal of Computer Mathematics*, 95(6–7):1340–1361, 2018.
- [136] Živorad Tomovski and Trifce Sandev. Distributed-order wave equations with composite time fractional derivative. *International Journal of Computer Mathematics*, pages 1–14, 2017.
- [137] Sheng Chen, Jie Shen, and Li-Lian Wang. Generalized jacobi functions and their applications to fractional differential equations. *Mathematics of Computation*, 85(300):1603–1638, 2016.
- [138] Stephen B Pope. Turbulent flows, 2001.

- [139] Massimo Germano, Ugo Piomelli, Parviz Moin, and William H Cabot. A dynamic subgrid-scale eddy viscosity model. *Physics of Fluids A: Fluid Dynamics*, 3(7):1760–1765, 1991.
- [140] Nicolas Mordant, Pascal Metz, Olivier Michel, and J-F Pinton. Measurement of lagrangian velocity in fully developed turbulence. *Physical Review Letters*, 87(21):214501, 2001.
- [141] M Buzzicotti, M Linkmann, H Aluie, L Biferale, J Brasseur, and C Meneveau. Effect of filter type on the statistics of energy transfer between resolved and subfilter scales from a-priori analysis of direct numerical simulations of isotropic turbulence. *Journal of Turbulence*, 19(2):167–197, 2018.
- [142] Yi Li and Charles Meneveau. Origin of non-gaussian statistics in hydrodynamic turbulence. *Physical review letters*, 95(16):164502, 2005.
- [143] Sarah T Gille and Stefan G Llewellyn Smith. Velocity probability density functions from altimetry. *Journal of physical oceanography*, 30(1):125–136, 2000.
- [144] IA Min, I Mezić, and A Leonard. Levy stable distributions for velocity and velocity difference in systems of vortex elements. *Physics of fluids*, 8(5):1169–1180, 1996.
- [145] Hudong Chen, Jackson R Herring, Robert M Kerr, and Robert H Kraichnan. Non-gaussian statistics in isotropic turbulence. *Physics of Fluids A: Fluid Dynamics*, 1(11):1844–1854, 1989.
- [146] XIA Yang, S Zafar, J-X Wang, and H Xiao. Predictive large-eddy-simulation wall modeling via physics-informed neural networks. *Physical Review Fluids*, 4(3):034602, 2019.
- [147] Pierre Sagaut. *Large eddy simulation for incompressible flows: an introduction*. Springer Science & Business Media, 2006.
- [148] Charles D Pierce and Parviz Moin. Progress-variable approach for large-eddy simulation of non-premixed turbulent combustion. *Journal of fluid Mechanics*, 504:73–97, 2004.
- [149] FA Jaberí, PJ Colucci, S James, P Givi, and SB Pope. Filtered mass density function for large-eddy simulation of turbulent reacting flows. *Journal of Fluid Mechanics*, 401:85–121, 1999.
- [150] Parviz Moin, Kyle Squires, W Cabot, and Sangsan Lee. A dynamic subgrid-scale model for compressible turbulence and scalar transport. *Physics of Fluids A: Fluid Dynamics*, 3(11):2746–2757, 1991.
- [151] Guixiang Cui, Haibing Zhou, Zhaoshun Zhang, and Liang Shao. A new dynamic subgrid eddy viscosity model with application to turbulent channel flow. *Physics of Fluids*, 16(8):2835–2842, 2004.
- [152] XIA Yang and A Lozano-Durán. A multifractal model for the momentum transfer process in wall-bounded flows. *Journal of Fluid Mechanics*, 824, 2017.

- [153] Fernando Porté-Agel, Charles Meneveau, and Marc B Parlange. A scale-dependent dynamic model for large-eddy simulation: application to a neutral atmospheric boundary layer. *Journal of Fluid Mechanics*, 415:261–284, 2000.
- [154] Gregory C Burton and Werner JA Dahm. Multifractal subgrid-scale modeling for large-eddy simulation. i. model development and a priori testing. *Physics of Fluids*, 17(7):075111, 2005.
- [155] U Rasthofer and Volker Gravemeier. Multifractal subgrid-scale modeling within a variational multiscale method for large-eddy simulation of turbulent flow. *Journal of Computational Physics*, 234:79–107, 2013.
- [156] Peter Hamlington and Werner Dahm. Reynolds stress closure including nonlocal and nonequilibrium effects in turbulent flows. In *39th AIAA Fluid Dynamics Conference*, page 4162, 2009.
- [157] Tyler Maltba, Pierre A Gremaud, and Daniel M Tartakovsky. Nonlocal pdf methods for langevin equations with colored noise. *Journal of Computational Physics*, 367:87–101, 2018.
- [158] John H Cushman and Monica Moroni. Statistical mechanics with three-dimensional particle tracking velocimetry experiments in the study of anomalous dispersion. i. theory. *Physics of Fluids*, 13(1):75–80, 2001.
- [159] Monica Moroni and John H Cushman. Statistical mechanics with three-dimensional particle tracking velocimetry experiments in the study of anomalous dispersion. ii. experiments. *Physics of Fluids*, 13(1):81–91, 2001.
- [160] Wen Chen. A speculative study of 2/ 3-order fractional laplacian modeling of turbulence: Some thoughts and conjectures. *Chaos: An Interdisciplinary Journal of Nonlinear Science*, 16(2):023126, 2006.
- [161] Alexander G Churbanov and Petr N Vabishchevich. Numerical investigation of a space-fractional model of turbulent fluid flow in rectangular ducts. *Journal of Computational Physics*, 321:846–859, 2016.
- [162] Peter W Egolf and Kolumban Hutter. Fractional Turbulence Models. *Progress in Turbulence VII*, pages 123–131, 2017.
- [163] Brenden P Epps and Benoit Cushman-Roisin. Turbulence Modeling via the Fractional Laplacian. *arXiv preprint arXiv:1803.05286*, 2018.
- [164] Yongtao Zhou, Jorge L Suzuki, Chengjian Zhang, and Mohsen Zayernouri. Fast imex time integration of nonlinear stiff fractional differential equations. *arXiv preprint arXiv:1909.04132*, 2019.
- [165] Hongfei Fu, Huan Liu, and Hong Wang. A finite volume method for two-dimensional riemann-liouville space-fractional diffusion equation and its efficient implementation. *Journal of Computational Physics*, 388:316–334, 2019.

- [166] Maryam Naghibolhosseini and Glenis R Long. Fractional-order modelling and simulation of human ear. *International Journal of Computer Mathematics*, 95(6-7):1257–1273, 2018.
- [167] Jorge L Suzuki, Pegah Varghaei, Ehsan Kharazmi, and Mohsen Zayernouri. Anomalous Nonlinear Dynamics Behavior of Fractional Viscoelastic Structures. *arXiv preprint arXiv:2009.12214*, 2020.
- [168] Anna Lischke, Guofei Pang, Mamikon Gulian, Fangying Song, Christian Glusa, Xiaoning Zheng, Zhiping Mao, Wei Cai, Mark M Meerschaert, Mark Ainsworth, et al. What is the fractional laplacian? *arXiv preprint arXiv:1801.09767*, 2018.
- [169] Constantine Pozrikidis. *The Fractional Laplacian*. Chapman and Hall/CRC, 2016.
- [170] Elias M Stein. *Singular integrals and differentiability properties of functions (PMS-30)*, volume 30. Princeton university press, 2016.
- [171] Joseph Smagorinsky. General circulation experiments with the primitive equations: I. The basic experiment. *Monthly weather review*, 91(3):99–164, 1963.
- [172] Sharath S Girimaji. Boltzmann kinetic equation for filtered fluid turbulence. *Physical review letters*, 99(3):034501, 2007.
- [173] Kannan N Premnath, Martin J Pattison, and Sanjoy Banerjee. Dynamic subgrid scale modeling of turbulent flows using lattice-Boltzmann method. *Physica A: Statistical Mechanics and its Applications*, 388(13):2640–2658, 2009.
- [174] Zhenhua Xia, Yipeng Shi, Yu Chen, Moran Wang, and Shiyi Chen. Comparisons of different implementations of turbulence modelling in lattice boltzmann method. *Journal of Turbulence*, 16(1):67–80, 2015.
- [175] Pierre Sagaut. Toward advanced subgrid models for Lattice-Boltzmann-based Large-eddy simulation: theoretical formulations. *Computers & Mathematics with Applications*, 59(7):2194–2199, 2010.
- [176] Vairis Shtrauss. Decomposition filters for multiexponential and related signals. *International journal of Mathematical Models and Methods in Applied Sciences*, 1(3):137–142, 2007.
- [177] Michael Rubinstein, Ralph H Colby, et al. *Polymer physics*, volume 23. Oxford university press New York, 2003.
- [178] Jesse Chu-Shore, M Brandon Westover, and Matt T Bianchi. Power law versus exponential state transition dynamics: application to sleep-wake architecture. *PLoS One*, 5(12):e14204, 2010.
- [179] Noëlle Pottier. *Nonequilibrium statistical physics: linear irreversible processes*. Oxford University Press, 2010.
- [180] Laure Saint-Raymond. *Hydrodynamic limits of the Boltzmann equation*. Number 1971. Springer Science & Business Media, 2009.

- [181] J Sun, D Kuhn, and G Naterer. Eddy viscosity and reynolds stress models of entropy generation in turbulent channel flows. *Journal of Fluids Engineering*, 139(3):034501, 2017.
- [182] Adrian Bejan. *Entropy generation minimization: the method of thermodynamic optimization of finite-size systems and finite-time processes*. CRC press, 2013.
- [183] M Oberlack. Invariant modeling in large-eddy simulation of turbulence. *Annual Research Briefs*, pages 3–22, 1997.
- [184] TG Thomas and HS Takhar. Frame-invariance of turbulence constitutive relations. *Astrophysics and space science*, 141(1):159–168, 1988.
- [185] Pablo L Nápoli et al. Symmetry breaking for an elliptic equation involving the fractional laplacian. *Differential and Integral Equations*, 31(1/2):75–94, 2018.
- [186] Guo Boling, Pu Xueke, and Huang Fenghui. *Fractional partial differential equations and their numerical solutions*. World Scientific, 2015.
- [187] E. Perlman, R. Burns, Y. Li, and C. Meneveau. Data exploration of turbulence simulations using a database cluster. In *SC ’07: Proceedings of the 2007 ACM/IEEE Conference on Supercomputing*, pages 1–11, Nov 2007.
- [188] C.D. Cantwell, D. Moxey, A. Comerford, A. Bolis, G. Rocco, G. Mengaldo, D. De Grazia, S. Yakovlev, J.-E. Lombard, D. Ekelschot, B. Jordi, H. Xu, Y. Mohamied, C. Eskilsson, B. Nelson, P. Vos, C. Biotto, R.M. Kirby, and S.J. Sherwin. Nektar++: An open-source spectral/*hp* element framework. *Computer Physics Communications*, 192:205 – 219, 2015.
- [189] David Moxey, Chris D. Cantwell, Yan Bao, Andrea Cassinelli, Giacomo Castiglioni, Sehun Chun, Emilia Juda, Ehsan Kazemi, Kilian Lackhove, Julian Marcon, Gianmarco Mengaldo, Douglas Serson, Michael Turner, Hongtao Xu, Joaquim Peiró, Robert Michael Kirby, and Spencer J. Sherwin. Nektar++: enhancing the capability and application of high-fidelity spectral/*hp* element methods. *arXiv preprint arXiv:1906.03489*, 2019.
- [190] Hao Lu, Christopher J Rutland, and Leslie M Smith. A priori tests of one-equation les modeling of rotating turbulence. *Journal of Turbulence*, (8):N37, 2007.
- [191] Jouke H.S. de Baar, Richard P. Dwight, and Hester Bijl. Improvements to gradient-enhanced kriging using a bayesian interpretation. *International Journal for Uncertainty Quantification*, 4(3):205–223, 2014.
- [192] Nikolay A Simakov, Renette L Jones-Ivey, Ali Akhavan-Safaei, Hossein Aghakhani, Matthew D Jones, and Abani K Patra. Modernizing Titan2D, a parallel AMR geophysical flow code to support multiple rheologies and extendability. In *International Conference on High Performance Computing*, pages 101–112. Springer, 2019.
- [193] Ali Akhavan Safaei. Analysis and Implementation of Multiple Models and Multi-Models for Shallow-Water Type Models of Large Mass Flows. Master’s thesis, State University of New York at Buffalo, 2018.

- [194] U Piomelli. Large eddy simulations in 2030 and beyond. *Philosophical Transactions of the Royal Society A: Mathematical, Physical and Engineering Sciences*, 372(2022):20130320, 2014.
- [195] Roland Bouffanais. Advances and challenges of applied large-eddy simulation. *Computers & Fluids*, 39(5):735–738, 2010.
- [196] Joshua Holgate, Alex Skillen, Timothy Craft, and Alistair Revell. A review of embedded large eddy simulation for internal flows. *Archives of Computational Methods in Engineering*, 26(4):865–882, 2019.
- [197] Yang Zhiyin. Large-eddy simulation: Past, present and the future. *Chinese journal of Aeronautics*, 28(1):11–24, 2015.
- [198] Andrea Beck and Marius Kurz. A Perspective on Machine Learning Methods in Turbulence Modelling. *arXiv preprint arXiv:2010.12226*, 2020.
- [199] Karthik Duraisamy, Gianluca Iaccarino, and Heng Xiao. Turbulence modeling in the age of data. *Annual Review of Fluid Mechanics*, 51:357–377, 2019.
- [200] Suraj Pawar, Omer San, Adil Rasheed, and Prakash Vedula. A priori analysis on deep learning of subgrid-scale parameterizations for Kraichnan turbulence. *Theoretical and Computational Fluid Dynamics*, 34(4):429–455, 2020.
- [201] Justin Sirignano, Jonathan F MacArt, and Jonathan B Freund. DPM: A deep learning PDE augmentation method with application to large-eddy simulation. *Journal of Computational Physics*, 423:109811, 2020.
- [202] G. D. Portwood, B. T. Nadiga, J. A. Saenz, and D. Livescu. Interpreting neural network models of residual scalar flux. *Journal of Fluid Mechanics*, 907:A23, 2021.
- [203] Manuel Arias Chao, Chetan Kulkarni, Kai Goebel, and Olga Fink. Fusing physics-based and deep learning models for prognostics. *arXiv preprint arXiv:2003.00732*, 2020.
- [204] Salar Taghizadeh, Freddie D Witherden, and Sharath S Girimaji. Turbulence closure modeling with data-driven techniques: physical compatibility and consistency considerations. *New Journal of Physics*, 22(9):093023, 2020.
- [205] Jared Willard, Xiaowei Jia, Shaoming Xu, Michael Steinbach, and Vipin Kumar. Integrating physics-based modeling with machine learning: A survey. *arXiv preprint arXiv:2003.04919*, 2020.
- [206] Mostafa Aghaei Jouybari, Junlin Yuan, Giles J Brereton, and Farhad A Jaberi. Supersonic turbulent channel flows over two and three dimensional sinusoidal rough walls. *arXiv preprint arXiv:2012.02852*, 2020.
- [207] Abani K Patra, Andrea Bevilacqua, and Ali Akhavan Safaei. Analyzing complex models using data and statistics. In *International conference on computational science*, pages 724–736. Springer, 2018.

- [208] Eduardo A Barros de Moraes, Jorge L Suzuki, and Mohsen Zayernouri. Atomistic-to-meso multi-scale data-driven graph surrogate modeling of dislocation glide. [arXiv preprint arXiv:2012.05223](#), 2020.
- [209] Huaiqian You, Yue Yu, Nathaniel Trask, Mamikon Gulian, and Marta D’Elia. Data-driven learning of nonlocal physics from high-fidelity synthetic data. [Computer Methods in Applied Mechanics and Engineering](#), 374:113553, 2021.
- [210] Marius Kurz and Andrea Beck. A machine learning framework for LES closure terms. [arXiv preprint arXiv:2010.03030](#), 2020.
- [211] Ali Akhavan-Safaei, Mehdi Samiee, and Mohsen Zayernouri. Data-Driven Fractional Subgrid-scale Modeling for Scalar Turbulence: A Nonlocal LES Approach. [arXiv preprint arXiv:2012.14027](#), 2020.
- [212] Albert Vincent and Maria Meneguzzi. The spatial structure and statistical properties of homogeneous turbulence. [Journal of Fluid Mechanics](#), 225:1–20, 1991.
- [213] JP Laval, B Dubrulle, and S Nazarenko. Nonlocality and intermittency in three-dimensional turbulence. [Physics of Fluids](#), 13(7):1995–2012, 2001.
- [214] Zhen-Su She, Eric Jackson, and Steven A Orszag. Intermittent vortex structures in homogeneous isotropic turbulence. [Nature](#), 344(6263):226–228, 1990.
- [215] Zhen-Su She and Emmanuel Leveque. Universal scaling laws in fully developed turbulence. [Physical review letters](#), 72(3):336, 1994.
- [216] Aashwin Ananda Mishra and Sharath Girimaji. Linear analysis of non-local physics in homogeneous turbulent flows. [Physics of Fluids](#), 31(3):035102, 2019.
- [217] Dhawal Buaria, Alain Pumir, and Eberhard Bodenschatz. Self-attenuation of extreme events in Navier–Stokes turbulence. [Nature communications](#), 11(1):1–7, 2020.
- [218] Guofei Pang, Marta D’Elia, Michael Parks, and George E Karniadakis. nPINNs: nonlocal Physics-Informed Neural Networks for a parametrized nonlocal universal Laplacian operator. [Algorithms and Applications](#). [Journal of Computational Physics](#), 422:109760, 2020.
- [219] Ali Akhavan-Safaei, S Hadi Seyed, and Mohsen Zayernouri. Anomalous features in internal cylinder flow instabilities subject to uncertain rotational effects. [Physics of Fluids](#), 32(9):094107, 2020.
- [220] Peter E Hamlington and Werner JA Dahm. Reynolds stress closure for nonequilibrium effects in turbulent flows. [Physics of Fluids](#), 20(11):115101, 2008.
- [221] Reginald J Hill. Exact second-order structure-function relationships. [Journal of Fluid Mechanics](#), 468:317–326, 2002.
- [222] Antoine Briard, Thomas Gomez, and Claude Cambon. Spectral modelling for passive scalar dynamics in homogeneous anisotropic turbulence. [Journal of Fluid Mechanics](#), 799:159–199, 2016.

- [223] BK Shivamoggi and N Tuovila. Direct interaction approximation for non-Markovianized stochastic models in the turbulence problem. *Chaos: An Interdisciplinary Journal of Nonlinear Science*, 29(6):063124, 2019.
- [224] Gregory C Burton and Werner JA Dahm. Multifractal subgrid-scale modeling for large-eddy simulation. II. Backscatter limiting and a posteriori evaluation. *Physics of Fluids*, 17(7):075112, 2005.
- [225] Alexis-Tzianni G Charalampopoulos and Themistoklis P Sapsis. Machine-learning energy-preserving nonlocal closures for turbulent fluid flows and inertial tracers. *arXiv preprint arXiv:2102.07639*, 2021.
- [226] Jérôme Jacob, Orestis Malaspinas, and Pierre Sagaut. A new hybrid recursive regularised Bhatnagar–Gross–Krook collision model for Lattice Boltzmann method-based large eddy simulation. *Journal of Turbulence*, 19(11-12):1051–1076, 2018.
- [227] Guodong Jin, Shizhao Wang, Yun Wang, and Guowei He. Lattice Boltzmann simulations of high-order statistics in isotropic turbulent flows. *Applied Mathematics and Mechanics*, 39(1):21–30, 2018.
- [228] Olena Burkowska, Christian Glusa, and Marta D’Elia. An optimization-based approach to parameter learning for fractional type nonlocal models. *arXiv preprint arXiv:2010.03666*, 2020.
- [229] Ehsan Kharazmi and Mohsen Zayernouri. Fractional sensitivity equation method: Application to fractional model construction. *Journal of Scientific Computing*, 80(1):110–140, 2019.
- [230] Peter William Egolf and K Hutter. Nonlinear, Nonlocal and Fractional Turbulence. *Graduate Studies in Mathematics*. Springer,, 2020.
- [231] P Clark Di Leoni, Tamer A Zaki, George Karniadakis, and Charles Meneveau. Two-point stress-strain rate correlation structure and non-local eddy viscosity in turbulent flows. *arXiv preprint arXiv:2006.02280*, 2020.
- [232] Mehdi Samiee, Ali Akhavan-Safaei, and Mohsen Zayernouri. A fractional subgrid-scale model for turbulent flows: Theoretical formulation and a priori study. *Physics of Fluids*, 32(5):055102, 2020.
- [233] Jorge L Suzuki and Mohsen Zayernouri. A self-singularity-capturing scheme for fractional differential equations. *International Journal of Computer Mathematics*, pages 1–28, 2020.
- [234] Jorge Suzuki, Yongtao Zhou, Marta D’Elia, and Mohsen Zayernouri. A thermodynamically consistent fractional visco-elasto-plastic model with memory-dependent damage for anomalous materials. *Computer Methods in Applied Mechanics and Engineering*, 373:113494, 2021.
- [235] FC Meral, TJ Royston, and R Magin. Fractional calculus in viscoelasticity: an experimental study. *Communications in nonlinear science and numerical simulation*, 15(4):939–945, 2010.

- [236] Mehdi Samiee, Ehsan Kharazmi, Mark M Meerschaert, and Mohsen Zayernouri. A Unified Petrov–Galerkin Spectral Method and Fast Solver for Distributed-Order Partial Differential Equations. *Communications on Applied Mathematics and Computation*, pages 1–30, 2020.
- [237] Mahmoud A Zaky, Ahmed S Hendy, and Jorge E Macías-Díaz. Semi-implicit Galerkin–Legendre spectral schemes for nonlinear time-space fractional diffusion–reaction equations with smooth and nonsmooth solutions. *Journal of Scientific Computing*, 82(1):1–27, 2020.
- [238] Changping Xie and Shaomei Fang. A second-order finite difference method for fractional diffusion equation with Dirichlet and fractional boundary conditions. *Numerical Methods for Partial Differential Equations*, 35(4):1383–1395, 2019.
- [239] Farzad Sabzikar, Mark M Meerschaert, and Jinghua Chen. Tempered fractional calculus. *Journal of Computational Physics*, 293:14–28, 2015.
- [240] Zhijiang Zhang, Weihua Deng, and George Em Karniadakis. A Riesz basis Galerkin method for the tempered fractional Laplacian. *SIAM Journal on Numerical Analysis*, 56(5):3010–3039, 2018.
- [241] Hudong Chen, Steven A Orszag, Ilya Staroselsky, and Sauro Succi. Expanded analogy between Boltzmann kinetic theory of fluids and turbulence. *Journal of Fluid Mechanics*, 519:301, 2004.
- [242] Orestis Malaspinas and Pierre Sagaut. Consistent subgrid scale modelling for lattice Boltzmann methods. *Journal of Fluid Mechanics*, 700:514–542, 2012.
- [243] G Evin, J Blanchet, E Paquet, F Garavaglia, and D Penot. A regional model for extreme rainfall based on weather patterns subsampling. *Journal of Hydrology*, 541:1185–1198, 2016.
- [244] Lorick Huang. Density estimates for SDEs driven by tempered stable processes. *arXiv preprint arXiv:1504.04183*, 2015.
- [245] Kamil Kaleta and Paweł Sztonyk. Estimates of transition densities and their derivatives for jump Lévy processes. *Journal of Mathematical Analysis and Applications*, 431(1):260–282, 2015.
- [246] Ali Akhavan-Safaei and Mohsen Zayernouri. A Parallel Integrated Computational-Statistical Platform for Turbulent Transport Phenomena. *arXiv preprint arXiv:2012.04838*, 2020.
- [247] Weihua Deng, Buyang Li, Wenyi Tian, and Pingwen Zhang. Boundary problems for the fractional and tempered fractional operators. *Multiscale Modeling & Simulation*, 16(1):125–149, 2018.
- [248] Eleonora Di Nezza, Giampiero Palatucci, and Enrico Valdinoci. Hitchhiker’s guide to the fractional Sobolev spaces. *Bulletin des sciences mathématiques*, 136(5):521–573, 2012.
- [249] David W Henderson and Daina Taimina. *Experiencing geometry*. Prentice Hall, 2000.
- [250] Rafał Weron. Levy-stable distributions revisited: tail index > 2 does not exclude the Levy-stable regime. *International Journal of Modern Physics C*, 12(02):209–223, 2001.